International Workshop

14th – 15th April 2014
Novosibirsk, Russian Federation

Integration of Point- and Area-wise Geodetic Monitoring for Structures and Natural Objects

Proceedings

Published by:
Siberian State Academy of Geodesy, Novosibirsk, Russian Federation
Institute of Engineering Geodesy, University of Stuttgart, Germany

International Workshop

Integration of Point- and Area-wise Geodetic Monitoring for Structures and Natural Objects

Proceedings

14th – 15th April 2014

Organizers:
Institute of Engineering Geodesy, University of Stuttgart
Siberian State Academy of Geodesy, Novosibirsk, Russian Federation

In collaboration with:
Leibniz University Hannover, Institute of Photogrammetry and GeoInformation, Germany
D. Serikbaev East Kazakhstan State Technical University, Republic of Kazakhstan

The Workshop is co-funded by the German Research Foundation (Deutsche Forschungsgemeinschaft – DFG).

Published by:

Alexander P. Karpik, Volker Schwieger, Argina Novitskaya, Otto Lerke

These proceedings can be ordered from:

rektorat@ssga.ru
sekretariat@ingeo.uni-stuttgart.de

ISBN: 978-3-00-045367-0

http://www.uni-stuttgart.de/ingeo/

Printed at Printing Laboratory, SSGA
8, Plakhotnogo St., Novosibirsk, 630108

Organizing Committee

Chairman:

Prof. Dr. **Alexander P. Karpik**	Rector, Siberian State Academy of Geodesy, Novosibirsk, Russian Federation
Prof. Dr.-Ing. **Volker Schwieger**	Director, Institute of Engineering Geodesy, University of Stuttgart, Chair of FIG Commissions 5 “Positioning and Measurement”, Germany
Prof. Dr.-Ing. **Christian Heipke**	ISPRS Secretary General, Leibniz University Hannover, Institute of Photogrammetry and Geoinformation, Germany

Vice Chairman:

Prof. **Vladimir A. Seredovich**	Vice Rector for Scientific and Innovative Activities, Siberian State Academy of Geodesy, Novosibirsk, Russian Federation
Dr. **Ivo Milev**	Managing Director, technet-rail 2010 GmbH, Chair of FIG Commission 6 “Engineering Surveys”, Germany

Members:

Prof. Dr.-Ing., **Uwe Stilla**	Vice President of the German Society of Photogrammetry, Remote Sensing and Geoinformation, Faculty of Civil, Geo and Environmental Engineering, Institute of Photogrammetry and Cartography, Technical University of Munich, Germany
Prof. Dr.-Ing. **Reiner Jäger**	University of Applied Sciences Karlsruhe, Institute of Geomatics, Honorary Professor of Siberian State Academy of Geodesy, Germany
Assoc. Prof. **Sergej V. Seredovich**, PhD	Director, Institute of Geodesy and Management, Siberian State Academy of Geodesy, Novosibirsk, Russian Federation
Prof. **Kaisar B. Khasenov**	Head, Department of Geodesy, Land Management and Cadastre, D. Serikbaev East Kazakhstan State Technical University, Republic of Kazakhstan
Prof. **Anatoly L. Okhotin**	Head, Department of Mine Surveying and Geodesy, National Research Irkutsk State Technical University, Director of I LLC NPC “Baikalgeoservice”, Russian Federation
Assoc. Prof. **Alexander V. Seredovich**, PhD	Head, Department of Engineering Geodesy and Mine Surveying, Siberian State Academy of Geodesy, Novosibirsk, Russian Federation
Prof. Dr. **Igor V. Minin**	Department of Metrology and Technologies in Optical Engineering, Siberian State Academy of Geodesy, Novosibirsk, Russian Federation

Secretaries

Argina Novitskaya	Siberian State Academy of Geodesy, Novosibirsk, Russian Federation
Otto Lerke	Institute of Engineering Geodesy, University of Stuttgart, Germany

General information

Monitoring of structures and natural objects with regard to movements and deformations is one of the main tasks of engineering geodesy. Geometric changes of points can be detected with geodetic instruments, such as level instruments, total stations and GNSS receivers. Beside tachymeters, only GNSS receivers are able to measure the three-dimensional positions point-wise automatically and continuously. The geodetic GNSS receivers can achieve accuracies in the sub-cm range up to mm e.g. by using different time-based one-dimensional filter algorithms in monitoring systems. The use of small low-cost atomic oscillators with a stability of about 10^{-12} and higher in GNSS receivers and satellites opens new opportunities for monitoring of structures, natural objects and phenomena to control the measurements and increase their accuracy.

In recent years, new area-wise measuring methods such as stereoscopic image sequence analysis, terrestrial laser scanning and ground-based radar have been introduced for practical applications. Terrestrial laser scanner (TLS) is a new measurement instrument to acquire area- wise deformations with high-resolution. Laser scanning technology can be successfully used for geospatial monitoring of complicated industrial objects and structures (dams, bridges, tunnels and other complex engineering structures) providing accuracy about 1-10 mm. There are many different approaches for the derivation of deformations.

The point-based methods provide highly precise information for individually characterized points. The area-based methods provide the complete shape of the object in a high resolution and with an often reduced accuracy. The accuracy and reliability of the area wise measurement method should be improved through the precise point wise measurement method.

Area-wise monitoring can be carried out using stereoscopic images or image sequences, followed by photogrammetric processing involving image orientation and image matching, and resulting in a 3D point cloud similar to that of laser scanning. As a consequence, further processing of this point cloud to derive object movement etc. is very similar to that for laser scanning point clouds. Image acquisition can be done from static cameras with known (pre-calibrated) image orientation, or from moving platforms, e. g. unmanned aerial vehicles (UAV).

The potential of the integration of precise point-wise measurements and high resolution area-wise measurements to lead to a rigorous statistical deformation analysis scheme has not yet been systematically investigated, which constitutes a gap within the recent research in engineering geodesy. The information from point-wise measurements including the complete stochastic description in time and space shall be used to strengthen the information from the area-wise information especially with respect to the accuracy of modeling of surfaces and the reliability to detect edges and corners. This integration may be realized in geodetic adjustment or in Kalman filter approaches. The alternative is a Baysian estimation approach to combine the two data sources e.g. using the point-wise data as prior information for the estimation of the surfaces by the area-wise data. For example GNSS and TLS can be used to improve functional safety of high liability hydro technical constructions and dams at hydroelectric power stations and, consequently, the safety of the population in the surrounding areas. The integration of point-wise measurements with physical models of structures by means of FEM in case of a static and dynamic behavior of structures leads to the topic of “Structural Health Monitoring”. In that integration case the point-wise geodetic geodetic displacements and the nodal point displacements can be leaded together by the FEM shape functions, and “unhealthy” physical structures, can be identified by adequate parametrizations or –parameter-changes in the characteristic FEM matrices (stiffness-, damping- and mass-matrix).

The round-table discussion will be devoted to leading research in the field of integration of point- and area-wise deformation analysis, and defining and developing future research targets.

Key issues are as follows:

Objects under observation: Industrial and civilian, public utilities (hydro technical constructions, atomic and thermal power plants), mining plants, minery, shafts, tunnels, linear structures (highways, roads, pipelines, power transmission lines), landslides, glaciers, etc.

Methods of observations and measurements: leveling, line-and-angle, laser scanning, Earth remote sensing, aerospace surveys (aerial and GPS surveys), radar. and georadar surveys, mine surveying, gravity surveys, interference control techniques, GNSS and MEMS technologies

Monitoring data processing and interpretation: software tools for geodata analysis, processing, interpretation and visualization, algorithmization and estimation concepts of geodetic observations and mathematical methods of analysis, integrated and system analysis related monitoring approaches, structural health-monitoring processing and interpretation, cloud computing technologies.

TECHNICAL PROGRAMME

<table>
<tr><td colspan="2">Monday, 14 April 2014</td></tr>
<tr><td>Monday
14 April 2014
09:00-09:45
SSGA, Novosibirsk
Room 402, Floor 4</td><td>Registration of participants and visitors</td></tr>
<tr><td>Monday
14 April 2014
09:45-10:00
SSGA, Novosibirsk
Room 402, Floor 4</td><td>Opening Ceremony of the workshop
“Integration of Point- and Area-wise Geodetic Monitoring for Structures and Natural Objects”
• Prof. Dr. Alexander P. Karpik, Rector of Siberian State Academy of Geodesy
• Prof. Dr.-Ing. Volker Schwieger, Director, Institute of Engineering Geodesy, University of Stuttgart, Chair of FIG Commissions 5 “Positioning and Measurement”, Germany</td></tr>
<tr><td rowspan="2">Monday
14 April 2014
10:00-12:00
SSGA,
Novosibirsk
Room 402, Floor 4</td><td>Technical session 1: Deformation Analysis and Modeling
Chair: Prof. Vladimir A. Seredovich, Vice Rector for Scientific and Innovative Activities, Siberian State Academy of Geodesy, Russian Federation
Co-Chair: Prof. Dr.-Ing. Reiner Jäger, University of Applied Sciences Karlsruhe (HSKA), Institute of Geomatics, Honorary Professor of SSGA, Germany
Secretary: Otto Lerke, Institute of Engineering Geodesy, University of Stuttgart, Germany</td></tr>
<tr><td>V. Schwieger, University of Stuttgart, Germany
Kinematic and Dynamic Deformation Modeling

A.V. Seredovich, V.A. Seredovich, A.A. Ivanov, Siberian State Academy of Geodesy,
Russian Federation
Modeling of Engineering Object Deformations by the Results of Point- and Area-Wise Observations

R. Jäger, University of Applied Sciences Karlsruhe (HSKA), Germany
Methods and Approaches for Integrated Deformation Analysis

I.G. Vovk, Siberian State Academy of Geodesy, Russian Federation
Modeling of Linear Objects by the Results of Geodetic Monitoring

U. Stilla, Technical University of Munich (TUM), Germany
Change Detection in Point Clouds</td></tr>
</table>

Monday 14 April 2014 13:00 – 15:30 SSGA, Novosibirsk Room 402, Floor 4	**Technical session 2: Geodetic Monitoring of Industrial Objects** Chair: Dr. **Ivo Milev,** Managing Director, "technet-rail 2010 GmbH", Beuth University of Applied Science Berlin, Chair of FIG Commission 6 "Engineering Surveys", Germany Co-Chair: Assoc. Prof. **Alexander V. Seredovich**, PhD, Department of Engineering Geodesy and Mine Surveying, Siberian State Academy of Geodesy, Novosibirsk, Russian Federation Secretary: **Ekaterina I. Gorokhova,** Senior Engineer, Department of Engineering Geodesy and Mine Surveying, Siberian State Academy of Geodesy, Novosibirsk, Russian Federation **A.P. Karpik, A.V. Dubrovsky**, Siberian State Academy of Geodesy, Russian Federation **Basic Principles of Geoinformation Solutions for Safe Operation of Nuclear Power Plants (NPPs)** **J. van Cranenbroeck**, Creative Geosensing sprl-s, Belgium, Europa **K. Y. Xiangjun, Hans Ni Xiangjun**, Beijing iSpatial Co Ltd PR China **SAMOS Switching Antenna Monitoring System Applied on Tailings Reservoir On-Line Monitoring Project** **K.B. Khasenov**, **M.Ye. Rakhymberdina**, D. Serikbaev East Kazakhstan State Technical University (EKSTU), Republic of Kazakhstan **K. M. Kaleeva,** S. Amanzholov East Kazakhstan State University (EKSU), Republic of Kazakhstan **Geodetic Monitoring of Gravity Dam Deformations on the Maloulbinsky Reservoir** **A.I. Fyodorov, N.V. Fyudorova**, Siberian State Academy of Geodesy, Russian Federation **Benchmark Stability Control in Geodetic Monitoring for Nuclear Power Plant Safety** **M. Reich, J. Unger, F. Rottensteiner, C. Heipke,** Institute of Photogrammetry and GeoInformation, Leibniz Universität Hannover, Germany **A New Approach for an Incremental Orientation of Micro-UAV Image Sequences** **V.F. Kanushin, I.G. Ganagina, D.N. Goldobin, A.M. Kosareva, L.R. Galimov**, Siberian State Academy of Geodesy, Russian Federation **The Impact of Nontidal Gravity Variations on the Results of Geodetic Monitoring of Hydrotechnical Constructions** **V.V. Loshchev**, Novosibirsk State University of Architecture and Civil Engineering, Russian Federation **A New Approach to the Problem of Monitoring Reinforced Geosynthetics Earth Structures**

Monday 14 April 2014 15:45 – 18:00 SSGA, Novosibirsk Room 402, Floor 4	**Technical session 3: Geodetic Monitoring of Natural Objects**
	Chair: Prof. **Evgeny I. Avrunev**, Department of Cadastre and Territorial Planning, Siberian State Academy of Geodesy, Novosibirsk, Russian Federation Co-Chair: Prof. **Alexander Zagibalov**, Department of Mine Surveying and Geodesy, National Research Irkutsk State Technical University, Russian Federation Secretary: **Ekaterina I. Gorokhova,** Senior Engineer, Department of Engineering Geodesy and Mine Surveying, Siberian State Academy of Geodesy, Novosibirsk, Russian Federation
	A.V. Seredovich, V.A. Seredovich, A.A. Ivanov, Siberian State Academy of Geodesy, Russian Federation **Landslide Hazard Assessment of Pit Mine Edges Using Laser Scanning Data** **E.I. Avrunev, I.A. Giniyatov, D.Yu. Terentyev, M.V. Meteleva,** Siberian State Academy of Geodesy, Russian Federation **Geodetic Monitoring of Natural Object Conditions (as an example of a landslide)** **V. S. Khoroshilov**, **O.G. Pavlovskaya,** Siberian State Academy of Geodesy, Russian Federation **Special Aspects of Mathematical Landslide Processes Modeling by Geodetic Data during Blasting Operations and Transportation of Big Soil Masses** **V.G. Kolmogorov**, Siberian State Academy of Geodesy, Russian Federation **Geodetic Monitoring of Contemporary Deformation Conditions of Near Surface Structures of South Siberia** **V.D. Han**, National Research Irkutsk State Technical University, Russian Federation **Proven Experience Using Satellite Measurements for Landslide Monitoring** **J. Unger, M. Reich, C. Heipke,** Institute of Photogrammetry and GeoInformation, Leibniz Universität Hannover, Germany **UAV-based Photogrammetry: Monitoring of a Building Zone**

Tuesday, 15 April 2014	
Tuesday 15 April 2014 09:00 – 11:00 SSGA, Novosibirsk Room 402, Floor 4	**Technical session 4: Construction Monitoring**
	Chair: Prof. **Anatoly L. Okhotin,** Head, Department of Mine Surveying and Geodesy, National Research Irkutsk State Technical University, Director of I LLC NPC "Baikalgeoservice", Russian Federation Co-Chair: Dr.-Ing. **Martin Metzner,** Deputy Director, Institute of Engineering Geodesy, University of Stuttgart, Germany Secretary: **Ekaterina I. Gorokhova,** Senior Engineer, Department of Engineering Geodesy and Mine Surveying, Siberian State Academy of Geodesy, Russian Federation

	I. Milev, D. Staykova, "technet-rail 2010 GmbH", Beuth University of Applied Science Berlin, Germany **TLS for Structure Monitoring** **I.V. Minin, O.V. Minin**, Siberian State Academy of Geodesy, Russian Federation **Strain Analysis in Explosion Physics Problems Using Cloud Photogrammetry** **A.V. Seredovich, V.A. Seredovich, A.A. Ivanov**, Siberian State Academy of Geodesy, Russian Federation **Geodetic Monitoring of Industrial Facilities Using Laser Scanning and Thermal Survey Data for Revealing Hazardous Areas** **I.V. Minin, O.V. Minin**, Siberian State Academy of Geodesy, Russian Federation **Diffractive Optics and its Application for 3D Scanners and Interferometry Deformation Measurements in Millimeter-wave** **M.A.**, **Altyntsev** Siberian State Academy of Geodesy, Russian Federation **Automated Recognition of Roadbed Deformations (defects) Using Laser Scanning Data**
Tuesday 15 April 2014 11:30 – 13:00 SSGA, Novosibirsk Room 402, Floor 4	**Technical session 5: Deformation Analysis and Time Series Analysis**
	Chair: Prof. Dr.-Ing. **Volker Schwieger**, Director, Institute of Engineering Geodesy, University of Stuttgart, Chair of FIG Commissions 5 "Positioning and Measurement", Germany Co-Chair: Prof. **Kaisar B. Khasenov,** Department of Geodesy, Land Management and Cadastre, D. Serikbaev East Kazakhstan State Technical University (EKSTU), Republic of Kazakhstan Secretaries: **Olga A. Situkha,** Regional Centre for Laser Scanning, Siberian State Academy of Geodesy, Novosibirsk, Russian Federation **Otto Lerke,** Institute of Engineering Geodesy, University of Stuttgart, Germany
	C. Heipke, Leibniz University Hannover, Germany **Dense Matching for Deformation Analysis** **M. Metzner**, University of Stuttgart, Germany **Time Series Analysis for Construction Monitoring** **A.V. Zagibalov**, National Research Irkutsk State Technical University, Russian Federation **Mathematic Modeling of Mineral Deposits** **L. Zhang**, University of Stuttgart, Germany **Time-Spatial Analysis for Low-Cost GPS Time Series**

Tuesday 15 April 2014 14:00 – 16:00 SSGA, Novosibirsk Room 402, Floor 4	**Technical session 6: Monitoring by Laser Scanning**
	Chair: Prof. Dr.-Ing. **Uwe Stilla,** Vice President of the German Society of Photogrammetry, Remote Sensing and Geoinformation, Faculty of Civil, Geo and Environmental Engineering, Institute of Photogrammetry and Cartography, Technical University of Munich (TUM), Germany Co-Chair: Prof. Dr. **Valery S. Khoroshilov**, Department of Physical Geodesy and Remote Sensing, Siberian State Academy of Geodesy, Novosibirsk, Russian Federation Secretaries: **Ekaterina I. Gorokhova,** Senior Engineer, Department of Engineering Geodesy and Mine Surveying, Siberian State Academy of Geodesy, Russian Federation **Maxim A. Altyntsev**, PhD, Senior Lecturer, Siberian State Academy of Geodesy, Russian Federation
	A.A. Tokin, National Research Irkutsk State Technical University, Russian Federation **Underground Laser Scanning for Testing of Constructions** **A. Schmitt**, University of Stuttgart, Germany **Combining Laser Tracker and Laser Scanner Data** **E. I. Gorokhova,** Siberian State Academy of Geodesy, Russian Federation **Terrestrial Laser Scanning for Monitoring of Tunnel Deformations** **B. Zheng**, University of Stuttgart, Germany **TLS for Calibrating Finite Element Models** **A. Scheider,** University of Stuttgart, Germany **Detecting and Modeling Fine Structures from TLS Data**
Tuesday 15 April 2014 16:30 – 17:15 SSGA, Novosibirsk Room 402, Floor 4	**Technical session 7: Geodetic Monitoring for Mining**
	Chair: Dr. **Ivo Milev**, Managing Director, "technet-rail 2010 GmbH", Beuth University of Applied Science Berlin, Chair of FIG Commission 6 "Engineering Surveys", Germany Co-Chair: Assoc. Prof. **Alexander V. Seredovich**, PhD, Head of the Department of Engineering Geodesy and Mine Surveying, Siberian State Academy of Geodesy, Novosibirsk, Russian Federation Secretary: **Olga A. Situkha**, Regional Centre for Laser Scanning, Siberian State Academy of Geodesy, Novosibirsk, Russian Federation
	A.L. Okhotin, National Research Irkutsk State Technical University, Russian Federation **UASs for Monitoring of Open Pit Mines** **K.M. Antonovich, N.S. Kosarev**, Siberian State Academy of Geodesy, Russian Federation **Future Challenges of Small Atomic Oscillators Used in GNSS Monitoring Systems for Structures and Natural Objects**

	T. T. Ipalakov, D. Serikbaev East Kazakhstan State Technical University, Republic of Kazakhstan **E. K. Nurzhumin**, S. Seyfullin Kazakh Agrotechnical University, Republic of Kazakhstan **The Assessment of Geomechanical Situation in the Neighborhood of Designed Open Pit-Side Contours Convergence with Shafts in Mine Development** **S.O. Gridnev**, National Research Irkutsk State Technical University, Russian Federation **New Method of Vertical Shaft Monitoring**
Tuesday 15 April 2014 17:15 – 18:00 SSGA, Novosibirsk Room 402, Floor 4	**Round-table discussion**
Tuesday 15 April 2014 18:00 SSGA, Novosibirsk Room 402, Floor 4	**Closure of workshop**

ПРОГРАММА КОНФЕРЕНЦИИ

<table>
<tr><td colspan="2">Понедельник, 14 апреля 2014</td></tr>
<tr><td>Понедельник
14 апреля 2014
09:00-09:45
СГГА, Новосибирск
ауд. 402, этаж 4</td><td>Регистрация участников конференции</td></tr>
<tr><td>Понедельник
14 апреля 2014
09:45-10:00
СГГА, Новосибирск
ауд. 402, этаж 4</td><td>Открытие международной конференции
“Интеграция данных наблюдений по маркам и за объектами в целом при геодезическом мониторинге инженерных сооружений и природных объектов”
• Карпик А.П., ректор СГГА, д.т.н., профессор, СГГА, Новосибирск, Россия
• Фолькер Швигер, директор Института инженерной геодезии, Университет Штутгарта, председатель FIG Комиссии 5 “Позиционирование и измерение”, доктор-инженер, профессор, Германия</td></tr>
<tr><td rowspan="2">Понедельник
14 апреля 2014
10:00-12:00
СГГА, Новосибирск
ауд. 402, этаж 4</td><td>Секция 1: Анализ и моделирование деформаций</td></tr>
<tr><td>Председатель: Середович В.А., проректор по научной и инновационной деятельности СГГА, профессор, Новосибирск, Россия
Зам. председателя: Райнер Ягер, Университет прикладных наук Карлсруэ, Институт геоматики, почетный профессор СГГА, доктор-инженер, профессор, Германия
Секретарь: Отто Лерке, Институт инженерной геодезии, Университет Штутгарта, Германия

Фолькер Швигер, Университет Штутгарта, Институт инженерной геодезии, Германия
Создание кинематических и динамических моделей деформаций

Середович А.В., Середович В.А., Иванов А.А., СГГА, Новосибирск, Россия
Моделирование деформаций инженерных объектов по данным наблюдений за марками и объектами в целом

Райнер Ягер, Университет прикладных наук Карлсруэ, Германия
Методы и подходы к комплексному анализу деформаций
Вовк И.Г., СГГА, Новосибирск, Россия
Моделирование линейных объектов по результатам геодезического мониторинга

Уве Штилла, Технический университет Мюнхена, Германия
Обнаружение изменений в облаке точек</td></tr>
</table>

<table>
<tr><td>Понедельник
14 апреля 2014
13:00-15:30
СГГА, Новосибирск
ауд. 402, этаж 4</td><td colspan="2">Секция 2: Геодезический мониторинг промышленных объектов</td></tr>
<tr><td></td><td>Председатель:

Зам. председателя:

Секретарь:</td><td>Иво Милев, генеральный директор фирмы “technet-rail 2010 GmbH”, Берлинский университет прикладных наук им. Бойта, председатель FIG Комиссии 6 “Инженерная геодезия”, доктор наук, Германия
Середович А.В., заведующий кафедрой инженерной геодезии и маркшейдерского дела, к.т.н., СГГА, Новосибирск, Россия
Горохова Е.И., ведущий инженер кафедры инженерной геодезии и маркшейдерского дела, СГГА, Новосибирск, Россия</td></tr>
<tr><td></td><td colspan="2">Карпик А.П., Дубровский А.В., СГГА, Новосибирск, Россия
Базовые принципы геодезического и геоинформационного обеспечения безопасной эксплуатации атомных станций

Джоэл ван Кроненброк, Creative Geosensing sprl-s, Бельгия
Карл Ю Сянцзюнь, Ганс Ни Сянцзюнь, Beijing iSpatial Co Ltd PR China, Китай
SAMOS - система мониторинга с коммутируемой антенной, применяемая в проекте по непрерывному контролю хвостохранилищ

Хасенов К.Б., Рахымбердина М.Е., Восточно-Казахстанский государственный технический университет им. Д. Серикбаева, Республика Казахстан

Калеева К.М., Восточно-Казахстанский государственный университет имени С. Аманжолова, Республика Казахстан
Геодезический мониторинг наблюдений за деформациями гравитационной плотины Мало-Ульбинского водохранилища

Федоров А.И., Федорова Н.В., СГГА, Новосибирск, Россия
К вопросу контроля устойчивости реперов при геодезическом мониторинге для безопасности АЭС

Мартин Рейх, Якоб Унгер, Франц Роттенштейнер, Кристиан Хайпке, Ганноверский университет им. Лейбница, Институт фотограмметрии и геоинформации, Германия
Новый подход к пошаговому ориентированию последовательности микроизображений, полученных с БПЛА

Канушин В.Ф., Ганагина И.Г., Голдобин Д.. Н., Косарева А.М., Галимов Л. Р. , СГГА, Новосибирск, Россия
Учет влияния неприливных изменений силы тяжести при геодезическом мониторинге гидротехнических сооружений</td></tr>
</table>

	Лощев В.В., Новосибирский государственный архитектурно-строительный университет (НГАСУ), Новосибирск, Россия *Новый подход к проблеме мониторинга армогрунтовых сооружений*
Понедельник 14 апреля 2014 15:45-18:00 СГГА, Новосибирск ауд. 402, этаж 4	**Секция 3: Геодезический мониторинг природных объектов**
	Председатель: Аврунев Е.И., зав. кафедрой кадастра и регионального планирования, СГГА, Новосибирск, Россия Зам. председателя: Загибалов А.В., научный сотрудник, кафедра маркшейдерского дела и геодезии, ИрГТУ, Иркутск, Россия Секретарь: Горохова Е.И., ведущий инженер кафедры инженерной геодезии и маркшейдерского дела, СГГА, Новосибирск, Россия
	Середович А.В., Середович В.А., Иванов А.А., СГГА, Новосибирск *Оценка масштабов оползней бортов рудников по данным лазерного сканирования* Аврунев Е.И., Гиниятов И.А., Терентьев Д.Ю., Метелева М.В., СГГА, Новосибирск, Россия *Мониторинг состояния природных объектов геодезическими методами (на примере оползня)* Хорошилов В.С., Павловская О.Г., СГГА, Новосибирск, Россия *Особенности математического моделирования оползневых процессов по геодезическим данным в условиях проведения взрывных работ и вывоза больших масс грунта* Колмогоров В.Г., СГГА, Новосибирск, Россия *Мониторинг современного деформационного состояния приповерхностных структур Южной Сибири* Хан В.Д., ИрГТУ, Иркутск, Россия *Успешный опыт применения спутниковых измерений для мониторинга оползня* Якоб Унгер, Мартин Рейх, Кристиан Хайпке, Ганноверский университет им. Лейбница, Институт фотограмметрии и геоинформации, Германия *Мониторинг районов застройки беспилотными летательными аппаратами (БПЛА) с использованием фотограмметрии*

Вторник, 15 апреля 2014

Вторник 15 апреля 2014 09:00-11:00 СГГА, Новосибирск ауд. 402, этаж 4	**Секция 4: Мониторинг сооружений** Председатель: Охотин А.Л., зав. кафедрой маркшейдерского дела и геодезии, ИрГТУ, директор ООО «Байкалгеосервис», профессор, Иркутск, Россия Зам. председателя: Мартин Мецнер, зам. директора Института инженерной геодезии, Университет Штутгарта, доктор-инженер, Германия Secretary: Горохова Е.И., ведущий инженер кафедры инженерной геодезии и маркшейдерского дела, СГГА, Новосибирск, Россия Иво Милев, Десислава Стайкова, "technet-rail 2010 GmbH", Берлинский университет прикладных наук им. Бойта, Германия *Наземное лазерное сканирование для мониторинга сооружений* Минин И.В., Минин О.В., СГГА, Новосибирск, Россия *Исследование деформаций в задачах физики взрывов методами облачной фотограмметрии* Середович А.В., Середович В.А., Иванов А.А., СГГА, Новосибирск, Россия *Геодезический мониторинг промышленных объектов по данным лазерного сканирования и тепловых съемок с целью выявления опасных участков* Минин И.В., Минин О.В., СГГА, Новосибирск, Россия *Дифракционная оптика: применение для 3D сканеров и интерферометрическим измерениям деформаций в миллиметровом диапазоне* Алтынцев М.А., СГГА, Новосибирск, Россия *Автоматизированное распознавание деформаций (дефектов) автодорожного полотна по данным лазерного сканирования*
Вторник 15 апреля 2014 11:30-13:00 СГГА, Новосибирск ауд. 402, этаж 4	**Секция 5: Анализ деформаций и временных рядов** Председатель: Фолькер Швигер, директор Института инженерной геодезии, Университет Штутгарта, доктор-инженер, профессор, Германия Зам. председателя: Хасенов К.Б., зав. кафедрой геодезии Восточно-Казахстанского технического университета им. Д. Серикбаева, к.т.н., Республика Казахстан Секретари: Ситуха О.А., инженер Регионального центра лазерного сканирования СГГА, Новосибирск, Россия Отто Лерке, Институт инженерной геодезии, Университет Штутгарта, Германия

	Кристиан Хайпке, Ганноверский университет им. Лейбница, Институт фотограмметрии и геоинформации, Германия *Согласование плотности изображений для анализа деформаций* Мартин Мецнер, Университет Штутгарта, Институт инженерной геодезии, Германия *Анализ временных рядов для мониторинга строительных объектов* Загибалов А.В., ИрГТУ, Иркутск, Россия *Математическое моделирование месторождений полезных ископаемых* Ли Чжан, Университет Штутгарта, Институт инженерной геодезии, Германия *Пространственно-временная фильтрация для временных рядов недорогих GPS*
Вторник 15 апреля 2014 14:00 – 16:00 СГГА, Новосибирск ауд. 402, этаж 4	**Секция 6: Мониторинг с применением лазерного сканирования**
	Председатель: Уве Штилла, вице-президент Немецкого общества фотограмметрии, дистанционного зондирования и геоинформации, Технический университет Мюнхена доктор-инженер, профессор, Германия Зам. председателя: Хорошилов В.С., кафедра физической геодезии и дистанционного зондирования, д.т.н., профессор, СГГА, Новосибирск Секретари: Горохова Е.И., ведущий инженер кафедры инженерной геодезии и маркшейдерского дела, СГГА, Новосибирск Алтынцев М.А., старший преподаватель, кафедры инженерной геодезии и маркшейдерского дела, к.т.н., СГГА, Новосибирск
	Токин А.А., ИрГТУ, Иркутск, Россия *Подземное лазерное сканирование для оценки состояния горных выработок* Аннетте Шмитт, Университет Штутгарта, Институт инженерной геодезии, Германия *Комбинирование данных лазерного трекера и сканера* Горохова Е.И., СГГА, Новосибирск, Россия *Мониторинг деформаций тоннелей методом наземного лазерного сканирования*

	Биминь Чжэнь, Университет Штутгарта, Институт инженерной геодезии, Германия *Наземное лазерное сканирование для калибровки моделей конечных элементов* Аннетте Шайдер, Университет Штутгарта, Институт инженерной геодезии, Германия *Моделирование тонкозернистых структур по данным лазерного сканера*
Вторник 15 апреля 2014 16:30 – 17:15 СГГА, Новосибирск ауд. 402, этаж 4	**Секция 7: Геодезический мониторинг в горной промышленности**
	Председатель: Иво Милев, генеральный директор фирмы “technet-rail 2010 GmbH”, Берлинский университет прикладных наук им. Бойта, председатель FIG Комиссии 6 “Инженерная геодезия”, доктор наук, Германия Зам. председателя: Середович А.В., заведующий кафедрой инженерной геодезии и маркшейдерского дела, к.т.н., СГГА, Новосибирск Секретарь: Ситуха О.А., инженер Регионального центра лазерного сканирования СГГА, Новосибирск
	Охотин А.Л., ИрГТУ, Иркутск, Россия *Беспилотные летательные комплексы для мониторинга карьеров* Антонович К.М., Косарев Н.С., СГГА, Новосибирск, Россия *Перспективы применения малогабаритных атомных генераторов частоты в системах геодезического мониторинга сооружений и природных объектов* Ипалаков Т. Т., Восточно-Казахстанский государственный технический университет им. Д. Серикбаева, Республика Казахстан Нуржумин Е.К., Казахский агротехнический университет им. С. Сейфуллина *Оценка геомеханической ситуации в районе сближения проектных контуров бортов карьеров со стволами шахт при комбинированной отработки месторождений* Гриднев С.О., ИрГТУ, Иркутск, Россия *Новый метод профилирования вертикальных шахт*

Вторник 15 апреля 2014 17:15 – 18:00 СГГА, Новосибирск ауд. 402, этаж 4	**Дискуссия**
Вторник 15 апреля 2014 18:00 СГГА, Новосибирск ауд. 402, этаж 4	**Закрытие конференции**

Content

Technical Session 1: Deformation Analysis and Modeling

Kinematic and Dynamic Deformation Modeling

Volker Schwieger
Institute of Engineering Geodesy, University of Stuttgart, Germany

Abstract
Monitoring measurements as well as deformation analysis have a long tradition in geodesy, especially engineering geodesy. The consideration of time allows to model the deformations kinematically. Taking into account the forces, e.g. loads on a bridge and factors, e.g. temperature changes influencing the deformations directly or indirectly, leads to a dynamic deformation model. This contribution will review the present status of quasi-static, static, kinematic and dynamic modelling. The present state is a point-oriented analysis. New developments in the measurement domain like terrestrial laser scanning yield to the possibility of modelling deformations of lines, surfaces and bodies. The author will discuss new aspects of deformation analysis with respect to freeform surface modelling with respect to kinematic and dynamical models.

Keywords
Monitoring, Kinematic Model, Dynamic Model, Deformation Analysis, Freeform Surfaces

1 INTRODUCTION

Monitoring measurements as well as deformation analysis have a long tradition in geodesy, especially engineering geodesy. This has yield to numerous symposia in this field: the most important are the *International FIG Symposia on Deformation Measurements* that has seen numerous realizations from 1975 in Poland up to 2003 in Greece. In 2006 it was joined in Austria for the first time with the IAG *Symposium on Geodesy for Geotechnical on Structural Engineering* that took place 2 times before. In 2011 the ISPRS joined the symposium series in Hong Kong, since then it has been called the *Joint International Symposium on Deformation Monitoring*. The last symposium was realized successfully in the UK 2013.

The main methodical innovations in the analysis domain were the mathematical-statistical algorithms to detect movements of points or point groups. It was a mathematical stringent way to deliver significant decisions. The base for the decisions were measurement quantities like distances and angles, height differences as well as GNSS coordinates or coordinate differences, meaning that all measurements are related to marked and defined points. The algorithms that were developed are mainly based on the comparisons of points measured in geodetic networks. Time and influencing forces were not considered at the beginning. Currently both model parts are included into research and into software development too.

Besides the trend of measurement technology is going towards techniques that do not acquire defined points automatically. Terrestrial Photogrammetry as well as terrestrial laser scanning may acquire up to a million points per second meaning that lines and surfaces as well as complete areas can be acquired in a very short time. This leads to the problem that the standard point-wise approaches cannot be used anymore. The question how to handle these new techniques in deformation modelling and detection is an open question that shall be discussed in this contribution.

2 CLASSICAL DEFORMATION ANALYSIS

One important component of classical deformation modelling is the discretization in time and space that is state of the art in monitoring applications. The definition of epochs, the measurements points or intervals of time, can be seen as a simple discretization in time. With respect to space the monitoring network points may be regarded as discretization. This relationship is shown in Figure 1. In the following the author firstly shows the way of spatial discretization in monitoring networks. Then the new developments with respect to quasi-continuous space modelling will be outlined in section 4.

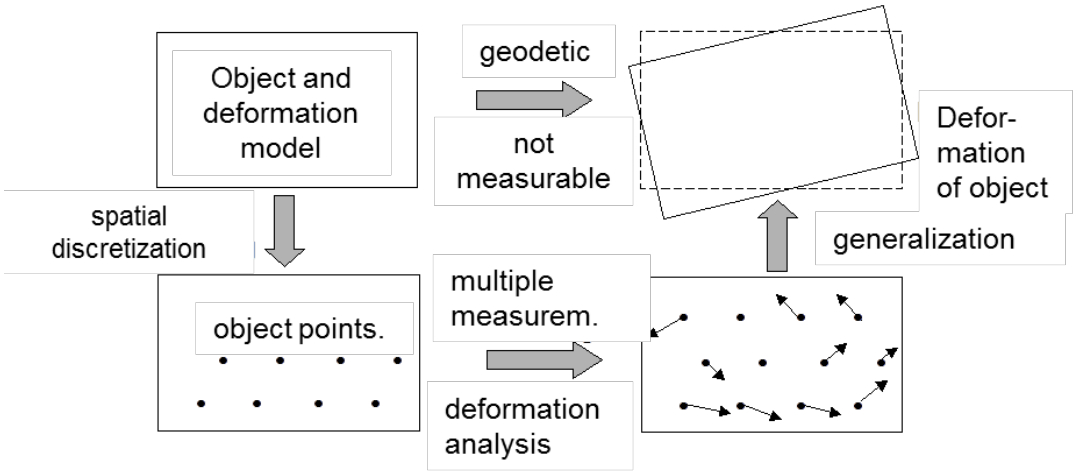

Figure 1: Discretization in space (after NIEMEIER, 1985)

As mentioned before classical deformation analysis deal with monitoring networks (geodetic network for monitoring tasks). Figure 2 shows an example for a monitoring network. In general the network is divided into control points and object points. The first being assumed to be not influenced by object deformations and accepted as stable; the latter assumed to be influenced by deformations. The main idea of the statistical method is to compare the coordinates measured at different points of time, the epochs. Between object points relative measurements are realized and towards control points the measurements are called absolute.

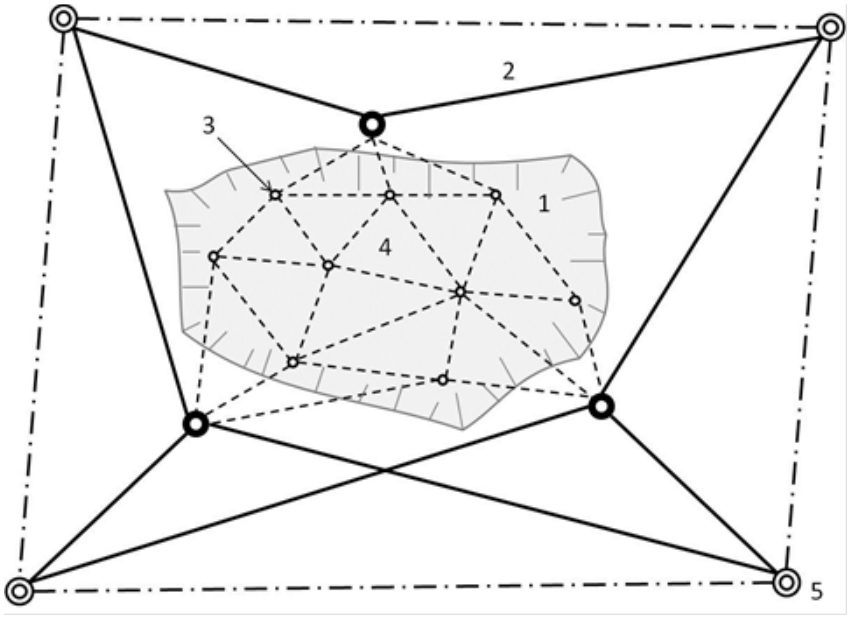

Figure 2: Example Monitoring Network (after PELZER, 1982); with 1 - monitoring object, 2 – absolute measurement, 3 – object point, 4 – relative measurement, 5 – control point

In Figure 1 the monitored object could be a subsidence area e.g caused by mining activities. The extension of this area is roughly estimated only, so that the separation into object and control is not clear and reliable. Therefore a detailed analysis procedure was developed.

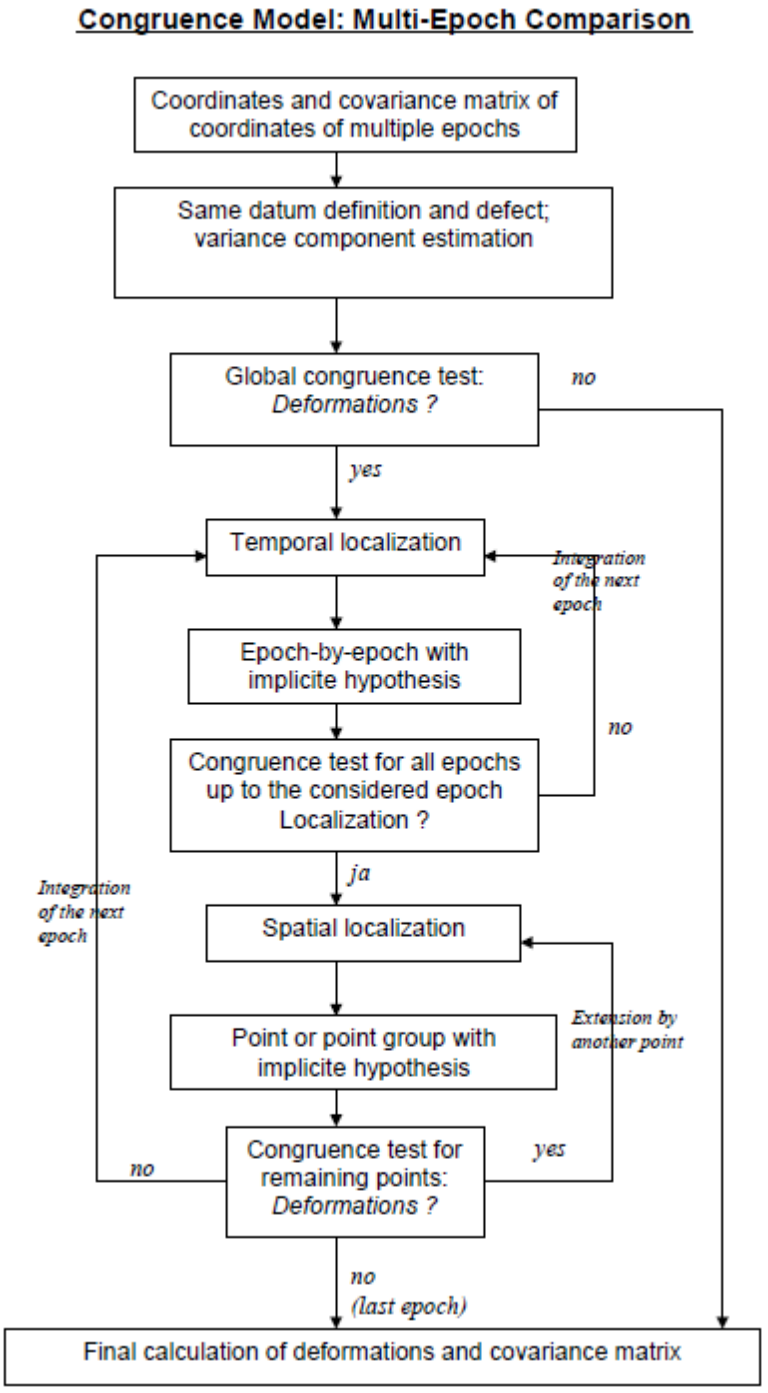

Figure 3: Congruence model: Multi-epoch deformation analysis procedure

The mathematical base was developed by numerous researchers; at this place PELZER (1971), NIEMEIER (1979) and CHEN (1983) should be mentioned. Based on these basic mathematical findings other researchers developed complete procedures. The developed algorithms can detect movements of points, point groups and the complete monitoring network based on statistical test. If more than two epochs are measures, a so called multi-comparison approach has to be realized. In this case three questions have to be answered:

1. Do deformations occur at all?
2. In which epoch(s) the deformations occur?
3. At which point(s) the deformations occur?

A complete exemplary procedure is outlined in Figure 3. For mathematical details the author refers to the literature mentioned above and PELZER (1985). These algorithms do not take the time into consideration and they do not deal with influencing factors or forces: the respective simplified model is called congruence model. More details will be given in the following section.

3 KINEMATIC AND DYNAMIC MODELLING

Every real object reacts dynamically, since it is influenced by time-dependent forces or other environmental influences. For modelling the objects frequently simplifications are realized, since some information are not available or the modelling effort would be too large. The consideration or neglect of time and influencing forces leads to different models: congruence model, kinematic model, static model and dynamic model. Table 1 gives an overview about the different models and shows the main differences. It adopted from WELSCH & HEUNECKE (2001).

Table 1: Models in deformation analysis

modelled are…	**geometry**	time-dependence	influencing forces
Congruence model	**yes**	no	no
Kinematic model	yes	yes	no
Static model	yes	no	yes
Dynamic model	yes	yes	yes

In the *congruence*, identity, random walk or quasi-static *model* geometric changes among minimum two epochs are investigated. The point movements are assumed to be zero meaning that the prediction is an unchanged extrapolation of the current epoch. Time and acting forces are not considered. As written before the main application is the statistical analysis of monitoring networks.
The *static model* of an object is investigated with respect to different acting forces. Time is not considered. Functional relationships among influencing forces and deformations lead to a causal prediction. A typical example is a load experiment on a bridge.
In contradiction the *kinematic model* allows a causal prediction only in case that the influencing parameters of the past will not change in the future. But in general time-related movements are described without consideration of acting forces. In general a kinematic model can be described in dependence of geometric quantities like the positions x, velocities $\dot{x}$ and accelerations $\ddot{x}$ of the pervious epochs *i, i-1*, etc.:

$$x_{i+1} = \varphi\left(x_i, \dot{x}_i, \ddot{x}_i, x_{i-1}, \dot{x}_{i-1}, \ddot{x}_{i-1}, \ldots\right). \quad (1)$$

PELZER (1987) introduces the general kinematic prediction model with Δt as time difference between two epochs. The model can be written in the form

$$x_{i+1} = x_i + \Delta t \cdot \dot{x}_i + \frac{\Delta t^2}{2} \ddot{x}_i . \quad (2)$$

Trend, periods and statistical properties can be determined e.g. using the methods of signal processing. Examples are movements of a glacier or of tectonic plates. UNTERBERG (1991) adopts the Kalman filter for height movements, SCHWIEGER et al. (1994) analyse vertical movements in the Carpathian Arc using the same method.
The most complete model is the *dynamic model*. Here the time-dependent movements are regarded as reactions of the object on the time-dependent acting forces u_{i-1}

$$x_{i+1} = \varphi\left(x_i, \dot{x}_i, \ddot{x}_i, x_{i-1}, \dot{x}_{i-1}, \ddot{x}_{i-1}, \ldots, u_i, u_{i-1}, \ldots\right). \quad (3)$$

This is the most realistic picture of reality. A complete causal prediction of deformations is possible. For dynamic models the question arises how structural characteristics can be modelled e.g. if a temperature change is measured how this temperature change influences geometric properties. Besides the measurement of the influencing factor like temperature, the engineer or the researcher needs an idea about the structure of the construction or the natural object to model the influence of the

temperature. This idea is very often modelled numerically e.g. using Finite Element Methods (FEM). BOLJEN (1983) made the first approaches to combine dynamic models and deformation analysis. HEUNECKE (1995) proposes a general procedure for integrating FEM and Kalman filter to determine point-wise movements and deformations as well as to calibrate the dynamic model or in any case some parameters (the process coefficients) of the model. GÜLAL (1997) adopts this approach for the calibration of a dam model. EICHHORN (2004) models the temperature flux driven deformations in a column by adaptive Kalman filtering and LIENHART (2007) adopts FEM for monolithic bridge monitoring and SZOSTAK-CHRZANOWSKI at al. (1999) investigates dynamic modelling of large earth dams. All these applications deal with real dynamic modelling of objects, but they all go back to control and calibrate the object behaviour by defined (and partly marked) points. Additionally the measurements are realized at these defined points. The area-wise consideration of object modelling is not realized up to now despite the fact dynamic models are surface or volume oriented and the measurement technologies are surface oriented too nowadays.

4 AREA-WISE DEFORMATION MODELLING

In general a surface or a body determined by terrestrial laser scanning can be modelled in three different ways: using the original or filtered point cloud (meshed or not meshed), estimating geometric primitives like cylinders or cones or estimating freeform surfaces (KERN, 2003).

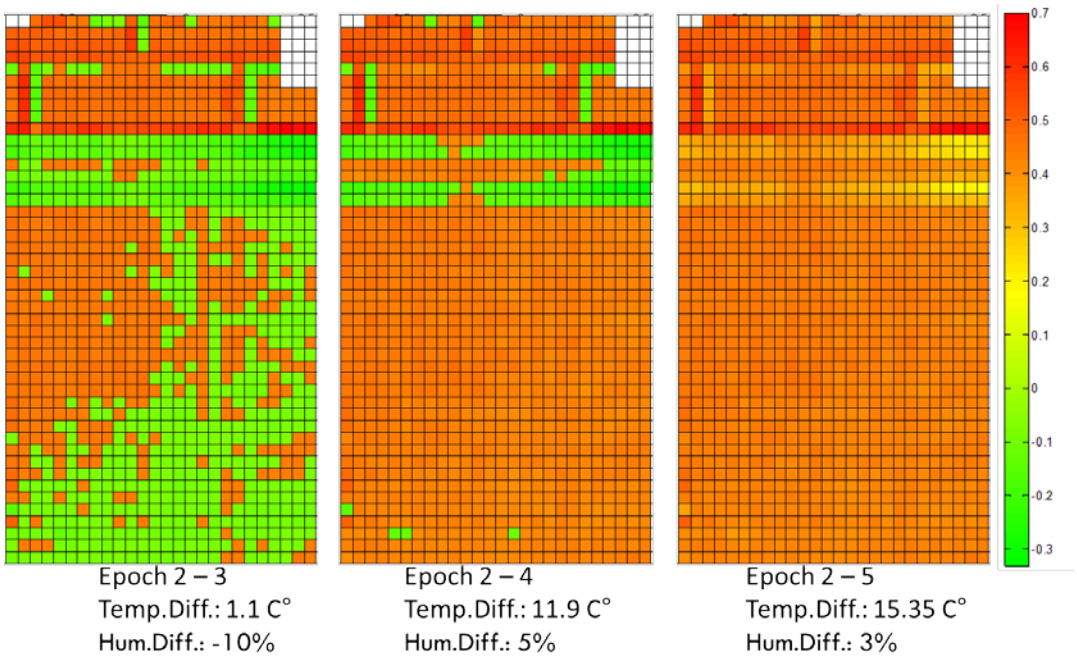

Figure 4: Comparison of volume change [cm^3] for a part of a sandstone façade (ZHENG et al., 2013)

The modelling using these options is well known and established within typical software packages like Cyclone or Geomagic. The problem arises when movements and deformations have to be detected. Here different approaches are currently under investigation. A very good overview is given by OHLMANN-LAUBER & SCHÄFER (2011). Basically one has to distinguish between two procedures. The first is based on the measured point clouds, the second realizes a model in a first step and analyses the geometrical changes in the second step. Most approaches deal with the second procedure. The model may consist for geometric primitives or freeform surfaces. For geometric primitives the question arises if one compares the change of the parameters describing the object e.g. the radius of a cylinder or, as described in section 2, compare points for their geometric changes. Again, the first seems is the more innovative approach that is e.g. put forward by GOSLIGA et al. (2006). The latter would again lead to a more or less arbitrary spatial discretization that will not reflect the model or object change as a whole. The other extreme are meshed point clouds that can be

compared point-wise only, a method that is wide-spread in cultural heritage modelling and analysis. Here ZHENG et al. (2013) investigate small rectangular surfaces for deformation analysis of volumes and normal vectors. Figure 4 shows an exemplary result for volume comparison. The method is based on the general findings of ELING (2009).

The most advanced idea to model surfaces are freeform elements. All freeform models should be two times differentiable. The most typical example are the Bezier-curves. They are based on the Bernstein polynomials. For further details the author refers to PIEGL & TILLER (1997). For a curve approximation the number of the polynomials and the location of the nodes have to be estimated. A Bezier curve of degree one includes two Bernstein polynomials and two nodes and results in a straight line. If degree two is chosen, three nodes and polynomials are considered. The location of the middle node can be placed in principle freely. In reality it should be chosen for optimal approximation of curve. Figure 5 presents examples for degrees 2 and 3, where P_i indicated the nodes.. The curves may be generalized to Bezier surfaces. Here the limiting curves of the surfaces are Bezier curves. The shape of the surface can be changed by the introduction of weights for each Bernstein polynomial. For these rational Bezier surfaces besides location of nodes and degree of polynomials the weights have to be estimated. All Bezier surface changes influence the complete modelled surface. This may be a problem if local deformations have to be detected, modelled and analysed.

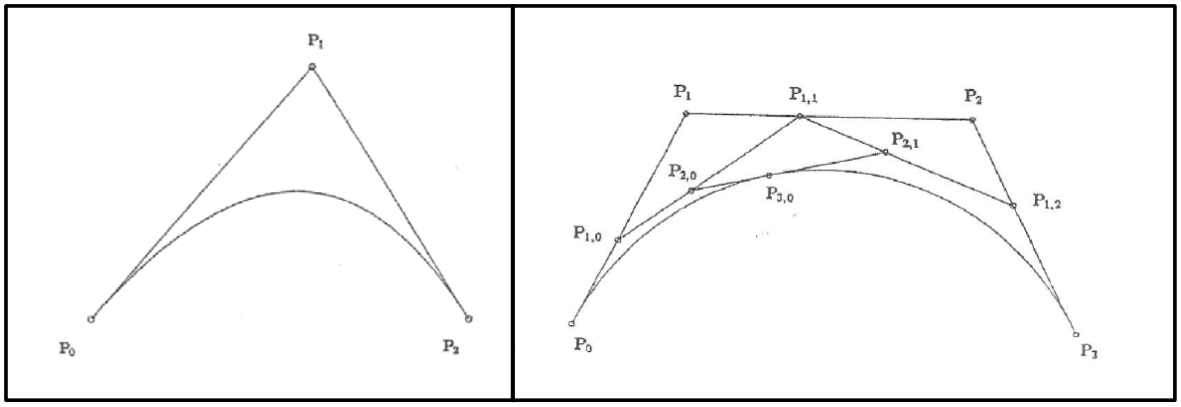

Figure 5: Bezier curves of degrees two and three (PIEGL & TILLER, 1997)

To overcome this problem the use of splines is the best procedure. Splines are defined for limited parts of the surface only, so they will not influence the other parts of the surface if parameters are changed. B-Splines approximate the surface by nodes and base functions modelled as piecewise polynomial functions. At the transition points between two parts the two-times differentiability has to be assured. Again the number of polynomial functions, the nodes in one part and the control points defining the transition lines are needed to optimally approximate the real surface. If weights for the polynomials are added non-uniform rational B-Splines (NURBS) as the most complete freeform model are available. Theoretically NURBS-surfaces consist of bi-variate rational base functions. For further details the author refers e.g. to PIEGL & TILLER (1997).

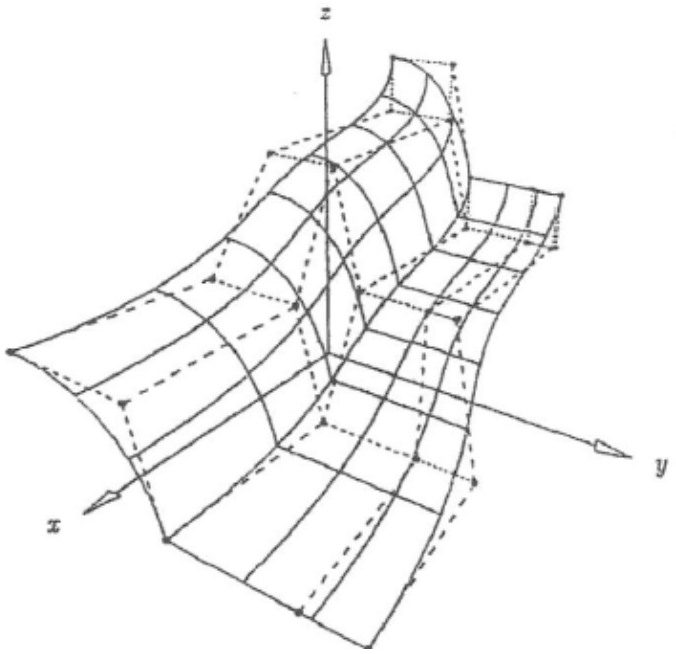

Figure 6: NURBS surface example (PIEGL & TILLER, 1997)

The remaining problem is that a purely data-driven approximation model may change all parameters: location of nodes (and control points) as well as the number and the weights of the polynomials. So it remains difficult to model geometric changes: should the analysis deal with fixed nodes or should the surfaces be modelled completely new in each epoch. This is the traget of current research.
All the mentioned modelling using freeform surfaces are still geometry oriented and, if time is considered, may be called kinematic. The difference to the classical methods is from point-wise to area-wise modelling and analysis. If the research should go towards dynamic modelling, the influencing forces have to be considered e.g. using an FEM model. Here a perfect matching could be realized in the future since body oriented deterministic dynamic FEM models could be combined with surface oriented measurement freeform modelling techniques. ZHENG (2014) presents some results en route to this aim. The geometry modelling is still mash-based and the compared FEM is in relation to this mesh.

5 CONCLUSIONS

This contribution outlines the basic ideas of classic deformation analysis based on the congruence model. Thereafter time dependence is introduced that leads to the kinematic deformation model. Finally the inclusion of influencing forces leads to dynamic deformation models. All these models base on point-wise analysis. Since measurement techniques are developing their way towards surface related measurements e.g. using terrestrial laser scanners, the current trend is towards area-wise deformation analysis. Here the current research is related to freeform surfaces and their changes in time, the deformations. It has to be decided if the deformation analysis has to be realized using points again of if significant changes of the freeform parameters like nodes, weights and number of polynomials are the relevant analysis target. Finally an integration with the surface related FEM modelling will lead to dynamic are-wise deformation analysis.

REFERENCES

Books:

BOLJEN, J.: *Ein dynamisches Modell zur Analyse und Interpretation von Deformationen*. Wissenschaftliche Arbeiten der Fachrichtung Vermessungswesen der Universität Hannover, No. 122, Hannover, 1983.

CHEN, Y.Q.: *Analysis of Deformation Surveys – A Generalized Method*. Department of Surveying Engineering, University of New Brunswick, Canada, Technical Report, No. 94, 1983.

EICHHORN, A.: *Ein Beitrag zur Identifikation von dynamischen Strukturmodellen mit Methoden der adaptiven KALMAN-Filterung*. Bayerische Akademie der Wissenschaften, DGK, Reihe C, No. 585, München, 2004.

ELING, D.: *Terrestrisches Laserscanning für die Bauwerksüberwachung*. Deutsche Geodätische Kommission, Reihe C, No. 641, München, 2009.

GÜLAL, E.: *Geodätische Überwachung einer Talsperre; eine Anwendung der Kalman-Filtertechnik*, Wissenschaftliche Arbeiten der Fachrichtung Vermessungswesen der Universität Hannover, No 224, Hannover, 1997.

HEUNECKE, O. (1995): *Zur Identifikation und Verifikation von Deformationsprozessen mittels adaptiver Kalman-Filterung (Hannoversches Filter)*. Wissenschaftliche Arbeiten der Fachrichtung Vermessungswesen der Universität Hannover, No. 208, Hannover, 1995.

KERN, F.: *Automatisierte Modellierung von Bauwerksgeometrien aus 3D-Laserscanner-Daten*. Geodätische Schriftenreihe der Technischen Universität Braunschweig, No. 19, 2003.

LIENHART, W. (2007): *Analysis of Inhomogeneous Structural Monitoring*. Shaker Verlag, Aachen, 2007

NIEMEIER, W.: *Zur Kongruenz mehrfach beobachteter geodätischer Netze*. Arbeiten der Fachrichtung Vermessungswesen, Universität Hannover, No. 88,1979.

PELZER, H.: *Zur Analyse geodätischer Deformationsmessungen*. Verlag der Bayerischen Akademie der Wissenschaften, Reihe C, No. 164, München, 1971.

PELZER, H.: *Geodätische Netze in der Landes- und Ingenieurvermessung II*. Konrad Wittwer, Stuttgart, 1985.

PIEGL, L.A.; TILLER, W.: *The Nurbs Book*. Springer Verlag, Berlin, 1997

UNTERBERG, U.: *Das KALMAN-Filter als Ansatz für die Auswertung weiträumiger kinematischer Höhennetze*. Arbeiten der Fachrichtung Vermessungswesen, Universität Hannover, No. 170,1979.

WELSCH, W.; HEUNECKE, O.: *Models and Terminology for the Analysis of Geodetic Monitoring Observations*. Official report of the Ad-Hoc Committee of FIG Working Group 6, 2001.

Journal articles:

GOSLIGA, R. v., LINDENBERGH, R., PFEIFER, N.: *Deformation Analysis of a bored tunnel by means of Terrestrial Laserscanning*. Proceedings on ISPRS Commission V Symposium, Dresden, 2006.

OHLMANN-LAUBER, J., SCHÄFER, T.: *Ansätze zur Ableitung von Deformationen aus TLS-Daten.* DVW, Volume 66, Wißner Verlag, Augsburg, 2011.

PELZER, H.: *Geodätische Modelle zur Erfassung von Deformationen, insbesondere von Rutscherscheinungen.* V. Internationales Symposium für Markscheidewesen, 1982.

PELZER, H.: *Deformationsmodelle auf Basis kinematischer Bewegungsmodelle.* Allgemeine Vermessungsnachrichten, Heft 2, 1987.

NIEMEIER, W.: *Anlage von Überwachungsnetzen*. In: PELZER, H.: *Geodätische Netze in der Landes- und Ingenieurvermessung II.* Konrad Wittwer, Stuttgart, 1985.

SCHWIEGER, V.; PELZER, H.; NEUNER, J.; RUS, T.: *Detection of Recent Crustal Movements in the Carpathian Arc by GPS.* Proceedings on Perelmuter Workshop on Dynamic Deformation Models. Haifa, Israel, 1994.

SZOSTAK-CHRZANOWSKI, A.; MASSIERA, M.; MUMA, M.; WHITAKER, C.: *Geotechnical Aspects of Erath Dam Deformation Monitoring*. Proceedings on 9th FIG International Symposium on Deformation Measurements, Olsztyn, Poland, 1999.

ZHENG, B.; SCHWIEGER, V.; GRASSEGGER-SCHÖN, G.: *Detection of hydrothermal deformations of sandstone using laser scanning*. 2nd Joint Symposium on Deformation Monitoring, Nottingham, UK, 2013.

ZHENG, B.: *TLS for Calibrating Finite Element Models.* International Workshop “Integration of Point- and Area-wise Geodetic Monitoring for Structures and Natural Objects”, Novosibirsk, Russia, 2014.

Methods and Approaches for Integrated Deformation Analysis

Reiner Jäger
University of Applied Sciences Karlsruhe, Germany

Abstract

The general term of geomonitoring includes RaD tasks and applications related to the disciplines of geodynamics, geology, engineering geodesy, civil engineering and geotechnics. It comprises early warning in case of natural disasters, monitoring of buildings, construction areas and engineering facilities (e.g. mines).

One modern international RaD topic is dedicated to the interdisciplinary field of structural health monitoring, also called “integrated” or “system-analysis” based deformation analysis. Integrated deformation analysis approaches and technical systems are directed to the identification of changes in the physical state parameters **p** of related geomonitoring objects by the use of different kind of sensors and/or derived geomonitoring data.

In the frame of the RaD project GOCA (www.goca.info) both, geodetic and integrated, FEM-based geomonitoring approaches have continuously been developed. The technical realization of the GOCA system covers the complete geomonitoring chain (data acquisition, modeling, reporting and alarm management) of a geodetic and integrated deformation analysis system. Based on network adjustment of GNSS, terrestrial total station and levelling sensor data, GOCA can presently provide 3D displacements, velocities and accelerations for object point dynamics up to 1 Hz. Concerning integrated deformation analysis and structural health monitoring, 1 Hz still means more less the static FEM case.
The article picks up both the technical realization of GOCA, serving over 15 years also as reference system for technical developments at the industry (technology transfer), as well as the state of the art of geodetic and FEM based integrated deformation analysis approaches being developed and continued in the RaD project GOCA. The presented FEM approaches cover both the use of geodetic displacement, velocity and acceleration estimations based on geodetic network adjustment, as well as the inclusion of local geotechnical sensor data.

While in the static case of FEM-based structural health monitoring, only changes in the para-metrized stiffness matrix $\mathbf{K}(\mathbf{p}_K)$ can be identified, dynamic FEM approaches enable additionally the identification of parameter changes in the damping and the mass matrix $\mathbf{C}(\mathbf{p}_C)$ and $\mathbf{M}(\mathbf{p}_M)$ of a structure, as shown in the contribution. As concerns the farer reaching integrated dynamical FEM deformation analysis, new local sensor technologies and respective estimation procedures for higher frequencies are however required. The ones presented in the article are based on low-cost GNSS/MEMS sensors and the estimation procedures originating from navigation. They enable high frequency estimates of local geodetic displacement, velocity, acceleration and rotation rates.

Keywords

Geomonitoring, geodetic and integrated deformation analysis, FEM, stiffness, damping and mass matrix, system analysis, inverse eigenvalue problems

1 INTRODUCTION

1.1 Geomonitoring Chain and Classical Geodetic Deformation Analysis

In its interdisciplinary structure the geomonitoring chain (Figure 1) breaks into the components of the data acquisition (sensor network operation and data communication), modeling (network adjustment and deformation analysis, statistically founded evaluation of the state parameters, detection of process changes, forecasting), the reporting (protocolling, web-/visualization and virtual sensor computation FUCHS (2010)) and reaction (alerting management). The central state variables $\mathbf{y}(t)$ of the modeling component, but also that of the of the reporting and alerting in the geodetic geomonitoring chain, are to be derived in subsequent classical least squares adjustments and modern robust M-estimations from the sensor data $\mathbf{l}(t)$. The basic standard state variable $\mathbf{y}(t)$ in a geodetic geomonitoring are the 3D displacement vectors $\mathbf{u}(t)$ of the object points $\mathbf{x}_O$ (Figure 2), as well the respective velocity and acceleration components $\dot{\mathbf{u}}(t)$ and $\ddot{\mathbf{u}}(t)$.

The georeferencing of the 3D object state variables $\mathbf{y}(t) = [\mathbf{u}(t), \dot{\mathbf{u}}(t), \ddot{\mathbf{u}}(t)]^T$ is performed in the unique reference point coordinate system $\mathbf{x}_R$ (Figure 2). The concept of geodetic geomonitoring - the state variables estimation $\mathbf{y}(t)$ in terms of a geodetic network adjustment using the data of networked sensors $\mathbf{l}(t)$ as the mathematical modeling core - has remained unchanged since the foundation and professional definition of the mathematical modeling of a classical deformation analysis in the 1970-ties (PELZER (1974), JÄGER & KÄLBER (1999-2014), JÄGER, WEBER & HAAS (1997), JÄGER, MÜLLER, SALER & SCHWÄBLE (2005), HECK & JÄGER (1986), SCHMITT, MOLDOVEANU, NICA & JÄGER (1990), HARTMANN & JÄGER (1997), HECK, ILLNER & JÄGER (1995), WELSCH & HEUNECKE (1999)).

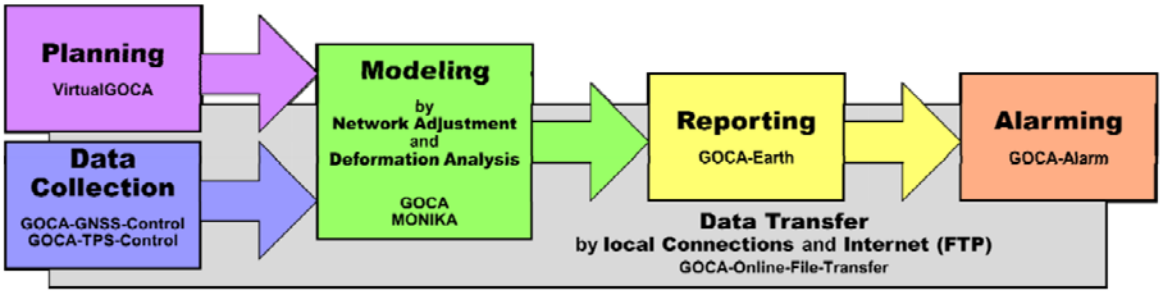

Figure 1: Components of the geodetic geomonitoring chain at the example of the GOCA-System

In the IT age, the technical innovation of the potentials through automation and real-time capability of the geomonitoring chain (Figure 1) allows - for about three decades now, in different stages of developments - the personal-free and permanent real-time use of geodetic geomonitoring systems such as GOCA JÄGER & KÄLBER (1999-2014) for disaster protection, and as early warning systems. The GOCA system can be used, in addition to the permanent real-time application, also for discrete epochal measurements and postprocessing. The GOCA system has become an established standard for geodesy, civil engineering and geotechnical engineering applications and research, as well as a reference for the developments of the industry, and has found its way into the relevant interdisciplinary literature (WITT (2009), JÄGER (2014)).

High-performance processors also allow the use of computationally intensive algorithms - such as robust adjustment methods and extended high frequency state estimations - in the modeling part (part 2) of the deformation analysis chain (Figure 1). Robust methods are necessary in view of high sensor data rates and an associated amount of gross sensor errors $\nabla\mathbf{l}(t)$, which occur naturally in the mass data amount of a continuous real-time operation in geomonitoring. Only in this way, a high deformation sensitivity (JÄGER, WEBER & HAAS (1997), HECK & JÄGER (1986)) can be guaranteed, while avoiding false alarms. Finally, the increasing spectrum of new geodetic, geotechnical and low cost

sensors (Figure 6) opens at present further potentials on the performance of geomonitoring, and poses new challenges in the modeling and prediction of deformation processes. These include the spatial and temporal scalability of the modeling (e.g. global plate modeling with spatially extended GNSS sensor networks, www.monika.ag, SPOHN & JÄGER (2007-2014)), as well as a scalability with respect to the sensor and model integration. The latter leads to the integrated deformation analysis (chap. 2).

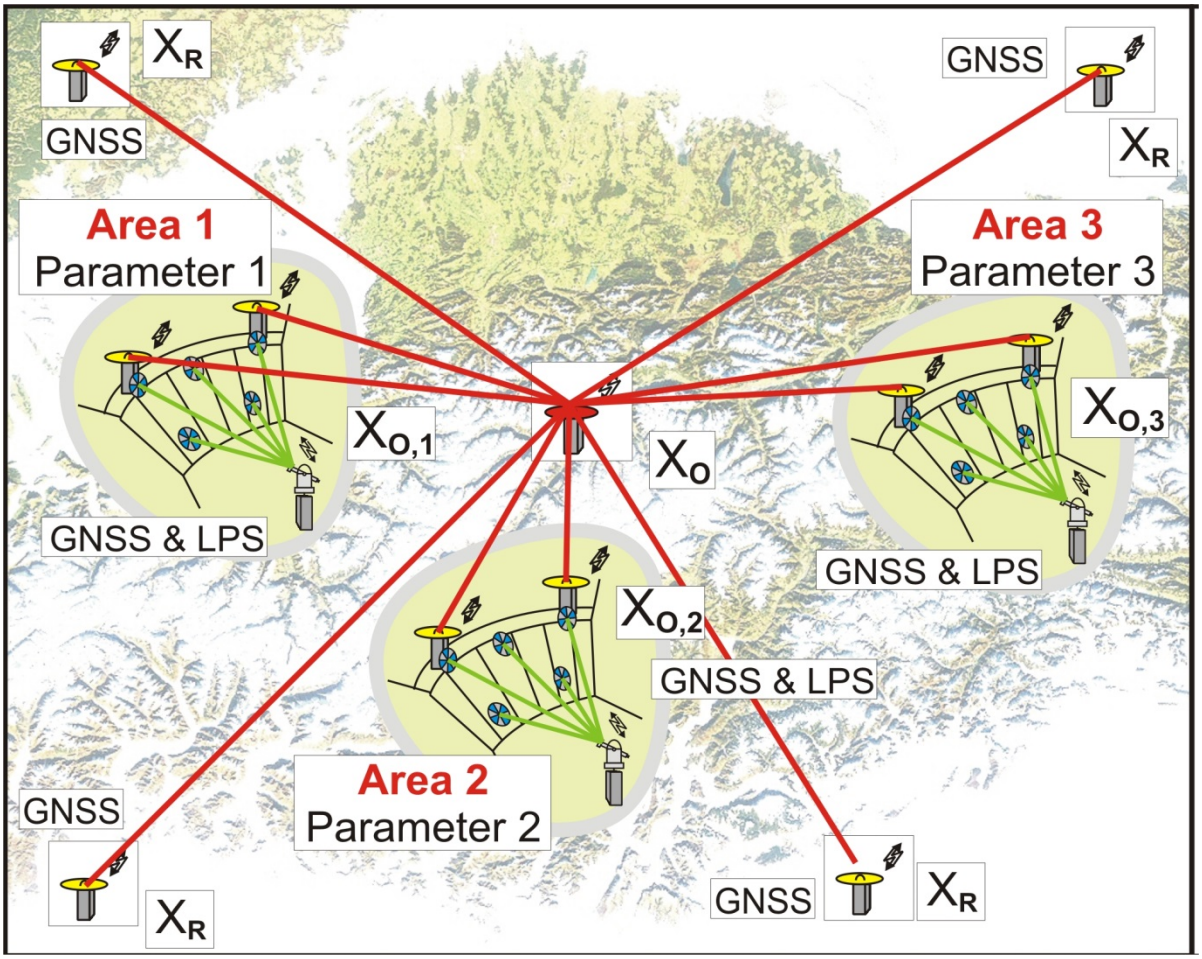

Figure 2: Geodetic network adjustment of geosensor network data as the basis of geodetic geomonitoring

The classical geodetic network adjustment in the Gauss-Markov model (GMM) JÄGER, MÜLLER, SALER & SCHWÄBLE (2005) and its extension to the integrated state estimation and deformation analysis (chap. 2) - but also the demand for prediction models for early warning systems - could not satisfy the continuously growing requirements on geomonitoring systems, without a progress and new developments in the field of the mathematical models, algorithms and software components. For these developments - but also in the planning and acquisition phase ("proof of concept") of geomonitoring arrays - the availability of virtual sensor raw data JÄGER, OSWALD & SPOHN (2010) provides crucial bilateral benefits, both for the systems developer and provider of systems, as well as for the user of geomonitoring systems and services.

1.2 Realization of the Geomonitoring Chain for the GOCA-System

The geodetic geomonitoring system GOCA (www.goca.info), developed at the Institute of Applied Research (IAF) of Karlsruhe University of Applied Sciences (HSKA), has been designed for an interdisciplinary profile of applications and research. These concern the protection from natural hazards (landslides, dislocations zones, volcanoes), deformation monitoring of geotechnical installations (mining, tunneling, etc.) as well as monitoring of deformations and changes in the

physical parameters of object in structural and civil engineering (dams, towers, bridges, buildings) (JÄGER, WEBER & HAAS (1997), JÄGER & KÄLBER (2000), LIENHART (2007), JÄGER & BERTGES (2004), PFEUFFER (1993), TESKEY (1988), WELSCH & HEUNECKE (1999)). Therefore, the GOCA system was consequently modularized along the geodetic geomonitoring chain (Figure 1), which is analogously structured and interfaced in other geomonitoring disciplines.

1.2.1 Data Acquisition - GOCA Geomonitoring Chain Component 1

For further processing of the sensor data resulting from the link 1 of the geomonitoring chain (Figure 1), an open data interface (GKA format) has been defined for GOCA. In that way, any GNSS and terrestrial sensors (LPS) can be connected to the GOCA modeling and deformation analysis software (chain link 2, Figure 1). By the open GKA interface the geomonitoring component 1 can be set up by any hardware and hardware control-software (see www.goca.info).

As components of the part 1 of the geomonitoring chain, the software packages GNSS-Control and TPS-Control have been developed in the RaD project GOCA (JÄGER & KÄLBER (1999-2014), KABASHI, ANGST, RAGOSSNIG-ANGST, JÄGER & SPOHN (2013), KABASHI, RAGOSSNIG-ANGST & JÄGER (2011)). These set up a TCP/IP-based sensor-communication and -control of GNSS, LPS and new local sensor (LS) types (see Figure 6), and provide the sensor data (GNSS baselines, GNSS raw data, TPS slope distances, directions, zenith distances, height differences of automated leveling/hydrostatic in the GKA format according to set data rates. GNSS arrays can be controlled and managed both in near online (RINEX data communication and processing) and in real-time (RTK). Due to the recent developments on new models as well as technical equipment (chap. 2) for an extended high rate geodetic deformation analysis and new integrated deformation analysis models, also high rate navigation state vector parameters (chap.2.3, (8)) have to be considered and communicated.

The software Virtual-GOCA JÄGER, OSWALD & SPOHN (2010) generates, Google-Earth® supported - virtual GNSS/LPS raw sensor data, allowing in that way an efficient and cost-effective development of geomonitoring systems and software such as GOCA JÄGER und KÄLBER (1999-2014) or MONIKA (www.monika.ag) SPOHN & JÄGER (2007-2014). By Virtual-GOCA the entire 4 parts geomonitoring chain (Figure 1) can be tested and optimization, planning, pre-analysis' (Figure 7) and "proof-of-concept-studies" can be done - in opposite to cost-intensive test installations with real sensors - without any technical, logistics and financial efforts. Using Virtual-GOCA together with the other software components of GOCA or MONIKA (Figure 1) also an assessment and expertise concerning existing geodetic geomonitoring projects can be done. Finally an efficient development and validation of the software components and the technical and IT operation procedures in geomonitoring scenarios can be done for all components along of the geomonitoring chain (Figure 1) by Virtual-GOCA.

1.2.2 GOCA Sensor Data Modeling and State Estimation - Geomonitoring Chain Component 2

1.2.2.1 Gauss - Markov Model of the Network Adjustment and State Estimation

Within the concept of a mathematically and statistically rigorous geodetic network adjustment in a so-called observation-related deformation-analysis (PELZER (1974), JÄGER, WEBER & HAAS (1997), JÄGER & KÄLBER (2000)) the GOCA sensor array is divided into a stable reference point frame $\mathbf{x}_R$ and a deformable object area $\mathbf{x}_O$ (Figure 2). The sensor points $\mathbf{x}_R$ set up the unique 3D coordinate reference frame for the network adjustment-based computation and further modeling of the object point positions $\mathbf{x}_O$ (2a,b) in the different areas. For this, the GNSS and LPS sensor data resulting from the geomonitoring chain part 1 (Figure 1) are transmitted online or near-online (in timely separated epoch-wise measurements also post-processed) further processed in a three steps network adjustment

and deformation state **y**(t) parameter estimation concept (based on least-squares, or robust M-estimations) as the subject of modeling in chain part 2 (Figure 1).

As concerns the GOCA network adjustment step 1, the initialization, the functional adjustment model is based on the observation equations **l**=**l**(t,**y**) (1a-e). The adjustment step 1 in geomonitoring chain part 2 aims at the determination of the 3D reference-point $\mathbf{x}_R$ frame and the respective covariance matrix $\mathbf{C}_{\mathbf{x},R}$ (Figure 2, Figure 7), in advance to the permanent monitoring. The GOCA step 2 covers then – by the online adjustment based on the GNSS (RINEX raw data, or RTK baseline vectors) and LPS data (TPS slope distances, directions, zenith distances and leveling data) and split into a horizontal (2D) and vertical (1D) component according to (1a-e) - the continuous 3D georeferencing of the object points $\mathbf{x}_O$ in the reference point datum $\mathbf{x}_R$ datum (2a,b).

The functional models of the 2D and 1D adjustments of the GOCA adjustments in steps 1 and 2 are based on the following observation-equations (functional Gauss-Markov models) (see also HECK & JÄGER (1986), SCHMITT, MOLDOVEANU, NICA und JÄGER (1990), HARTMANN & JÄGER (1997), JÄGER, MÜLLER, SALER & SCHWÄBLE (2005)):

GNSS Horizontal Baselines (2D):

$$\begin{bmatrix} \Delta x_{ij} \\ \Delta y_{ij} \end{bmatrix}_{GNSS} + \begin{bmatrix} v_{\Delta x,ij} \\ v_{\Delta y,ij} \end{bmatrix}_{GNSS} = \begin{bmatrix} \Delta \hat{x}_{ij} \\ \Delta \hat{y}_{ij} \end{bmatrix} \tag{1a}$$

Horizontal Distances (2D):

$$s_{ij} + v_{s,ij} = s \cdot \sqrt{\Delta \hat{x}_{ij}^2 + \Delta \hat{y}_{ij}^2} \tag{1b}$$

Directions (2D):

$$r_{ij} + v_{r,ij} = \arctan\left(\frac{\Delta \hat{y}_{ij}}{\Delta \hat{x}_{ij}}\right) - \hat{o}_i \tag{1c}$$

GNSS Vertical Baselines (1D):

$$\Delta h_{GNSS,ij} + v_{\Delta h,ij} = \Delta \hat{h}_{ij} \tag{1d}$$

Terrestrial Height Difference (1D):

$$\Delta H_{terr,ij} + v_{\Delta H,ij} = \Delta s_h^m \cdot \Delta \hat{h}_{ij} + (\hat{a}_{00} + \hat{a}_{10} \cdot x_j + \hat{a}_{01} \cdot y_j)^m - (\hat{a}_{00} + \hat{a}_{10} \cdot x_i + \hat{a}_{01} \cdot y_i)^m \tag{1e}$$

With m the area index (Figure 2) and with Δs_h^m and a_{ik}^m the scale difference and the polynomial coefficients for the modeling of the height reference surface (geoid, Q-geoid) in the different local area parts m (Figure 2) are described in (1e). As the stochastic component of the Gauss-Markov model JÄGER, MÜLLER, SALER & SCHWÄBLE (2005) based deformation state **y**(t) estimation, the covariance matrices $\mathbf{C}_l$ of the individual observation components (1a-e) are used. As concerns GNSS, the GOCA system treats both, RTK baselines as well as near-online GNSS raw data (RINEX) through the integration of different real-time (RTK) and near-online modules in the software component GOCA-GNSS-Control (part 1 of the geomonitoring chain). As a result of the chain part 1, the 3D GNSS baselines are provided in the above mentioned open GKA format for the further 2D/1D modeling according to (1a-e) in chain part 2 by the GOCA-software (Figure 1).

In the GOCA-adjustment step 2, the 3D permanent georeferencing of the object-point positions $\mathbf{x}_O(t)$ in the reference point frame $\mathbf{x}_R$ is done, making again use of the observation equations **l**=**l**(t,**y**) in the 2D/1D concept given by (1a-e). The step 2 step is running online and the resulting estimated object-

point positions $\mathbf{x}_O(t)$ and their covariance matrix $\mathbf{C}_O(t)$ are stored in daily object-point FIN-files containing the positions and the covariance information as

$$\mathbf{x}_O(t) \text{ and } \mathbf{C}_O(t). \qquad (2a,b)$$

The visualisation of the object-point position $\mathbf{x}_O(t)$ time-series in 2D horizontal position (x (green), y (blue)) in the earth fixed frame or local building systems, and 1D height position h (red) is shown in Figure 3.

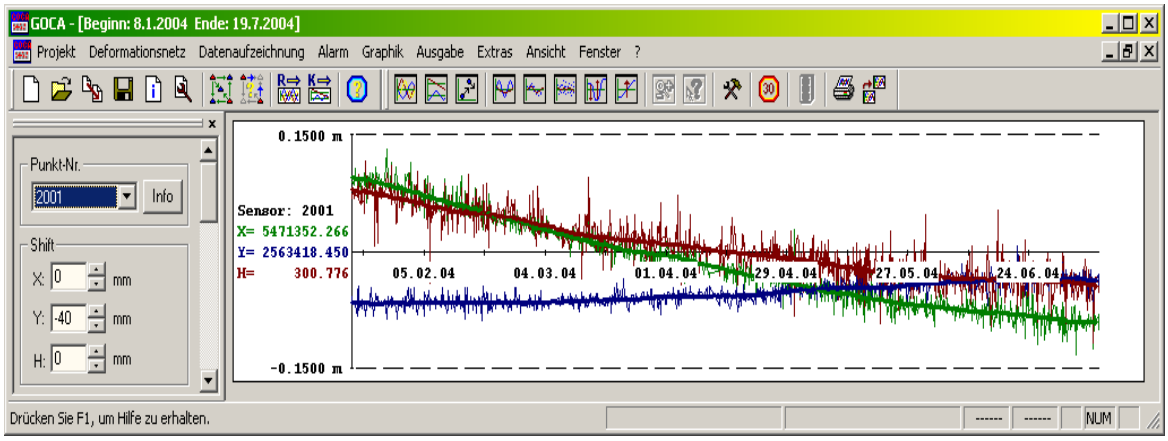

Figure 3: GOCA object-point time series xO(t) as the result of the GOCA adjustment step 2. Thick lines show smoothing by a moving average estimation (MVE) of the GOCA adjustment step 3.

The reference frame coordinates $\mathbf{x}_R$ and the above additional and observation specific parameters $\mathbf{s}$, Δs_h^m and a_{ik}^m (1a-e) are (except the orientation-unknowns o_i) kept as fix parameters in GOCA step 2 according to the results of the initialization step 1. In that way any influence of observation errors on the respective geo-monitoring frame $\mathbf{x}_R$ is avoided, and the risk of a wrong alarm is reduced. The covariance matrix of the fixed set of parameters within all parameters **y** is however strictly considered in the computation of the covariance matrices $\mathbf{C}_O(t)$ (2b) of the object points.

The GOCA adjustment step 3, namely the deformation analysis, deals with the estimation of the parameters **y**(t) of different deformation functions. It is again based either on least squares (L2 norm) or on robust M-estimations. The parameter-estimation runs online and parallel to GOCA step 2. The observation input for the different deformation state **y**(t) estimations is the observation data ($\mathbf{l}(t), \mathbf{C}_l(t)$) in terms of the object-point position time series $\mathbf{x}_O(t)$ and $\mathbf{C}_O(t)$ (2a,b), which have been stored in the simultaneous running GOCA adjustment step 2 as FIN-files in the GOCA project folder.

A first and simple object-point related deformation function **y**(t), provided by the GOCA deformation analysis software, is the moving average estimation (MVE), where $\mathbf{x}_O(t)$ (2a) and $\mathbf{C}_O(t)$ (2b) are direct observations with respect to the least squares (L2) or robust L1 MVE-position $\mathbf{y}(t)^T = (x(t), y(t), h(t))$ in each adjustment interval. The thick lines in Figure 3 show the smoothed values of the three components of the MVE estimation $\mathbf{y}(t)$. The MVE-estimation in GOCA includes an alarm-setting due to critical displacements compared to the current displacements $\mathbf{u}(t) = \mathbf{y}(t) - \mathbf{x}_O(t_0)$, derived with respect to initial object-point positions $\mathbf{x}_O(t_0)$.

A second deformation function and parameter state vector **y**(t) of the deformation analysis step 3 of GOCA is the online displacement estimation (SHT), see also Figure 4a and Figure 4b, between different "extended epochs" t_0 and t_i. Extended epochs means again, that the two epochs t_0 and t_i start at individual times t_0 and t_i, and have interval lengths Δt_o and Δt_i (Figure 4a,b), e.g. one hour. The start of the first epoch t_0 may be the initialization time (GOCA step 1). Alternatively t_0 can be

defined in the GOCA deformation analysis software settings (Figure 4a) either by an arbitrary fixed or by a dynamically moving time mark.

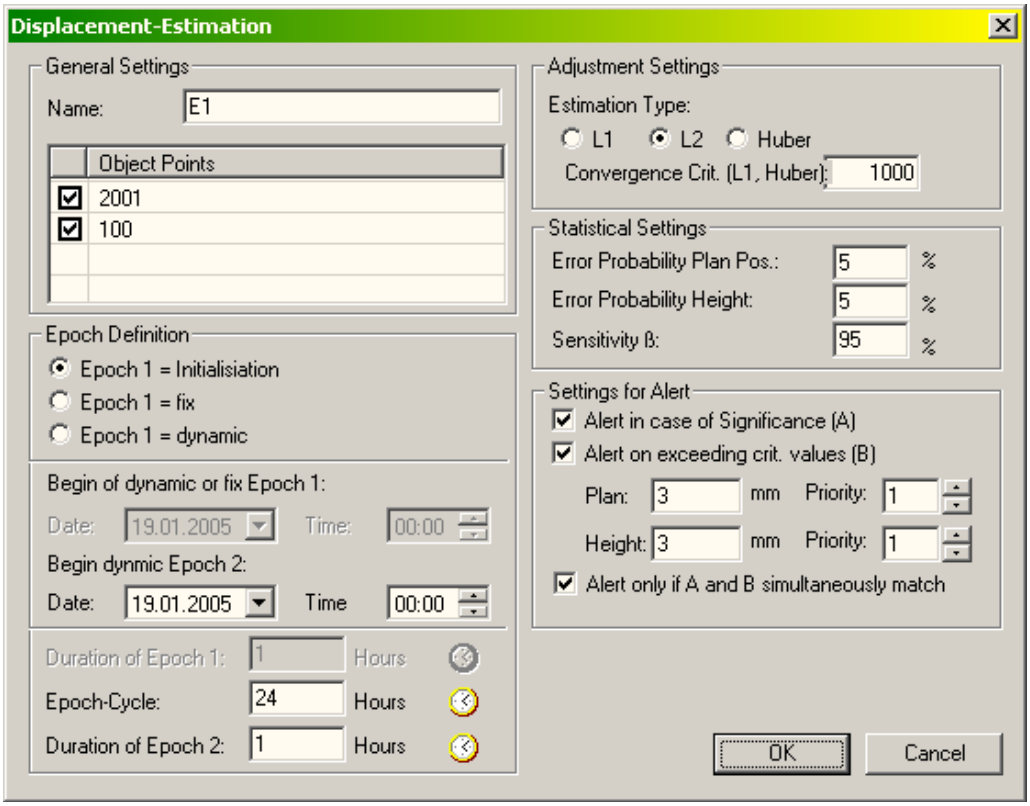

Figure 4a: Settings for the GOCA online displacement (SHT) estimation and alerting.

The functional model of the object point displacement estimation is reading:

$$\begin{bmatrix} \mathbf{l}_{t_0} \\ \mathbf{l}_{t_i} \end{bmatrix} + \begin{bmatrix} \mathbf{v}_{t_0} \\ \mathbf{v}_{t_i} \end{bmatrix} = \begin{bmatrix} \mathbf{E}_1 & \mathbf{0} \\ \mathbf{E}_2 & \mathbf{E}_2 \end{bmatrix} \cdot \begin{bmatrix} \hat{\mathbf{x}}_0 \\ \hat{\mathbf{u}}(t) \end{bmatrix} = \mathbf{A} \cdot \hat{\mathbf{y}} \qquad \text{and} \qquad \hat{\mathbf{y}} = [\hat{\mathbf{x}}_0(t_0), \hat{\mathbf{u}}(t_0, t_i)]^T \qquad (2c,d)$$

The two observation groups $\mathbf{l}_{t_0}$ and $\mathbf{l}_{t_i}$ in (2c,d) and their covariance matrices are taken out of the object-point time series information $(\mathbf{x}_O(t), \mathbf{C}_O(t))$ (2a,b) (Figure 3, thin lines). With $\mathbf{v}$ we introduce again the observation residuals in (2c).

The deformation state parameters $\hat{\mathbf{y}}(t)$ are for each object point the three-dimensional adjusted dynamic state position $\hat{\mathbf{x}}_0(t_0) = [\hat{x}, \hat{y} \,|\, \hat{h}]^T$ for the fixed on at t_0, and the 3D displacements $\hat{\mathbf{u}}(t_0, t_i) = [u_x, u_y \,|\, u_h]^T_{t_0,t_i}$ between t_0 and t_i. The design matrices $\mathbf{E}_1$ and $\mathbf{E}_2$ are column matrices composed of (3x3)-unit matrices for each three-dimensional point observation $\mathbf{x}_O(t)$ in the respective epoch intervals Δt_0 and Δt_i. Figure 4a shows the GOCA-software settings for the online displacement estimation according to (2c,d). The different settings concern the selection of the object points, the epoch definition for the displacement estimation, the settings for adjustment and statistical testing, and the settings for an automatic alert.

As mentioned above the automatic displacement estimation between different extended epochs $\Delta t(t_i)$ (e.g. 3 hours) can be done in three different modes, namely (Figure 4a)

- 1st epoch = Static namely initialization (GOCA step 1). 2nd epoch repeated periodically (e.g. every 24 hours)
- 1st epoch = Static and fixed by user definition. 2nd epoch repeated periodically

- 1st epoch = Repeated also periodically, such as the 2nd epoch.

Figure 4b shows by the thick horizontal line left the estimation of $\hat{\mathbf{x}}_0(t_0)$ (2c,d) by a number of observations $\mathbf{x}_O(t_i)$ (2a) belonging to the reference time t_0 and the estimation interval $\Delta t(t_0)$ .The thick horizontal lines (Figure 4b) on the right show the estimated position $\hat{\mathbf{x}}(t_i) = \hat{\mathbf{x}}_0(t_0) + \hat{\mathbf{u}}(t_0, t_i)$ at time t_i, and thick arrow shows the estimated displacement $\hat{\mathbf{u}}(t_0, t_i)$, here the in the vertical component.

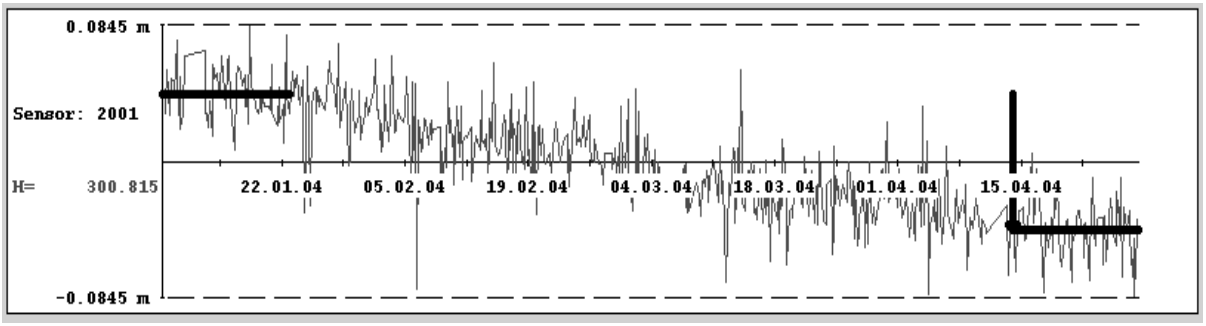

Figure 4b: Visualization of the GOCA displacement estimation in GOCA step 3

The Kalman filter estimation **y**(t) of displacements $\mathbf{u}(t)$, velocities $\dot{\mathbf{u}}(t)$ and accelerations $\ddot{\mathbf{u}}(t)$ of the object points $\mathbf{x}_O(t)$ movements, and the prediction of displacements are discussed in chap. 1.2.2.3. The respective results are stored in the GOCA project folder as KAL- and VHS-Data.

The stability and congruency of the reference points $\mathbf{x}_R$ (Figure 2) can also be statistically analyzed, as described in KÄLBER & JÄGER (2000).

1.2.2.2 Robust M-Estimation instead of Least-Squares (L2 Norm)

Gross sensor data errors $\nabla\mathbf{l}(t)$ and other systematic errors (e. g. incorrect ambiguities in GNSS) KÄLBER und JÄGER (2000) would – in case of the fully automated ("24 hours a day - 7 days a week") GOCA real-time adjustment steps 2 and 3 – draw erroneous results in the sensor data modeling and parameter estimations **y**(t), respectively, in the geomonitoring chain part 2 (Figure1). False alarms, or complementarily, a high risk of - falsely - suppressed alarm situations in critical conditions, would be the consequences. To eliminate or at least to minimize these risks, the parameter estimations **y**(t) in the GOCA deformation analysis in the real-time steps 2 and 3 are based on the concept of robust M-estimations. The characteristics of the robustness of a M-estimation is due to a bounded first derivative of the estimation function $\rho(\bar{v}_k)$ KÄLBER & JÄGER (2000). The M-estimation of parameters **y**(t) in a Gauß-Markov-Model (GMM) is reading KÄLBER & JÄGER (2000):

$$\sum_{k=1}^{n}\rho(\bar{v}_k) = \sum_{k=1}^{n}\rho\left((\mathbf{C}_l^{-\frac{1}{2}}\cdot\mathbf{A})_k\cdot d\hat{\mathbf{y}} - (\mathbf{C}_l^{-\frac{1}{2}}\cdot(\mathbf{l}-\mathbf{l}(\mathbf{y}_0))_k\right) \quad , \quad \text{with} \tag{3a}$$
$$= \sum_{k=1}^{n}\rho(\bar{\mathbf{A}}_k\cdot d\hat{\mathbf{y}} - (\bar{\mathbf{l}}-\bar{\mathbf{l}}(\mathbf{y}_0))_k) = \text{Min}|_{d\hat{\mathbf{y}}}$$

$$\hat{\mathbf{y}} = \mathbf{y}^0 + d\hat{\mathbf{y}} \tag{3b}$$

The estimation function $\rho(\bar{v}_k)$ and the minimization concept together (3a,b) define the general M-estimation type. It includes the robust L1-norm ($\rho(\bar{v}_k) = |\bar{v}_k|$), which is breaking-point resistant to gross observations errors $\nabla\mathbf{l}(t)$ in the sensor data, as well as least squares (L2-norm, with $\rho(\bar{v}_k) = \bar{v}_k^2$) as a special non-robust case, and many other robust and non-robust estimation concepts KÄLBER & JÄGER (2000). The dashes in the M-estimation formula (3a) are denoting the so-called homogenized

design-matrix $\bar{\mathbf{A}}$ and the homogenized reduced observations $(\bar{\mathbf{l}} - \bar{\mathbf{l}}(\mathbf{y}_0))$ KÄLBER & JÄGER (2000). With $\mathbf{y}_0$ the approximate values of the state parameters are denoted.

The results of the GOCA adjustment steps 2 and 3 of the geomonitoring chain part 2 (Figure 1), are numerically provided as well as visualized in graphical windows (Figure 3, Figure 4b, Figure 9). The numerical results are also available as general output interfaces (FIN-, MVE-, SHT-, KAL-, VHS-files), e.g. for the integrated deformation analysis (chap. 2). An alarm can be carried out on the direct comparison of the estimate of the numerical values of the deformation parameters **y**(t) (such as (2c,d) or (4c)) with the corresponding critical values of the state variables, or by statistical significance tests of the deformation parameters **y**(t), as well as by an "and" or by an "or" with respect to the combination of both cases.

1.2.2.3 GOCA Kalman-Filtering and Prediction and Early Warning Concept

The GOCA Kalman filtering as a further component of the GOCA - step 3 state estimation **y**(t) in the geomonitoring chain, modeling part 2 (Figure 1), is based on the following state transition matrix for the state vector **y**(t) from the past $t-\Delta t$ to the time t KÄLBER & JÄGER (2000)

$$\mathbf{y}(t) = \mathbf{T}(t) \cdot \mathbf{y}(t-\Delta t) \qquad \text{with} \qquad (4a)$$

$$\begin{bmatrix} \mathbf{u}(t) \\ \dot{\mathbf{u}}(t) \\ \ddot{\mathbf{u}}(t) \end{bmatrix} = \begin{bmatrix} \mathbf{I} & [\Delta t] & \left[\frac{1}{2}\Delta t^2\right] \\ \mathbf{0} & \mathbf{I} & [\Delta t] \\ \mathbf{0} & \mathbf{0} & \mathbf{I} \end{bmatrix} \cdot \begin{bmatrix} \mathbf{u}(t-\Delta t) \\ \dot{\mathbf{u}}(t-\Delta t) \\ \ddot{\mathbf{u}}(t-\Delta t) \end{bmatrix} \qquad \text{and} \qquad (4b)$$

$$\mathbf{y}(t) = [\mathbf{u}(t), \dot{\mathbf{u}}(t), \ddot{\mathbf{u}}(t)]^T \qquad (4c)$$

The state vector **y**(t) in (4a,b,c) comprises the 3D displacements, velocities and accelerations of the 3D object points $\mathbf{x}_O$ between successive time intervals $t-\Delta t$ and t. The state transition model (4b) implies a truncated Taylor series of the unknown displacement function **u**(t), and thus the assumption of a constant acceleration $\ddot{\mathbf{u}}(t)$ in the time interval Δt. This assumption is either almost always feasible in the geodetic geomonitoring of many objects (e.g. dams, landslides, mines etc.) and naturally slow (static) processes (chap. 2.1), or it can be achieved by applying correspondingly high data sampling and processing rates MÖNICKE (1991). The covariance matrix of the prediction (4a,b) - as stochastic component of the Gaussian Markov model KÄLBER & JÄGER (2000) based estimation of **y**(t) at time t - is evaluated by the law of error-propagation applied to (4b) and the covariance matrix of the previous estimation of the state vector $\mathbf{y}(t-\Delta t)$.

The Kalman-Filtering means (generally) the common adjustment of a prediction, here **y**(t) (4c) and the state-related observations **l**=**l**(**y**,t), in the following the displacement observations **l**(t), resulting from the time series (2a,b) in the parallel running GOCA adjustment step 2. The observation component **l**=**l**(**y**,t) is reading:

$$\mathbf{l}(t) = \mathbf{l}(\mathbf{y}(t)) =: \mathbf{u}(t) = \mathbf{x}_O(t) - \mathbf{x}_O(t_0), \text{ with} \qquad (4d1)$$

$$\mathbf{C}_l = \mathbf{C}_{x_O}(t) + \mathbf{C}_{x_O}(t_0) \qquad (4d2)$$

In case of a least-squares estimation (L2-norm), the above common adjustment can be written in the classical notation, using explicitly the Kalman-Matrix **K**. In case of a generalized M-estimation, the common adjustment of the state parameters of the state prediction component **y**(t) (4b) and **l**=**l**(t,**y**) (4d1), and the associated stochastic model $\mathbf{C}_y$ resulting from (4b), and $\mathbf{C}_l$ (4d2), respectively. It can be leaded back to an iterative Kalman-Filtering process (j=j-th iteration) according to the following

computation scheme (JÄGER, HOSCISLAWSKI & OSWALD (2009), JÄGER & GONZALES (2005), HOSCISLAWSKI(2009)):

$$\hat{\mathbf{y}}(t)^{(j)} = \mathbf{y}(t) + \mathbf{K}^{(j)} \cdot (\bar{\mathbf{l}}(t) - \bar{\mathbf{l}}(\mathbf{y}(t)) \quad , \qquad \text{with} \tag{4e}$$

$$\mathbf{K}^{(j)} = (\mathbf{C}_y^{-\frac{1}{2}} \mathbf{W}_y^{(j)} \mathbf{C}_y^{-\frac{1}{2}} + \bar{\mathbf{A}} \mathbf{W}_l^{(j)} \bar{\mathbf{A}})^{-1} \cdot \bar{\mathbf{A}} \mathbf{W}_l^{(j)} \quad . \tag{4f}$$

In (4e,f) the Kalman-Matrix $\mathbf{K}^{(j)}$ (4f) is updated in the j-th step with the diagonal weight matrices $\mathbf{W}_y^{(j)}$ and $\mathbf{W}_l^{(j)}$. These are set up by the residuals of the two observation components (4a) and (4d1) according to the individual weight function JÄGER, MÜLLER, SALER & SCHWÄBLE (2005) of the specific M-estimation. In GOCA, both the displacement estimation (2c,d) and the Kalman-Filtering (4e-f) can be done using by choice and respective dialogue settings, either as a least-squares (L2), a robust L1-norm or a robust Huber-estimation. The Kalman-Filtering results **y**(t) (4e) and the covariance matrix are stored in the GOCA project folder as so-called Kalman-Files (KAL).

1.2.2.4 State Prediction and Predictive Alarming in the GOCA-System

The state prediction equations (4b) can also be used for the determination of the time Δt remaining until a predetermined critical state vector **y**(t) (4c) will be achieved. If an evacuation time bound Δt_{crit} is exceeded by the computed Δt, the GOCA system module GOCA-Alarm (Figure 1) sets a so-called prediction alarm, and informs by sending the respective information out of the stored VHS-files to the alarm-management group. In that way, GOCA can be used as early warning system.

1.2.3 Reporting and Alarming - GOCA Geomonitoring Components 3 and 4

As concerns the geomonitoring chain components 3 and 4 (Figure 1) the GOCA software components GOCA-Earth and GOCA-Alarm have been developed. GOCA-Earth visualizes - based on Google Earth (Figure 7) - the deformation states **y**(t) (2d), (4c) and also provides the respective numerical values. Designed for alarm management, the software component GOCA-Alarm sets alarm - e.g. by a hooter, light-signal, SMS, email etc. - when critical values for the state parameter estimations or predictions **y**(t) and/or statistical significance levels (Figure 4a) are exceeded. GOCA-Alarm then transmits a respective short information out of the stored results files (FIN, MVE, SHT, KAL, VHS).

2 INTEGRATED DEFORMATION ANALYSIS AND STRUCTURAL HEALTH MONITORING

The further developments in the deformation analysis and in geodetic monitoring are aiming at the integration of the state parameters $\mathbf{y}(t) = [\mathbf{u}(t), \dot{\mathbf{u}}(t), \ddot{\mathbf{u}}(t)]^T$ of the above geodetic ("pure geometric") geomonitoring - together with additional geometric or physical observations **l**(t) of local sensors (LS), such as classical geotechnical sensors or new ones, e.g. for high deformation rates and structural vibrations (Figure 6) - into appropriate common parametric models **y**(t).

Since the geodetic sensor data and the geotechnical LS sensor observations TESKEY (1988), considered as the output parameters of a physical object (e.g. dams), can be related to the parameter set $\mathbf{y}(t) = [\mathbf{u}(t), \dot{\mathbf{u}}(t), \ddot{\mathbf{u}}(t)]^T$ of a classical geodetic geomonitoring (see (2c), (4e)) these are regarded as the common denominator of an integrated deformation analysis (JÄGER, WEBER & HAAS (1997), JÄGER & KÄLBER (2000)). The geometric parameters $\mathbf{y}(t) = [\mathbf{u}(t), \dot{\mathbf{u}}(t), \ddot{\mathbf{u}}(t)]^T$ can be used commonly with physical system parameters **p** in an integrated deformation analysis, which then allows to detect changes $\Delta \mathbf{p}$ in the physical parameters **p** of structures, meaning "structural health monitoring".

In the general classification of integrated deformation analysis in black, grey and white box system descriptions (PFEUFFER (1993), WELSCH & HEUNECKE (1999), JÄGER, WEBER und HAAS (1997), JÄGER & KÄLBER (2000)), the class of finite-element models (FEM) belongs to the white-box category. And FEM (Figure 5a, Figure 5b) models are thereby parameterized both by different kind of physical parameters p (chap. 2.1, 2.2) and by the state variables $\mathbf{y}(\mathbf{t}) = [\mathbf{u}(\mathbf{t}), \dot{\mathbf{u}}(\mathbf{t}), \ddot{\mathbf{u}}(\mathbf{t})]^{\mathbf{T}}$ ((2c,d) and (4a-e), chap. 1, 2) estimated from the geodetic network coordinates $\mathbf{x}_0(\mathbf{t})$ (2a).

Networked geodetic sensors (GNSS, LPS, automatic leveling, laser-trackers, laser-scanners, radar-sensors, cameras), geo-referenced local geometric LS sensors (tilt, strain) and geotechnical LS sensors (force, pressure sensors) can all be used in an integration by FEM approaches, by making use of the so-called FEM shape functions (ZIENKIEWICZ (1984), JÄGER & BERTGES (2004)) in the common georeferencing. Here, the different types of local sensors are mostly related both to the common geodetic and integrating displacement-based parameters **y**(t) and to the physical parameters **p** of a structure (JÄGER, WEBER & HAAS (1997), JÄGER & KÄLBER (2000), JÄGER, HOSCISLAWSKI & OSWALD (2009), JÄGER & BERTGES (2004)). So FEM with the displacement-related parameters **y**(t) together with physical parameter part **p** are - in the static and dynamic FEM case - the key to integrated deformation analysis (also called "system analysis" or "structural health monitoring").

While in the static case (chap. 2.1) of an FEM-based structural health monitoring, only changes in the parametrized stiffness matrix $\mathbf{K}(\mathbf{p}_K)$ (Figure 5a) can be identified, dynamic FEM approaches (chap. 2.2) enable additionally the identification of parameter changes in the damping and the mass matrix $\mathbf{C}(\mathbf{p}_C)$ and $\mathbf{M}(\mathbf{p}_M)$, respectiuvely of a structure, as shown below. The new type of a GNSS/MEMS local sensor (chap. 2.3, Figure 6) is under development in the RaD project GOCA. It fits both to a use for integrated deformation analysis in the static (chap. 2.2) and in the dynamic FEM approach (chap. 3.2).

Due to the interdisciplinary task, new sensor developments are also done e.g. by the civil engineering discipline GROSSE & KRÜGER (2011).

Structural health monitoring for static (chap. 2.1) and for dynamic (chap. 2.2) parameter identification problems is a permanent and current international research topic of the FIG commissions 5 and 6 (www.fig.net). The GOCA-project related RaD is integrated here by the author membership in the FIG Working Group 5.4 ("Kinematic Measurements").

2.1 FEM based Integrated Geomonitoring – Static Case

The integrated deformation models for the static case, developed in the GOCA - project (JÄGER, WEBER & HAAS (1997), JÄGER & KÄLBER (2000)), and successfully applied and further developed by LIENHART (2007), are based on the well-known relationship ZIENKIEWICZ (1984)

$$\mathbf{u}_{\mathrm{FEM}} = \mathbf{K}(\mathbf{p}_k)^{-1} \cdot \mathbf{f} \tag{5a}$$

between the nodal displacements **u**, the parameterized stiffness matrix $\mathbf{K}(\mathbf{p}_k)$ and the nodal force vector **f** (Figure 5a). Based on Neumann series of matrices applied to (5a), changes $\Delta\mathbf{p}_k$ in the physical parameters – like a lack of stiffness due to material deficiency (Figure 5a) - can directly be used to parametrize geodetic displacements $\mathbf{u}_{\mathrm{geod}}$. We arrive at:

$$\begin{aligned} \mathbf{u}(\Delta\mathbf{p}_k)_{geod} &= \mathbf{u}_{FEM} - \mathbf{K}(\mathbf{p}_k)^{-1} \cdot d\mathbf{K}(\Delta\mathbf{p}_k)) \cdot \mathbf{K}(\mathbf{p}_k)^{-1} \cdot \mathbf{f} \\ &= \mathbf{K}(\mathbf{p}_k)^{-1} \cdot (\mathbf{I} - d\mathbf{K}(\Delta\mathbf{p}_k) \cdot \mathbf{K}(\mathbf{p}_k)^{-1}) \cdot \mathbf{f} \end{aligned} \tag{5b}$$

Formula (5b) directly shows for the static FEM case the benefit of integrated deformation analysis and "structural health monitoring", respectively, where geodetic displacements $\mathbf{u}_{geod}$ contribute to model and to detect physical changes $\Delta\mathbf{p}_k$, e.g. a respective lack of stiffness of a structure (Figure 5a). FEM-based simulation of changes of $\Delta\mathbf{p}_k$ and the effect on the difference between the above $\mathbf{u}_{geod}$ and the expected $\mathbf{u}_{FEM}$ (5a.b) are given in KÄLBER & JÄGER (2000).

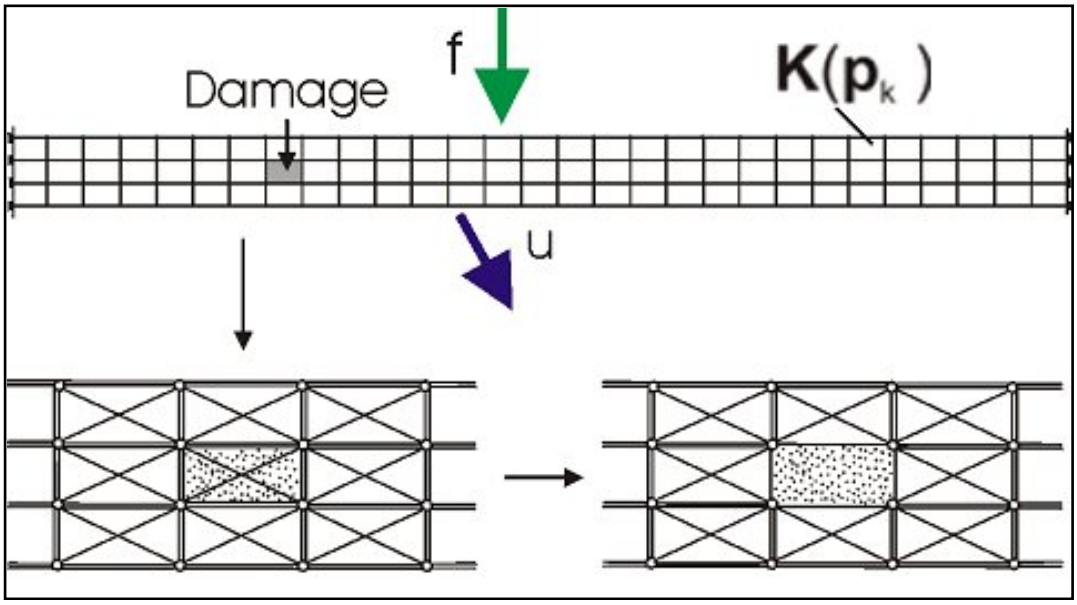

Figure 5a: Integrated deformation analysis in the static FEM approach at the example of a dam. Integrating physical parameters pk and detecting changes $\Delta\mathbf{p}_k$ according to Jäger, R., Weber, A. & Haas, R. (1997), Kälber, S. & Jäger, R. (2000)

Following the ideas of TESKEY (1988), a sophisticated FEM based integrated deformation analysis and structural health monitoring approach for the static case was presented in JÄGER & BERTGES (2004). The mathematical model of that structural health monitoring approach developed in the GOCA RaD project, includes - again as a Gauß-Markov-Model (GMM) JÄGER, MÜLLER, SALER & SCHWÄBLE (2005) - the components of the FEM model itself, as being parametrized by $\mathbf{p}_k$ and respective changes $\Delta\mathbf{p}_k$, the data of assumed stochastic physical parameters $\mathbf{p}_k$, the data of estimated geodetic displacements $\mathbf{u}(t)_{geod}$, and the data $\mathbf{l}(t)$ of different kind of local geotechnical sensors (LS). The integrated model was successfully evaluated and further developed in the thesis LIENHART (2007).

2.2 FEM based Integrated Geomonitoring – Dynamic Case

The above integrated deformation model for the static case (5a,b), and the illustration (Figure 5a), hold for deformation processes, where the reaction of the structure on the velocity $\dot{\mathbf{u}}(t)$ and acceleration $\ddot{\mathbf{u}}(t)$ can be neglected for physical process reasons, and it can be renounced therefore on a related appropriate FEM modeling. The geodetic model (4a,b,c) - assuming $\ddot{\mathbf{u}}(t) = \ddot{\mathbf{u}}(t - \Delta t)$ - can still be kept for higher rate deformation processes, just by increasing the sampling frequency $f = 1/\Delta t$ by use of suitable sensor types MÖNICKE (1991), see e.g. the Robinette sensor, Figure 6.

In opposite to (5a,c) the geometric model (4a,b,c) remains however, unnecessarily, non-informative for fast moving deformation processes (e. g. vibrations of objects). The vibration case of structures, is reading in case of a dynamically acting external force $\mathbf{f}(t)$, and in case of so-called natural vibrations or eigenvibrations wíth $\mathbf{f}(t)=0$), respectively:

General Damped Vibrations: $$\mathbf{K}(\mathbf{p}_K)\cdot\mathbf{u}(t)+\mathbf{C}(\mathbf{p}_C)\cdot\dot{\mathbf{u}}(t)+\mathbf{M}(\mathbf{p}_M)\cdot\ddot{\mathbf{u}}(t)=\mathbf{f}(t) \quad (6a)$$

Damped Eigenvibrations: $$\mathbf{K}(\mathbf{p}_K)\cdot\mathbf{u}(t)+\mathbf{C}(\mathbf{p}_C)\cdot\dot{\mathbf{u}}(t)+\mathbf{M}(\mathbf{p}_M)\cdot\ddot{\mathbf{u}}(t)=\mathbf{0}\ . \quad (6b)$$

The dynamic FEM models (6a,b) opens, besides the access to the parameters and changes $\Delta\mathbf{p}_k$ of the a structure, also the parameters and changes $\Delta\mathbf{p}_C$ of the damping $\mathbf{C}(\mathbf{p}_C)$ and the parameters and changes $\Delta\mathbf{p}_M$ of the ass-matrix $\mathbf{M}(\mathbf{p}_M)$. By drawing also a first parallel to chap. 1.2.2.3 and (4c), we continue with the case of the eigenvibrations (6b). Here we arrive after few steps at the recursive formula, which means directly the state transition for the above state variables $\mathbf{y}(t)=[\mathbf{u}(t),\dot{\mathbf{u}}(t),\ddot{\mathbf{u}}(t)]^T$ (4c) in case of an integrated structural health monitoring. It is reading (JÄGER & BERTGES (2004)):

$$\begin{bmatrix}\mathbf{u}(t)\\ \dot{\mathbf{u}}(t)\\ \ddot{\mathbf{u}}(t)\end{bmatrix}=\begin{bmatrix}\mathbf{I} & [\Delta t] & \left[\frac{1}{2}\Delta t^2\right]\\ \mathbf{0} & \mathbf{I} & [\Delta\mathbf{t}]\\ \mathbf{0} & [-\mathbf{M}(\mathbf{p_M})^{-1}\cdot\mathbf{K}(\mathbf{p_K})\cdot\Delta t] & [\mathbf{I}-\mathbf{M}(\mathbf{p_M})^{-1}\cdot\mathbf{C}(\mathbf{p_C})\cdot\Delta t]\end{bmatrix}\cdot\begin{bmatrix}\mathbf{u}(t-\Delta t)\\ \dot{\mathbf{u}}(t-\Delta t)\\ \ddot{\mathbf{u}}(t-\Delta t)\end{bmatrix} \quad (6c)$$

In opposite to the pure geometric modeling (4a,b,c), the state transition of the FEM-based physical FEM (6c) of a damped eigenvibration integrates - associated with the difference in the rows three between (4b) and (6c) - both the geometrical FEM nodal point (Figure 5b) movements $\mathbf{y}(t)=[\mathbf{u}(t),\dot{\mathbf{u}}(t),\ddot{\mathbf{u}}(t)]^T$, and all groups of physical structural parameters in the complete set $\mathbf{p}=(\mathbf{p_K},\mathbf{p_C},\mathbf{p_M})^T$. Compared to the static FEM (5b), the above state transition equations (6c) of the dynamic FEM, enabled by make use of structural vibrations, now provides the structural health monitoring for the complete structural physics, namely $\mathbf{p}=(\mathbf{p_K},\mathbf{p_C},\mathbf{p_M})^T$.

In the dynamic case, the parameter estimation can again be based on a Kalman-Filtering approach, with the nonlinear state transition (6c), and the integration of different kind of sensor (e.g. the "Robinette", Figure 6) with observations $\mathbf{l}(t)=l(t,\mathbf{y})$. Now we have to do with the extended parameter state vector $\mathbf{y}(t)_{\text{Integrated}}=[\mathbf{u}(t),\dot{\mathbf{u}}(t),\ddot{\mathbf{u}}(t)\,|\,\mathbf{p_K},\mathbf{p_C},\mathbf{p_M}]^T$ in that respective first approach to be proposed as an integrated dynamics deformation analysis model.

In analogy to the GMM parametrization (5b), and as an alternative approach to the use of (6c) for structural health monitoring, a so-called spectral approach JÄGER (1988) for integrated deformation analysis and structural health monitoring can be set up. For this, we remain at the above case of structural eigenvibrations (6b). In order to keep the limited space of the paper, and to get simultaneously in spite still the full insight into the spectral structural health concept, we assume undamped eigenvibrations, meaning $\mathbf{C}(\mathbf{p}_C)=\mathbf{0}$. Starting with the harmonic model for the time dependent displacements $\mathbf{u}(\mathbf{x},t)$

$$\mathbf{u}(\mathbf{x},t)=\mathbf{a}\cdot\phi(\mathbf{x})\cdot\cos(\omega\cdot t-\varphi)\,, \quad (7a)$$

in case of structural vibrations (Figure 5b), we arrive from (6c) and $\mathbf{C}(\mathbf{p}_C)=\mathbf{0}$ at the general eigenvalue problem for undamped vibrations of structures, reading ZIENKIEWICZ (1984):

$$[\mathbf{K}(\mathbf{p}_K)-\omega^2\cdot\mathbf{M}(\mathbf{p}_M)]\cdot\phi(\mathbf{x})=\mathbf{0}\ . \quad (7b)$$

The solution of (7b) leads to n (n=dimension of **K, M**) eigenfrequencies ω_i and respective n – location **x** dependent - eigenmodes $\phi_i(\mathbf{x})$ as the normalized eigenvectors in (7b). The location dependent $\phi_i(\mathbf{x})$ modes provide the shapes of the vibration displacements $\mathbf{u}(\mathbf{x},t)$ of the structure (see Figure 5b),

while the sizes of the amplitudes $\mathbf{a}(\omega_i)$ (7a) of the possible vibrations remain undetermined. Physically, the amplitudes $\mathbf{a}(\omega_i)$ depend on the kind of induction of the eigenvibrations of a structure (e.g. wind, earthquakes, traffic, etc.).
By making use of the first order differentiation of (7b), we can - in analogy to the static case (5b) – set up a parametrization of the spectral changes, namely these of the vibration frequencies ω_i and the $\phi_i(\mathbf{x})$ vibration modes. Using the derivations of (7b) evaluated by the author in the context with geodetic network optimization JÄGER (1988), we directly arrive at the parametrization of the spectral characteristics ω_i and $\phi_i(\mathbf{x})$ concerning - presumably "unhealthy" - changes $\Delta\mathbf{p}_K, \Delta\mathbf{p}_M$ in the physical parameters of structures (e.g. towers, bridges, etc.). We get:

$$\Delta\boldsymbol{\omega}_i^2(\Delta\mathbf{p}_K, \Delta\mathbf{p}_M) = \boldsymbol{\varphi}_i^T \cdot [\mathbf{dK}(\Delta\mathbf{p}_K) - \boldsymbol{\omega}_i^2 \cdot \mathbf{dM}(\Delta\mathbf{p}_M)] \cdot \boldsymbol{\varphi}_i \qquad (7c)$$

and

$$\Delta\boldsymbol{\varphi}_i(\Delta\mathbf{p}_k, \Delta\mathbf{p}_M) = -\frac{\boldsymbol{\varphi}_i^T \cdot \mathbf{dM}(\Delta\mathbf{p}_M) \cdot \boldsymbol{\varphi}_i}{2} \cdot \boldsymbol{\varphi}_i + \sum_{\substack{j=1 \\ j \neq i}}^{n} \left[\frac{1}{\boldsymbol{\omega}_i^2 - \boldsymbol{\omega}_j^2} \boldsymbol{\varphi}_i^T \cdot [\mathbf{dK}(\Delta\mathbf{p}_K) - \mathbf{dM}(\Delta\mathbf{p}_M)] \cdot \boldsymbol{\varphi}_j \right] \cdot \boldsymbol{\varphi}_j \quad (7d)$$

The approach and the respective parameterizations (7c, 7d) imply a so-called inverse eigenvalue-eigenvector problem, meaning the task to conclude from changes in the respective spectral characteristics (left) to changes in the parametrization (right) of the general eigenvalue problem (7b) itself.

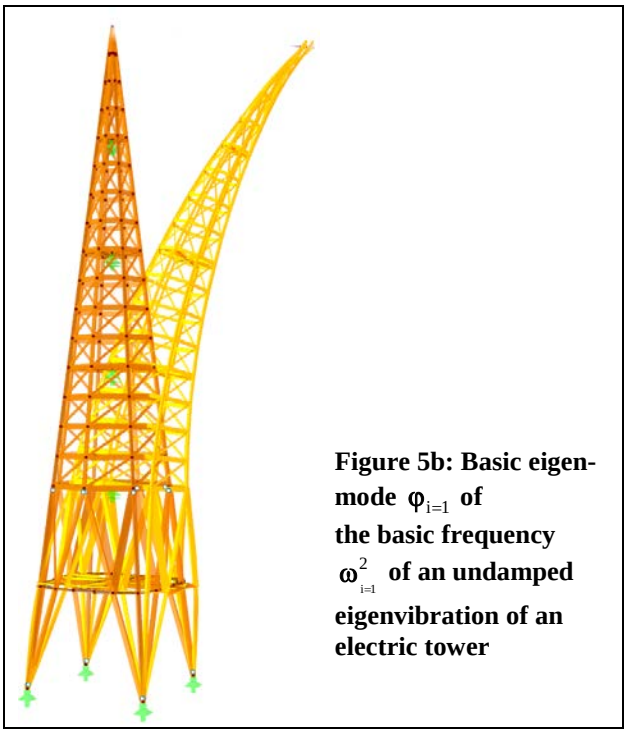

Figure 5b: Basic eigenmode $\varphi_{i=1}$ of the basic frequency $\omega^2_{i=1}$ of an undamped eigenvibration of an electric tower

Both, the proposed time-domain approach represented by (6c), using the time-domain $\mathbf{y}(t) = [\mathbf{u}(t), \dot{\mathbf{u}}(t), \ddot{\mathbf{u}}(t)]^T$ and observations $\mathbf{l}=\mathbf{l}(\mathbf{y},t)$, and the spectral domain approach, using "observed or monitoring-data derived" changes in the vibration frequencies $\Delta\omega_i^2$ (7c), and/or "observed or monitoring-data derived" changes in the eigenmodes $\Delta\boldsymbol{\varphi}$ (7d), are both proposed as candidates (after being extended as well to the damped case (6b) and the general case (6a)) for further RaD on integrated deformation analysis and structural health monitoring, respectively, concerning the structural health state, which can be concluded from the parameters $\mathbf{p}_K, \mathbf{p}_C, \mathbf{p}_M$ and their changes.

A further recent method for the validation of structural models and system-identification using autoregressive processes in combination with FEM simulations is presented in HÄKELL, HAAKE & ROLFES (2014).

2.3 GNSS and GNSS/MEMS Developments for Structural Health Monitoring

The current developments in the geomonitoring project GOCA are dealing also with mathematical models, algorithms and software concerning the integration of GNSS and suitable MEMS sensor types (in that case accelerometers and gyroscopes) for an application in structural health monitoring. In the

frame of the RaD project "GNSS&MEMS multi-sensor navigation and object georeferencing (DIEKERT, HOSCISLWASKI, JÄGER, LORENZ, BATKE & ZWIENER (2010-2013), JÄGER (2013), JÄGER (2014)) at IAF/HSKA, the industrial RaD consortium member, teXXmo Mobile Solutions, developed the hardware and data-communication of sensor box, called "Robinette" (www.robinette.de), Figure 6. The bootable firmware has been developed by IAF/HSKA. The Robinette is available as pure GNSS (G) and as GNSS&MEMS (GM) version.

The GNSS Robinette (G) can be used via TCP/IP communication interface in differential GNSS mode, either with a local or with an external reference station or GNSS-positioning service and geodetic low-cost GNSS antennas (Figure 6). Controlled by GOCA-GNSS-Control (geomonitoring chain, part 1, Figure 1) it can be applied as sensor for a classical networked deformation state estimation based on the observations **l**(t) according to (1a-d) and the GOCA standard deformation state estimation models (2a,b) and (4a-f).

Figure 6: (Left) GNSS&MEMS navigation-box "Robinette" with interfaces. (Right) GNSS low-cost antenna used together with the "Robinette" in geomonitoring

As holds for the GNSS&MEMS Robinette GM the state estimation **y**(t) for the geomonitoring use will be based on a modification of the mathematical models for the estimation of the global navigation state vector **y**(t) of a body (b) in earth-framework (e) (JÄGER (2013), JÄGER (2014)), reading:

$$\mathbf{y}(t) = [x^e\ y^e\ z^e \mid \dot{x}^e \dot{y}^e \dot{z}^e \mid r^e\ p^e\ y^e \parallel \ddot{x}^e\ \ddot{y}^e\ \ddot{z}^e \mid \omega^b_{eb,x}\ \omega^b_{eb,y}\ \omega^b_{eb,z} \mid \mathbf{s}]^T \tag{8}$$

The general navigation state vector **y**(t) (8) comprises the 3D position $\mathbf{x}(t)^e$, velocity $\dot{\mathbf{x}}(t)^e$, acceleration $\ddot{\mathbf{x}}(t)^e$, orientation (roll (r), pitch (p), yaw (y)), rotation rates $\omega^b_{eb,x}\ \omega^b_{eb,y}\ \omega^b_{eb,z}$ and different kind of sensor calibration parameters **s**. Making use of the georeferencing of the structure (Figure 5a, Figure 5b) in regard, the essential part $\mathbf{y}(t) = [\mathbf{x}(t)^e, \dot{\mathbf{x}}(t)^e, \ddot{\mathbf{x}}(t)^e]^T$ of the state vector **y**(t) (8) used for structural health monitoring can be rotated to the body frame (b) of the building.

In case of geomonitoring the estimation of **y**(t) (8) will be based on a robust L1-norm estimation (3a,b). Instead of an iterative least squares solution JÄGER, MÜLLER, SALER & SCHWÄBLE (2005), simplex algorithms (Barrodale-Roberts type) will be used, because these allow the simultaneous introduction of inequations concerning the variables of the parameter state vector **y**(t) (8).

As concerns the development of mathematical models for the use of GNSS/MEMS and the Robinette GM (Figure 6), respectively for the classical geometric geomonitoring (represented by (2a,b), (2c,d)

and (4a-f)) and for structural health monitoring represented by (5b), (6c) and (7c,d)) both - DGNSS and absolute GNSS or SSR based absolute OPPP (Online Precise Point Positioning) - are regarded as candidates for the estimation of the full state vector **y**(t) (8) in rates of 400 Hz and higher. So, for high rate deformation monitoring, the use of the GM Robinette as a local sensor (LS) enables both, a high rate classical deformation state estimation (4a-e), as well the dynamic cases (6c) or (7c, d) of the proposed structural health monitoring for the detection of “unhealthy” structural parameters.

In that context it is to be mentioned, that the topic of bridge monitoring is a RaD project item in the so-called “skating project” (optimization of the conditions of study in engineering) at the University of Karlsruhe of Applied Sciences (HSKA).

3 CURRENT GOCA PROJECT EXAMPLES

As concerns the geodetic and integrated GNSS/LPS/LS based geomonitoring system GOCA, the basic concepts and mathematical models of the network adjustment based deformation analysis in the so-called observation-related approach are based on the geodetic network adjustment based geomonitoring models PELZER (1974), HECK & JÄGER (1986), SCHMITT, MOLDOVEANU, NICA & JÄGER (1990), HARTMANN & JÄGER (1997), HECK; ILLNER & JÄGER (1995) and JÄGER (1988) with further-developments starting in 1998.

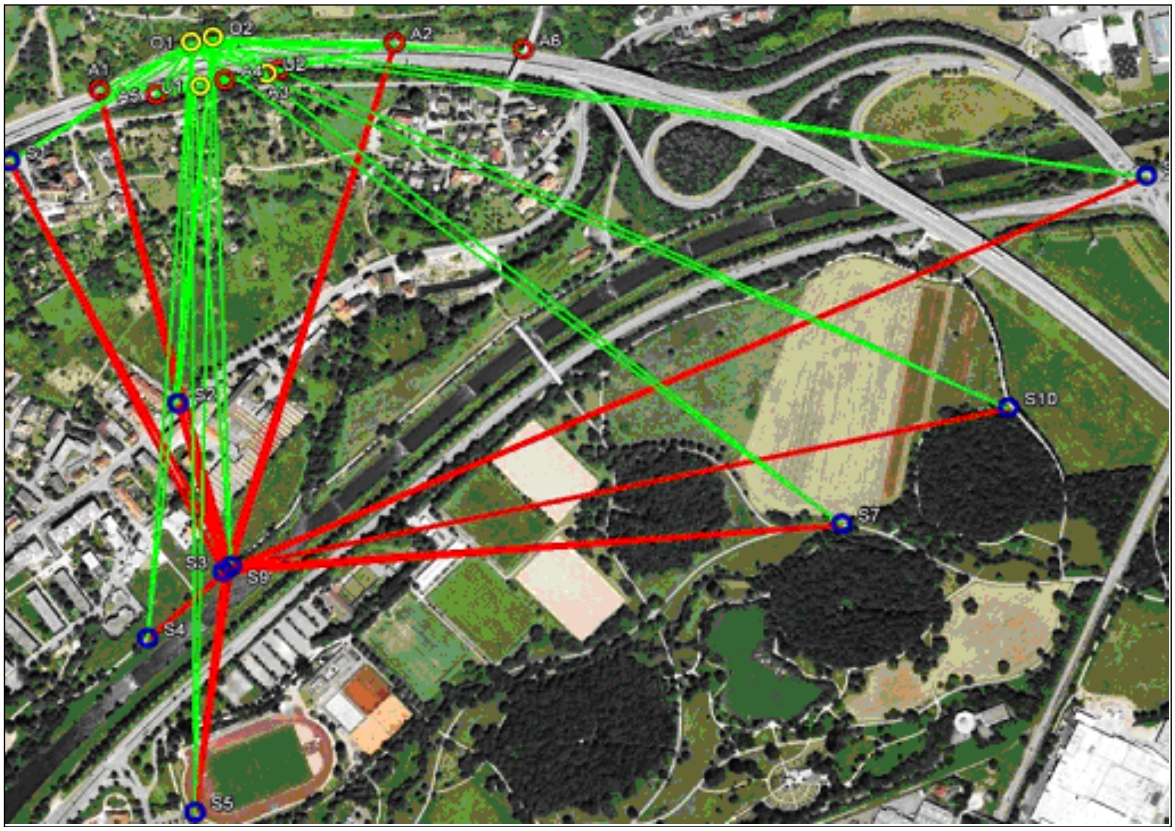

Figure 7: GOCA-Project Stützmauer (abutment wall) A98 at Rötteln/Germany. Screenshot of the project planning and tests, using the software Virtual-GOCA instead of real sensors. Red: GNSS-Baselines with stable reference points xR in the southern part. Yellow: TPS sensor points on and in front of the abutment wall, modelled as object points xO in the North of the area. Green: TPS-sights.

The GOCA system is used since with a broad range of applications in more than 100 installations as an epochal, short and long-time permanent online geomonitoring system in civil engineering, geotechnical engineering and natural disaster protection. Project overview, see JÄGER & KÄLBER (1999-2014).

Purely with GNSS-sensors, GOCA is currently used in many mining projects, as well as a permanent early warning system in different slide areas in the Austrian Alps WUNDERLICH (2006). In Russia, the GOCA system is used for GNSS-based monitoring of constructions by the cooperation partner GNSSplus, Moscow (www.gnssplus.ru). As concerns recent monitoring projects using the combination of GNSS and TPS sensors for construction monitoring, the new railway tunnel in Cochem and the monitoring of the abutment wall along the highway A 98 near the town of Rötteln, Germany (Figure 7) are mentioned. Figure 7 above shows the design for the planning and pre-analysis and"proof of concept" of this GOCA-project concerning the achievable sensitivity JÄGER, WEBER & HAAS (1997) for the determination of 3D displacements in the state estimation (2c,d).

Figure 8 shows the Rethe lift bridge and the local TPS sensor installation on the bridge, situated in the port of Hamburg. Here the GOCA-system is used by the Hamburg Port Authority (HPA) for the continuous monitoring of the 3D displacements during the ongoing construction of a new bridge, close aside to the old Rethe lift bridge.

Figure 8: GOCA project Rethe lift-bridge maintained by Hamburg Port Authority (HPA) in the Hamburg port. Building monitoring during the construction of a new bridge close aside. Middle: installation of the total station (TPS) sensor.

Figure 9 shows the 3D time-series (2a,b) resulting form the continuous online adjustment, GOCA step 2 of the modeling part in the geomonitoring chain, part 2 (Figure 1) for the Rethe bridge (Figure 8).

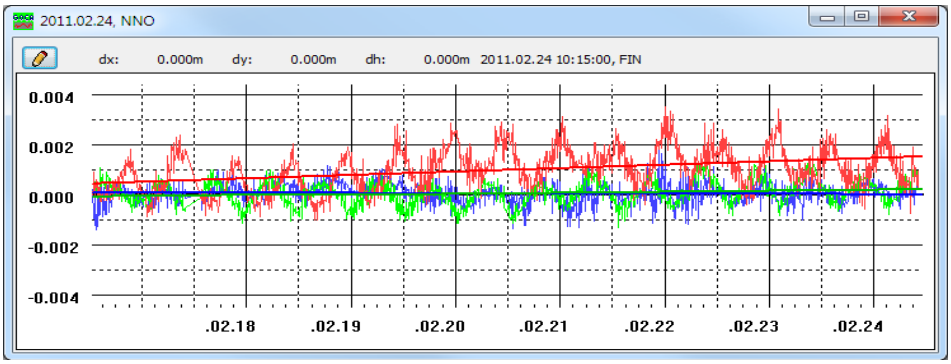

Figure 9: Online adjustment GOCA step 2. Object point NNE located on the Rethe lift-bridge with linear trend estimate for 7 days. Green / Blue: displacements along and cross the bridge. Red: height displacement

Like for all object points, also the displacements of object point "NNO" (Figure 9) are superposed by daily cycles of tide variations. The visualized linear trend estimate (red line) for the time series (2a,b) of "NNO" shows, for the period of one week, an uplift of the bridge of 0.5 mm, which is reversed again by the trend of the following week.

Figure 10 shows the dam Jablanica in Bosnia-Herzegovina, as one of two other dams (Grabovica and Salakovac), which are since 2011 subjected to a modernization and automation of the geodetic dam monitoring concept of all three dams, as a project of the Austrian GOCA cooperation partner, Angst ZT GmbH, Vienna (KABASHI, ANGST, RAGOSSNIG-ANGST, JÄGER & SPOHN (2013), KABASHI, RAGOSSNIG-ANGST, & JÄGER (2011)). Like a number of other GOCA based geodetic geomonitoring projects of buildings and structures of the cooperation partner Angst ZT GmbH (www.angst.at), the geodetic geomonitoring of the above three dams are currently done with total stations (TPS) and leveling sensors. The integration of GNSS into the local TPS networks (like in Figure 7) - as well as the integration of all three dams (Figure 10) into a unique reference system $\mathbf{x}_R$ (Figure 2) - are possible at any time, and have already been taken into account in the project planning

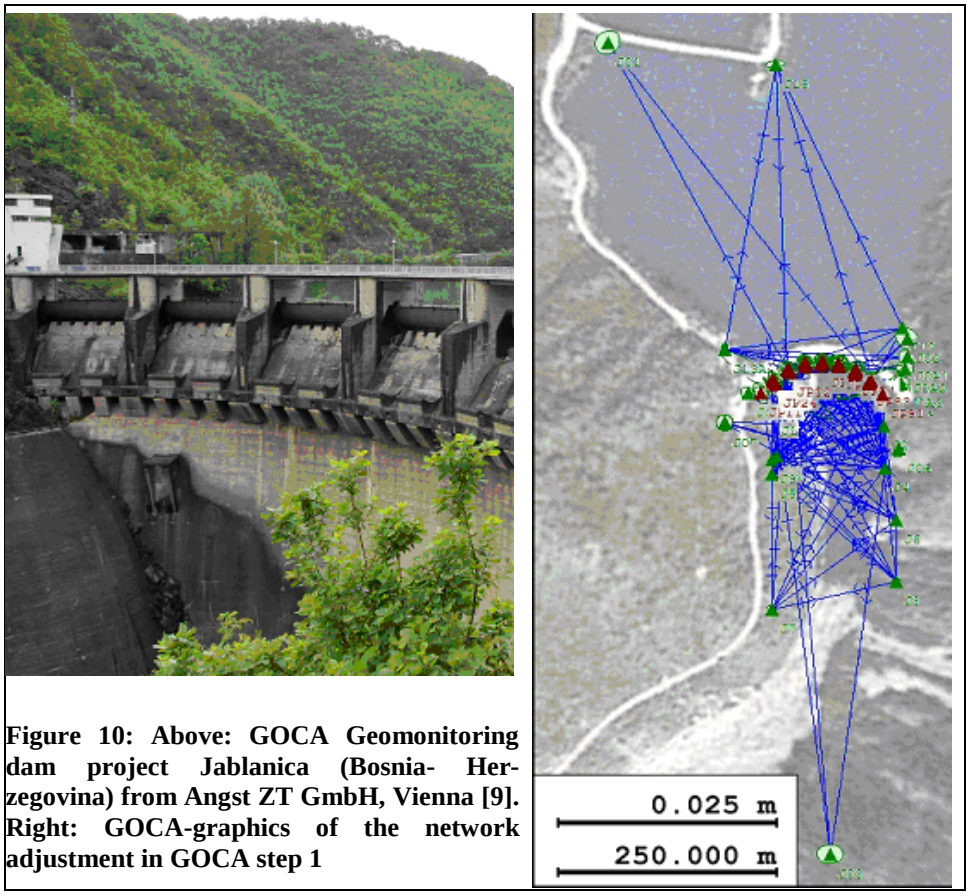

Figure 10: Above: GOCA Geomonitoring dam project Jablanica (Bosnia- Herzegovina) from Angst ZT GmbH, Vienna [9]. Right: GOCA-graphics of the network adjustment in GOCA step 1

In the context with the RaD projects GOCA and MONIKA (JÄGER & KÄLBER (1999-2014), SPOHN & JÄGER (2007-2014)) IAF/HSKA presently does research and developments (RaD) in the area of sensor developments (chap. 2.3) for geodetic and integrated geomonitoring, on the further development of the mathematical models and software for a scalable classical geomonitoring (fig .2), and on structural health monitoring (chap. 2.1; chap. 2.2). All RaD on the above mathematical models, algorithms, software and system components, as well as the transfer of modern geodetic monitoring technologies concerning the systems GOCA JÄGER & KÄLBER (1999-2014 and MONIKA SPOHN & JÄGER (2007-2014) into the practice, contribute to the reduction of the hazard potentials and risks for people and for the environment, which are caused both by natural disasters sources (volcanos, fault-dislocations, land-slides) and by the risks of deformation of different types of technical facilities (e.g. construction areas, tunnels, dams, buildings, mines, etc.).

The GOCA RaD team of IAF/HSKA would like to thank therefore in this way all GOCA project partners and users, applying the systems GOCA (since 1998) and MONIKA (since 2007) in practice and research round the world, for providing their feedback and valuable suggestions, as contributions for IAF/HSKA concerning and benefiting the RaD on the further and new developments of the mathematical model approaches and the technical components of both systems.

REFERENCES

Books:

JÄGER, R., WEBER, A. & HAAS, R. (1997): *Ein ISO 9000 Handbuch für Überwachungsmessungen*, DVW-Schriftenreihe, Heft Nr. 27, Wichmann Verlag, Karlsruhe.

JÄGER, R., MÜLLER, T., SALER, H. und SCHWÄBLE, R. (2005*): Klassische und robuste Ausgleichungsverfahren - Ein Leitfaden für Ausbildung und Praxis von Geodäten und Geoinformatikern*. Wichmann-Verlag, Heidelberg. ISBN 3-87907-370-8.

LIENHART, W. (2007): *Analysis of Inhomogeneous Structural Monitoring Data. Dissertation*, Series Engineering Geodesy TU Graz. Shaker, Verlag Aachen.

PELZER, H. (1974): *Zur Analyse geodätischer Deformationsmessungen*. DGK, Reihe C, Nr. 164, München.

HECK, B., ILLNER, M. und JÄGER, R. (1995): *Deformationsanalyse zum Testnetz Karlsruhe auf der Basis der terrestrischen Messungen und aktueller GPS-Messungen*. Festschrift Draheim-Kuntz-Mälzer. Universität Karlsruhe.

WITT, K. J. (2009): *Grundbautaschenbuch – Teil 1: Geotechnische Grundlagen*. 7. Auflage. Ernst&Sohn.

FUCHS, K. (2010): *Konzipierung und Implementierung einer modularen Software (GOCA-Virtual Sensor) sowie Algorithmen für virtuelle Sensoren im Geomonitoring und Anwendung auf die historischen Daten des Moskauer Kreml*. Masterthesis Studiengang Geomatik (MSc). Hochschule Karlsruhe Technik und Wirtschaft.

HOSCISLAWSKI, A. (2009): *Konzeption und C++-Softwareentwicklung eines M-Schätzer Kalmanfilters zur Zustandsschätzung, -Vorhersage und Alarmmanagement für das Geomonitoringsystem GOCA*. Diplomarbeit am Studiengang Vermessung & Geomatik. Hochschule Karlsruhe Technik und Wirtschaft.

TESKEY, W. (1988): *Integrierte Analyse geodätischer und geotechnischer Daten sowie physikalischer Modelldaten zur Beschreibung des Deformationsverhaltens großer Erddämme unter statischer Belastung*. Deutsche Geodätische Kommission, Reihe C, München.

JÄGER, R. (1988) *Analyse und Optimierung geodätischer Netze nach spektralen Kriterien und mechanische Analogien*. Deutsche Geodätische Kommission. Reihe C (Dissertationen), Nr. 342, München.

ZIENKIEWICZ, O.C. (1984): *Methode der finiten Elemente*. Carl Hanser Verlag, München, Wien.

HÄCKELL, C., HAAKE, G. und ROLFES, R. [2014]. *Beiträge zum DVW-Seminar „Validierte Strukturmodelle und Systemidentifikation. „Zeitabhängige Meßgrößen ihre Daten haben (Mehr)-Wert“*. DVW Schriftenreihe, Band 74.

Journal articles:

KÄLBER, S. and JÄGER, R. (2000): *Realization of a GPS-based Online Control and Alarm System* (GOCA) and Preview on Appropriate System Analysis Models for an Online Monitoring. Proceedings 9th FIG-Symposium on Deformation Measurement and Analysis. Sept. 1999, Olsztyn, Poland. p. 98 - 117.

KABASHI, I., ANGST, J., RAGOSSNIG-ANGST, M., JÄGER, R. und SPOHN, P. (2013): *Automatisiertes geodätisches Monitoring an den Staudämmen* Jablanica, Grabovica und Salakovac. (In: Hanke, K.; Weinold, T. Hrsg.). 17. Internationale Geodätische Woche Obergurgl 2013. Wichmann. ISBN 978-3-87907-526-3.

KABASHI, I., RAGOSSNIG-ANGST, M. und JÄGER, R. (2011): *Geodätisches Online-Monitoring von alten Bauwerken in gefährdungskritischem Zustand im Zuge von Sanierungen*. 16. Internationale

SCHMITT, G., MOLDOVEANU, T., NICA, T. and JÄGER, R. (1990): *Deformation Analysis of a Local Deformation Analysis of a Local Terrestrial Network in Romania with respect to the Vrancea Earthquake of August 30 1986*. In: Ivan I. Mueller (ed.). International Association of Geodesy Symposia. Symposium No. 101: 'Global and Regional Geodynamics', Edinburgh/Scotland, Aug. 7-8, 1989. Convened and edited by P. Vyskocil, C. Reigber and P. A. Cross, Springer Verlag: 211-221.

HARTMANN, P. and JÄGER, R. (1997): *GPS-Integration including terrestrial Data Combination in large and local plane and height networks with a view to quality control and automatation - Strada&Netz, development of a geodetic software-application for Microstation ®*. In: M. Roic and Z. Kapovic (Eds). Proceedings of the 1st Croatian Congress on Cadastre. Multigraf, Zagreb. ISBN 953-97081-0-9.

MÖNICKE, H.-J. (1991): *Measurements of high-frequency oscillations by optoelectric and inertial sensors in a hybrid measurement system. In: International Association of Geodesy Symposia. Applications of Geodesy to Engineering*, No. 108. Springer, Heidelberg, New York.

WELSCH, W. and HEUNECKE O. (1999): *Terminology and classification of deformation models - final report of FIG ad-hoc-Committee of WG 6.1*. Proceeding of the 9th International FIG Symposium on Deformation Measurements, Olsztyn, 27-30 September, 1999.

JÄGER, R., HOSCISLAWSKI, A. und OSWALD, M. (2009): *GNSS/LPS/LS based Online Control and Alarm System (GOCA) – Mathematical Models and Technical Realization of a Scalable System for Natural and Geotechnical Deformation Monitoring and Analysis*. In (E. Bauer, S. Semprich and G. Zenz (Eds.)): Proceedings of the 2nd International Conference “Long Term Behaviour of Dams”, Oct. 2009. Verlag der Technischen Universität Graz, University of Technology. ISBN 9783851250701. p. 387 – 394

JÄGER, R. und BERTGES, M. (2004): *Integrierte Modellbildung zum permanenten Monitoring von Bauwerken und geotechnischen Anlagen*. Beitrag zum 61. DVW-Fortbildungsseminar, 27./28. September 2004, Bauhaus-Universität Weimar. DVW-Schriftenreihe, Band 46/2004. ISBN 3-89639-451-7. S. 101-140.

WUNDERLICH, T. A. (2006): *Geodätisches Monitoring – ein fruchtbares Feld für interdisziplläre Zusammenarbeit*. VGI - Österreichische Zeitschrift für Vermessung & Geoinformation. 1+2/2006. Österreichische Geodätische Kommission, Wien. S. 50-76.

Geodätische Woche Obergurgl 2011.Grimm-Pitzinger, A. ; Weinhold, T. (Hrsg.) Wichmann Verlag, Heidelberg. ISBN 978-3-87907-505-8. Seiten 53-65.

PFEUFFER, A. (1993): *Analyse und Interpretation von Überwachungsmessungen - Terminologie und Klassifikation*. ZfV 1993, Heft 8/9, S. 470-476.

JÄGER, R. (2014*): GNSS/LPS based Online Control and Alarm System (GOCA) - Konzept, Modellbildung und Realisierung eines Systems zum Geomonitoring in Bauwesen, Geotechnik und Naturkatastrophenschutz*. Proceedings, 9. Kolloquium Bauen in Boden und Fels. Technische Akademie Esslingen (TAE). Januar 2014. ISBN 978-3-943563-08-05, Registered at http://dnb.dnb.de. Seiten 359-368.

JÄGER, R. (2014): *Navigation mit verteilten GNSS/MEMS Sensoren - Mathematische Modelle, Algorithmen und Anwendungspotenziale*. Horizonte (43). ISSN 1432-0174. Pages 7-10.

JÄGER, R., OSWALD, M. und SPOHN, P. (2010): *VirtualGOCA – Generierung von Sensordaten zur Modell- und Softwarevalidierung sowie zur Planung und Analyse von Monitoringszenarien in virtuellen Geosensornetzen mittels Google-Earth. Wasserwirtschaft* - Zeitschrift für Wasser und Umwelt 10/2010, Vieweg Verlag, Stuttgart.

JÄGER, R. and GONZALEZ, F. (2005): GNSS/GPS/LPS based *Online Control and Alarm System (GOCA) - Mathematical Models and Technical Realisation of a System for Natural and Geotechnical Deformation Monitoring and Hazard Prevention*. ISGDM IAG-Symposium 2005, University of Escuela Politécnica Superior de Jaén. Spain. (F. Sanso and A. J. Gil (Eds.): Geodetic Deformation

Monitoring: From Geophysical to Engineering Roles. IAG Series on Geodesy Symposia. Springer Heidelberg and New York. ISBN 3-540-38595-9. S. 293 – 304.

HECK, B. und JÄGER, R. (1986): *Zur Sensitivität von Strecken- und Streckenverhältnisbeobachtungen in Deformationsnetzen*. Zeitschrift für Vermessungswesen (111): 459-468.

Links:

JÄGER, R. und KÄLBER, S. (1999-2014): GOCA-WebSite. URL: www.goca.info.

DIEKERT, J., HOSCISLAWSKI, A., JÄGER, R., LORENZ, A., BATKE, B. und ZWIENER, J. (2010-2013): NAVKA-Webseite. URL: www.navka.de .

SPOHN, P. und JÄGER, R. (2007-2014): MONIKA-WebSite. URL: www.monika.ag .

GROSSE, C.U. and KRÜGER, M. (2011): *Inspection and Monitoring of Structures in Civil Engineering*. Internet-Publication http://www.ndt.net/article/v11n01/grosse/grosse.htm

JÄGER, R. (2013): *Mehr als Positionierung - Präzise Out-/Indoor Navigation mit verteilten Sensoren*. Vortrag zur INTERGEO 2013. Download:
http://www.kongress.intergeo.de/share/public/Intergeo/Archiv/2013/Jaeger_Vortrag.pdf

Modelling Linear Objects by the Results of Geodetic Monitoring

Igor G. Vovk
Siberian State Academy of Geodesy, Russian Federation

Abstract
We call linear objects those having one dimension considerably exceeding the other two. Linear objects can be of either natural or artificial origin. Thus, for instance, all rivers and springs are linear objects of natural origin whereas all roads and channels, communication lines and conductors of some products, mines and tunnels are man-made and so they have artificial origin. To study linear objects is a modern challenge of applied geoinformatics. This task is to be solved on the basis of the principles of the systemic-and-purposeful approach because of its complexity. Mathematic modeling is the major method used to study the complex systems.
Geometric modeling of linear objects comprises the solution of two tasks : geometric modeling of a curve which is the axis of the linear object and geometric modeling of its cross-section. The article studies the task of geometric modeling of some abstract linear objects and there are several examples of geometric modeling given here.

Keywords
Linear objects, semi-cylindrical surfaces, algorithm, mathematic modeling, geometric modeling

Linear objects are those with one dimension considerably exceeding the other two. Linear objects can be of either natural or artificial origin. Thus, for instance, all rivers and streams are linear objects of natural origin whereas all roads and channels, communication lines and product pipelines, mines and tunnels are man-made and so they have artificial origin. The distinctive feature of most linear objects is that they may be presented by the quadric surface. For example, the road is a stripe whose axis is a curve, product pipelines are cylindrical surfaces with different cross-sections and their axis is also a curve. Rivers, streams and channels are presented by semi-cylindrical surfaces with variable cross-sections, etc. Study of linear objects is an objective of applied geoinformatics LOVYAGIN (2003). Due to the task complexity it is to be solved on the basis of the system-and-target approach principles VOVK (2012), BUGAKOVA & VOVK (2012), VOVK & BUGAKOVA (2011). Mathematical simulation is a major technique to study complex systems BELOV (2003), VOVK (2011), VOVK (2012).

Computer technologies are now widely used for modeling geometrical objects. Hereupon two new branches referred to as computational geometry and geometrical modeling appeared. Though not identical they have much in common.

The main objective of computational geometry is transformation of geometrical problems into computational form PREPARATA & SHEYMOS (1989), i.e. construction of algorithm for numerical solution of the geometrical problem, while the main task of geometrical modeling is computer representation, analysis and synthesis of the geometric image data PRATT & FOX (1982), VOVK (2013). Both branches are based on the discrete information to be used for computer representation of geometric images in accordance with the problem solution algorithm.

Applying the techniques of computational geometry and geometric modeling for developing models of linear objects one can computerize information on the object shape, its appearance, size, geometric characteristics, and features in space-saving analytical form. Thus, information on the object shape and its geometric properties may be digitized, the object model decomposed with these data easily visualized in numerical and graphical form. Graphic presentation of the linear object on the display

makes it possible to see how the mathematically formulated system looks from any point of the environment.
With a great arsenal of geometric models available we can aggregate them and model the shape of the object under consideration according to the set requirements and the task. The requirements may be set exactly or qualitatively. Therefore aggregation should be performed interactively so that with the system image on the display you could manage the procedure of aggregation to meet the formal and heuristic requirements imposed on the result.

Geometric modeling of linear objects comprises the solution of two problems: geometric modeling of the curve which is the axis of the linear object and that of its cross-section.

The theory of modeling curves and surfaces is considered in the course of geometry PRATT & FOX (1982), LAPTEV (1975), POSTNIKOV (1979). Some examples of geometric modeling of curves and surfaces are presented in works VOVK (2013), VOVK (2012c), VOVK (2012d). Based on these works, geometric modeling of an abstract linear object may be carried out for the set axis line and different variants of cross-section (Figure 1).

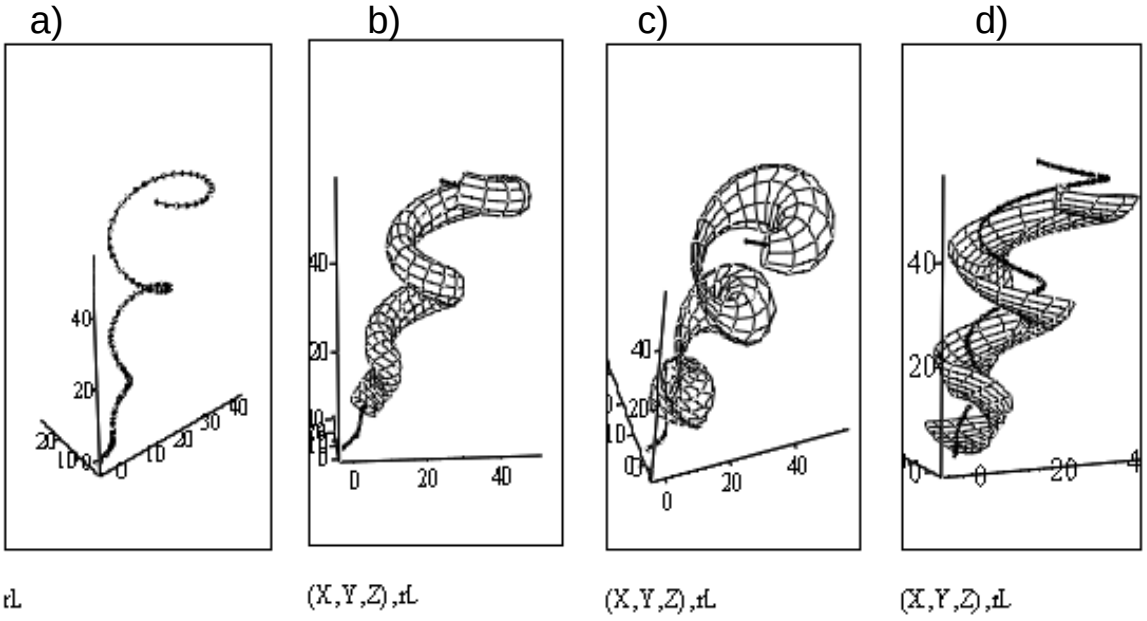

Figure 1: Example of geometrical models for an abstract linear object:

a) axis of the object
b) pipe with constant cross-section
c) pipe with variable cross-section
d) tray with semi-circle cross-section

The example considered demonstrates applications of computational geometry and geometric modeling techniques for mathematical formulation of linear objects. Changing the axial line of the linear object and the form of its cross-section we can obtain different variants of its models. The fact makes it possible to develop different models of the same object, to conduct comparative analysis, estimate efficiency index for modeling goal achievement, and solve the problem of the best alternative choice.

Now we can develop geometrical model of the linear object on the Earth physical surface. To this end we have to determine the model of the Earth surface features and the axial line of the linear object on this surface. These problems solutions are not considered in this article. Therefore let us suppose these models are known and presented in Figure 2.

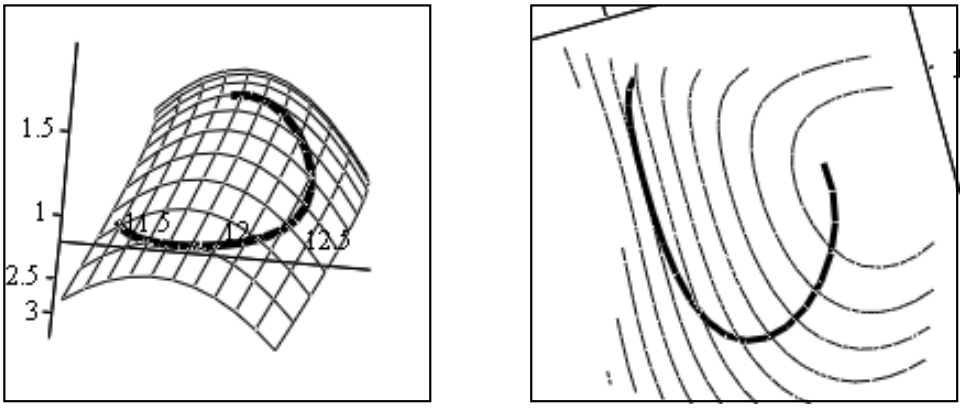

Figure 2: Geometrical model of the linear object axis (heavy line) and surface (left-hand surface is shown with parametric lines, right–hand one with equal-height lines)

This data is sufficient to develop geometrical models of linear objects (with different cross-sections) laid on the set surface relief. Figure 3 is an example of the pipe model (with circular cross-section), laid on the set relief.

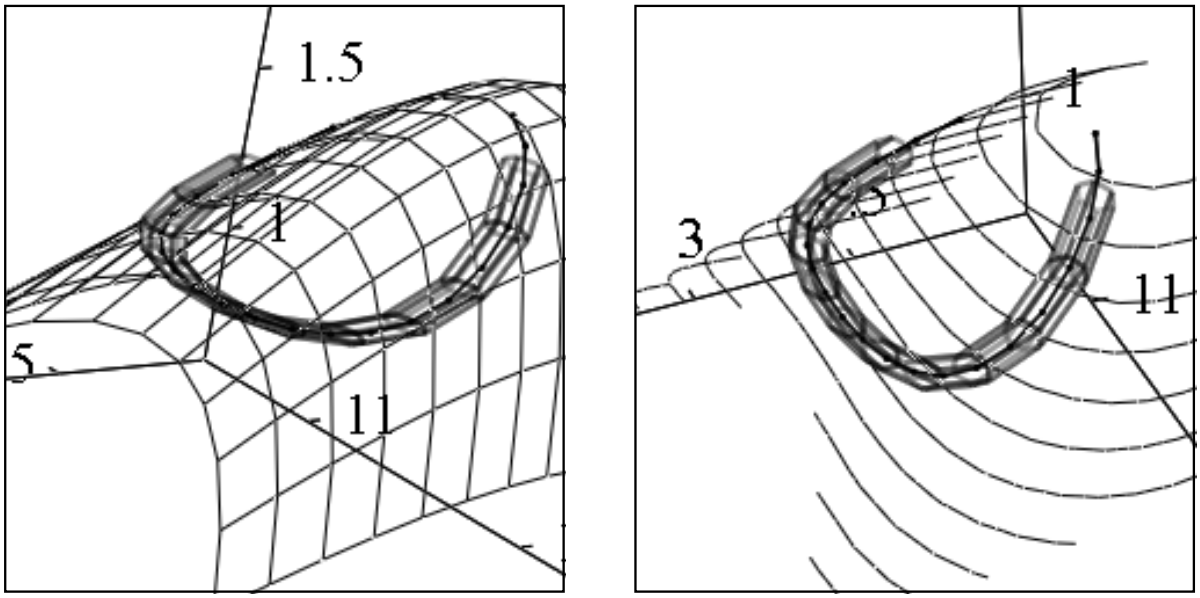

Figure 3: Geometrical model of the linear object (pipe with constant diameter) laid on the physical surface relief.

The form of the cross-section may be changed. Figure 4 presents an example of a model for the linear object in the form of the tunnel with triangular cross-section and for that in the form of the plane band. Figure 4 does not present surface features, as distinct from Figure 3, with only linear object models being shown.

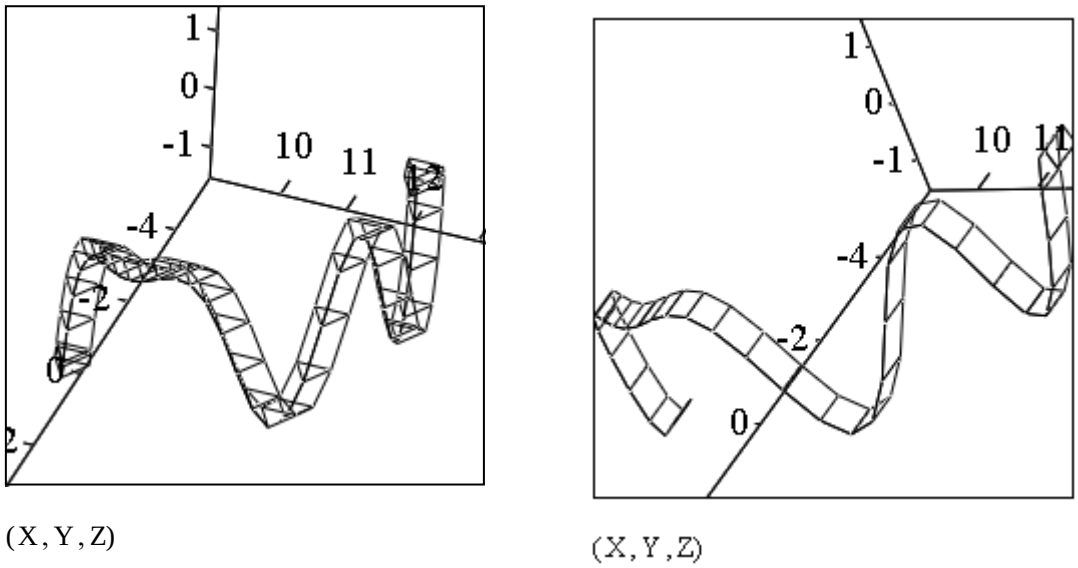

Figure 4: Geometric models of the linear object with different cross-sections

The geometric models alternatives for linear objects may be numerous: they may be situated not only on the Earth surface, but also in its interior or above it. To develop these models, it is necessary to properly set physical surface and the linear structure axis, and determine the cross-section of the object to be modeled. The data may be used for assessing different invariant characteristics of the linear object and, if necessary, reveal the sites where man-made transformations of the object are necessary to achieve the assigned tasks.

Thus, the techniques of classical geometry combined with modern computer technologies give new opportunities for investigating complex objects like linear objects of natural and artificial origin. Modeling linear objects of different location on the Earth surface makes it possible to calculate or pre-calculate their geometrical characteristics, estimate labour-intensiveness of their construction or transformation, the resources required, ecological risk as well as acquire some other relevant information including that on the best alternative choice.

REFERENCES

Books:

BELOV, P.G. *System analysis and modeling of dangerous processes in technosphere*. Moscow: Publishing house “Akademiya”, 2003, p. 512. ISBN 5-7695-1039-0.

VOVK, I.G., BUGAKOVA, T.Y. *Fundamentals of system-and-target approach and decision-making*. Novosibirsk: SSGA, 2011, p. 152. ISBN 978-5-87693-461-1

LAPTEV, S.F. *Elements of vector calculus*. Moscow ; Nauka, 1975, p. 336

POSTNIKOV, M.M. *Lectures on geometry*. Semester II. Moscow: Nauka, 1979. p. 312.

Journal articles:

LOVYAGIN, V.F. *Methodological aspects of defining the problem of routes optimization by system-and-structural approach*. Herald of Siberian State Academy of Geodesy.2003, 8, pp. 60 -67.

BUGAKOVA, T.Y., VOVK, I.G. *Mathematical modeling of space-time state of systems by geometrical properties and technogenic risk assessment by exponential smoothing*. Herald of Siberian State Academy of Geodesy. 2012, 4, pp. 47 – 58.

VOVK, I.G. *Modeling in applied geoinformatics*. Herald of Siberian State Academy of Geodesy. 2011, 1(14), pp. 69 – 76.

VOVK, I.G. *System-and-target approach in applied geoinformatics*. Herald of Siberian State Academy of Geodesy. 2012 a, 3(19), pp. 52 – 61.

VOVK, I.G. *Mathematical modeling in applied geoinformatics*. Herald of Siberian State Academy of Geodesy. 2012 b, 1 (17), pp, 94 -103.

VOVK, I.G. *Determination of geometric invariants of surface in applied geoinformatics*. Herald of Siberian State Academy of Geodesy. 2012 c, 4 (20), pp. 59 - 69

VOVK, I.G. *Determination of geometric invariants of spatial curve in applied geoinformatics*. Herald of Siberian State Academy of Geodesy. 2012 d, 3 (19), pp. 51 - 62

VOVK, I.G. *Modeling of form and estimation of system size in applied geoinformatics*. Herald of Siberian State Academy of Geodesy. 2013, 2(22), pp. 115 - 124

FOX, A., PRATT, M. *Computational geometry*. *Application in designing and production*. Moscow: “Mir”, 1982, pp. 304.

PREPARATA, F., SHEYMOS, M. *Computational geometry*: Introduction. (edited) Y.M. Bayakovsky. Moscow: “Mir”, 1989, p. 478. ISBN 5-03-001041-6.

Change Detection of Urban Objects Using Point Clouds

Uwe Stilla[1], Sebastian Tuttas[1], Marcus Hebel[2]
[1]Technische Universitaet Muenchen, Germany
[2]Fraunhofer Institute of Optronics, System Technologies and Image Exploitation, Germany

Abstract
Change detection in urban areas requires the comparison of multi-temporal data. In contrast to broad research activities in remote sensing this contribution addresses the topic using 3D data (point clouds) instead of 2D data (images). For further discussion, two strategies in the field building monitoring are presented, which address change detection based on point clouds. The first example deals with change detection on construction sites using a building information model (BIM). The second example uses airborne laser scanning data to discover changes in the built environment.

Keywords
Change detection, point clouds, buildings, construction sites, urban areas, multi-view stereo images, multi view laser scanning

1 INTRODUCTION

Automatic identification of urban structures and the analysis of their changes are important steps to provide a basis for monitoring and planning. Common tasks in this context are the documentation of urban development, surveying of construction sites, or damage inspection after disasters. In particular, the automatic acquisition of buildings and their 3D geometry is of great interest, which is confirmed by the growing number of scientific papers on this topic ROTTENSTEINER et al. (2013).

Generally, photogrammetry and remote sensing allow contactless observations of urban objects using varying geometric resolution and aerial coverage by using several platforms (terrestrial, airborne, space-borne). Change detection in urban areas requires the comparison of multi-temporal data. The flexibility in observation techniques and temporal resolution of multi-temporal data typically depends on the technical conditions of the involved platform and sensor which cover a broad field, e.g. from terrestrial observations using a mobile video camera with a frame rate of some milliseconds up to orbit fixed observation from satellites with a revision interval of some days. It has to be mentioned that in the field of remote sensing the topic ‘change detection’ is discussed very often on the basis of 2D data (images). In contrast to this, in this paper change detection will be addressed on the basis of 3D data (point clouds).

Beside the variation in different acquisition methods of buildings we can find a variety of ways to describe the geometric and semantic structure of buildings, e.g. by labelled point clouds, Geographic Information Systems (GIS), Building Information Models (BIM), Industry Foundation Classes (IFC) etc. Facing the challenge of combining and exploiting different models, a research center of digital methods for the built environment was founded at Technische Universitaet Muenchen (TUM). A particular emphasis is put on researching digital methods which are able to bridge the multiple scales involved with modelling and simulating the built environment – from the scale of a few millimeters to the scale of a whole country TUM-LOC (2014).

In this context it is intended to stimulate the research on general strategies for change detection methods based on point clouds. For preparing the discussion in this paper the topic of change detection is described by two examples using different views and data acquisition techniques.

1.1 Example I: Comparison model-to-point cloud

Automatic construction site monitoring aims to support the efficiency of the construction process. For this the current state of the building (as-built) has to be acquired at successive time steps. This state has to be matched with the planned state of the building (as-planned) for the respective time step to detected deviations from the scheduled progress or the geometry. The as-planned state is extracted from a building information model (BIM). This model contains the schedule of the construction project, the 3D geometry of the building and information about the components and the costs. The as-built state can be acquired by laser-scanning or images. The image based strategy was chosen to get a higher flexibility in contrast to laser scanning for data acquisition on a construction site (e.g. from the crane). In Chapter 2 a procedure for change detection is described which focuses on the comparison between a dynamic model and point clouds from images TUTTAS et al. (2014).

1.2 Example II: Comparison point cloud-to-point cloud

In this example, we address change detection in urban areas in the case that both the reference data and the current data are given as 3D point clouds. Airborne laser scanning (ALS) is well suited to provide 3D measurements allowing a direct comparison of geometric features. A basic requirement for detecting differences between multiple ALS point clouds is an accurate registration and alignment of the multi-temporal data HEBEL & STILLA (2012). In contrast to classical nadir data acquisition we assume that the scene is captured with an oblique forward-looking airborne laser scanner. During acquisition of the reference data, multiple criss-crossing flight lines are used. This setup has the additional advantage of full terrain coverage, for example allowing further analysis of building facades TUTTAS & STILLA, (2012, 2013). In Chapter 3 a procedure for change detection is described which focuses on the comparison between two point clouds HEBEL et al. (2013).

2 EXAMPLE I: CHANGE DETECTION ON CONSTRUCTION SITES

2.1 Data acquisition

For generating point clouds from images it is necessary to acquire multiple images which are appropriate for stereo matching. The reliability can be increased by regions of interest which are visible at least in three images. For the comparison of the model and the point clouds of different time steps or the comparison of subsequent point clouds a reliable co-registration is required. This can be ensured by performing the following two main tasks:

- The images have to be registered in the coordinate system of the building model. In the ideal case the coordinate system of the model is realized on the construction site and control points in this system can be measured in the images.
- Images of subsequent time steps can be registered consistently by adjusting them in a common bundle block adjustment. For this, homologous points have to be identified in images of both time steps. In this case, the difficulty is that the sensed scene has changed. For this reason the tie points have to be restricted to areas where no construction activity has taken place during the two acquisition times. All available control points shall be used if they are visible.

The described tasks can be embedded in a structure-from-motion process which is extended with the introduction of the control point information and tracking of stable features over subsequent time steps.

2.2 Point cloud generation

In the next step dense point clouds from the images are generated using semi-global-matching (SGM). As a first step, appropriate stereo pairs are chosen based on the orientation parameters which are received from the bundle adjustment. The selection of the pairs is based on (i) the baseline length, (ii) the viewing direction of the camera (z-axis of the camera system), and (iii) the angle between z-axis and baseline. All stereo pairs are matched with SGM to create depth images for each stereo pair. Then for a certain master image all available depth maps are fused. For that the depth values which are given for different rectified images are transformed to the pixel of the undistorted master image and a

final depth value is calculated. After that the 3D points are triangulated. For this procedure all images are used as master images once and finally all point clouds are fused. This approach is based on the procedure of ROTHERMEL et al. (2013).

2.3 Comparison of model and measured point cloud

The matching of the model with the as-built point cloud can be divided into different processing steps. These are (i) the direct verification of construction parts by the points, (ii) the indirect verification based on constraints derived from the model, and (iii) the handling of points which cannot be aligned to model objects.

In this contribution a simple measure for the direct verification of construction parts is introduced, which shall indicate areas of the construction parts being covered by as-built points. For that, points are extracted which are within the distance Δd in front of and behind the model plane. The plane is split into quadratic raster cells with the edge length of x_r. For every raster cell the points belonging to this cell are used to calculate the measure M, which is used to decide whether the points confirm the construction part or not:

$$M = \frac{1}{\mu_d} \cdot \sum_i \left(\frac{1}{d_i \cdot \sigma_{d_i}} \right) \quad \text{mit} \quad d_i = \begin{cases} d_i = d_i & \text{für } d_i > d_{\min} \\ d_i = d_{\min} & \text{für } d_i \le d_{\min} \end{cases}$$

Here d denotes the orthogonal distance between a point (having the average point error σ_d) and the model and μ_d denotes the mean value of all distances per raster cell. This measure includes the distance, the accuracy and the amount of points in one raster cell. In order to prevent that a single point, which is close to the plane, obtains a very large weight, the minimal distance $d_{\min}$ is set additionally. This value should be chosen in the range of the best expected point accuracy (or larger) and limits the maximum weight of a single point. The threshold to decide if a (quadratic) cell verifies the construction part is calculated by

$$S_M = \left(\frac{x_r}{\delta_d \cdot p_d} \right)^2 \cdot \frac{1}{\sigma_{3D}} \; .$$

Here p_d denotes the expected point density (represented by the distance of two adjacent points), δ_d denotes the tolerated distance to the plane and σ_{3D} denotes the required point accuracy. Generally it cannot be assumed that the complete construction part is covered with points, e.g. because of occlusions caused by a scaffold or construction machines or because of limited acquisition positions. Because of this a simple threshold on the percentage of verified cells cannot be used to refuse a part, but a high percentage can be used to confirm it.

2.4 Test scenario

As test scenario a construction site of a multistory building in the inner city of Munich was chosen. An overview of the construction site is shown by an image taken from a stationary crane camera (Figure 1a). The photogrammetric image acquisition of different construction states are made without any disturbance of the building activities. Figure 1b shows the positions of all 80 images taken for a certain time step. The used sensor is an off-the-shelf digital single lens reflex camera (Nikon D3), which was calibrated in advance. In Figure 1c the state of the model for a certain time step and in Figure 1d the acquired point cloud can be seen.

The orientation of all images has been determined by a bundle adjustment together with the images of previous time steps. Control points have been extracted from a laser scan which was accomplished at the beginning of the execution of the construction work. The control points are defined by four rotatable signal disks which are mounted on stable concrete piles as well as defined by features on adjacent buildings. The point cloud was calculated from 213 stereo pair combinations and has about 25.000.000 points. The average point error is between 1-5 cm. Points with larger errors are not further considered.

The co-registration of point cloud and model is performed based on eleven control points on already built construction parts. The average residual of these points after the transformation is 1.9 cm (with a standard deviation of 1 cm).

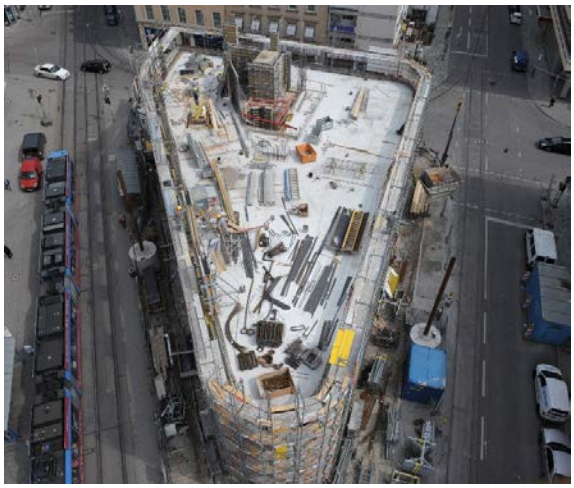

a)

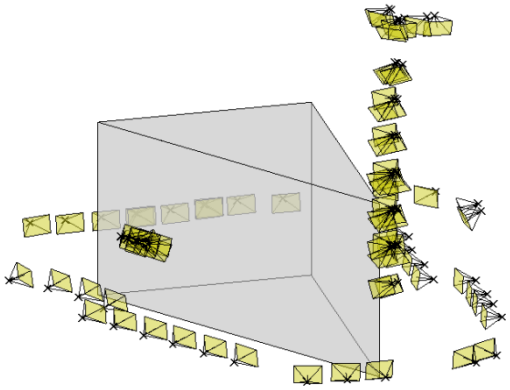

b)

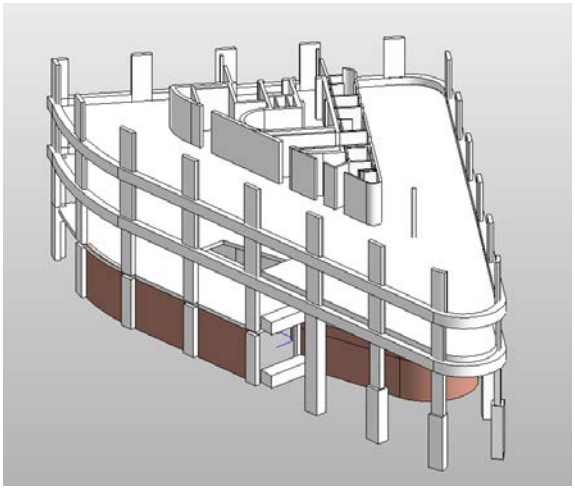

c)

d)

Figure 1: Construction site in Munich, Germany, TUTTAS et al., (2014).
a) View from the monitoring crane camera (stationary), b) camera positions for temporary acquisition, c) building information model (BIM) showing intended construction progress on step 42 (May, 2013), d) reconstructed point cloud from photos taken in May, 2013.

2.5 Experiments

The verification step is tested on a small part consisting of 13 construction parts. The surrounding of the test area can be seen in Figure 2a without model and in Figure 2b with the model. The area marked with a red rectangle in this figure contains the 13 construction parts, which are shown in detail in Figures 2c and 2d. In Figure 2c the points extracted with the threshold Δd = 5 cm can be seen. In Figure 2d these model parts, which are verified by the introduced measure M, using a raster size x_r = 10 cm, are marked in red. For the calculation of the threshold S_M the following values are chosen: p_d = 2 cm for the point distance, δ_d = 2 cm for the tolerated distance, σ_{3D} = 1 cm for the point accuracy and d_{min} = 0,5 cm for the minimal distance.

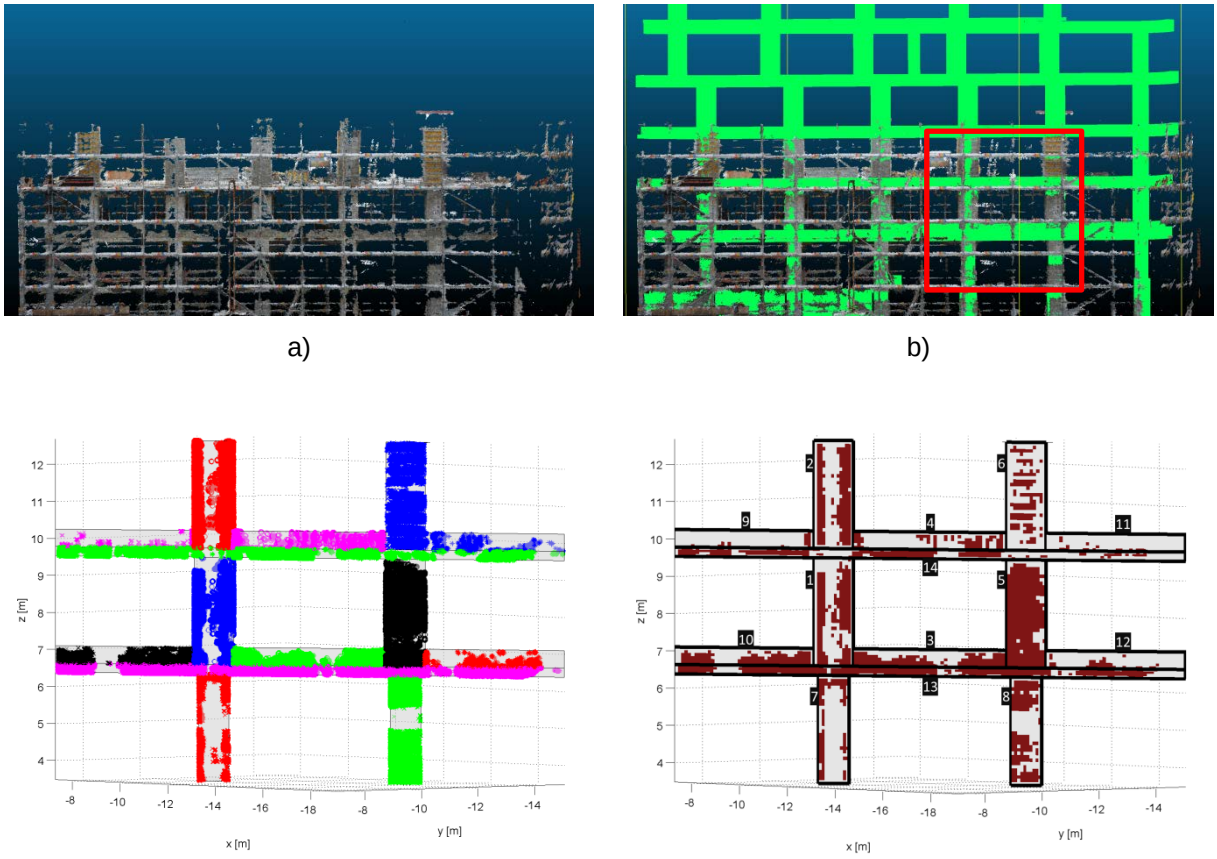

Figure 2: Comparison of model and point cloud, Tuttas et al., (2014). a) Point cloud, b) points together with model, c) extracted points assigned to building component (different colors show assignments to different components), d) confirmed areas (red) of the building components (1 to 13) by reconstructed points from photogrammetry.

3 EXAMPLE II: CHANGE DETECTION IN URBAN AREAS

For ALS data acquisition and analysis two different stages are distinguished. In stage I a database (reference) for time step (t_1) is built up and a 3D voxel grid that covers the complete urban area is filled with information. During stage II it will be decided whether current ALS measurements (t_2) confirm or contradict this information in the database. Instead of evaluating the occupancy of space for the voxels themselves, the grid structure is used only to store information on the proximity of laser beams (and points). Once established, this data structure enables to identify all candidates of old laser range measurements that may interfere with a new one. Furthermore, the cell size can be chosen comparatively wide (e.g., five times the average point-to-point distance), resulting in a moderate amount of data. Since the grid is only used as a search structure, the selection of the cell size has only minor impact on the results.

3.1 Generation of the database

Reference data captured at time step t_1 contain the classified and co-registered laser measurements L of multiple overlapping ALS stripes. For each point $\boldsymbol{p}_i$ the sensor position $\boldsymbol{p}_N$ and the range vector $\boldsymbol{r}$ are known. For storing the indices in the 3D space two voxel grids V_P and V_R with same size are defined. The cells of both grids are filled with indices from L (see Figure 3). Each index i is included in a single cell of V_P according to the 3D position of the laser point $\boldsymbol{p}_i$ that corresponds to this index. Therefore, V_P simply represents a rasterization of the point cloud. Beyond that, V_R is used to store all indices of laser beams that traverse the voxels. Each cell in V_P or V_R can receive either none, one or multiple

indices, depending on the number of laser points contained in this voxel, or depending on the number of laser beams that run through this voxel, respectively.

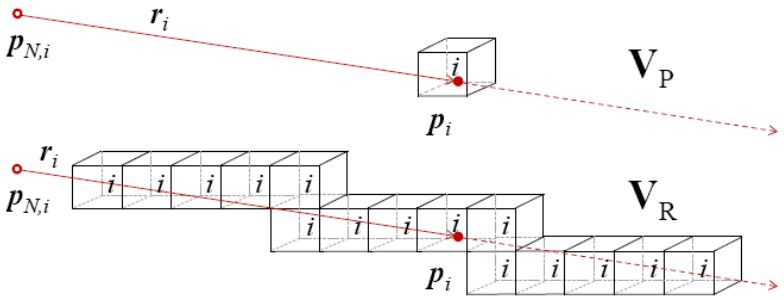

Figure 3: Filling the voxel grids V_P and V_R with indices for a laser measurement, i: index of the measurement, p_{Ni}: sensor position, p_i: laser point, r_i: direction vector.

3.2 Modeling the occupancy of space

For a laser measurement, the occupancy of space can be assumed as *empty* between sensor and laser point, as *occupied* at the laser point itself, and as *unknown* behind the laser point in direction of the ray. In case multiple laser measurements are related to the same area in space, the question comes up how the different and probably contradicting information can be fused. A possible strategy for fusion is based on the evidence theory by DEMPSTER (1967) and SHAFER (1976) which explicitly handles the state of uncertainty or vagueness. The application of this theory has some advantages for the here mentioned nexus: On one side the uncertainty or vagueness allows to model occlusions and the resulting lack of information. On the other side the combination rule of Dempster allows to assess conflicts of information which is interesting for automatic change detection. The space occupancy using the Dempster-Shafer approach can be described by functions assigning each element a so-called 'belief mass' in the interval [0,1]. Figure 4 shows the spatial modeling of point $\boldsymbol{q}$ with transversal and longitudinal distance (d_x,d_y) related to a laser measurement $\boldsymbol{p}$ for the states *occupied*, *empty* and *unknown* by the mass functions $m_{q,p}(\{occ\})$, $m_{q,p}(\{emp\})$, and $m_{q,p}(U)$. In this model the three parameters (λ,c,κ) determine the uncertainty of the laser beam and the points and have to be chosen according to the physical properties and technical limitations of the ALS measurements (for details see HEBEL & STILLA, (2012)). Especially $m_{q,p}(\{occ\})$ should be designed regarding the acquired point density and position accuracy which depend on the range resolution of the laser scanner, the accuracy of the scan, and the size of the laser footprint.

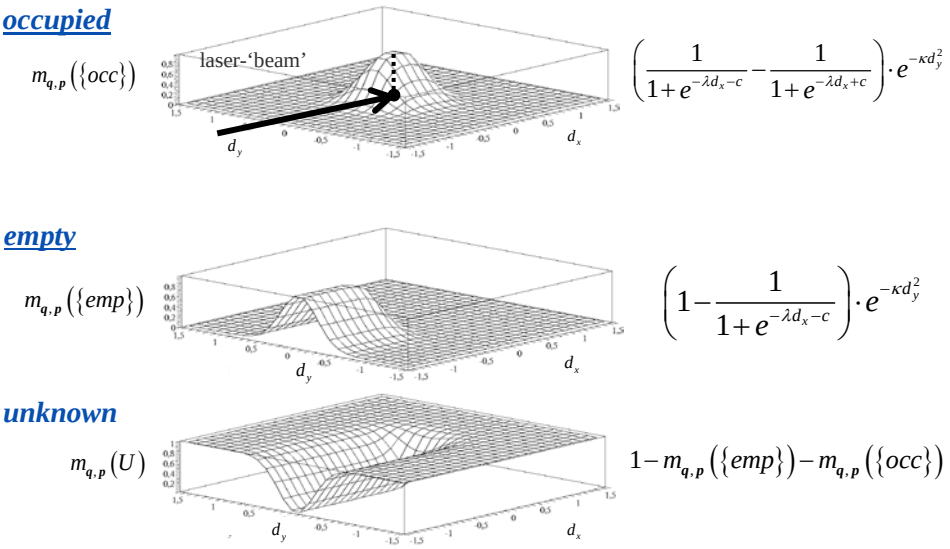

Figure 4: Belief masses *occupied*, *empty* and *unknown* in the surrounding *q* near the laser point *p*

3.3 Combination of evidences

In case of two or more laser beams which come across in the surrounding of $\boldsymbol{q}$, the corresponding mass assignments have to be combined. For calculation of a fused mass function the combination rule of DEMPSTER (1967) is used. For instance, a conflict C caused by two independent laser measurements $\boldsymbol{p}_1$ and $\boldsymbol{p}_2$ (*empty* in m_1 and *occupied* in m_2, or *occupied* in m_1 and *empty* in m_2) is calculated by $C = m_{q,p1}(\{emp\})\ m_{q,p2}(\{occ\}) + m_{q,p1}(\{occ\})\ m_{q,p2}(\{emp\})$. Further details can be found in the paper of HEBEL et al. (2013).

3.4 Detection of changes by space conflicts

During the phase of comparisons at time step t_2 the previous defined model of space occupancy is used to assess whether a new single ALS measurement $\boldsymbol{q} = \boldsymbol{q}_N + \boldsymbol{r}_q$ confirms or contradicts the existing mass assignments in space. In this context 'existing assignment' means the local combination of mass functions which stem from ALS measurements of the reference data at time step t_1. Changes in the scene will be visible as contradictions or conflicts in space occupancy. Such conflicts occur in two cases, namely, if the laser beam $(\boldsymbol{q}_N, \boldsymbol{r}_q)$ traverses a volume in space which is marked as occupied (Figure 5b) or if a laser point $\boldsymbol{q}$ is measured in a volume in space which should be empty (Figure 5a).

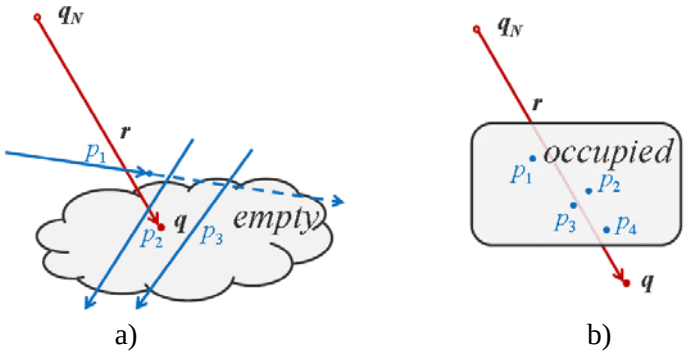

a) b)

Figure 5: Conflicts between reference data (blue) and the current measurement (red).
a) Conflict *Cq*: A new measurement gives a laser point *q* in a space which is labeled as *empty*,
b) Conflict *Cp*: A new measurement $q=q_N+r_q$ (laser-'beam') traverses an *occupied* space.

3.5 Considering additional attributes

In the current beam model it was not considered that objects may lead to multiple reflections based on discontinuities of the surface or due to a small size. In case of a partial penetration of vegetation a single pulse will label same places along the measuring direction as *occupied* and *empty*. These conflicts will occur also using different laser measurements of the same unchanged space of the vegetation. Furthermore, vegetation is subject to seasonal changes. If the detection of such changes is of minor importance, it is advisable to treat vegetation in a different way than ground level, buildings, or other man-made objects. Besides full waveform analysis REITBERGER et al., (2010), local principal component analysis (PCA) and region growing HEBEL & STILLA, (2012), YAO et al., (2010) are common approaches to classify ALS points belonging to vegetation. For these measurements an additional weighting factor is derived from local PCA that increases the amount of $m(U)$. Additionally, a special uncertainty is considered for this space.

3.6 Experiments

The data that we analyzed for this study were acquired during field campaigns in 2008 and 2009, using a laser scanner (RIEGL LMS-Q560) in combination with an inertial navigation system (Applanix POS AV 410). With our configuration and settings, each scan line of the laser scanner covered a field of view of 60° subdivided into 1000 angular steps. The laser scanner was set to a forward looking inclination angle (45°) and acquired strips with a width of 500 m and an average point-to-point distance of 0.5 m. The cell size of V_R and V_P was chosen to be $2\times2\times2$ m^3, resulting in two cell arrays of the dimensions $300\times300\times50$ (which corresponds to $600\times600\times100$ m^3) to cover the area in question.

In April 2008, the test site Abenberg (Bavaria) was covered by four strips in a cross pattern, resulting in an accumulated point cloud which includes 5,400,000 points with an average point density of 16 pts/m^2. Fig. 6a shows a rendered visualization of these reference data, where each point is gray-value coded according to the echo amplitude, which is derived from full waveform analysis of the backscattered pulse.

a) Reference data: Abenberg, 18.04.2008

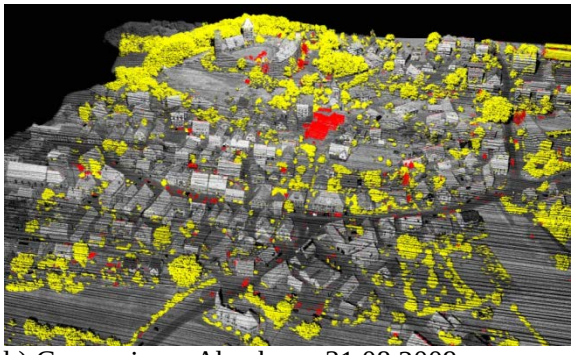

b) Comparison: Abenberg, 31.08.2009

c) Details Abenberg (2008):

d) Details Abenberg (2009):

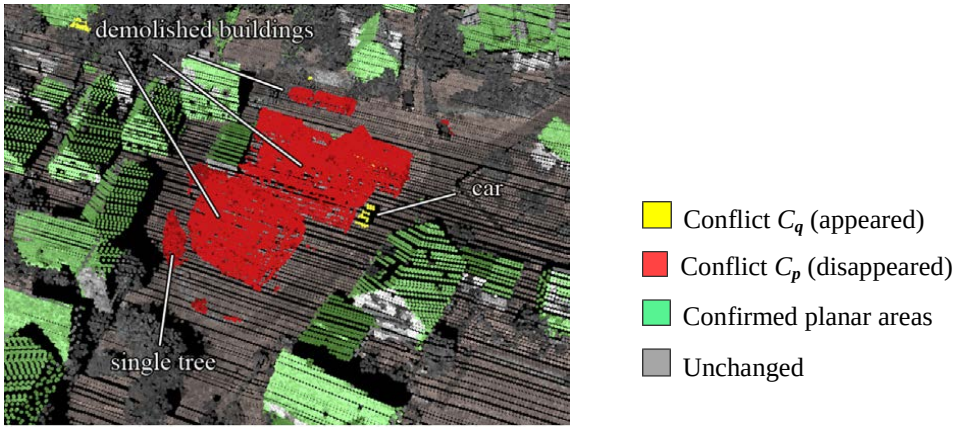

e) Considering additional attributes

Figure 6: Results and different types of detected changes: e.g., demolition of buildings, new car.

The test site was scanned again in August 2009, using the same sensors and a similar setting. Based on the recorded data stream of a single strip from south to north (1,500,000 points), we successively applied the methods described in the previous sections. The parameters of functions shown in Figure 4 were set to λ=12, c=5 und κ=8. Figure 6b shows conflicts $C_p \geq 0{,}5$ (objects that have disappeared) in red and the conflicts $C_q \geq 0{,}5$ (objects that have appeared) in yellow. In this example, vegetation obviously causes a lot of conflicts C_q, which can be ascribed to seasonal influences (April vs. August). In case we want to focus on man-made changes, according to section 3.5 additional attributes and a

classification of reference data into *ground*, *vegetation*, and *building* can be used to reduce changes induced by vegetation. Such a result is shown in Figure 6e. In addition to the previous color-coding, green points now indicate that these are (most likely) part of an unchanged building. The remaining conflicts are mainly caused by moved cars, newly constructed and demolished buildings.

4 CONCLUSION

Both examples show procedures for monitoring the persistence or detection of changes concerning urban objects. Both solutions are based on point clouds, but depend on typical border conditions for the domain and the type of comparison. Generally, the consideration of uncertainties for the comparison plays an important role. While for the example described in Chapter 3 uncertainties are already modelled by Dempster-Shafer theory, the change detection in Chapter 2 needs to be further developed by considering visibility and uncertainties in the next working steps. Related work concerning change monitoring of 3D building elements using point clouds from unordered images sequences and building information models (BIM) was carried out by GOLDPARVAR-FARD et al. (2011). For determining the progress of the construction process a probabilistic approach within a voxel data structure was used. In further work it should be investigated to which extent the strategy described in Chapter 3 can be adapted to the problem described in Chapter 2. A comparison of pros and cons with the related work is intended.

REFERENCES

Books:

DEMPSTER A: *Upper and lower probabilities induced by a multivalued mapping*. Annals of Mathematical Statistics, 38 (2): 325-339.,1967

HEBEL M, STILLA U: *Simultaneous calibration of ALS systems and alignment of multiview LiDAR scans of urban areas*. IEEE Transactions on Geoscience and Remote Sensing, 50(6): 2364-2379. [doi: 10.1109/TGRS.2011.2171974], 2012

SHAFER G: *A mathematical theory of evidence.* Princeton University Press, 1976

YAO W, HINZ S, STILLA U *Automatic vehicle extraction from airborne LiDAR data of urban areas aided by geodesic morphology*. Pattern Recognition Letters, 31(10): 1100-1108. [doi: 10.1016/j.patrec.2010.02.006], 2010

Journal articles:

GOLPARVAR-FARD M, PEÑA-MORA F, SAVARESE S: *Monitoring changes of 3D building elements from unordered photo collections*, Computer Vision Workshops (ICCV Workshops), 2011 IEEE International Conference on, p. 249-256., 2011

HEBEL M, ARENS M, STILLA U: *Change detection in urban areas by object-based analysis and on-the-fly comparison of multi-view ALS data*. ISPRS Journal of Photogrammetry and Remote Sensing 86 (2013): 52–64. [doi: 10.1016/j.isprsjprs.2013.09.005], 2013

REITBERGER J, SCHNOERR Cl, KRZYSTEK P, STILLA U *3D segmentation of single trees exploiting full waveform LIDAR data*. ISPRS Journal of Photogrammetry and Remote Sensing, 64(6): 561-574. [doi:10.1016/j.isprsjprs.2009.04.002], 2009

ROTHERMEL M, WENZEL K, FRITSCH D, HAALA N: *SURE Photogrammetric surface reconstruction from imagery*. LC3D Workshop, Berlin. 2013

TUTTAS S, STILLA U: *Reconstruction of rectangular windows in multi-looking oblique view ALS data*, ISPRS Ann. Photogramm. Remote Sens. Spatial Inf. Sci., I-3, p. 317-322. [doi: 10.5194/isprsannals-I-3-317-2012]., 2012

TUTTAS S., STILLA, U: *Reconstruction of façades in point clouds from multi aspect oblique ALS*, ISPRS Ann. Photogramm. Remote Sens. Spatial Inf. Sci., II-3/W3, p. 91-96, 2013. [doi: 10.5194/isprsannals-II-3-W3-91-2013]., 2013

TUTTAS S., BRAUN A, BORMANN A, STILLA U: *Konzept zur automatischen Baufortschrittskontrolle durch Integration eines Building Information Models und photogrammetrisch erzeugten Punktwolken.* 34. Wissenschaftlich-Technische Jahrestagung der DGPF e.V. 2014

Links:

ROTTENSTEINER F, STILLA U, HINZ S (2013) CMRT13 – City Models, Roads and Traffic 2013. ISPRS Annals – Volume II-3/W3, 2013 http://www.isprs-ann-photogramm-remote-sens-spatial-inf-sci.net/II-3-W3/, last accessed on March 10, 2014

TUM-LOC *Leonhard Obermeyer Center - TUM Center of Digital Methods for the Built Environment.* http://www.loc.tum.de , last accessed on March 10, 2014

Technical Session 2: Geodetic Monitoring of Industrial Objects

Basic Principles of Geoinformation Solutions for Safe Operation of Nuclear Power Plants (NPPs)

Alexander P. Karpik, Alexey V. Dubrovsky
Siberian State Academy of Geodesy, Russian Federation

Abstract
The article describes practical experience of providing the situational center with a set of geographic maps of the Russian NPP territories. There are examples of finished products and possible ways of its use when monitoring the territory, the organization of emergency response measures and elimination of the NPPs possible accidents consequences.

Keywords
Geoinformation solutions, nuclear power plants (NPPs), evacuation plans, digital maps.

The origin and extension of emergency situations depends on many factors. These factors, in turn, are caused by different objects, processes and phenomena, taking place on the Earth's surface, in geological and space environments DUBROVSKY (2010). Emergency of catastrophes on a global scale are usually multi-environmental. During a short period of time the emergency geospace (geoenvironment) can undergo significant changes, both qualitatively and quantitatively DUBROVSKY (2012). Technogenic natural-territorial complexes of NPPs appear to be the areas of possible radiation catastrophe and territories experiencing protracted influence of anthropogenic radiation contamination KOLTIK (1997). Such a dual territories condition requires a particular approach to their use and organization of a continuous monitoring system. One of the elements of the monitoring system is a monitoring subsystem for radiation polluted lands in the area of NPPs.

According to two largest nuclear disasters – on the Chernobyl NPP (USSR, 1986) and Fukushima NPP (Japan, 2011), the governments and emergency services of these countries weren't prepared for catastrophes of such a scale. On-line mapping of radiation situation remains one of the many technical issues while liquidating the accidents consequences at NPPs. Data received from the radioactive contamination monitoring were processed for a long time and their use was not possible because of the absence of geoinformation provision that could meet the requirements of urgency, accessibility and universality in the area of NPP.

The term "geoinformation solutions" denotes the new kind of activity, that is developing on the basis of computer technologies and that is developed to meet economic and social needs in geo-information for a particular territory by means of its collection, modeling of geoenvironment, spatial analysis, preparation of spatial solutions, integration and dissemination by means of GISs. KARPIK (2004)

Up-to-date development of GIS technology allows carrying out various types of thematic digital mapping projects. The government policy is oriented to early warning of crisis management, that's why the development for modeling, analysis and prevention of emergency situations is very urgent.

Up-to-date means of spatial data acquisition contribute greatly to the development in this field. First of all, they space mapping systems and various sensors, including those integrated with the technologies of global navigation satellite systems (GNSS) that are used for monitoring the health of industrial facilities and the condition of natural objects.

Geoinformation solutions for crisis management can be divided into three main types DUBROVSKY (2012):

- timely and dynamically changing monitoring data of spatial objects condition;

- predictive spatial analytical models that describe various scenarios of crisis situations and elimination of their consequences;
- statistical spatial-situational models of crisis management.

While organizing crisis management of industrial objects of a high hazard level, such as NPP, these types of geoinformation solutions are used.

The continuous space monitoring of an object and the neighboring territory condition is provided in a dynamic mode. Sensor-based mapping systems, including GNSS, provide control of the object geometric characteristics. Up-to-date robotized electronic total stations with GLONASS/GPS enable to monitor the condition of objects and pick up the slightest changes of their spatial characteristics. The Automated System for Monitoring Radiation Situation (ASKRO) in constant stream mode provides the information about the radiation level.

Predictive spatial analytical models describe various scenarios of crisis situations. Thus, it is important to create the most complete list of situation development options and its possible consequences. Different mathematical models and analytical data on earlier crises are used to fulfill these tasks. As a rule, these models created are ranked in accordance with the possibility of their origin and the amount of damage, etc. SVERD (2005), DUBROVSKY (2010). Received data from ASKRO enable to approximately assess the land condition pollution.

The third type of geoinformation solutions for crisis management (that is statistical spatial-situational models) is based on the created emergencies scenarios. These models of a generalized character serve for efficient crisis management when they emerge. As an example, the simplest situational models are the plans of people evacuation of from buildings, and the more complicated plans are those of population evacuation from the regions affected by radioactive contamination in case of accidents at NPPs), Figure 1.

The peculiarities of this plan are the following:

- combined representation of thematic symbols and digital topographic map on the territory integrated territory plan ;
  the fragment of a digital map limited by 100 kilometers zone around NPP that is used as a topographic substrate. Territories of several regions of the Russian Federation may belong to this zone. Foreign territories can be shown on a map if necessary;
- all thematic information without any generalization is plotted on the evacuation plan;
- except the main evacuation plan of scale 1:100,000, the industrial zone of NPP and the residential area near the station are shown in the form of insert maps in a larger scale. To compile insert maps, satellite images or airphotoplans of high resolution can be used.

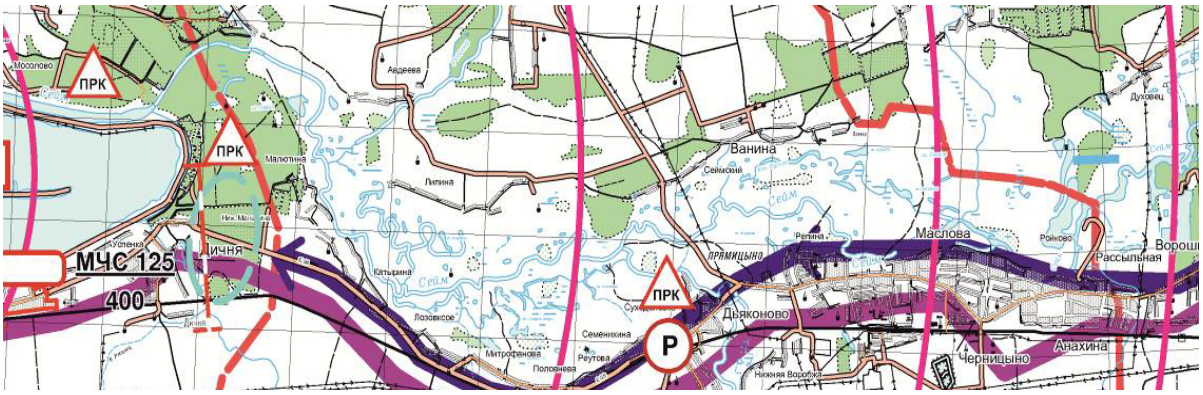

Figure 1 Fragment of digital evacuation plan from NPP area.

The following results have been achieved:

- digital maps (in vector form) of ten Russian NPPs locations of scale 1:200000 and 1:100000 (respectively 100 and 30 km area) can be published in GIS MapInfo format;
- separate thematic map layers of 10 Russian NPPs that are used for planning and carrying out measures to eliminate accidents consequences at nuclear power plants have been prepared;
- electronic layouts of 100 and 30 km area near Russian NPPs are prepared on the basis of digital maps and separate thematic layers;
- rigid map tablets in the amount of 40 pieces, representing NPPs locations of scale 1:200,000 and 1:100,000 (respectively 100 and 30 km area) have been made;
- four map-cases and six wall sets for hanging tablets have been made.

Evacuation plans were introduced at the situation center. Metal-base evacuation plans nowadays represent the key element of the emergency management center's technological infrastructure, Figure 2.

Figure 2: Wall maps in the emergency operations center.

The digital plans of NPPs area can be used while conducting geoinformation analysis and modeling, for the following:

- to interpolate the contamination according to ASKRO sensors data (Figure 1 a);
- to detect automatically the number of polluted settlements and their citizens in the constructed buffer zone (Figure 3 b);
- to model radiation contamination depending on the wind speed and its direction (Figure 3 c);
- to generate reports for evacuation echelons routes (Figure 3 c) SVERD (2005);
- on-line updating the evacuation plans.

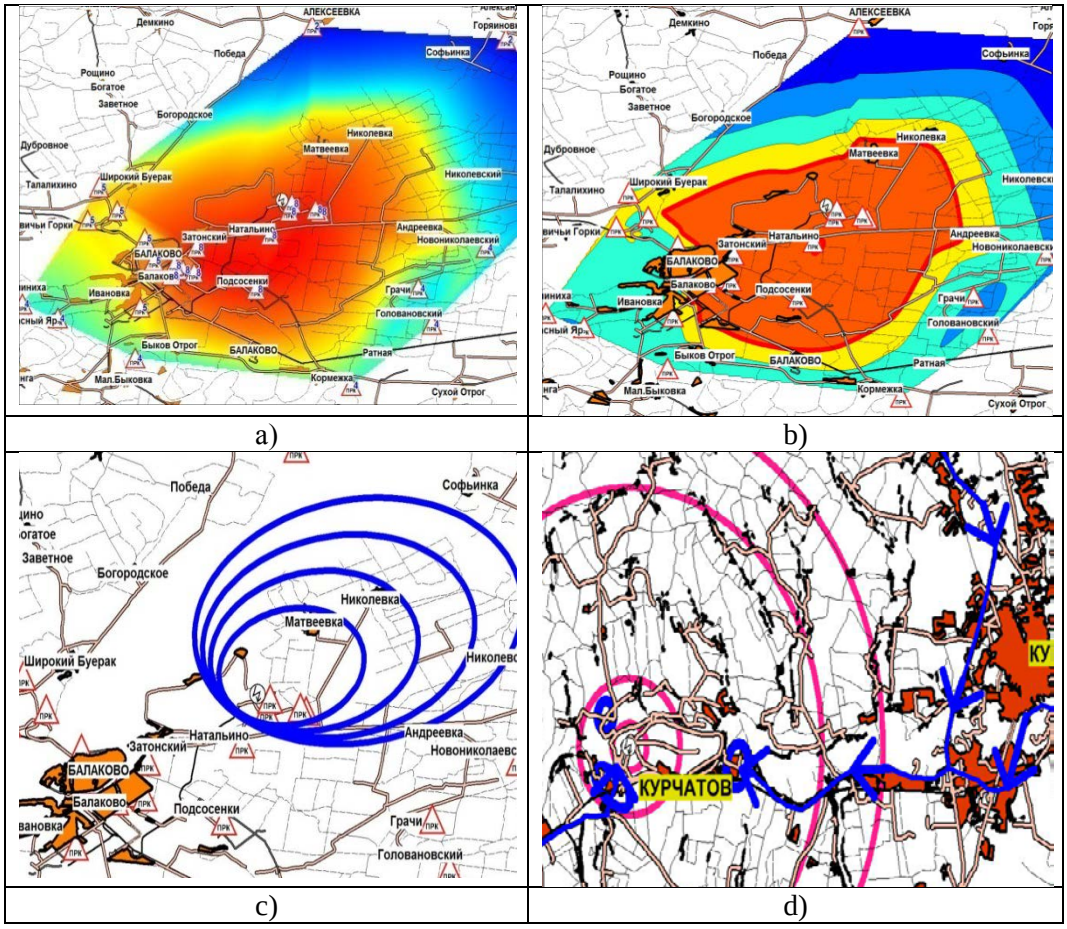

Figure 3: Examples of GIS analysis and modeling with digital evacuation plans of NPP area: a - interpolation of contamination according to ASKRO sensors data ;b - construction of polluted buffer zone; c - modeling of radiation contamination depending on the wind speed and its direction;d – reports generation of evacuation echelons routes.

GIS technology for territory monitoring near NPPs represents a complex system of interacting elements. The geoinformation land monitoring in the area of NPP except for its main functions: “monitoring, analysis, forecast and management” TSVETKOV (2005), has some peculiarities:

- it controls the radiation situation in the area of NPP, which is part of a unified state environmental monitoring system (USEMS) ;
- monitoring faces some problems connected with negative factors of radiation contamination;
- borders of the monitoring zone coincide with those of emergency situation geoenvironment and they change dynamically due to the degree of radiation influence of various factors;
- the life and health of people who don’t only live in the region monitored , but also use food produced in this region depends on the efficiency and reliability of land monitoring data;
- geoinformation basis of land monitoring must contain the systematized complex of the region (territory) data about various groups of spatial objects, processes and phenomena;
- the effectiveness of the monitoring depends on the information exchange comprehensiveness between the land monitoring system and the monitoring systems controlling the condition of such environments as water, air, geological.

Figure 4 shows the enlarged scheme of geoinformtion monitoring in the area of NPPs.

The fully-functional system of GIS collection, representation, analysis and predictive modeling with the ability of transferring the received data to the competent services and agencies to control the situation must be a basic component of the monitoring system in the area of NPPs.

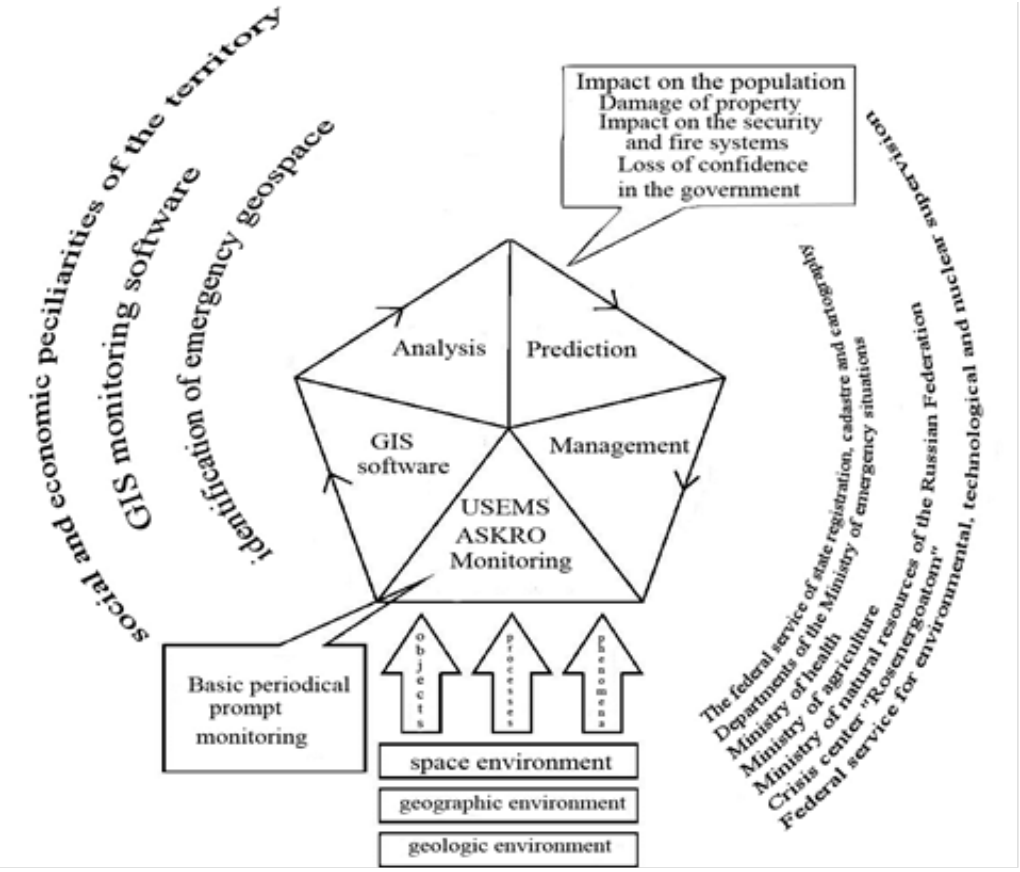

Figure 4: Generalized scheme of GIS monitoring in the area of NPPs.

Thus, the basic principles of geoinformation solutions for the NPPs safe maintenance are the following:

- to create the network of active base stations to organize high-precision satellite positioning system, to increase the accuracy of geodetic measurements and to control the NPP technological fcilities;
- to develop and introduce the high-precision coordinate system of NPP;
- to create the unified GIS basis in the area of NPP, including large-scale digital plans of NPP industrial site and the residential area near the station (the scale is 1:100 - 1:1 000); digital maps of a sanitary protection zone (at scale 1:10,000); digital maps of 30 km monitoring zone (at scale 1:100, 000); digital maps of 100 km evacuation zone (at scale 1:200,000) KARPIK (2013);
- to create spatial 3D models of technological objects and the machinery at NPPs that are digitally integrated into unified GIS basis (environment) of a given territory;
- to create the complex monitoring system of the area near NPP, including geodetic monitoring system, hydrometeorological observations, automated system of radiation control, the environmental control system. Information received from various sensors must have a coordinate referencing and is to be integrated into the unified GIS basis of a given territory;

- to develop the mobile navigation software to solve the problems of emergency response, navigation, mapping the NPP territory, the increase of geodetic measurements accuracy;
- to introduce the GIS and create the automated workstations (AW) in the departments of NPP office, situation center, Municipal Bodies administration of NPP area, Civil Defense and Emergencies divisions;
- computer simulation modeling of probable emergencies scenarios of natural and technogenic character;
- to develop catastrophe (accident) – prevention plans and evacuation measures with a GIS application.

Figure 5 shows the interaction scheme of basic principles of geoinformation solutions for the NPPs safe maintenance.

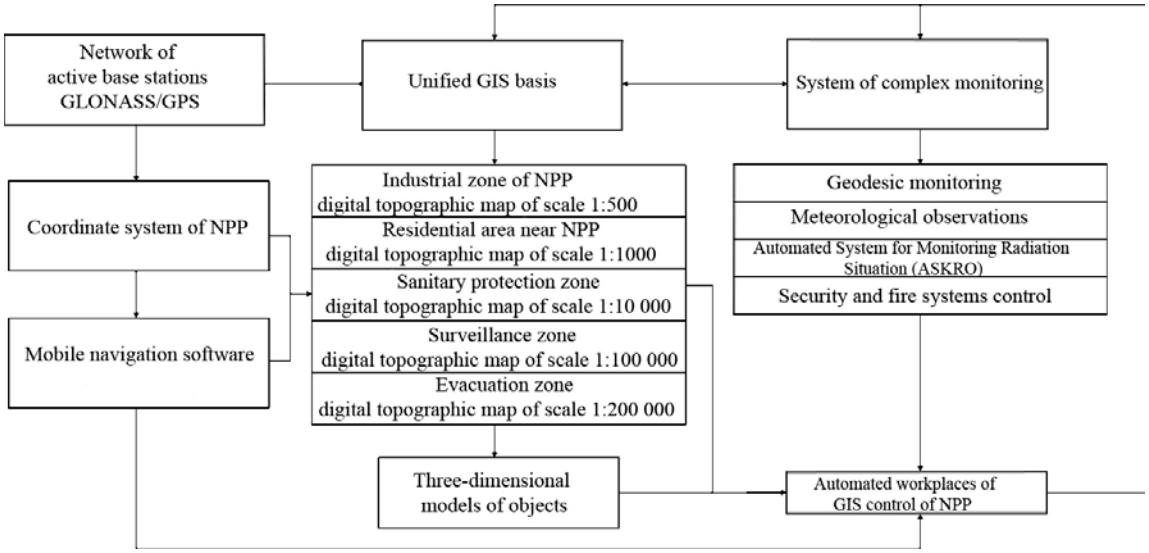

Figure 5: Interaction scheme of basic principles of geoinformation solutions for the NPPs safe maintenance.

Specialists from the Siberian State Academy of Geodesy (SSGA) have developed methodological and technological approaches to realize basic principles of geoinformation solutions for the NPPs mentioned above. Our developments in the field of geoinformation solutions have been tested and successfully implemented in a complex of works carried out at the Leningrad, Kursk, Beloyarsk NPPs. Geoinformation solutions for catastrophe (accident) – prevention plans and evacuation measures developed by our specialists is nowadays widely used at all Russian NPPs.

References

Books:

DUBROVSKY, A.V. *Cadastre and Land Information Systems* [Text]: methodical manual / A.V. Dubrovsky. – Novosibirsk: SSGA, 2010.-112 p.

KOLTIK, I.I. *Development of methodical principles of radiation contamination assessment in the area of NPP (example of Beloyarsk NPP).* [Text] / I. I. Koltik. – Abstract - Yekaterinburg: 1997.

KARPIK A.P. *Methodological and technological fundamentals of geoinformaation solutions for a particular territory*: Monograph [Text] / A.P. Karpik – Novosibirsk: SSGA, 2004. – 260 p.

SVERD, H. *Analysis and risk management* [Text] / Hans-Ivar Sverd - Russian and European experience of using the complex coastal zone management model at the regional and municipal levels. Seminar materials. – Saint-Petersburg, 2005 – 74 p.

DUBROVSKY, A.V. *Geoinformation space research of a town for the people's life danger prevention* [Text] / A. Dubrovskiy // Early warning and crises/disaster and emergency management. – Novosibirsk: SSGA, 2010 – P. 118–124.

Journal articles:

DUBROVSKY, A.V. *Analysis of natural and technogenic peculiarities of emergency situation geospace* [Text] / A.V. Dubrovsky, A.P. Karpik, E.L. Kim / Interexpo GEO-Siberia - 2012. VIII International scientific congress, the 10-20th of April 2012, Novosibirsk: International scientific congress "Geodesy, geoinformatics, cartography, mine surveying": collection of works in three volumes. V.3. – Novosibirsk: SSGA, 2012 – p. 171-177.

DUBROVSKY, A.V. *Geoinformation solutions for early warning and crisis management*. [Text] Dubrovsky, A.V., Kim E.L. – *Collection of works. The international scientific Congress* "Sibsafety-Spassib-2012" the 25-27th of September 2012, Novosibirsk. – Novosibirsk: SSGA, 2012 - p. 51-56.

TSVETKOV, V. Y. *GIS monitoring* [Text] / V.Y. Tsvetkov - News of higher education institutions "Geodesy and Aerial Photography". – Moscow, 2005 - №5. - P. 151-155.

KARPIK A.P. *Geospatial Solutions Providing Access to Territorial Databases for Increasing the Quality of Surveying Works for the State Immovable Property Cadastre* [Text] / A.P. Karpik, V.I. Obidenko – Interexpo GEO-Siberia-2013. IX International scientific congress, the 15-26th of April 2013, Novosibirsk: collections of plenary papers– Novosibirsk: SSGA, 2013. – P. 1-9.

KARPIK A.P. *The Experience of Creating Evacuation Plans for Districts within Nuclear Power Station Areas.* [Text] / A.P. Karpik, A.V. Dubrovsky, Ya.G. Poshivaylo – Interexpo GEO-Siberia-2013. IX International scientific congress, the 15-26th of April 2013, Novosibirsk: collections of plenary papers – Novosibirsk: SSGA, 2013. – P. 45-54.

SAMOS Switching Antenna Monitoring System Applied on Tailings Reservoir On-Line Monitoring Project

Joel van Cranenbroeck[1], Karl You Xiangjun[2], Hans Ni Xiangjun[2]
[1]Creative Geosensing sprl-s, Belgium, Europa
[2]Beijing iSpatial Co Ltd, PR China

Abstract
Tailings reservoir has become the 19th state-level danger source of China government, which could cause permanent damage to the local environment and kill hundreds of thousands of people if the dam earthen made collapse.

SAMOS, Switching Antenna Monitoring System, is derived from GNSS, Global Navigation Satellite System (GPS, GLONASS and COMPASS/BEIDOI), which enables a single GNSS receiver to monitor more than just one monitoring point according to the specified accuracy requirement. This method helps to save lots of GNSS receivers while always keeping the high performance of accuracy and online monitoring features.

This paper introduces how Beijing iSpatial experts deployed that technology for a tailings reservoir dam online monitoring application and the practical performances of SAMOS and the software in a slow-deformation project.

Keywords
Tailings reservoir, online monitoring, SAMOS, Switching Antenna, GNSS monitoring, software, Kalman Filtering

1 ONLINE MONITORING SYSTEM FOR TAILINGS RESERVOIR

Tailings reservoir is a large pool which is usually built at the foot of mountain with long earthen dam to collect the waste material of metal ore dressing industry. There are more than 7 thousand normal tailings reservoirs, and nearly 5 thousand abnormal tailings reservoirs still running across the whole China.

This huge danger source has already been recognized and paid great attention by the China State Administration of Work Safety (SAWS) since 2006. Online monitoring system became an important technical support and handle for detailed administration measures It took years of technical investigations and pilot project, such 9 GPS for 700 meters Zhejiang Litie tailing reservoir and 44 GPS for 4.5km earth dam of Anhui MaSteel tailing reservoir, to finally qualify the concept.

GNSS monitoring system became then the indispensable online monitoring method to check the displacement of the earthen dam because of three important features of such system, all-weather supported, continuously operational 24/7 and high accuracy in displacement monitoring.

But due to the high cost of the high performance GNSS receiver and communication system to support huge amount of GNSS raw data transmission, GNSS online monitoring system is still nowadays an expensive technology considering the equipment for 12 thousand tailings reservoir dams. In fact the huge cost of the traditional GNSS installation is preventing the authority to invest and fulfil their obligations.

2 SAMOS – THE PARADIGM SHIFT IN GNSS MONITORING

SAMOS is an abbreviation of “Switching Antenna Monitoring System”, a professional GNSS monitoring system with innovative GNSS signal processing technology, which is specifically designed for high performance low cost GNSS monitoring solution, such as Hydro Power Dam, landslide, bridge, subsidence areas and high-rise building GNSS monitoring application to only cite a few.

In tailings reservoir dam monitoring case, the continuous processed observation represents every day a 3D displacement value for each monitoring point since the deformation of earthen dam is rather slow motion with total deformation range that can reach few centimetres.

Based on such application requirement, SAMOS offers a solution where there is no need to setup at every monitoring point a full pair of GNSS receiver and antenna but only one antenna per point of interest connected to a switch where only one GNSS receiver is attached. Using a timer, the switch can connect the GNSS receiver to a particular antenna and log the corresponding observations. When the quantity of observation has been reached, the switch disconnects the antenna from the GNSS receiver and automatically establishes the connection to another antenna. After a complete cycle, the switch is re-addressing again the entire antenna network. This solution can greatly mitigate the cost of the installation by reducing the number of high performance GNSS receivers.

3 THE ARCHITECTURE OF SAMOS

SAMOS system is selected for monitoring projects where a large amount of GNSS receivers is needed. The reference station remains mandatory but can easily doubled as the budget allows that.

SAMOS hardware system is designed with a number of GNSS antennas, a GNSS receiver connected to the switch, the switching hardware, the coaxial antenna cabling and at least one GNSS receiver base station. In that architecture, several switches can be placed for addressing specific group of GNSS antennas in a common project. The system is very scalable and modular. If monitoring points cannot fit with cabling connection, we can still setup the GNSS receiver and antenna pair like traditionally.

Figure 1: an example of SAMOS architecture

The length of the coaxial antenna cable can be extended up to 500 meters with special GNSS signal amplifier placed every 90 meters adding 29db signal gain each section.

GNSS signal is collected by GNSS receiver through the antenna switch from each antenna periodically under control of antenna switch timing system.

The raw GNSS data can be logged onto the SD card inside the GNSS receiver attached to the switching hardware in a survey campaign mode (for one or two days) and data post processing will be handled manually afterwards. The other possibility is the capacity of the system to transmit directly to the central monitoring software the data using any communication possibilities. IS-MonNet, runs on a PC server and access the data through serial com port or Ethernet LAN port the data to perform real-time or post processing automatically online with several parameters that the user will control.

Figure 2: GNSS antenna switch

Figure 3: GNSS signal amplifier

Figure 4: IS-X300M GNSS receiver

4 GNSS MONITORING SOFTWARE

SAMOS MonNet software is advanced GNSS kinematic positioning software developed by Shanghai iSpatial Co., Ltd., processing short to medium baseline length within millimetre level of accuracy and coping with switching antenna scheme.

The software uses epoch data to distinguish which data is from which antenna to organise the raw data's transmitted by the switch.

The ASW (average sliding window) method is applied.

The key for achieving high accuracy performances is to fix the ambiguities and for carrier-based relative positioning between a rover **r** and a base-station **b**, the following double-differencing measurement equations for **carrier phase Φ** and **pseudo range P** are used.

$$\phi_{rb}^{ij} = \rho_{rb}^{ij} + \lambda(B_{rb}^{i} - B_{rb}^{j}) + \varepsilon_{\phi} \quad (1)$$

$$P_{rb}^{ij} = \rho_{rb}^{ij} + \varepsilon_{P} \quad (2)$$

Where $()^{ij}$ and $()_{rb}$ represent a single-difference between satellites and between receivers, respectively, ρ is the geometric range, λ is the carrier wave length and ε is the measurement error of the observables. B_{rb}^{i} is the single-difference of carrier phase ambiguities in cycle.

We settle the unknown vector as:

$$x = \left(r_r{}^T, B_{L1}{}^T, B_{L2}{}^T\right)^T \qquad (3)$$
$$B_{Lj} = (B^1_{rb,Lj}, B^2_{rb,Lj}, ..., B^m_{rb,Lj})^T$$

Where r_r is the antenna position expressed in the ECEF frame.

The measurement vector y_k at epoch t_k is:

$$y_k = (\phi^T_{L1}, \phi^T_{L2}, P^T_{L1}, P^T_{L2})^T \qquad (4)$$

By using standard EKF (extended Kalman filter), the state vector **x** and its covariance matrix **P** can be estimated by:

$$\begin{aligned} \hat{x}_k(+) &= \hat{x}_k(-) + K_k(y_k - h(\hat{x}_k(-))) \\ P_k(+) &= (I - K_k H(\hat{x}_k(-)))P_k(-) \\ K_k &= P_k(-)H(\hat{x}_k(-))(H(\hat{x}_k(-))P_k(-)H(\hat{x}_k(-))^T + R_k)^{-1} \end{aligned} \qquad (5)$$

Where $h(x)$, $H(x)$ and R_k are the measurements vector, the matrix of partial derivatives and the covariance matrix of measurement errors, respectively.

For the standard deviation σ of carrier phase or pseudo range error, SAMOS employs an elevation-dependent model with user-defined parameters:

$$P = 2(a \cdot a + b \cdot b / \sin(e) / \sin(e) + c \cdot c \cdot bl) + C \cdot sclk \cdot dt \qquad (6)$$

Where the elevation angle of satellite is e, bl is the base-line length, C is the speed of light, dt is the time period. $a, b, c, sclk$ are user defined parameters.

Time update of the state vector and its covariance matrix from epoch t_k to t_{k+1} by EKF is expressed as:

$$\begin{aligned} \hat{x}_{k+1}(-) &= F_k^{k+1}\hat{x}_k(+) \\ P_{k+1}(-) &= F_k^{k+1}P_k(+)F_k^{k+1T} + Q_k^{k+1} \end{aligned} \qquad (7)$$

Where F is the transition matrix and Q is the system noise covariance matrix.

By solving the EKF formulas, the estimated rover antenna position and the single-differenced carrier-phase ambiguities are obtained. Then the float carrier-phase ambiguities should be resolved into integer values in order to improve accuracy and convergence time. The well-known efficient strategy LAMBDA and its extension MLAMBDA are used by the software. After the validation by the simple ratio-test, the fixed solution of the rover antenna position is provided.

5 THE YUANPING TAILINGS RESERVOIR IN SHANXI ROVINCE

SAMOS technologies has been used to connect 9 GNSS monitoring points as well as 9 Osmometer (An Osmometer is a device for measuring the osmotic strength of a solution, colloid, or compound) along a 2000 meters earthen dam length, which belongs to “Shanxi Aluminum Co. ltd, China Power

Investment Corporation (CPI)", in order to monitor both the displacement of dam and the water level inside the dam.

Z0 is the base point of the system and Z1 up to Z9 are monitoring points. Z0 and Z1 use common single antenna paired with one GNSS receiver. Z2 up to Z9 points are controlled by two data collection cabinet, with 4 GNSS points and osmometer devices for each. The data are transferred by RS232 or RS485 serial interface and then mapped into Ethernet signal to be transferred via optical fibre cables up to the central monitoring room.

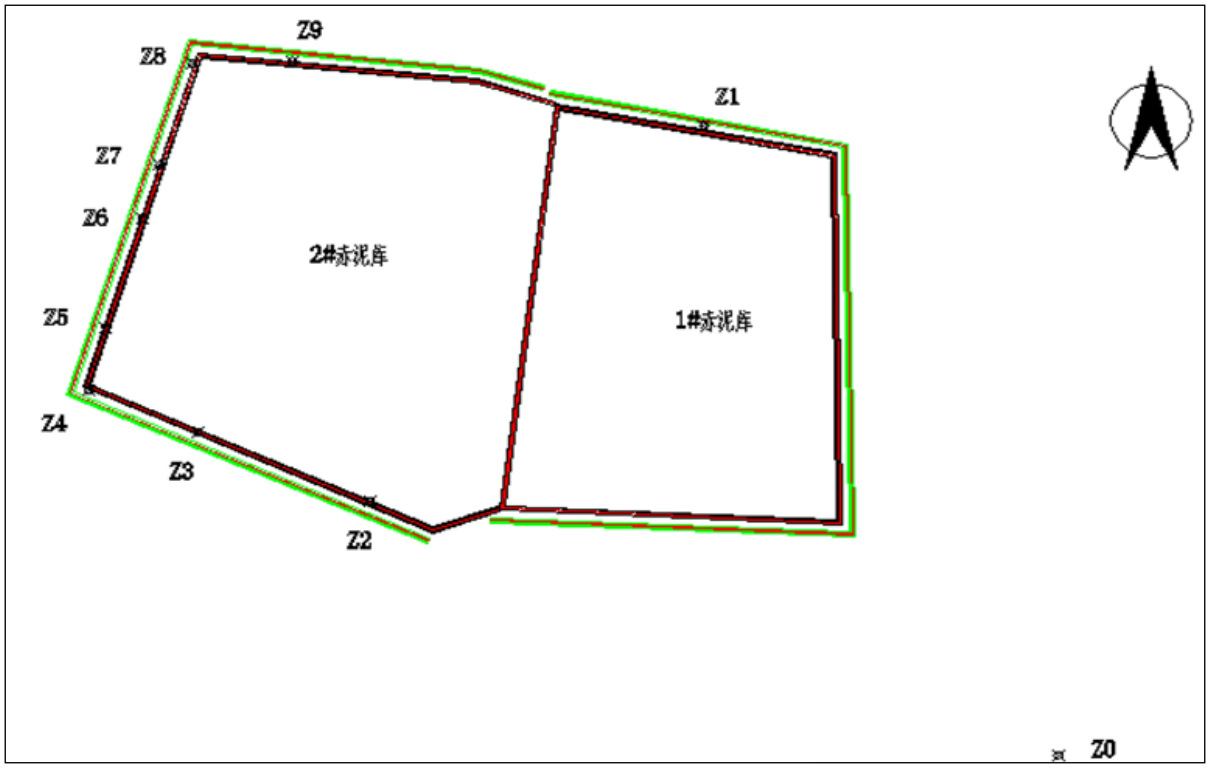

Figure 5: Overview of the point deployment

Figure 6: A view of this 2000 meter reservoir dam

Figure 7: Base point and the central monitoring room behind

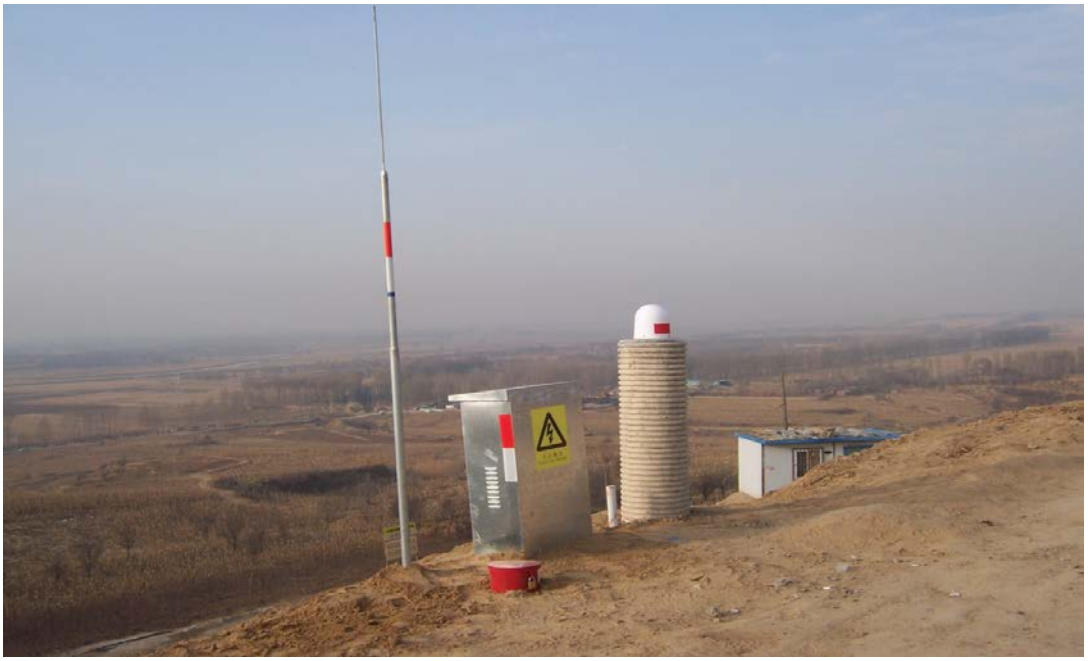

Figure 8: A typical switching antenna monitoring point with data collection cabinet and osmometer (red cylinder is the cover of osmometer pipe)

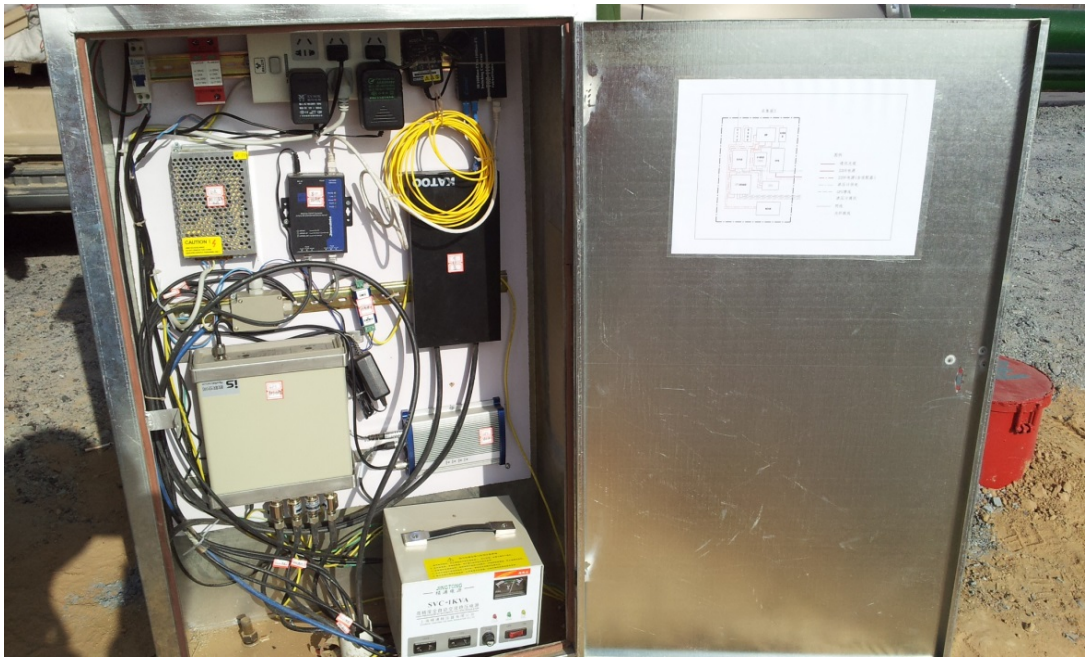

Figure 9: Data collection cabinet with antenna switch and all data communication, power supply, lighting protecting devices

Figure 10: Central monitoring room

Figure 11: Sensor management GUI

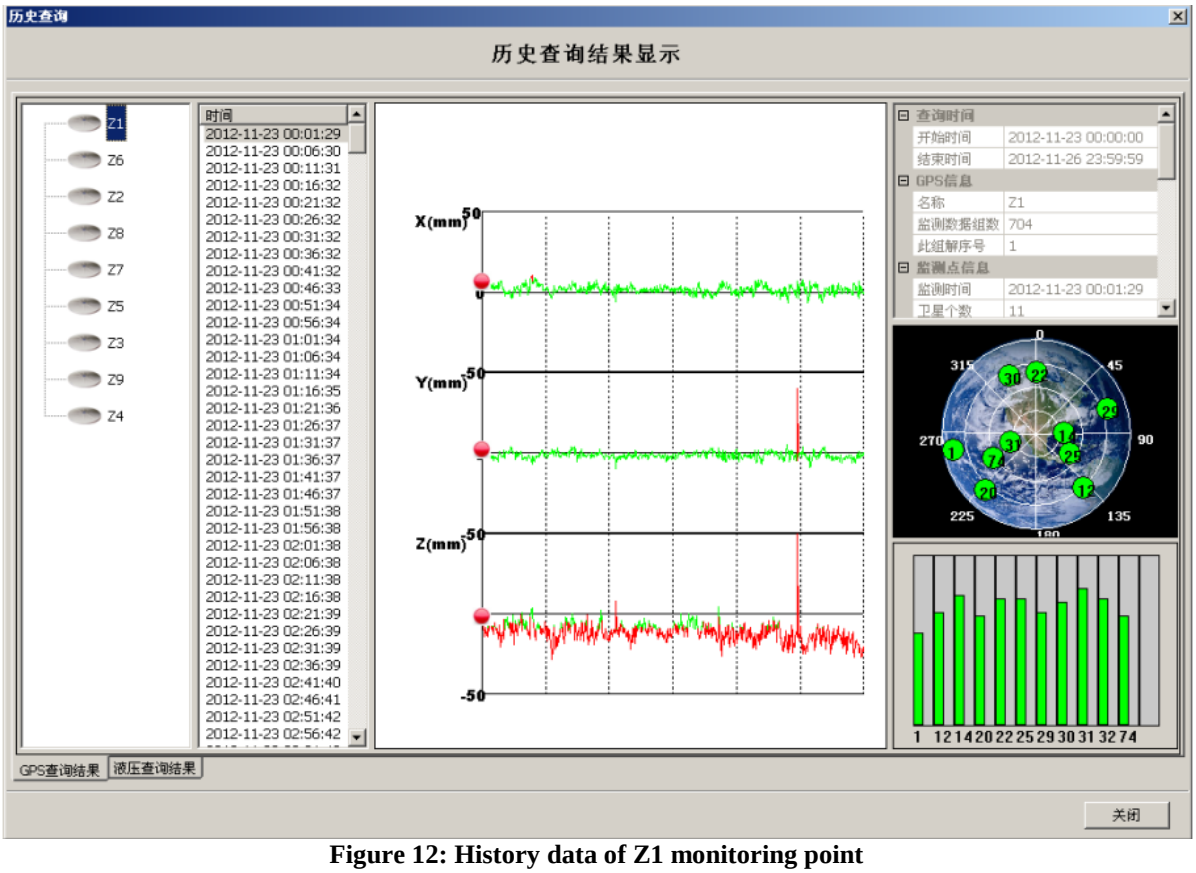

Figure 12: History data of Z1 monitoring point

6 CONCLUSIONS

SAMOS technology and software have been designed and developed to meet the expectations of managers and engineers in charge of maintaining engineering infrastructures situated in risky

environments with the need to have a full picture of the movements to feed deformation models and take appropriated decision accordingly to the feedback of the system.

The “Switching Antenna Monitoring System” namely SAMOS has been developed with the highest quality of technology and know-how and by specialists in GNSS hardware and firmware technology. The software that is part of the complete system has proven to deliver on a 24/7 rate the best linear unbiased estimators using advanced filtering techniques on mm level of accuracy.

Without any comprise on accuracy, the switching antenna system has demonstrated on many other projects such hydro power dams, landslides and subsidence areas that monitoring solutions can and must be affordable when respect to human live and environment are the concern.

The authors have no doubt that more and more engineers involved or confronted to permanent monitoring of their infrastructures will consider SAMOS as the most appropriated solution to get high accuracy results at an affordable budget level.

Geodetic Monitoring of Gravity Dam Deformations on the Malo-Ulbinsky Reservoir

Kaisar B. Khasenov[1], Marzhan. Y. Rakhymberdina[1], Kulzina M. Kaleeva[2]
[1]D. Serikbayev East Kazakhstan State Technical University, Republic of Kazakhstan
[2]S. Amanzholov East Kazakhstan State University, Republic of Kazakhstan

Abstract
Assessments of major engineering structures during the operational period, which include hydraulic structures, can be obtained only by using various methods and techniques of geodetic measurements. Further mathematic treatment represents generally complete and accurate information of the observed object condition and stiffness.

Keywords
Gravity (rock-fill) dam, range line observations, horizontal and vertical displacements, geometric levelling.

1 INTRODUCTION

The Malo-Ulbinsky reservoir was made in the late 1930s for covering water deficit of Ridder industrial hub, public water and energy supply. The reservoir is located 35 miles south-east of Ridder in the upper reaches of the Malaya Ulba at about 1,500m above sea level.

The reservoir is made in the riverbed of the Malaya Ulba by means of rock-fill dam with 34.5m height and 367m crest length. The dam crest width is 5m, maximum width at the bottom - 74.5 m, the dam crest level – 1,574.00 m.

Estimated reservoir capacity at NWL 1,572.00m is 88.3 million m^3, the minimum level of drawdown – 1,549.00m and, respectively, the effective storage capacity - 84.2 million m^3. The length of the Malo-Ulbinsky reservoir is 5 km, maximum width is 3 km, average depth is 13.4 m, and maximum depth of 31.5 m, the catchment area that feeds the reservoir is 40.5 km^2.

Filling of the reservoir occurs during spring and summer flood, and, in winter, when the natural runoff decreases sharply, storage water supplies are dumped into the Left Gromotukha, then the water flows to the hydro-electric power station and to other consumer of Ridder.

The rock-fill dam of Malo-Ulbinsky reservoir is one of the few dams of that type. The dam has an abrupt upstream face. In plan view the dam is given a curved outline, which is made purposely to reduce the volume of rock fill (Figure 1).

Figure 1: the Malo-Ulbinsky reservoir rock-fill dam

The upstream wedge piece of the dam body represents a masonry wall with slope 3: 1. The foundation bed for masonry wall is untouched with rotting rocks (granite).

The material for filling as well as for dry masonry is grey granite with ultimate compressive strength from 800 to 2,500 kg/cm^2.

To increase the stiffness of downstream side large rocks with selection are put down, and by their junction with the rock foundation bed along the whole length of the dam a rubble concrete retaining prism is constructed.

For preventing filtration under constructions in dam foundation a concrete-filled trench is placed, which is sunk in rocks at a depth of 6m to 11m, under the trench cement-grout curtain is disposed. The trench is sunk to a depth of at least 1 m in granite without signs of weathering and cracking.

2 GEODETIC OBSERVATIONS OF HORIZONTAL AND VERTI-CAL DISPLACEMENTS AT THE CREST OF THE MALO-ULBINSKY RESERVOIR ROCK-FILL DAM

The main method of monitoring hydraulic structures settlement is a method of geometric levelling with short rays. This method allows covering a very wide range of accurate measurement of difference in elevation (from 0.05 till 5mm for one station), allows keeping measurement in a wide range of external and internal impacts of natural and industrial environment, has higher productivity in comparison with other methods and lower working costs.

At the present time while monitoring the engineering objects settlement the following types of classifications and techniques of geometric levelling are used:

a) state levelling of I, II, III and IV classes;
b) grade levelling for measuring hydraulic structures settlement;
c) grade levelling for measuring bedding deformation of buildings and constructions;
d) levelling of special classes for engineering-geodetic works.

By a variety of reasons the levelling method, applied for waterworks facilities to determine the settlements, is different from methods, recommended by state instruction:

- levelling, as a rule, is carried out according to non-removable change points,
- the length of collimating ray is limited by the distance between contiguous graduation marks,
- marking and fixing the places of level and laths installation are performed in advance, etc.

Oriented on long experience of waterworks facilities settlement observations, 3 classes of hydrotechnic levelling are emphasized in references, characteristics of which are given in the Table 1.

Table 1: Technical characteristics of hydrotechnic levelling classes

Class of levelling	Root-sum-square uncertainty excess at the station , mm	Extreme discrepancy of direct and reverse running, mm	Measurement capacity at the station
I	0,08	$0{,}3\sqrt{n}$	Direct and reverse with two heights of instrument
II	0,13	$0{,}5\sqrt{n}$	Direct and reverse with one height of instrument
III	0,40	-	In one direction with one height of instrument

While observing the settlements of earth dams, earthflows and in some other cases, where high accuracy is not required, recommended state levelling instruction of III and IV classes is applied.

Table 2 represents the recommended extents of root-sum-square uncertainties of determining absolute settlements and horizontal displacements, which were derived from the summary of foreign and native experience of observation activities of various hydraulic structures and their foundation beds taking into account fully developed at the present time correspondence between observation problems and geodetic methods possibilities.

Determination accuracy of relative deformation must be higher in several times. Inaccuracy of their determination is normally 0.2 – 0.3 mm for concrete constructions and their foundation bed and 0.5 – 1.5 mm for earthwork structures.

In some instances, in considerable deformation inaccuracy their determinations might be increased as, for example, for marks disposed in the key at the crest of arch dam. It is often enough to keep inaccuracy in determining earthflow displacement just for the first time for detection of the process beginning. Later on, for higher shift values, it is possible to decrease the accuracy of their determination.

Table 2: Root-sum-square uncertainty of determining absolute settlements and horizontal displacements

Objects of observations	Root-sum-square uncertainty of deformation determining, mm	
	settlements	horizontal displacements
Concrete constructions at rock bed	1	1
Concrete constructions at compressible soil	2	2
Earthwork structures:		
Construction period	10	5 - 10
Maintenance period	5	3 - 5

The rock-fill dam has been exploited since the end of thirties. Observations of horizontal and vertical deformation of the rock-fill dam were started in 1943. Since 1947 till 1963 dam observations were not carried out, the allocation scheme of graduation lines and range beacons was lost. in 1963 the

allocation scheme of graduation lines was reconstructed. Further observations were fulfilled periodically by various specialized enterprises: since 1969 till 1973, since 1980 till 1983, since 1997 till present.

Vertical shift is determined by geometric levelling according to observation marks (Figure 2), placed in the dam body (Figure 3). Monumented bench marks № 200, 201 were taken as datum points.

Horizontal displacement is determined with the cross-section method direct distance observations from section lines to mark center:

1) from BP – 2 on CP – 2 – displacement of marks 9, 11;
2) from BP – 3 on CP – 3 – displacement of marks 13, 15;
3) from BP – 3 on CP – 3 – displacement of marks 15, 13;
4) from M – 39 on CP – 4 – displacement of marks 17, 19, 21,…, 37.

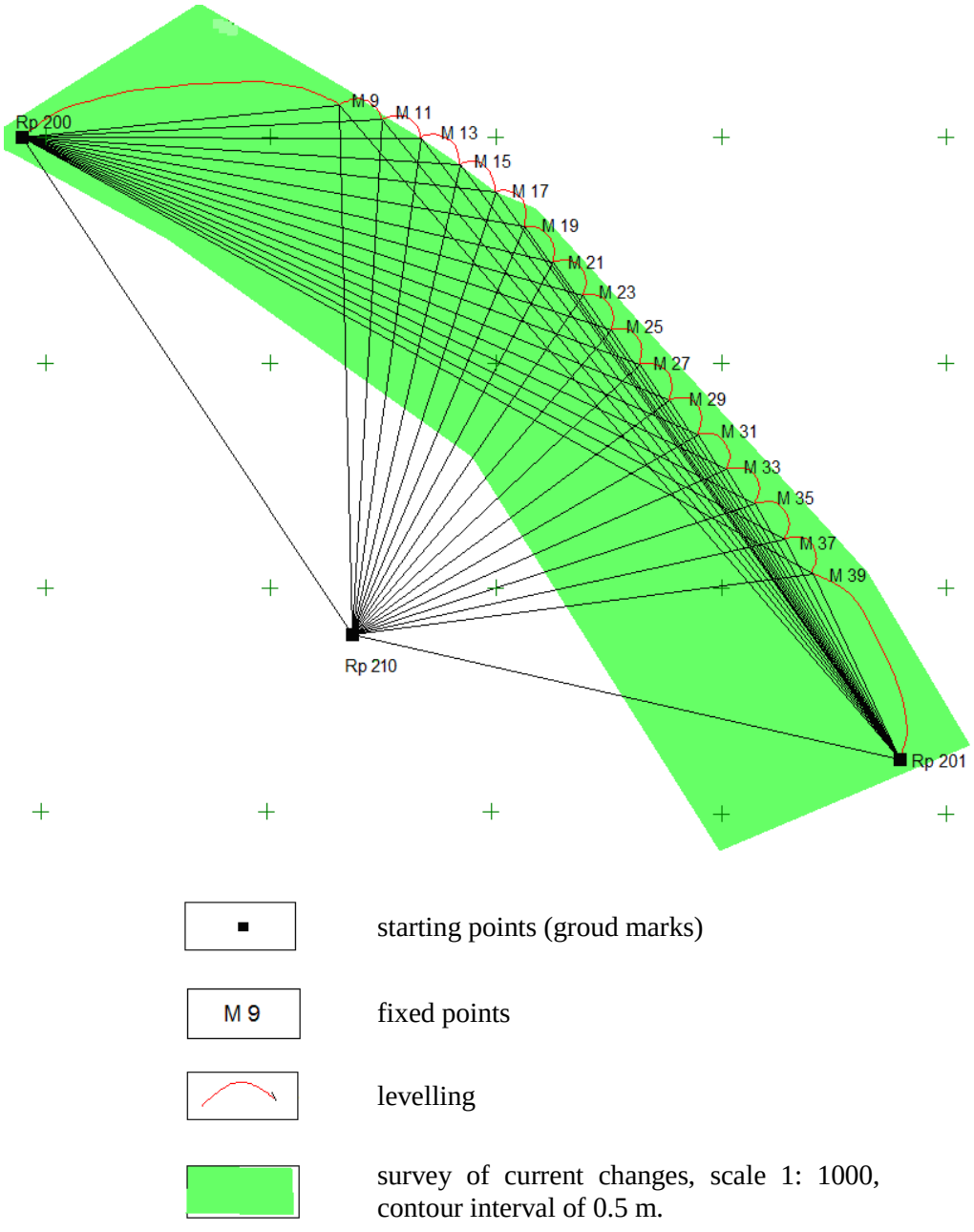

Figure 2: Scheme of surveyor' pickup

In accordance with observation results a graphic chart of marks' horizontal displacement at the dam crest is drawn (Figure 4) and corresponded conclusions are made.

Since the dam has a curved outline, the observations of horizontal displacement are realized according to 3 section lines. As base points (BP) were taken BP-2, BP-3 and mark 39, placed in 1997. As collimating points (CP) were taken CP-2, CP-3 and CP-4. According the results of range line measurement a graphic chart of horizontal displacements is drawn up and displacement analysis with preceding years is carried out.

Figure 3: Observation mark

For observation of marks' vertical displacements the levelling line of IV class is run with the help of a batter level N-3 and 3-meter surveying rod (Figure 5). Based on the results of fulfilled observations a graphic chart of vertical displacements of marks at the crest of the Malo-Ulbinsky reservoir dam is drawn up (Figure 6) and displacement analysis with preceding years is carried out.

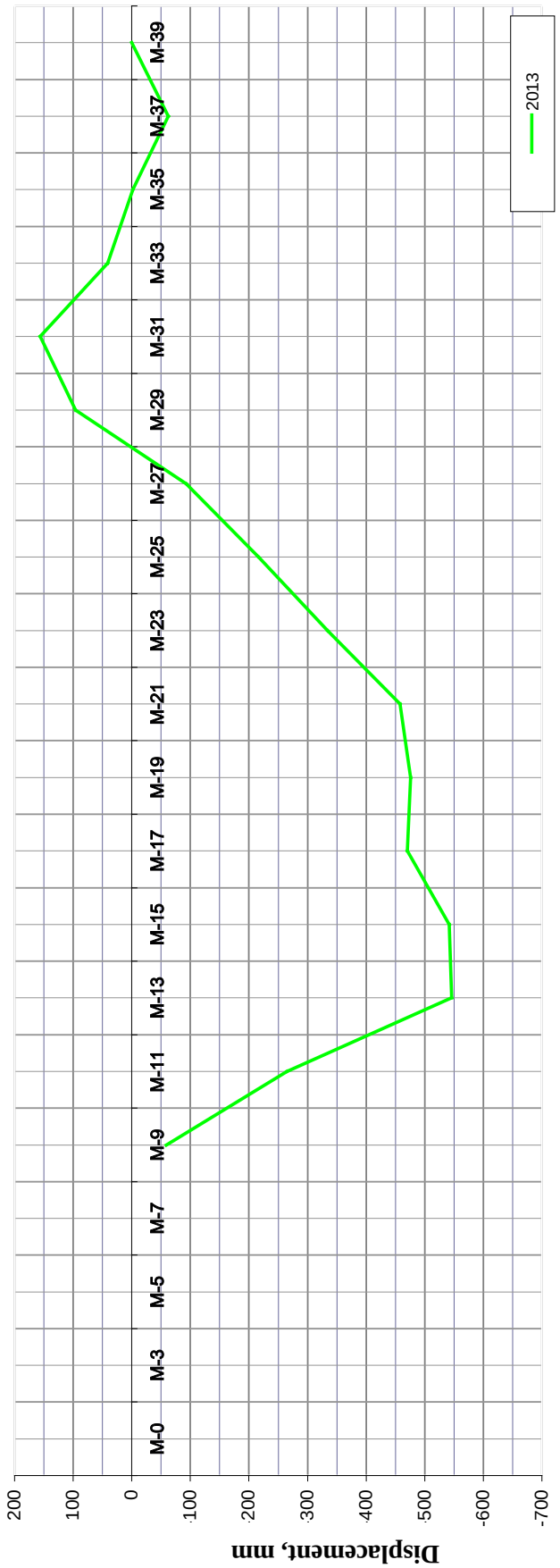

Figure 4: Graphic chart of marks' horizontal displacements at the crest of the Malo-Ulbinskoe reservoir rock-fill dam

Figure 5: Marks levelling at the dam crest

Figure 6: Graphic chart of marks vertical displacements at the crest of the Malo-Ulbinskoe reservoir rock-fill dam

3 USING GEOMOS ADJUSTMENT SOFTWARE IN PROCESSING THE RESULTS OF GEODETIC OBSERVATIONS AT THE ROCK-FILL DAM OF THE MALO-ULBINSKY RESERVOIR

Network adjustment and deformation analysis is one of the most difficult tasks in the field of geodesy. In processing the results of geodetic observations at the Malo-Ulbinsky reservoir rock-fill dam GeoMoS Adjustment module was used in experimental mode (Levelling).

In observing the displacements at the crest of the Malo-Ulbinsky reservoir rock-fill dam, except the listed observation methods, a method of linear-angular constructions operated by means of total station is applied, the results of which can be further processed in a software product GeoMoS Adjustment.

The results of observations by means of total station performed with fixed monumented bench marks on observation marks are imported, in clean layout, into the program GeoMoS Adjustment. The input data are the coordinates of the base and collimating points, the output is a deformation analysis of the data with an accuracy appraisal of the fulfilled works.

The observation results might be presented in the graphic charts form of control points displacements from collimated section line of X and Y-axes (Figure 7).

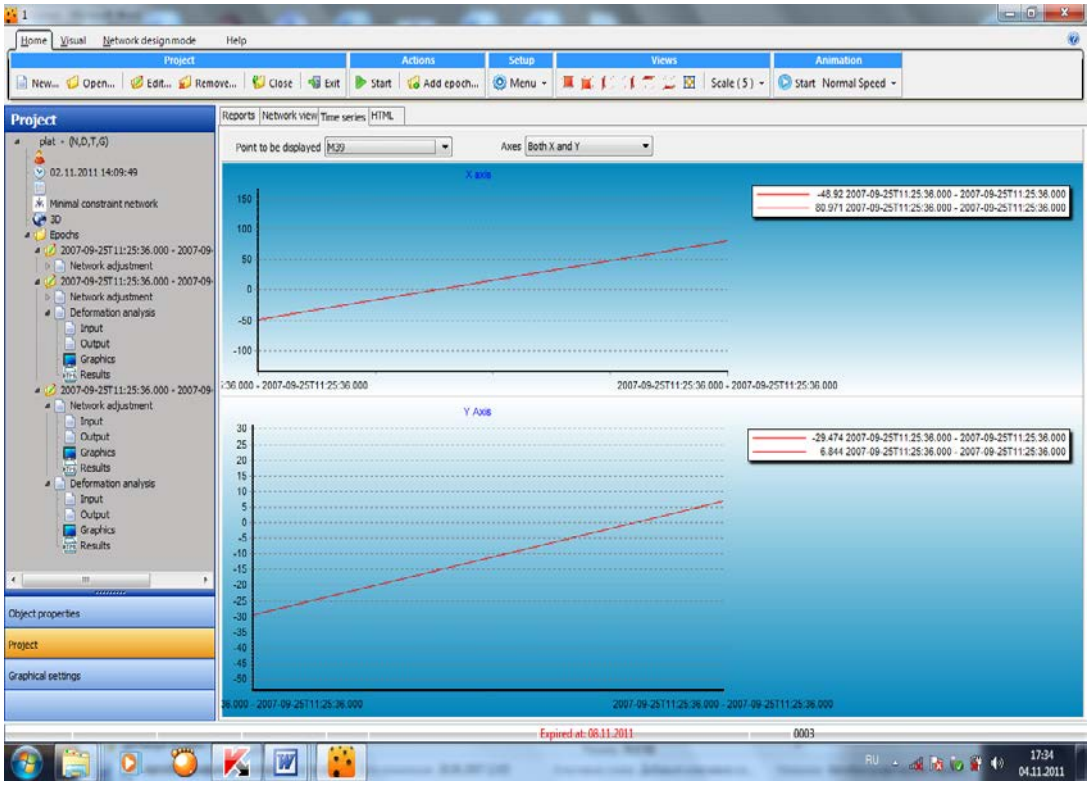

Figure 7: Graphic chart of control points displacements of X and Y-axes

Observation data of X, Y, Z are imported into the program GeoMoS Adjustment and based on the data a network is drawn up (Figure 8). Next the angular and linear values for the coordinates of each of the observation periods are calculated, and the program executes the deformation analysis for a certain period of observation (Figure 9).

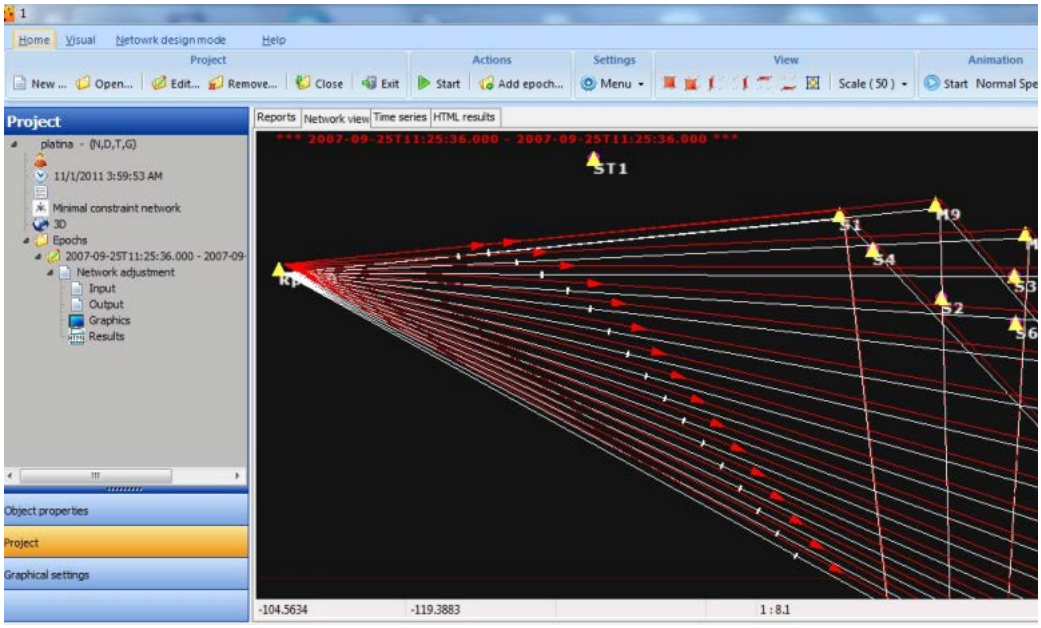

Figure 8: Network adjustment and its construction

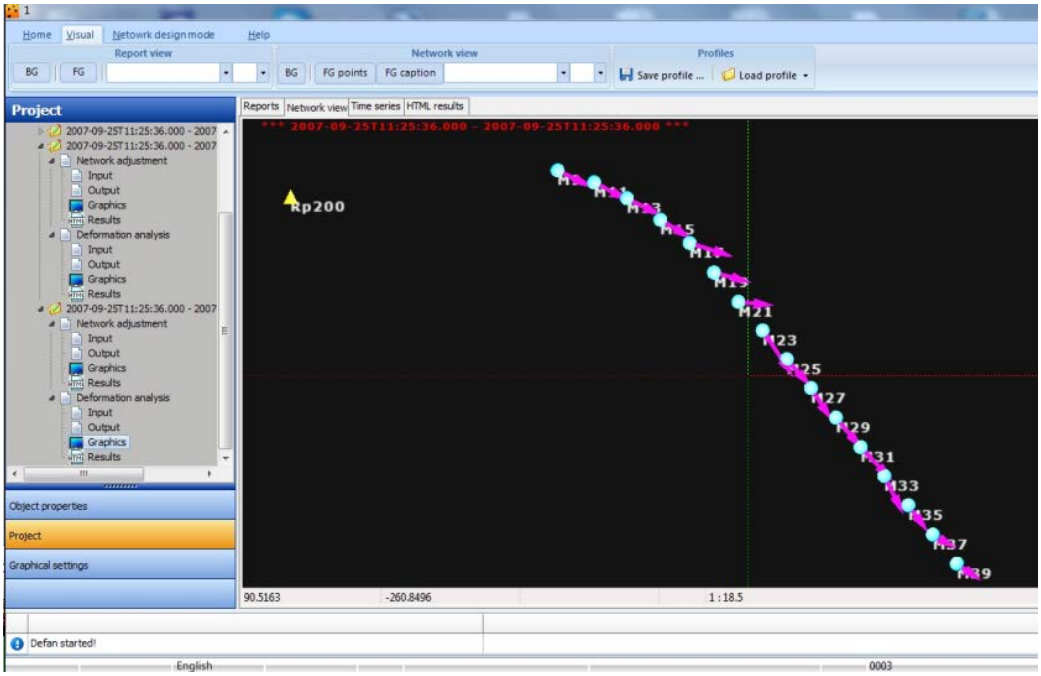

Figure 9: Deformation analysis

4 CONCLUSIONS

Analysis of observations of horizontal displacements shows that the west wing of dam is subject to most of the deformation and displacements are directed both toward the upstream side, so the downstream side. It should be noted that until 1969 the displacements on the entire length of the dam had steady rate to the downstream side. Since 1969, marks displacements between cycles have fluctuations to the upstream side.

Analysis of the observations results of marks vertical displacements at the crest of the dam shows that the average value of the vertical displacement is (-4) - (-8) mm comparatively to the observations results in 2012.

Considering the importance and the uniqueness of the Malo-Ulbinsky reservoir for life support and safety of the city of Ridder, it is necessary to continue monitoring of the given object condition using modern geodetic technologies

REFERENCES

Books:

ZHUKOV, B.N. *Geodetic monitoring of plant and equipment expenditures of production enterprises*. Monograph. – Novosibirsk: SSGA, 2003 (in Russian)

ZHUKOV, B.N. *Guidelines on geodetic monitoring plant and equipment expenditures of production enterprise while*.– Novosibirsk: SSGA, 2004 (in Russian)

LEBEDEV, N.N. *Practical course of applied geodesy*. – Moscow: Subsurface resources, 1977 (in Russian)

CARLSON, A.A. *Measuring deformations of hydraulic structures*. - Moscow: Subsurface resources, 1984 (in Russian)

State production committee on energetics and electrification of USSR ORGRES. Technical report on inspection of dams of the Malo-Ulbinsky reservoir – Moscow, 1964 (in Russian)

Republican specialized manufacturing enterprise «Kazenergonaladka». Report on instrumental surveying of deformation of the Malo-Ulbinsky gravity (rock-fill) dam, - Alma-Ata, 1981 (in Russian)

Guidelines on field surveys for deformation of hydraulic structures and their foundation beds using geodetic methods. П-648. Hydroproject, Moscow: Energy, 1980 (in Russian)

Journal articles:

VESELOV, V. V. *On digit leveling.* / V.V. veselov, O.V. Esennikov, A.N. Sjachinov //Vestnik of Voronezh State Agricultural University. – 2010 - № 2(25). - pp. 87 – 93

Benchmarks Stability Control in Geodetic Monitoring for Nuclear Power Plant Safety

Alexander.I. Fyodorov, Natalia V. Fyodorova
Siberian State Academy of Geodesy, Russian Federation

Abstract
The benchmarks displacement calculation as their stability determination is relative. As a result, the stability evaluation problem does not have a single solution. The existing analysis methods have revealed that one and the same displacement model is applied in the benchmarks stability research. The rating system suggestion involves the benchmark ratings calculation, i.e. the digital parameters that characterize the relative benchmark stability.

Keywords
Benchmarks stability, benchmarks displacement, benchmark stability, rating

Nuclear power plants belong to the engineering structures which require individual planning high precision and special surveying works. The main objective of geodetic observations during the maintenance period of such structures is the technical supervision and detailing computing techniques for the finite subsidence values. The vertical control benchmarks chosen as a starting points created on the territory of the NPP for the purposes of monitoring vertical displacements should provide the benchmark stability during the whole period of observations and guarantee the determination of subsidence with required accuracy.

In the theory of benchmarks stability investigations there exists a common practice to distinguish the actual benchmark displacement and possible errors in determining their elevations depending mainly on the order of leveling. If the calculated benchmark displacement exceeds the doubled (or tripled) mean-root-square error of the displacement, it is regarded as a real displacement. Otherwise, the benchmark is considered to be stable.

The mathematical processing of engineering structures subsidence observations includes the leveling adjustment and calculation of vertical displacements of benchmark and marks in each cycle. The serious theoretical problem is the choice of the initial reference plane with respect to which the benchmark elevations and their vertical displacements should be calculated, and the development of procedure for benchmarks stability assessment.

The solution of these problems has engaged many scientists and geodesists. All research methods of benchmark stability involve the same initial data – the difference of heights between benchmarks from cycle to cycle. The variety of methods concerns the choice of true elevation while repeated leveling, that is why in GANSHIN, STOROZHENKO & ILYIN (1981) all the methods are divided into two groups. The first group includes the methods that are based on the principle of invariable elevation of the most stable benchmark in the network. The second group includes the methods that implement the principle of unchanged mean elevation of all benchmarks or a group of the most stable benchmarks.

All methods of benchmarks stability investigation are divided into three groups: the first group includes methods based on the analysis of elevation differences; the second group - those using additional mathematical condition imposed on the measurement results; the third group – the methods using the adopted hypothesis of the benchmarks displacement MIHELYOV, RUNOV & GOLUBTSOV (1977).

From a mathematical standpoint, in order to determine the benchmark displacements (ΔH) it is necessary to solve the following system of equations:

$$\Delta H_j - \Delta H_i = \Delta h\,, \qquad (1)$$

where Δh – the change in the adjusted elevation along with the line connecting the *i*- and *j*-benchmarks for the period between two cycles of network leveling.

The number of equations of the kind (1) equals *n* – the number of measured differences in elevation; the number of unknown benchmarks displacements equals *t.* In the real leveling network it is always *n>t,* but because of the fact that part of the equations (1) are a linear combination of other equations, the number of independent equations of the kind (1) is equal to *t-1*. To solve the system, it is necessary to set an additional condition that will allow writing the missing equation.

The difference of all known methods for analysis of benchmark displacements can be only in the choice of the missing equation to solve the system (1). In this sense, none of them may be of any advantages over other methods.

The analysis of particular methods shows that there is no essential difference between classifications of GANSHIN, STOROZHENKO and ILYIN (1981) and MIHELYOV, RUNOV & GOLUBTSOV (1977); thus, the first group of methods in both cases includes those suggested by A. Kostekhel, G.K. Botyan, A.M. Zelenskiy and V.V. Dorofeyeva, I.V. Runova. The second one in both classifications is the methods by P. Marchak and V.F. Chernikov.

It is known that the determination of benchmarks displacements, as well as the confirmation of their stability, is relative. As a result, the objective of the benchmarks stability assessment and the choice of the most stable benchmark as the reference benchmark does not have a single solution MIHELYOV, RUNOV & GOLUBTSOV (1977).

The analysis of existing methods showed that the analysis of benchmark stability involved the same model for benchmark displacements, in which some benchmarks are influenced by a subsidence, while the others uplift, and the benchmark stability is determined with respect to the rest of network benchmarks. The relativity of this problem solving is evident and mentioned by many authors. Therefore, such solution cannot be considered to be final. It is possible to make this solution more specified, if take into account the external data with regard to this leveling network when elevations can be periodically transferred to one or several benchmarks from the precise leveling benchmark or final conclusion on a character of vertical deformations at the object under study given by geologists and hydrogeologists.

For such cases, the rating system of benchmarks stability assessment is suggested DYAKOV (1992). The idea of a rating assessment is identical to the I.V. Runov method RUNOV (1976) and similar methods. It implies the calculation of benchmark ratings, that is, of some numerical parameters characterizing the relative benchmark stability. According to DYAKOV (1992), it is necessary to distinguish the four rating types: the average and weight sign ratings, the average and modular ratings.

In the initial cycle of leveling, all the network benchmarks are assigned by are a zero value of all ratings; in each subsequent cycle the rating will be changed by an increment value for the period between two adjacent cycles. The total value of benchmark rating consists of it's rating value in the previous (k-1) cycle and its increment for the current *k*- cycle.

The average sign rating increment of the *i*-benchmark is calculated according to the formula:

$$\Delta RZ_i = \frac{\sum_1^t \delta h_{i,j}}{t}, \qquad (2)$$

and the average modular rating increment - by the formula

$$\Delta RM_i = \frac{\sum_1^t \left|\delta h_{i,j}\right|}{t}, \qquad (3)$$

where t - the number of benchmarks in the network, $\delta h_{i,j}$ - the displacement of the i-benchmark with respect to the j- benchmark of the network.

As noted in DYAKOV (1992), the average sign and average modular ratings satisfy the condition of their independence from the choice of the reference benchmark in the network, but in formulas (2) and (3) the weights of $\delta h_{i,j}$ displacements are not taken into account. If the displacement weights are to be taken into account, the ratings will be called the weight ratings; the values of weight ratings depend on a choice of the reference benchmark, and therefore, the weight ratings are less convenient for practical application.

The analysis of numerical weight rating values revealed that the replacement of the reference benchmark leads to a change in the reference point of ratings, and the sequence of benchmarks according to the values of weight rating remains the same. Moreover, it corresponds to a sequence of benchmarks in accordance with the average rating. Thus, in order to investigate the benchmarks stability it is enough to calculate the average sign and modular ratings of network benchmarks. Table 1 illustrates the average and modular ratings for the leveling network benchmarks according to seven cycles.

Table 1: Calculation of network benchmark average ratings

Benchmark number	Average ratings according to the cycles, mm						
	1	2	3	4	5	6	7
Benchmark 1– RZ	/0,0	–0,7/–0,7	0,0/–0,7	+0,6/–0,1	–0,4/–0,5	+0,7/+0,2	–0,8/–0,6
RM	/0,0	0,7/ 0,7	0,1/ 0,8	0,4/ 1,2	0,4/ 1,6	0,7/ 2,3	0,8/ 3,1
Benchmark 2– RZ	/0,0	–0,2/–0,2	+0,3/+0,1	–0,6/–0,5	–0,2/–0,7	–0,3/–1,0	–0,7/–1,7
RM	/0,0	0,4/ 0,4	0,3/ 0,7	0,4/ 1,1	0,3/ 1,4	0,5/ 1,9	0,8/ 2,7
Benchmark 3- RZ	/0,0	+0,3/+0,3	–0,2/+0,1	–0,2/–0,1	+0,9/+0,8	–0,8/ 0,0	+0,3/+0,3
RM	/0,0	0,4/ 0,4	0,2/ 0,6	0,4 1,0	0,9/ 1,9	0,8/ 2,7	0,8/ 3,5
Benchmark 4- RZ	/0,0	+0,6/+0,6	0,0/+0,6	+0,2/+0,8	–0,2/+0,6	–0,1/+0,5	+1,3/+1,8
RM	/0,0	0,6/ 0,6	0,1/ 0,7	0,4/ 1,1	0,3/ 1,4	0,5/ 1,9	1,3/ 3,2
Note: numerator – the rating increment denominator –the total rating value							

Having the values of sign rating, the most stable benchmark can be determined for any model of benchmark displacements. For instance, if it is known that some benchmarks are affected by a subsidence, while others – uplift, the most stable benchmark is close to a zero rating. According to the processing results for seven cycles it is the benchmark 3. Such conclusion is in good agreement with A. Kostekhel and P. Marchak methods. If only the benchmark subsidence takes place, the most stable benchmark will be that with the average sign rating is the highest and positive. The results of seven processing cycles show that such benchmark is the benchmark 4. If all the benchmarks uplift, the most stable one has the highest negative rating. According to Table 1 it is the benchmark 2.

Modular rating characterizes the irregularity and absolute values of benchmark displacements. Numerical modular rating equals to the total movement of the benchmark for the period from the initial cycle to the current one. The average value of modular rating for the given benchmark ($RM_{cp} = \frac{RM}{k}$, where k-number of cycles) characterizes its average displacement within one cycle. If the ratio of average modular rating value calculated for the whole network to the maximum benchmark displacement error at the weakest point does not exceed unity, the benchmark network as a whole can be considered stable. Otherwise, it is fair to say that some benchmarks have significant

vertical displacements relative to one another and there arises a problem of finding the most stable benchmark that can be considered as a reference benchmark.

In conclusion, some recommendations are suggested for geodesists who investigate the reference benchmark displacements choosing one or another method. The simplest and most obvious method is that ratings. In addition, it can be easily automated, and therefore, its application is a prime necessity. As regards the calculation of benchmarks subsidence, P. Marchak method (or V.F. Chernikov's) is more preferable, if the character of vertical deformations is unknown or if the benchmarks subsidence or their uplift are equally probable. When the character of vertical displacements is known with high probability, the benchmark displacements should be calculated with regard to the most stable benchmark chosen by sign rating values.

REFERENCES

Books:

GANSHIN, V.N., STOROZHENKO, A.F., ILYIN, A.G. *Measurement of structure vertical displacements and benchmark stability analysis.* Moscow, 1981.

MIHELYOV, D. Sh., RUNOV I.V., GOLUBTSOV, A.I. *Geodetic measurements while studying large engineering structure deformations.* Moscow, 1977.

Journal articles:

RUNOV, I.V. *Benchmark stability analysis of geodetic control network.* Surveying and Mapping, 7/1976, p.15-17, 1976.

DYAKOV, B.N. *Benchmark stability analysis of a free vertical control network.* Surveying and Mapping, 4/1992, -p.15-17, 1992.

A new Approach for an Incremental Orientation of Micro-UAV image sequences

Martin Reich, Jakob Unger, Franz Rottensteiner, Christian Heipke[1]
Institute of Photogrammetry and GeoInformation, Leibniz Universität Hannover, Germany

Abstract
Civil applications for small size unmanned aerial vehicles (UAV) have become quite important in recent years and so have accurate orientation and navigation of these devices in unknown terrain. In this work we focus on on-line compatible positioning in façade observation based on monocular low resolution still images acquired by a camera mounted on a UAV. Also, a 3D point cloud of the facade is generated. This allows further processing steps, e. g. navigation assistance, collision avoidance or the evaluation of the point cloud density, verifying completeness of the data. To be able to deal with the increasing amount of observations and unknown parameters we implement an incremental bundle adjustment based on automatically determined tie points and sliding image triplets. The tripletwise orientation allows for an efficient double cross-check of the detected feature points and hence guarantees reliable initial values for the nonlinear bundle adjustment. The initial values are estimated within a convex formulation delivering a sound basis for the incremental adjustment. Our algorithm is evaluated by means of imagery we took of the facade of the Welfenschloss in Hannover, captured from a manually flown Microdrones md4-200 micro-UAV.We compare the orientation results of our approach with an approach in which initial values for the unknown object coordinates are computed algebraically.

Keywords
Orientation, UAV, convex optimisation, incremental bundle adjustment

1 INTRODUCTION

Comprehensive information about facades is important e. g. For different fields like architecture, cultural heritage or the construction of realistic 3D city models. UAVs allow for an efficient observation of facades because of their high flexibility and thus fill the gap between terrestrial and aerial photogrammetry which are often constrained by an inappropriate observation angle. Nowadays high-performance stabilising devices as well as light weight imaging sensors allow a manual navigation of a small UAV through narrow streets or close to buildings. Since the complexity of a building is not always known in advance, the completeness of the collected data cannot be guaranteed and a potential lack of data is not revealed until postprocessing. In order to avoid missing relevant information, the user must be able to adapt the flight path during the capture, which requires among other results, an on-line orientation of the UAV and a sparse point cloud of the environment.

In this work we present a new incremental orientation approach based on image triplets, which is able to deliver the position and orientation of the UAV and a sparse point cloud of the observed object in near real-time. We use image triplets to increase the robustness of image matching because triplets allow a double cross-check on the consistency of the keypoint matches between all image pairs that can be formed of an image triplet. We use a combination of projective and perspective geometry. The former is used to obtain initial values for the first image triplet. The latter forms the foundation of an incremental bundle adjustment. In this way we avoid effects of over-parametrisation and furthermore are able to integrate results of a precalibration of the camera in a straightforward way. A previous version of this approach is also described in (Reich et al., 2013), this paper contains two important extensions: Firstly, the estimation of initial values for the unknown object coordinates of the

[1] This paper has been published in The International Archives of the Photogrammetry, Remote Sensing an Spatial Information Sciences, Vol. XL-3/W1, p. 93-98, 2014.

homologous feature points is formulated as a convex optimisation problem. Hence the risk of getting stuck into a local minimum leading to a distortion of the adjustment can be eliminated. Secondly, in the new version we adaptively remove already oriented images from incremental adjustment based on the number of supporting object points measured in the related image to keep computation time constant.

The remainder of this paper is structured as follows. Section 2 gives an overview of work related to this topic. In section 3 the used hardware, namely the UAV and the camera are presented. In section 4 we describe the methodology of this approach with a focus on the convex formulation of three-image spatial intersection. Experiments and results are shown in section 5. Finally, section 6 summarises this work and gives an outlook into future prospects.

2 RELATED WORK

An extensive overview of UAV applications and experiments can be found in (Remondino et al., 2011). For our approach we need an on-line compatible implementation. The idea of on-line user assistance in UAV mapping is given in (Hoppe et al., 2012). Simultaneous georeferencing of images and 3D point cloud generation in real- or near real-time based on monocular imagery, which is also called simultaneous localisation and mapping (SLAM), has been in the focus of several publications: On-line orientation and dense-matching implementations based on projective geometry alone can be found in (Klein and Murray, 2009) and (Wendel et al., 2012), respectively. In these approaches a local and a global bundle adjustment optimise all unknown parameters in parallel to avoid drifting effects. In (Cesetti et al., 2011) a so called ”visual global positioning system” is presented in which the position is estimated based on the matching of the acquired images with freely available georeferenced satellite imagery. A vision-aided navigation for UAVs based on a fusion of relatively oriented image pairs and data of an inertial measurement unit (IMU) is presented in (Wang et al., 2013). Steffen and Förstner (2008) describe the real-time orientation of a UAV for mapping purposes formulated in an unscented Kalman filter. The approach also deals with the drift problem in performing a loop closure based on points structured in a 3 dimensional octree.

The incremental bundle adjustment is comprehensively derived in (Beder and Steffen, 2008). Using an incremental bundle adjustment with a functional model different from ours, Meidow (2012) presents a loop closure approach for the purpose of stitching subsequent images. The idea of using triplets of images for the orientation of image sequences can be found in (Nistér, 2000). A hierarchy of trifocal tensors is used for the whole sequence without incremental estimation. The nature of the trifocal tensor and its estimation is described in a general context in (Hartley and Zisserman, 2000). The formulation of optimisation problems via a convex objective function is of increasing interest in research in many different disciplines. The entire derivation of its principles can be found in (Boyd and Vandenberghe, 2004). One of the first works integrating this technique into geometric reconstruction problems is (Hartley and Schaffalitzky, 2004). In (Ke and Kanade, 2007), the geometric interpretation of reconstruction problems is pointed out. Furthermore they propose an L_1-norm based reprojection error integrated into the objective function. The works of Olsson and Kahl (2010) and Kahl and Hartley (2008) describe the spatial intersection problem from three images and show that there is only one minimum in optimisation with the L_∞-norm.

In our approach we combine projective and perspective geometry and implement an on-line compatible orientation within an incremental bundle adjustment. The initial values for the bundle adjustment are estimated using convex optimisation.

3 PRELIMINARIES

There are many types of UAVs. We use a *Microdrones md4-200* micro-UAV[1], a vertical take-off and landing quadrocopter. It has a maximum payload of 300 g, which is enough for a high quality compact camera. We use a *Canon PowerShot S110*[2] in combination with the *Canon Hack Development Kit*[3].

This software allows to manipulate many relevant parameters including exposure time, sensor sensitivity and focal length. Furthermore it enables automatic capturing based on a fixed time interval. The camera is calibrated before the flight based on a five-parameter-distortion model, three parameters for radial and two parameters for tangential distortion, respectively (Laganière, 2011).

During the flight images are acquired with a time interval of two seconds. In the following we tackle the transmission of the imagery as a problem that is solvable but whose solution is not in the focus of this work. We perform the estimation in postprocessing, although our implementation allows for a near real-time orientation and point cloud computation.

4 METHODOLOGY

The orientation of the UAV is based on imagery captured by a precalibrated camera, though our implementation is able to estimate the parameters of the interior orientation and lens distortion during bundle adjustment for refinement. For each incoming image SIFT features are extracted and matched (Lowe, 2004), which are the basis for the subsequent orientation work-flow. This workflow can be divided into two steps. The first one deals with the initial image triplet and is explained in section 4.1. The second part covers the spatial resection of subsequent images and convex spatial intersection of feature points for the derivation of initial values (section 4.2) as well as the incremental bundle adjustment, in which the unknown parameters are refined (section 4.3).

4.1 Initial Image Triplet

The computation starts as soon as features of the three first images are available. Matching of feature points in image triplets is more robust than in image pairs. Based on a pair of matching feature points $[x^I, x^{II}]$ in two images $[I, II]$ one can perform a double cross-check, because for a triple $[x^I, x^{II}, x^{III}]$ also $[x^I, x^{III}]$ and $[x^{II}, x^{III}]$ have to be a match. Nevertheless, erroneous matches generally still remain after double cross-check. Therefore, the estimation of the trifocal tensor, based on seven three-point correspondences, is carried out based on RANSAC (Fischler and Bolles, 1981). Inliers that support an estimation are found by a point transfer into the third image using the fundamental matrix of the first two images derived from the tensor. More details can be found in (Reich et al., 2013) and (Hartley and Zisserman, 2000, Chapter 15).

The first image triplet defines the local coordinate system of the whole block. A certain number of supporting matches has to be found to consider the estimation of the trifocal tensor as valid and to proceed with the following steps. Otherwise the first image is rejected and computation starts again with the three subsequent images.

When a valid initial image triplet is found, we derive the fundamental matrices of the first two images from the trifocal tensor and estimate the relative orientation of the two images based on the calibration data of the camera. The local coordinate system (XYZ) is defined as follows: The origin is located in the projection centre of the first image, the X and Y axes are parallel to the x and y axes in the image, respectively. The Z axis coincides with the negative viewing direction. The scale is given by the distance between the projection centres of the first and the second image. That base length is set to one.

Initial values for the unknown object points are estimated by convex spatial intersection (see 4.2) and the relative orientation of the third image is computed by a RANSAC-based spatial resection (Kraus, 1997). Having initial values for all unknowns a robust bundle adjustment based on non-linear collinearity equations can be performed. Observations are iteratively re-weighted based on their residuals so that their contribution on the adjustment result can be controlled. In this way outliers in the observations can be detected and excluded from further estimation.

4.2 Convex Spatial Intersection

Subsequent images are added to the existing block based on spatial resection. First we perform a matching between the feature points of the new image and the ones of the previous images for which object coordinates have already been estimated. This allows us to compute the relative orientation of the new image analogously to the way described for the third image of the initial triplet in section 4.1.

In order to extend the existing 3D point cloud, we are interested in finding additional homologous points between the three images. The related 3D coordinates are to be estimated via incremental bundle adjustment, which needs appropriate initial values. These initial values are computed using convex spatial intersection.

$$f_{res,i}(\mathbf{X}) = \left\| \mathbf{x}_{proj,i} - \mathbf{x}_i \right\|_m \tag{1}$$

with

$$x_{proj} = -c \frac{\mathbf{r}_{i,1}^T (\mathbf{X} - \mathbf{X}_0)}{\mathbf{r}_{i,3}^T (\mathbf{X} - \mathbf{X}_0)} + x_0,$$

$$y_{proj} = -c \frac{\mathbf{r}_{i,2}^T (\mathbf{X} - \mathbf{X}_0)}{\mathbf{r}_{i,3}^T (\mathbf{X} - \mathbf{X}_0)} + y_0. \tag{2}$$

$f_{res,i}(\mathbf{X})$ is the residual function for each image *i* based on the three-dimensional parameter vector $\mathbf{X}$, the object coordinates of the point to be intersected. It is the difference between the projected 3D point $\mathbf{x}_{proj}$ and the observation $\mathbf{x}_i$ in some norm *m*. *c* and (x_0, y_0) are the focal length and the principal point of the image, respectively, determined in camera calibration and considered to be constant. $\mathbf{X}_{0,i}$ is the position of the projection centre and $\mathbf{R}_i^T$ the transposed rotation matrix of image *i* with $\mathbf{r}_{i,j}^T$ being its *j*th row.

In the case of two images taking the midpoint of the shortest line that connects the two image rays which, in fact, is an algebraic minimisation with no obvious geometrical or statistical meaning (Hartley and Schaffalitzky, 2004), may not lead to suitable results. It is shown in (Kahl and Hartley, 2008) that algebraic minimisation in special cases may result in very high reprojection errors. Olsson and Kahl (2010) show that the reprojection error as a function of $\mathbf{X}$ (equation (1)) is quasiconvex. Since quasiconvexity is not preserved under summation (Boyd and Vandenberghe, 2004), L_2-minimisation (minimising the sum of squares) of the reprojection error does not represent a convex (or quasiconvex) optimisation. L_2-minimisation of the spatial intersection problem with three images mathematically means finding the minimum of a 47th order polynomial (Stewenius et al., 2005). Kahl and Hartley (2008) and Olsson and Kahl (2010) illustrate the chance to get stuck in a local minimum in three-image spatial intersection based on L_2-minimisation.

Therefore, we carry out an L_∞-minimisation as proposed in (Hartley and Schaffalitzky, 2004) and (Olsson and Kahl, 2010). This allows a quasiconvex formulation of the three-image spatial intersection problem:

$$\text{minimise} \qquad \max_{i=1\ldots3} f_{res,i}(\mathbf{X}) \tag{3}$$

Taking the pointwise maximum of the three quasiconvex residual functions preserves quasiconvexity (Olsson and Kahl, 2010).

We reformulate (3) to derive a quasiconvex formulation for which an effective solver can be generated. By substituting equation (2) into equation (1) we obtain (note that while equation 3 represents the L_∞-norm, each reprojection error itself can be expressed in any norm m):

$$f_{res,i}(\mathbf{X}) = \left\| \begin{pmatrix} -c\dfrac{\mathbf{r}_{i,1}^T(\mathbf{X}-\mathbf{X}_0)}{\mathbf{r}_{i,3}^T(\mathbf{X}-\mathbf{X}_0)} + x_0 - x_i \\ -c\dfrac{\mathbf{r}_{i,2}^T(\mathbf{X}-\mathbf{X}_0)}{\mathbf{r}_{i,3}^T(\mathbf{X}-\mathbf{X}_0)} + y_0 - y_i \end{pmatrix} \right\|_m . \tag{4}$$

This can be extended to:

$$f_{res,i}(\mathbf{X}) = \left\| \begin{pmatrix} \dfrac{-c\cdot\mathbf{r}_{i,1}^T + (x_0-x_i)\mathbf{r}_{i,3}^T(\mathbf{X}-\mathbf{X}_0)}{\mathbf{r}_{i,3}^T(\mathbf{X}-\mathbf{X}_0)} \\ \dfrac{-c\cdot\mathbf{r}_{i,2}^T + (y_0-y_i)\mathbf{r}_{i,3}^T(\mathbf{X}-\mathbf{X}_0)}{\mathbf{r}_{i,3}^T(\mathbf{X}-\mathbf{X}_0)} \end{pmatrix} \right\|_m$$

$$= \left\| \begin{pmatrix} \dfrac{\left(-c\cdot\mathbf{r}_{i,1}^T + (x_0-x_i)\mathbf{r}_{i,3}^T\right)\mathbf{X} - \left(-c\cdot\mathbf{r}_{i,1}^T + (x_0-x_i)\mathbf{r}_{i,3}^T\right)\mathbf{X}_0)}{\mathbf{r}_{i,3}^T\mathbf{X} - \mathbf{r}_{i,3}^T\mathbf{X}_0} \\ \dfrac{\left(-c\cdot\mathbf{r}_{i,2}^T + (y_0-y_i)\mathbf{r}_{i,3}^T\right)\mathbf{X} - \left(-c\cdot\mathbf{r}_{i,2}^T + (y_0-y_i)\mathbf{r}_{i,3}^T\right)\mathbf{X}_0)}{\mathbf{r}_{i,3}^T\mathbf{X} - \mathbf{r}_{i,3}^T\mathbf{X}_0} \end{pmatrix} \right\|_m . \tag{5}$$

Now we can write equation (5) as

$$f_{res,i}(\mathbf{X}) = \frac{\|\mathbf{A}_i\mathbf{X} + \mathbf{b}_i\|_m}{\mathbf{c}_i^T\mathbf{X} + d_i}, \tag{6}$$

with

$$\mathbf{A}_{i_{2x3}} = \begin{pmatrix} -c\cdot\mathbf{r}_{i,1}^T + (x_0-x_i)\mathbf{r}_{i,3}^T \\ -c\cdot\mathbf{r}_{i,2}^T + (y_0-y_i)\mathbf{r}_{i,3}^T \end{pmatrix}, \qquad \mathbf{c}_{i_{1x3}}^T = \mathbf{r}_{i,3}^T,$$

$$\mathbf{b}_{i_{2x1}} = \begin{pmatrix} -\left(-c\cdot\mathbf{r}_{i,1}^T + (x_0-x_i)\mathbf{r}_{i,3}^T\right)\mathbf{X}_0 \\ -\left(-c\cdot\mathbf{r}_{i,2}^T + (y_0-y_i)\mathbf{r}_{i,3}^T\right)\mathbf{X}_0 \end{pmatrix}, \qquad d_{i_{1x1}} = -\mathbf{r}_{i,3}^T\mathbf{X}_0.$$

Equation (6) is a quasiconvex function on the set $\mathbf{c}_i^T\mathbf{X} + d_i \geq 0$, implying that the point $\mathbf{X}$ is in front of the camera (Hartley and Schaffalitzky, 2004), (Kahl and Hartley, 2008). Equation (6) can geometrically be interpreted as a convex cone of norm *m* (Boyd and Vandenberghe, 2004) in front of the camera *i* with its apex in the projection centre. This cone intersects with the image plane defining some uncertainty measure (e. g. circle in case of the L_2-norm and square in case of the L_∞-norm).

Taking the pointwise maximum of equation (6) generally implies that the resulting function at some points is not differentiable anymore. Hence the minimum cannot be found by gradient based methods. Kahl and Hartley (2008) propose to write the minimization of (6) as a convex feasibility problem

$$\begin{aligned} &\text{find} && \mathbf{X} \\ &\text{subject to} && \|\mathbf{A}_i\mathbf{X} + \mathbf{b}_i\|_2 - \mu\left(\mathbf{c}_i^T\mathbf{X} + d_i\right) \leq 0, \\ &i = 1 \ldots 3, \end{aligned} \tag{7}$$

with a fixed $\mu > 0$. Note that a L_2-norm is used for representing the reprojection error. The minimisation problem (7) can be geometrically thought of as finding the intersection of the three convex cones located at each of the projection centres of the three images. The size of the cones is controlled by the factor μ, which, in fact, is the radius of the intersecting circle in image plane. The problem (7) is feasible if μ is large enough so that the cones intersect (Ke and Kanade, 2007). Such a

feasibility problem can be solved by a bisection algorithm (Olsson and Kahl, 2010), (Kahl and Hartley, 2008).

In our work we modify the feasibility problem (7) according to (Ke and Kanade, 2007) and reformulate it as a minimisation problem. μ is kept fixed and we try to minimise the distance ϵ to the cones defined by μ.

$$\begin{aligned} &\text{minimise} && \epsilon \\ &\text{subject to} && \|\mathbf{A}_i\mathbf{X} + \mathbf{b}_i\|_\infty - \mu\left(\mathbf{c}_i^T\mathbf{X} + d_i\right) \leq \epsilon, \\ &i = 1 \dots 3, \end{aligned} \tag{8}$$

In this way the intersection of the three cones defined by μ may be empty. If this is the case the minimal distance ϵ^* will be positive. If $\epsilon^* \leq 0$ an intersection of the cones exists and the optimal point $\mathbf{X}^*$ lies in that intersection. The implementation of the optimisation procedure is based on CVXGEN[4] (Mattingley and Boyd, 2012), which produces a C-based solver for convex optimization problems. Note that in contrast to (Kahl and Hartley, 2008) we use a L_∞-based reprojection error, because CVXGEN is for quadratic programs only and using the L_2-norm would imply [2]solving a second order cone program (Kahl and Hartley, 2008).

We are aware of the fact, that the L_∞-norm is sensitive to outliers. Hence, after the optimisation the reprojection error of each point (in each image) is required to lie below a certain maximum value.

4.3 Incremental Bundle Adjustment

As we want to provide an on-line compatible orientation procedure, unknown parameters are estimated incrementally. For each incoming image there are six parameters for the exterior orientation, namely the position and the orientation of the camera, and three object coordinates for each point measured in the current image triplet for the first time, enlarging the set of parameters of the whole block. Besides, already estimated parameters that are related to the current image triplet, can be improved by incremental bundle adjustment. For each triplet, two different types of unknowns occur:

1. unknowns which have already been estimated in previous triplets. These are
    a. orientation parameters of the $N-1$ already oriented images remaining in the incremental bundle adjustment
    b. object coordinates of points that have been estimated in previous triplets and are used to tie the new image to the existing block (see beginning of section 4.2)
2. unknowns that are estimated for the first time, i. e.
    a. orientation parameters of the new image
    b. object coordinates of points that have been measured and triangulated in the current image triplet for the first time (see section 4.2).

The parameter vector $\mathbf{p}$ is split into two components, $\mathbf{p}_1$ and $\mathbf{p}_2$ for the first and second type of parameters, respectively. Similarly, we split the observation vector l into two components, $\mathbf{l}_1$ and $\mathbf{l_2}$. $\mathbf{l}_1$ contains all observations that were used in previous triplets, whereas $\mathbf{l_2}$ contains observations derived in the current image triplet. The incremental bundle adjustment can now be formulated as:

$$\begin{pmatrix} \mathbf{l}_1 + \mathbf{v}_1 \\ \mathbf{l}_2 + \mathbf{v}_2 \end{pmatrix} = \begin{pmatrix} \mathbf{A}_{11} & 0 \\ \mathbf{A}_{21} & \mathbf{A}_{22} \end{pmatrix} \begin{pmatrix} \mathbf{p}_1 \\ \mathbf{p}_2 \end{pmatrix}. \tag{9}$$

[4]http://cvxgen.com/

As one can see in equation (9) the new observations $\mathbf{l}_2$ are related to both types of parameters $\mathbf{p}_1$ and $\mathbf{p}_2$ via the design matrices $\mathbf{A}_{21}$ and $\mathbf{A}_{22}$, respectively. Therefore, not only the new parameters can be estimated ($\hat{\mathbf{p}}_2$) but also the previous parameters are improved ($\hat{\mathbf{p}}_{1,+}$):

$$\begin{pmatrix} \hat{\mathbf{p}}_{1,+} \\ \hat{\mathbf{p}}_2 \end{pmatrix} = \mathbf{N}_+^{-1} \begin{pmatrix} \mathbf{A}_{11}^T \mathbf{P}_{11} \mathbf{l}_1 + \mathbf{A}_{21}^T \mathbf{P}_{22} \mathbf{l}_{22} \\ \mathbf{A}_{22}^T \mathbf{P}_{22} \mathbf{l}_2 \end{pmatrix}, \tag{9}$$

with $\mathbf{N}_+^{-1}$ being the inverse normal equation matrix of the incremental adjustment and $\mathbf{P}_{11}$ and $\mathbf{P}_{22}$ the weight matrices derived from the inverse covariance matrices of the observations $\mathbf{l}_1$ and $\mathbf{l}_2$, respectively. The dimensions of the matrices involved in the estimation equations, thus the normal equation matrix of the already estimated parameters and $\mathbf{A}_{21}$, do increase over time. At some point older images (and their orientation parameters plus points that have been measured in that image for the first time) have to be removed from the orientation process to keep the size of the matrices small enough for near real-time processing. For each incoming image a minimum number of points found in the oldest image involved in the estimation process and re-measured in the current image has to be present to keep that image in the estimation process. Otherwise this old image is eliminated. For a complete derivation of the incremental bundle adjustment the reader is referred to (Beder and Steffen, 2008) or (Reich et al.,2013).

5 EXPERIMENTS

The evaluation of the presented approach is based on imagery showing the facade of the Welfenschloss in Hannover. The images were taken by the camera and micro-UAV presented in section 3 with a fixed focal length and with a time interval of two seconds between neighbouring images. The UAV was manually controlled in front of the facade in several distances and heights. We ended up with three separate flights each consisting about 250 images.

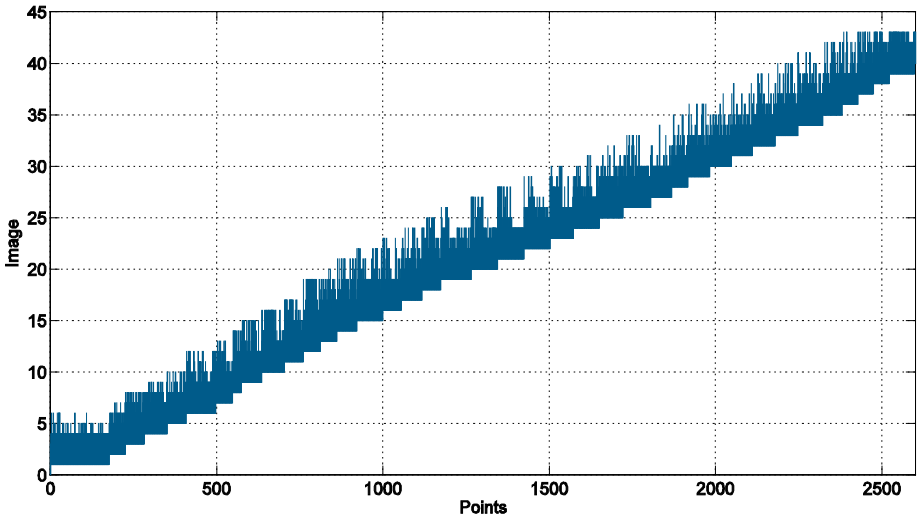

Figure 2: Indices of the images in the sequence in which each object point was visible.

The analysis of these image sequences is focused on two specific aims. First, we want to show the general performance of our algorithm. Hence, we show if the computation time per image is kept constant and the effects of older images removed from the estimation if they are not relevant any more. Second, we demonstrate the improvement of the convex formulation of the estimation of the initial values with respect to an algebraic estimation that was presented in (Reich et al., 2013). The following analysis is based on one image sequence consisting of 233 images.

As mentioned in section 4.3 the criterion for keeping an image in the estimation process is a minimal number of points found in that image which are re-measured in the current image. In our experiments we set that number to 20 points. Figure 1 shows the distribution of points with respect to the images they are measured in for the first part (43 images) of the image sequence. The number of images involved in one iteration of the incremental bundle adjustment varies between five and seven. This interval is somehow restricted since we limit the number of new observations connected to already estimated points to 50 due to reasons of computation time. Furthermore, we select all observations depending on their location in image space to achieve a well distributed set of observations. A maximum number of 200 new observations is involved into each incremental bundle adjustment. The computation time per image is kept constant and amounts to about ten seconds on a standard desktop computer in a nonoptimised implementation. This timing includes the computation of the whole covariance matrix of the parameters to be able to extract its precision. We estimate that an improvement by a factor of five is achievable, which delivers real-time results based on the time interval of two seconds between neighbouring images.

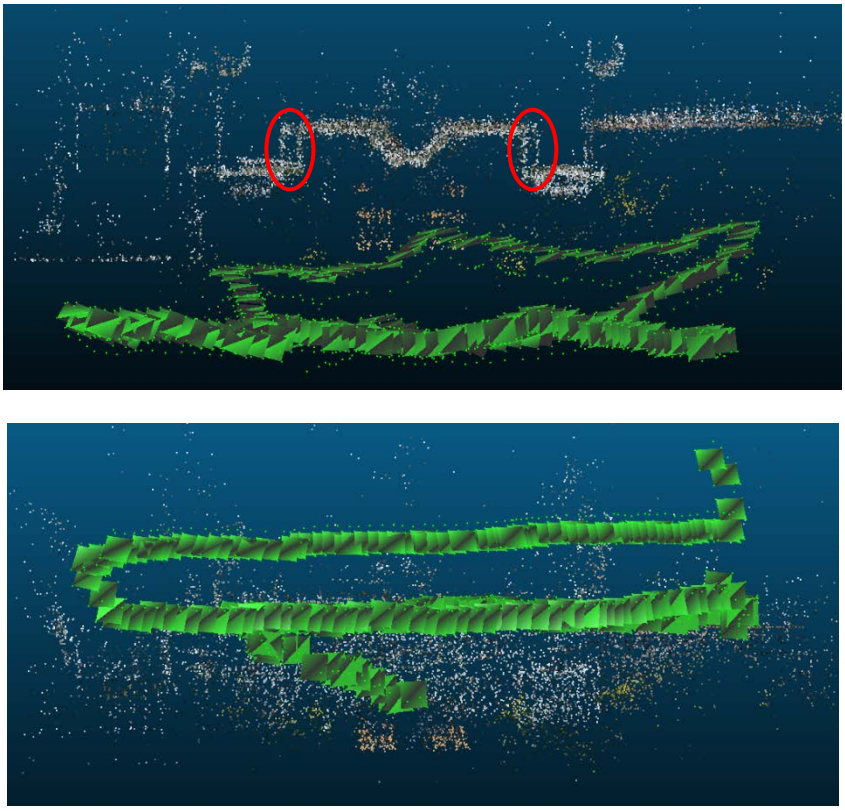

Figure 2: Point cloud and oriented images of an image sequence consisting of 233 images seen from above (first row) and from the front (second row). Regions that are highly affected by an offset are highlighted in red.

In figure 2 the point cloud and the orientation results of the whole image sequence are illustrated. One can see the uppermost image strip is captured in a rather oblique orientation so that also surface elements and trees are detected. Although the point cloud appears noisy it has to be said that the facade is quite rough with many decorative elements, window sills and balconies. Nevertheless, offset effects are present. The regions that are obviously affected either in scale or in translation are highlighted in red. The facade at that part of the building consists of a planar wall.

In a second experiment we compared the results of our approach with results for which the initial values of the object coordinates have been estimated using the shortest distance between the related rays (called ’algebraic approach’ below). After each incremental bundle adjustment we extracted the standard deviations from the covariance matrix of the newly estimated parameters $\Sigma_{\hat{\mathbf{p}}_2\hat{\mathbf{p}}_2}$. We

computed the trace of that part of the matrix concerning the position of the projection centre and its three rotation angles, respectively, representing the sum of the standard deviations of the projection centre and that of the three rotation angles. Furthermore, we extracted the mean precision of all new object points after each incremental bundle adjustment iteration by averaging the trace of $\Sigma_{\hat{\mathbf{p}}_2\hat{\mathbf{p}}_2}$ concerning the object points. Figure 3 illustrates the mean standard deviations of the estimated positions, rotations and object point coordinates of the first part of the sequence after each incremental bundle adjustment iteration. The color and type of the curve decode the type of initial value computation. The solid green curve shows the standard deviations for our approach, whereas the dotted blue curve shows the standard deviations for the algebraic approach. It can be seen that the precision of the orientation parameters in the case of convexly estimated initial values is nearly always better than for the algebraic approach, in particular for the images around image 13. The precision of the object points is rather equal for both approaches except for a few images near image 26. The fact, that differences in precision between the two approaches are visible for different images in the case of figure 3(a) and 3(b) compared to figure 3(c), may be an indication that the initial values itself play a secondary role only for the solution of the incremental bundle adjustment. Nevertheless, the way of initial value computation causes another factor influencing the precision of the bundle adjustment results as there is the number and distribution in space of points used. In fact, the distribution of object points observed in image 13 is better in our approach (std. deviation with respect to its centre of gravity: 3:2 [*baselengths*]) than for the algebraic approach (2:8 [*baselengths*]).

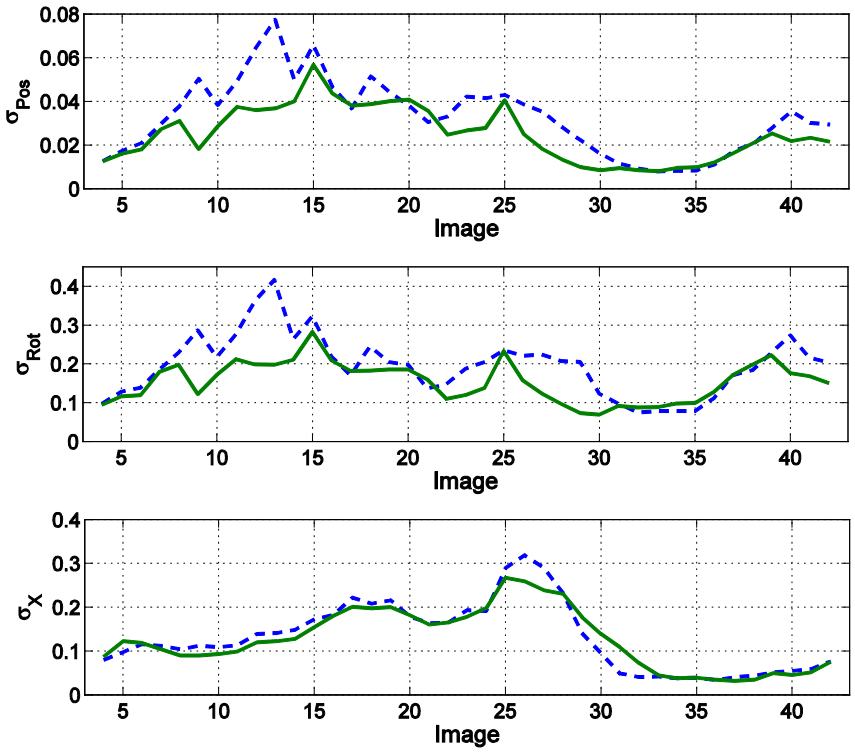

Figure 3: Mean standard deviations of the position $\mathbf{X}_0$ (a) and the rotation parameters $[\omega, \phi, \kappa]$ of the projection centre (b) and the object points (c) in [*baselengths*] and [*gon*] after each incremental bundle adjustment iteration for our approach (green/solid) and the algebraic approach (blue/dotted).

Differences can also be seen in the point cloud. Figure 4 shows the resulting point clouds of the image sequence used above. The white point cloud results from our approach. A second point cloud estimated using the algebraic approach is depicted in colour where different colours depict different distances between the two point clouds. One can see that the observations and hence the estimated object points differ between the two approaches. The wall on the left side only exists in the result of our approach. As can be seen, the differences between the point clouds increase with each iteration (UAV flew from right to left). This can be explained by a rotation between the two solutions.

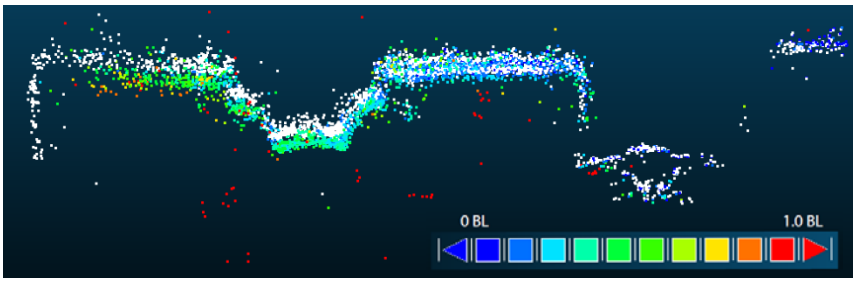

Figure 4: Comparison of the two resulting point clouds using our approach (white) and algebraically estimated initial values (coloured, depending on the distance to the other point cloud).

6 CONCLUSIONS

In this work we have presented a new incremental orientation approach of a micro-UAV based on triplets of images acquired at a certain time interval. We use convex estimation of the object coordinates as initial values for the incremental bundle adjustment. Furthermore, older images that become irrelevant for the orientation process are automatically removed from computation. We were able to show that our implementation estimates the orientation and a sparse point cloud of a whole flight consisting of hundreds of images with a constant computation time per image. In addition, we investigated the influence of different initial values for the unknown object point coordinates stemming from an algebraic computation and from our new approach.

However, there are several problems which need further investigation. Firstly, the comparison of the two approaches computing initial values for the bundle adjustment revealed differences in the estimation results. Whether the use of convexly optimised initial values itself or a deduced effect like the distribution of the object points in space is a significant reason for the enhanced quality of the results of our approach could not finally be verified. This will be part of our future work. Secondly, to be able to analyse the reliability and geometrical quality of our results we need a reference model with predefined and precisely measured points. Finally, the implementation is far from being applicable in realtime. But, irrespective of computation time, our approach is realtime compatible in terms of its incremental implementation.

REFERENCES

Books:

BOYD, S. P. and VANDENBERGHE, L.: *Convex Optimization*. Cambridge University Press, 2004.

HARTLEY, R. and ZISSERMAN, A.: *Multiple view geometry*. Vol. 642, Cambridge University Press, 2000.

KRAUS, K. *Photogrammetry*. Vol. 2, 3rd edition, Dümmler Verlag, Bonn, 1997.

LAGANIÈRE, R. *OpenCV 2 Computer Vision*. Packt-Publishing, 304 pages, 2011.

Journal articles:

BEDER, C. and STEFFEN, R. *Incremental estimation without specifying a-priori covariance matrices for the novel parameters.* IEEE Computer Society Conference on Computer Vision and Pattern Recognition Workshops, 2008. CVPRW '08., Anchorage, USA, pp. 1–6. 2008.

CESETTI, A., FRONTONI, E., MANCANI, A., ASCANIi, A., ZINGARETTI, P. and LONGHI, S. *A visual global positioning system for unmanned aerial vehicles used in photogrammetric applications.* Journal of Intelligent & Robotic Systems 61(1-4), pp. 157–168. 2011.

FISCHLER, M. A. and BOLLES, R. C. *Random sample consensus: a paradigm for model fitting with applications to image analysis and automated cartography*. Commun. ACM 24(6), pp. 381–395. 1981.

HARTLEY, R. and SCHAFFALITZKI, F. *L_∞ minimization in geometric reconstruction problems*. In: Computer Vision and Pattern Recognition, 2004. CVPR 2004. Proceedings of the 2004 IEEE Computer Society Conference on, Vol. 1, pp. I–504–I– 509 Vol.1. 2004.

HOPPE, C., KLOPSCHITZ, M., RUMPLER, M., WENDEL, A., KLUCKNER, S., BISCHOF, H. and REITMAYR, G. *Online feedback for structure-from-motion image acquisition*. In: British Machine Vision Conference, pp. 1–12. 2012.

KAHL, F. and HARTLEY, R. *Multiple-view geometry under the L_∞-norm*. Pattern Analysis and Machine Intelligence, IEEE Transactions on 30(9), pp. 1603–1617. 2008.

KEe, Q. and KANADE, T. *Quasiconvex optimization for robust geometric reconstruction*. Pattern Analysis and Machine Intelligence, IEEE Transactions on 29(10), pp. 1834–1847. 2007.

KLEIN, G. and MURRAY, D. *Parallel tracking and mapping on a camera phone.* In: Proc. 8th IEEE and ACM International Symposium on Mixed and Augmented Reality (ISMAR'09), Orlando. 2009.

LOWE, D. *Distinctive image features from scale-invariant keypoints.* International Journal of Computer Vision 60(2), pp. 91–110. 2004.

MATTINGLEY, J. and BOYD, S. *CVXGEN: a code generator for embedded convex optimization*. Optimization and Engineering 13(1), pp. 1–27. 2012.

MEIDOW, J. *Effcient multiple loop adjustment for computer vision tasks.* Photogrammetrie-Fernerkundung-Geoinformation 2012(5), pp. 501–510. 2012.

NISTÈR, D. *Reconstruction from uncalibrated sequences with a hierarchy of trifocal tensors*. In: European Conference on Computer Vision, LNCS, Vol. 1842, Springer Berlin Heidelberg, pp. 649–663. 2000.

OLSSON, C. and KAHL, F. *Generalized convexity in multiple view geometry*. Journal of Mathematical Imaging and Vision 38(1), pp. 35–51. 2010.

REICH, M., UNGER, J., ROTTENSTEINER, F. and HEIPKE, C. *Online compatible orientation of a micro-UAV based on image triplets*. International Annals of the Photogrammetry, Remote Sensing and Spatial Information Sciences II-3/W2, pp. 37–42. 2013.

REMONDINO, F., BARAZZETTI, L., NEX, F., SCAIONI, M. and SARAZZI, D. *Uav photogrammetry for mapping and 3d modeling–current status and future perspectives*. International Archives of the Photogrammetry, Remote Sensing and Spatial Information Sciences XXXVIII-1/C22, pp. 25–31. 2011.

STEFFEN, R. and FÖRSTNER, W. *On visual real time mapping for unmanned aerial vehicles*. In: International Archives of the Photogrammetry and Remote Sensing, Vol. XXXVII-B3a, Beijing, pp. 57–62. 2008.

STEWENIUS, H., SCHAFFALITZKY, F. and NISTÈR, D. *How hard is 3-view triangulation really?* In: Computer Vision, 2005. ICCV 2005. Tenth IEEE International Conference on, Vol. 1, IEEE, pp. 686–693. 2005.

WANG, T., WANG, C., LIANG, J., CHEN, Y. and ZHANG, Y. *Vision-aided inertial navigation for small unmanned aerial vehicles in GPS-denied environments.* International Journal of Advanced Robotic Systems 10(276), pp. 1–12. 2013.

WENDEL, A., MAURER, M., GRABER, G., POCK, T. and BISCHOF, H. *Dense reconstruction on-the-fly.* In: IEEE Conference on Computer Vision and Pattern Recognition, pp. 1450–1457. 2012

The Impact of Non-tidal Gravity Variations on the Results of Geodetic Monitoring of Hydrotechnical Constructions

Vadim F. Kanushin, Irina G. Ganagina, Denis N. Goldobin,
Alexandra M. Kosareva, Lenar R. Galimov
Siberian State Academy of Geodesy, Russian Federation

Abstract
The impact of anthropogenic variations of gravity potential on the results of geodetic deformational monitoring of hydrotechnical constructions is described. The calculation of attractive potential variations and its derivatives to determine the influence of reservoir water mass on geodetic position of control points and geodetic observations can be realized by specially developed software.

Keywords
Anthropogenic variations of gravity potential, hydrotechnical constructions, geometrical and hydrostatic leveling, dynamic models of water masses, algorithm, software

1 INTRODUCTION

Major hydraulic facilities construction inevitably brings about concentration of a great amount of water near power dam (billions of cubic meters) in a short period of time. This necessitates regular dam monitoring and its foundation. Reliable control based on in-situ observations is an integral part of the geodetic monitoring which includes: multi-cycle high-precision geodetic observations of spatio-temporal changes in the hydraulic structure under study; mathematical treatment of these observations results to estimate and improve their accuracy; substantial analysis, and interpretation. Among different events of the monitoring special attention is paid to mathematical modeling of the processes under observation, including predictive estimate of intermediate and successor state of the engineering structure.

The results of geodetic observations may be distorted due to various errors and depend on the external factors, such as gravity field variations, caused by reservoir water mass changes. Gravity variations do not cause spatial dislocation of the control points on the hydraulic facility and around it, they just bring about some changes in the values of their points positions.

The changes in hydrosystem's geodetic position of control points obtained from high-cycle geodetic measurements are used to determine structure settlements and horizontal displacements as well as vertical deflection, inclination, declination and other deformation characteristics. The effect of gravity field variations, resulting from the changes of reservoir water mass between geodetic measurements cycles, should be eliminated from the registered changes of the positions.

According to Construction rules and regulations 3.01.03-84 the root-mean-square error in the determined dam settlement and foundation values as well as its horizontal displacement may not exceed 1mm for buildings and structures erected on the rock bed.

Gravity variations caused by the changes of reservoir water mass may reach absolute value of $(1-2)\cdot 10^{-5}\,\frac{m}{s^2}$ and the changes of the marks normal heights that of 1-15 mm, i.e. the same as the admissible error.

The effect of water mass attraction on geodetic measurements may be taken into account by two ways. The first is based on the repeated gravimetric observations with different water levels. However according to the results of the repeated gravimetric measurements it does not always happen that the gravity variations can be detected (everywhere and at any time) in the reservoir neighborhood accurately enough to calculate corrections to be introduced into geodetic measurements.

Thus, gravimetric measurements made on the dam and nearby may be of low accuracy due to the dam vibration. Moreover, to calculate variations of plumb line deviation by the results of repeated measurements of gravity using Vening Meinis formula, it is necessary to conduct comprehensive high-cycle gravimetric resurvey around the reservoir within the range of 100 km including that on the reservoir surface. This gravimetric survey requires a great amount of field works and the labor-intensive operation of gravity determination on the water surface

The second way to take into consideration the effect of water mass on geodetic observations is based on calculation of the attractive potential and its derivatives by the known volume and the form of water mass (surface), enclosed between the two levels of the reservoir, i.e. by solving the primal problem of potential theory. As we know the volume and the form of variable water mass, the attractive potential and its derivatives, caused by these masses may be obtained unambiguously at any point P (x, y, z) of the reservoir neighborhood with higher accuracy and lower working hours than with repeated gravimetric measurements.

2 INITIAL DATA AND TECHNIQUES

The calculation of the attractive potential variations and its derivatives to determine the influence of reservoir water mass on geodetic position of control points and geodetic observations can be realized as follows:

- Dynamic (mathematical) modeling of water masses;
- Development of algorithm and software modules for calculating the potential and its derivatives values;
- Development of techniques and algorithm design for taking into account the influence of attractive potential and its derivatives variations on geodetic measurements results.

Gravity field variation, spatial displacement of potential reference surfaces, changes in their curvature and a gravity vector direction become apparent in the results of geodetic measurements as changes in latitudes, longitudes and normal heights of observation points.

Let P be a point on the Earth's physical surface, on the reservoir shore (Figure 1). Applying rectangular coordinate system 0XYZ, we direct axis 0Y along the dam, axis 0X in the direction of the head race, and axis 0Z –down the plumb line.

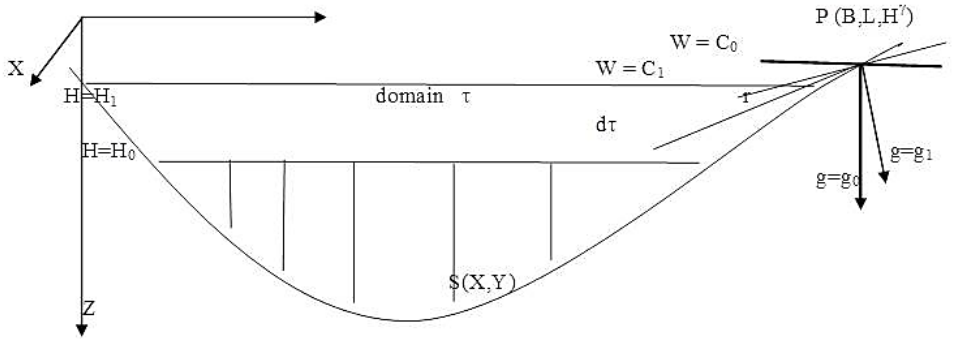

Figure 1: Cross-section of reservoir

With water level $H=H_0$ in the reservoir the reference surface of gravity potential $W(X,Y,Z) = C_0$ and the normal vector to this surface go through point $P(B,L,H^{\gamma})$

$$\bar{g}_0 = \{g_{X_0}, g_{Y_0}, g_{Z_0}\}.$$

Due to the change of water level from mark $H = H_0$ to $H=H_1$ potential $W(X,Y,Z)$ will change by value $V(P)$, and reference surface $W_1(X,Y,Z)$ will cross point P:

$$W_1(x, y, z) = C_1 = C_0 + V(P)\,. \tag{1}$$

Normal vector to this reference surface is

$$\overline{g}_1 = \{g_{x_1}, g_{y_1}, g_{z_1}\}. \tag{2}$$

In this case coordinates of point P will change by quantities:

$$\Delta B = -\frac{g_{x_1} - g_{x_0}}{\gamma(P)} = -\frac{V_X(P)}{\gamma(P)}, \tag{3}$$

$$\Delta L = -\frac{g_{y_1} - g_{y_0}}{\gamma(P)} = -\frac{V_Y(P)}{\gamma(P)}, \tag{4}$$

$$\Delta H^{\gamma} = \frac{C_1 - C_0}{\gamma(P)} = -\frac{V(P)}{\gamma(P)}, \tag{5}$$

where $\gamma(P)$ is a normal gravity force at point P.

Thus, to estimate changes of coordinates B, L, H^{γ} with the change of water level in the reservoir, we must know variations of the attractive potential ΔV and its first derivatives in coordinate axes V_x, V_y, V_z directions.

To calculate variations of the gravity potential and its characteristics (first and second derivatives), the disturbing masses of water enclosed in the corresponding area are approximated by the mathematical model, consisting of homogeneous elementary rectangular parallelepipeds. The model is constructed by approximating the reservoir volume by the system of elementary disjoint parallelepipeds $\Delta\tau_i$, whose facets are parallel to coordinate planes. Evidently, the smaller are the dimensions of elementary parallelepipeds $\Delta\tau_i$, the more accurate will be the volume approximation. However, unlimited reduction of dimensions $\Delta\tau_i$ results in the unlimited increase in the number of summands in formulas, thus, complicating experimental investigations.

Therefore the dimensions problem of elementary parallelepipeds$\Delta\tau$, approximating the area, should be treated individually for every specific case, taking into account initial data, the topographic map scale, configuration of integration domain τ**,** the required accuracy, and capabilities of computing aids to be applied.

On choosing the criterion of accuracy ε (determination of gravity potential variations and characteristics) we may obtain interval estimation of approximation accuracy. To this end the accuracy is to be estimated several times with gradual reduction of $\Delta\tau_I$

$\Delta\tau_I$. may be reduced until the difference of the two progressive approximations is less than the chosen criterion ε

$$\varepsilon(V) \le |V_i - V_{i-1}|\,. \tag{6}$$

The given technique for choosing elementary parallelepipeds dimensions makes it possible to achieve the required accuracy in solving the set problem. However it is a very laborious method. It needs multiple processing of a great amount of the initial data. To reduce the scope of computations for this problem solution, it makes sense to divide the reservoir volume into two areas: τ_1 – the central area of the reservoir and τ_2. – its shore. The central area τ_1 is approximated by the system of constant elementary parallelepipeds with the base side dimension to be chosen depending on the reservoir bed features to comply with condition (6).

Experimental computations for the interval estimation of approximation accuracy are conducted several times (separately for the shore τ_2 and central τ_1 areas) with gradual reduction of elementary parallelepipeds sides dimensions.

Each uniform rectangular parallelepiped is used to integrate and calculate elementary values of gravity potential (and its derivatives) variations, and to determine their complete values for the point under study.

3 SOFTWARE

Special software (Figure 2) has been developed to calculate gravity response of reservoir mass variations approximated by parallelepipeds with different densities.

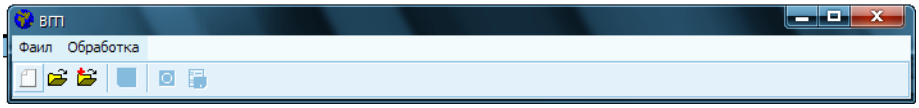

Figure 2: Active window

A software package contains two files: the executable and Model.dat-file with digital model of the Sayano-Shushenskaya HPP reservoir.

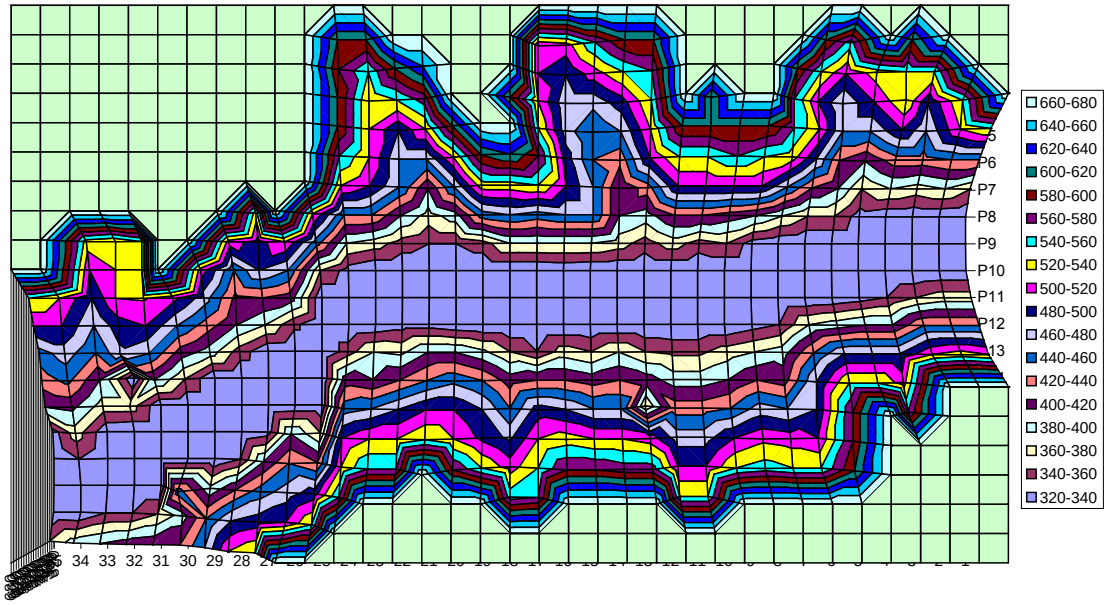

Figure 3: Digital model of the Sayano-Shushenskaya HPP reservoir dam area

The software includes the list of points to calculate variations of the gravity potential and its characteristics in accordance with the digital model of the reservoir. The lists of points may be created just in the program or beforehand.

The initial model does not contain information on the changes of reservoir water level. It is added in the program for each point separately. When initial list is opened the maximum, possible change of the water level (m) is automatically set for each point.

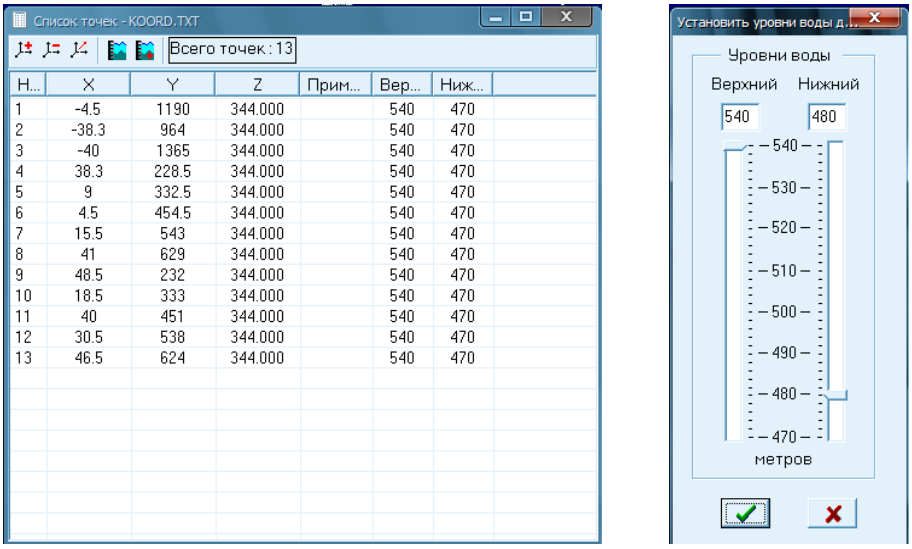

Н...	X	Y	Z	Прим...	Вер...	Ниж...
1	-4.5	1190	344.000		540	470
2	-38.3	964	344.000		540	470
3	-40	1365	344.000		540	470
4	38.3	228.5	344.000		540	470
5	9	332.5	344.000		540	470
6	4.5	454.5	344.000		540	470
7	15.5	543	344.000		540	470
8	41	629	344.000		540	470
9	48.5	232	344.000		540	470
10	18.5	333	344.000		540	470
11	40	451	344.000		540	470
12	30.5	538	344.000		540	470
13	46.5	624	344.000		540	470

Figure 4: Data processing screen

4 THE RESULTS

Special software is used for computation of gravity potential variations and its characteristics (Table 1) for the fixed points.

Table 1: Program results

ВП	potential variation (cm^2/s^2)
ВВ	height variation (cm)
ВС	vertical component (mGal)
ГС-Х	horizontal component in X (mGal)
ГС-Y	horizontal component in Y (mGal)
МСТ	gravity module (mGal)

To visualize the obtained gravity field variation characteristics in the reservoir neighborhood contour maps are created (Figure 5).

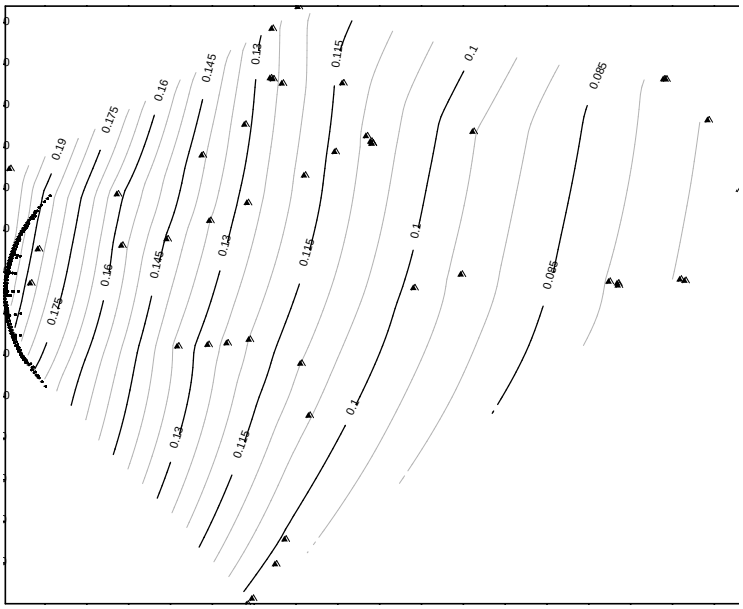

Figure 5: An example of results obtained (height variations diagram)

The developed software has been successfully tested to be used for calculation of gravity effects in construction world major reservoirs, and implemented into the Sayano-Shushenskaya HPP's automated process control system.

REFERENCES

Books:

KARLSON, A.A., PIK, L.I., PONOMAREV, O.A., SERDYUKOV, V.I.: *Engineering geodetic surveys for designing and construction of power plants* /Textbook for technical secondary school/, Nedra, Moscow, 1986.

GANAGINA, I.G., KANUSHIN, V.F., GOLDOBIN, D.N.: *Modern problems of physical geodesy* /Textbook/, SGGA, Novosibirsk, 2012.

OGORODOVA, L.V., SHIBIREV, B.P., YUZEFOVICH, A.P.: *Gravimetry*, Nedra, Moscow, 1978.

GANAGINA, I.G., KANUSHIN, V.F.: *Modern problems of physical geodesy*, SSGA, Novosibirsk, 2013.

Journal articles:

YELAGIN, S.V.: *Gravity correction in deformational monitoring of high dams,* Gidrotechnicheskoye stroitelstvo, 5/1966, p. 26 -28, 1966.

VOVK, I.G., KANUSHIN, V.F., RALCHENKO, V.F.: *Non-tidal variations of gravity around a reservoir.* Proceedings: Repeated gravimetric observations: theory and results, p. 78 – 85, 1980.

KANUSHIN, V.F., GANAGINA, I.G., GOLDOBIN, D.N., STEFANENKO, N.I. *Assessment of gravity response of reservoir mass variations on the results of deformational monitoring of main Sayano-Shushenskaya HPP facilities.*Vestnik SGGA, 7/2003, p. 44 - 46, 2003.

Technical Session 3: Geodetic Modeling of Natural Objects

Geodetic Monitoring of Natural Object Conditions (as an example of a landslide)

E.I. Avrunev, I.A. Giniyatov, D.Yu. Terentyev, M.V. Meteleva
Siberian State Academy of Geodesy, Russian Federation

Abstract
Theoretical issues of geodetic monitoring of natural object conditions are outlined. The techniques offered were used for designing a special geodetic network for monitoring landslide displacements and mathematical processing and interpretation of vertical landslide movement.

Keywords
National land monitoring, landslide, terrestrial geodetic network, horizontal and vertical movements, mathematical model of movements

The investigation of movements and deformations of natural and artificial geodynamic objects and is one of the most important challenges in contemporary science and practice. The information about movements and stressed-deformed state of the earth surface and Earth's crust caused by endogenetic and endogenic and exogenic factors is the most important in the view of forecasting disastrous geodynamic phenomena such as earthquakes, volcanic eruptions, landslides, glacier descents, rock bumps and ground subsidence in regions of mineral resources development, etc. AVRUNEV (2010). Anomalous technogeneics geodynamic processes cause X-shifts of the Earth's crust, faults formation, underground damages, inundations; not only industrial projects, engineering constructions, residential building, but also people suffer from it.

In recent years applied geodynamics data is used in new spheres: information got during investigation of the local Earth's crust areas movements and deformation is and should be used for state property cadastre and national land monitoring goals KARPIK (2004), KARPIK (2013), KARPIK (2012). It is so especially since ground area that is part of the earth surface which borders are set in accordance with federal legislation is a general accounting unit in monitoring lands and cadastre.

The values of movements and deformation parameters of the local Earth's crust zones are obtained from the mathematical processing and interpretation of multivariate time series of geodetic and other observations for object monitoring AVRUNEV (2010), SEREDOVICH (2004).

The solution of the one problem concerned the investigation of the earth surface physical state caused by landslide activity is considered in this research. Landslides are one of the most widespread physical and geological phenomena in our country resulting in considerable changes in the earth surface state STEPANYAN (1979), SHVEDOV (1997). They are abundant in valleys of the Volga, the Oka, the Kama, the Ob and other rivers and along the Black and the Sea of Azov and Lake Baikal coasts. The Crimean, Volzhsk and Baikal landslides are well-known by their caused damages.

Systematic observations are carried out for forecasting landslides and depend on landslide motion character. Today it is a common feeling that geodetic methods permit to get the most accurate quantitative data of the earth surface movements including landslides AVRUNEV (2010), SEREDOVICH (2004).

The investigation of landslide motion path and velocity is carried out during observations of deformation mark behavior located on the landslide body and during following mathematical processing and interpretation of observation results. This problem can be solved if coordinates of deformation marks at time point t1 (x', y', h') and time point t2 (x”, y”, h”) will be defined in three-

dimensional space X, У, H relative to the fixed reference system origin after specified time interval Δt = t2-t1. Then following parameters can be received: deformation mark displacement D, horisontal D_H and vertical D_V components of total deformation mark displacement, velocity of the displacement V with it horisontal and vertical components V_H and V_V and displacement direction α.

A special geodetic network used for current coordinate determination is designed and consists of deformation marks embed in a landslide body, control points embed on fixed base in the immediate vicinity of the landslide, and initial points. Making geodetic measurements in such network with given time interval Δt , the current position of deformation mark is calculated and landslide motion path and velocity t are determined.

Besides, designers impose the condition that accuracy of determined deformation mark position with regard to the geodetic datum should not be more than m_0 in plane and mHo in height AVRUNEV (2010). In this case during geodetic network designing there should be done a priori estimation of measurement accuracy - angles (m_β), sides (m_s) and heights (m_h) — according to specified mean-squared error (m_0 and m_{Ho}) and mark position in the weakest point of the network.

The presence of random errors in geodetic measurements causes an error (m_D) in deformation mark displacement in calculations. Under small velocities V_H and V_v and time interval Δt appears the situation when deformation mark displacement is within the accuracy of calculation (m_D). In this case deformation mark displacement is considered to be undetermined and deformation mark – stable. Thus during a priori estimation of geodetic network accuracy there should be determined a criterion that is used to estimate the significance of deformation mark displacement obtained from mathematical processing.

The next important point is the determination of time interval Δt between cycles of geodetic observation. Incorrectly defined time interval can cause the situation when displacement will not be detected or when deformation mark displacement path will not be determined with sufficient particularity level. That is why during the time interval Δt determination a priori set displacement velocity (V'_H and V'_v) and deformation mark displacement calculation accuracy (m_D) should be taken into account.

The algorithm of a priori estimate of measurement precision and mathematical processing of observations during projecting of the geodetic network for monitoring earth surface physical state by the example of landslide is represented in the following way.

The required accuracy of angular and linear measurements is calculated according to given mean-squared error of horisontal position for the network weakest point $m_{0.}$

$$m_\beta = \mu = \frac{m_0}{\sqrt{(Q_{Xi} + Q_{Yi})_{M\ A\ X}}},$$
$$m_S = \frac{m_\beta}{\sqrt{K}}. \qquad (1)$$

where Qij – inverse weighting matrix coefficients for corrections equations in measured values.

The required accuracy of measured heights in a designed levelling network is calculated according to a given mean-squared error of vertical position for the weakest reference point m_{H0}.

$$\mu = m_{1km} = \frac{m_{H0}}{\sqrt{Q_{H\max}}}. \qquad (2)$$

During the mathematical processing of geodetic network it is necessary to determine whether D is a displacement of deformation mark or this value D is caused only by the influence of random

observation errors in two cycles of geodetic observations. To solve this problem the following criterion is recommended AVRUNEV (2010):

$$D > D_{min}, \tag{3}$$

where D_{min} is a minimal displacement of deformation mark that can be detected during mathematical processing of geodetic network. Horizontal component is calculated by the following formula:

$$Д_{MINH} = t * m_{DH} = t * \sqrt{2} * m_{\beta H} \sqrt{\cos^2 \alpha * Q_X + \sin^2 \alpha * Q_Y}, \tag{4}$$

where t is a statistic coefficient that depends on confidence probability of the displacement significance estimation (P= 95% - t = 2; P= 99% - t = 2.5; P= 99.73% - t = 3); α - directional angle of deformation mark displacement, Q_X, Q_Y – weight coefficients of deformation mark, corresponding to the weakest point of the geodetic network; m_{DH} – accuracy of calculation of the displacement in horizontal plane.

The science-based time interval Δt_H between geodetic measurements cycles in horizontal geodetic network is calculated according to landslide body velocity and accuracy of deformation mark coordinate calculation by the following formula:

$$\Delta t_H = \frac{m_{DH}}{\sqrt{0.11} * V_H^э} = \frac{\sqrt{2} * m_{\beta H} \sqrt{\cos^2 \alpha * Q_X + \sin^2 \alpha * Q_Y}}{\sqrt{0.11} * V_H^{'}}, \tag{5}$$

where V'_H – a priori given movement velocity in horizontal plane.

A time interval Δt_V for levelling network is calculated by the following formula:

$$\Delta t_V = \frac{m_{DV}}{\sqrt{0.11} * V_V^{'}} = \frac{\sqrt{2} * m_{hH} \sqrt{Q_H}}{\sqrt{0.11} * V_V^{'}}, \tag{6}$$

where V'_V – a priori given landslide motion velocity in vertical plane.

Let's illustrate the work of the described algorithm by processing linear-angle network shown in Figure 1.

In the network under consideration we have three deformation marks located on the landslide body - №№ 5, 6, 7; two benchmarks located on stable base - №№ 3 and 7; two initial points - №№ 1 and 2. Having approximate coordinates of all points of the network and information about measured values, we can get inverse weighting matrix in which we are interested only in diagonal elements that are inverse weights of points coordinates under determination. In our case we have:

$$Q = \text{diag} \{\underline{0,2394; 0,2126;} 0,0706; 0,1064; 0,0181; 0,1073; 0,0880; 0,3303; 0,1215; ,1794\}. \tag{7}$$

In accordance with available numbering and calculated weight coefficient values the weakest point in the network is point №3, which weight coefficients sum is maximal (elements are underlined). Having performed all further calculations in accordance with algorithm given before, we get following results (Table 1).

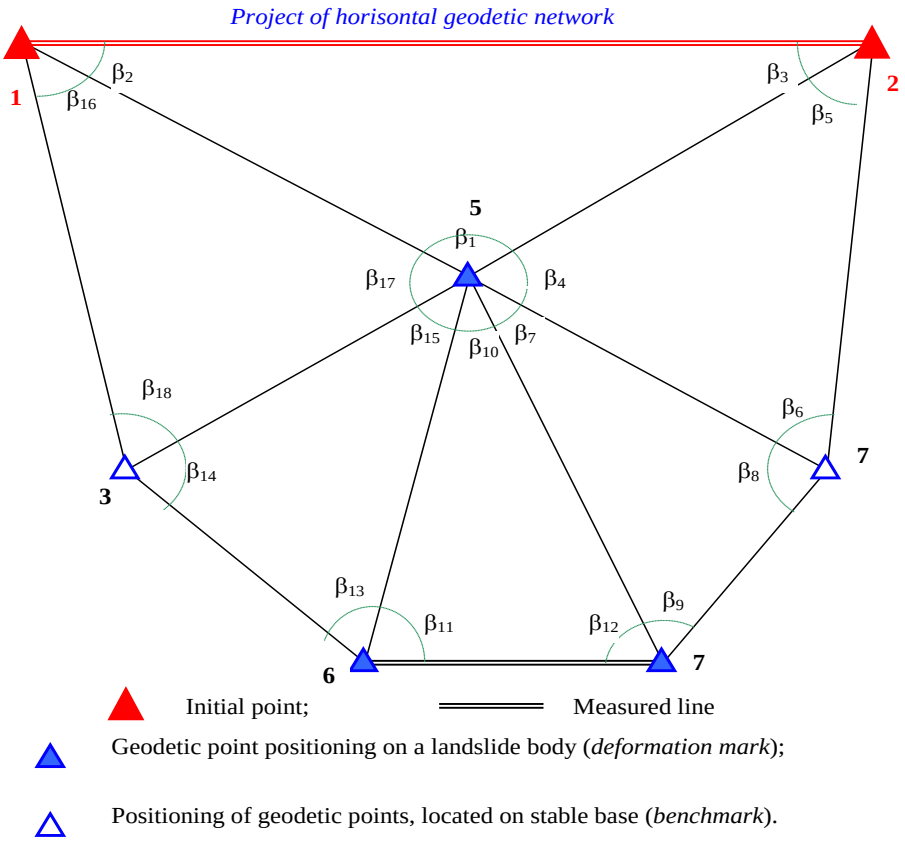

Figure 1: A project of horizontal geodetic network

Table 1: The results of a priori evaluation of horisontal geodetic network characteristics

№№	Network characteristics	
1	A method of horisontal geodetic network design	Combined network
2	The number of measurements/observations	n = 19
3	The number r of parameters to be defined	t = 10
4	The number redundant measurements	r = n – t =9
5	Line lengths in horisontal geodetic network	S_{av} = 1.5 km. S_{max} = 2.0 km S_{min} = 0.98 km
6	Site perimeter	∑S = 9.5 km
7	A weak network point and its weight coefficients	№3, Q_{X3} = 0.2394,Q_{Y3} = 0.2126
8	Minimal deformation mark displacement	$D_{min\ H}$ = 6.6 cm
9	Time interval between observation cycles	Δt_H = 33 days

CONCLUSIONS

The solution only of one problem obtained during national land monitoring and connected with investigation of the earth surface physical state modifications produced by landslides is considered in this research. Obtained results can be used in projecting specific geodetic networks to observe landslides movements (including choice of the network type, tools and methods of measurements, calculation minimal value of deformation mark displacement, that can be determined in this case, and definition optimal time interval between measurement cycles) and are recommended for practical use. It should be pointed out that only horisontal landslide movements are considered in this research, whereas similar conclusions are made also for vertical landslide movement and can be found by all interested persons.

REFERENCES

Books:

AVRUNEV E.I. *Geodetic supplying of state property cadastre* / E.I.Avrunev. Novosibirsk. SSAG, 2010.

KARPIK A.P. *Methodological and technological basis for GIS support of the territories*: Monograph. – Novosibirsk: Siberian State Academy of Geodesy (SSAG), 2004 – 260 p

SEREDOVICH V.A. et al. *Movements and stressedly-deformed state of self-organizing geodynamic systems identification by complex geodetic and geophysical observations*: Monograph / V.A.Seredovich, V.K. Pankrushin, Y.I.Kyznecov, B.T.Mazurov, V.F.Lovyagin; SSAG.- Novosibirsk, 2004. - 356 p.

STEPANYAN G.I. *Geodetic methods of landslides dynamics research*. – M.: Nedra, 1979.

SHVEDOV G.I. *Engineering geology, soil mechanics, foundations*. – M.: Higher School, 1997

Journal articles:

KARPIK A.P. *Creation of territories uniform geo-environment to improve geodetic dataware for state property cadastre* / A.P.Karpik, V.I. Obidenko.-Interexpo Geo-Siberia-2013. T. 1. Economics of nature management and property. P. 1: proceeding of IX International Scientific Congress and Exhibition Interexpo Geo-Siberia -2013, 24-26 April 2013, Novosibirsk.- Novosibirsk: SSAG.

KARPIK A.P., *Horoshilov V.S. Essense of territories GIS environment as common base for state property cadastre development* // News of higher educational institutions. Geodesy and Aerophotography. – 2012. – № 2/1. – p. 134–136.

Special Aspects of Mathematical Landslide Processes Modeling by Geodetic Data during Blasting Operations and Transportation of Big Soil Masses

Valery Khoroshilov, Olga Pavlovskaya
Siberian State Academy of Geodesy, Russian Federation

Abstract
The article describes the technique of landslide dynamics analysis and estimation through the results of long-term geodetic observations over the landslide benchmarks vertical movements on the bank of the Angara river in the zone of construction a rockfill dam of the Boguchanskaya HPP while carrying out blasting works and earth disposal from open-cast mines because of lack of information concerning the time and intensity of the impact.

Keywords
Geodetic observations, negative and positive components of landslide movements process, movements rate, inter-cycle time interval, process modeling

1 INTRODUCTION

The relevance of studying the landslide movements dynamics is determined, primarily, by landslide hazard areas while constructing and maintaining of engineering structures such as large hydroelectric plants, dams, bridges, etc. The subject of our research was the landslide process developing in the area of construction a rockfill dam of the Boguchanskaya HPP while carrying out blasting operations and the disposal of earth from the open-cast mines. This process was presented with the geodetic data concerning landslide slopes vertical displacements because of lack of information about particular places, time and intensity effects.

The investigation of the landslide slope reaction to blasting operations and earth disposal was conducted by means of geodetic data concerning the vertical displacements of the five benchmarks, fixed at the surface. These benchmarks were not destroyed by the explosions and have been preserved for 9 years. Vertical movements were determined by a third-class leveling conducted along the entire right bank landslide zone. Intercycle leveling network adjustment was conducted by VASILIEV, GULYAEV and PAVLOVSKAYA (2010). The basic data for further research was introduced by cycle standardized benchmark elevations and their mean errors. The study of vertical displacements changes in time showed that the number of observation cycles and calendar periods of their implementation didn’t allow revealing the seasonal influence of natural factors, suppressed by a technogenic impact. However, the influence of explosions and disposal of earth in the form of successive alternations of negative and positive values of landslide benchmark displacements took place.

2 THE METHOD OF LANDSLIDE DYNAMIC ASSESSMENT

The proposed assessment method of landslide mobility consists of two components PAVLOVSKAYA, KHOROSHILOV & NOSKOV (2012), PAVLOVSKAYA, KHOROSHILOV & NOSKOV (2013). The first component relates to the search of invariants of stable or more stable reference stations out of a landslide benchmark group in terms of their mobility. The second component refers to a landslide mobility assessment through geodetic observation results. Determination of invariants of stable or the most stable observed landslide benchmarks allows

representing more objectively the real landslide processes evolution in the conditions of some uncertainty of geodetic information. The method of investigation of the reference stations mutual stability, suggested by Fedoseyev J.E. (KLYUSHIN, MIKHELEV & BARKOV (1993)) was used as a mathematical algorithm. This technique allows not only to identify unstable benchmarks through the inter-cycle heights variations of the observed benchmark group in the system of their average height, but also to establish the degree of their displacement. Using this method all the benchmarks elevations in the group under study were corrected, i.e. the results of the actual benchmark heights were obtained GULYAEV & PAVLOV (1993), VASILIEV, GULYAEV & PAVLOVSKAYA (2010).

In the next step according to the corrected benchmark elevations there was a transition from the values of displacements observed at different inter-cycle time intervals to the velocities of these movements. This was the way we standardized the controlled parameters of the process investigated regardless of inter-cycle time intervals. In the stage of transition from the adjusted benchmark elevations and from the movements rates, being observed at different inter-cycle time intervals, to the velocities of these movements, the comparative analysis showed that in only 24 cases out of 120 the velocities values were less than the errors of their calculation. The short interval close to the absolute values between rates and their errors was caused by slow speeds during short inter-cycle time intervals, as well as insufficient precision of the third-class leveling. It was also taken into account that the value of the plus velocities were reduced due to continuing landslide natural movements down while disposing of earth, but the minus velocities were decreased due to inertial effect of earlier disposal of earth. Figure 1 shows temporal development of negative and positive values of the observed sliding process. Thus, the different reaction of the landslide slope on blasting operations and earth disposal was proved. In the next stage this data provided the basis for a separate analysis of negative and positive values of vertical displacements in accordance with their deterministic - probabilistic nature.

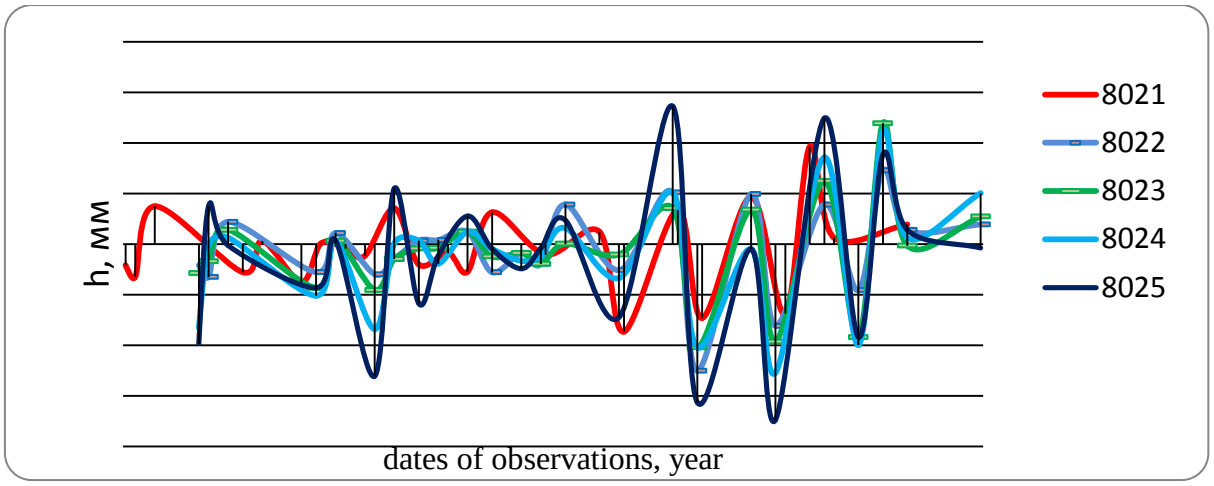

Figure 1: Positive and negative components of a vertical displacement process due to blasting works and landslide earth disposal

The following stage of the negative and positive landslide displacement research involved mathematical modeling of this process, consisting of a number of procedures. The initial procedure consisted of grouping of negative and positive movements, reflecting the different nature of the slope reaction to the explosive and earth disposal works (Figure 2).

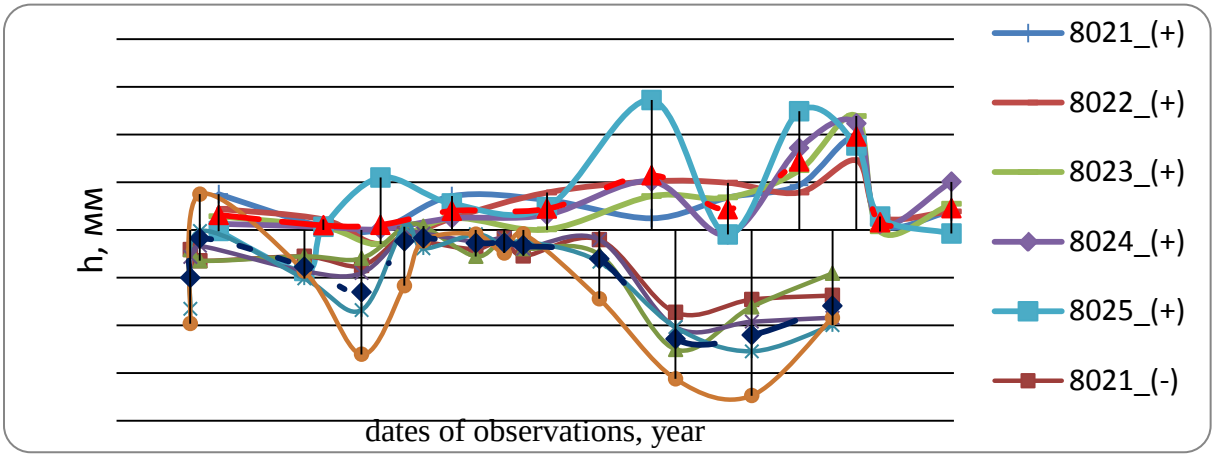

Figure 2: Results of a separate design of the negative and positive components of the vertical movement process

Further the process of a separate center assignment of the above mentioned components was carried out, which has resulted in the character of a two-way human impact in the form of temporal changes of average displacement values, recorded during the observations (Figure 3, 4).

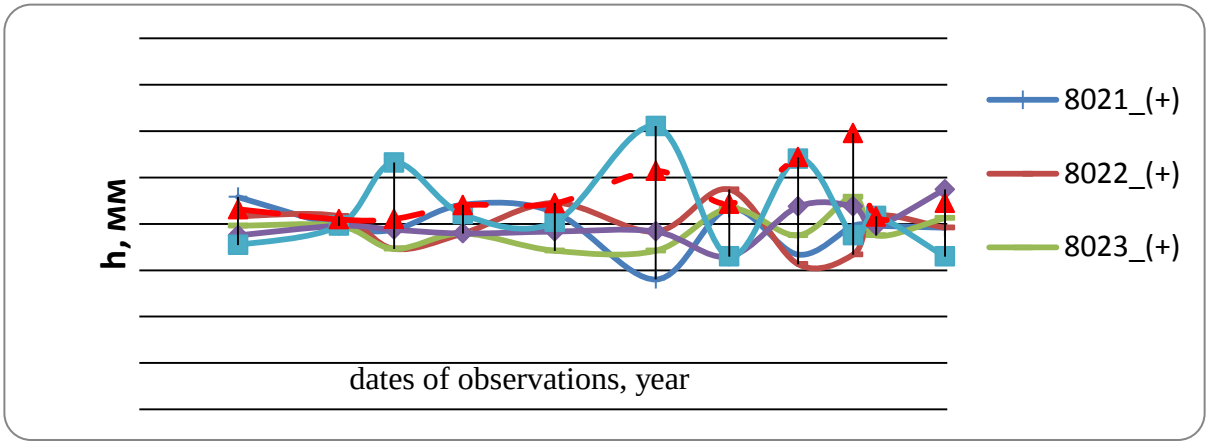

Figure 3: The centering of the positive component of the vertical movement process during blasting operations and landslide earth disposal

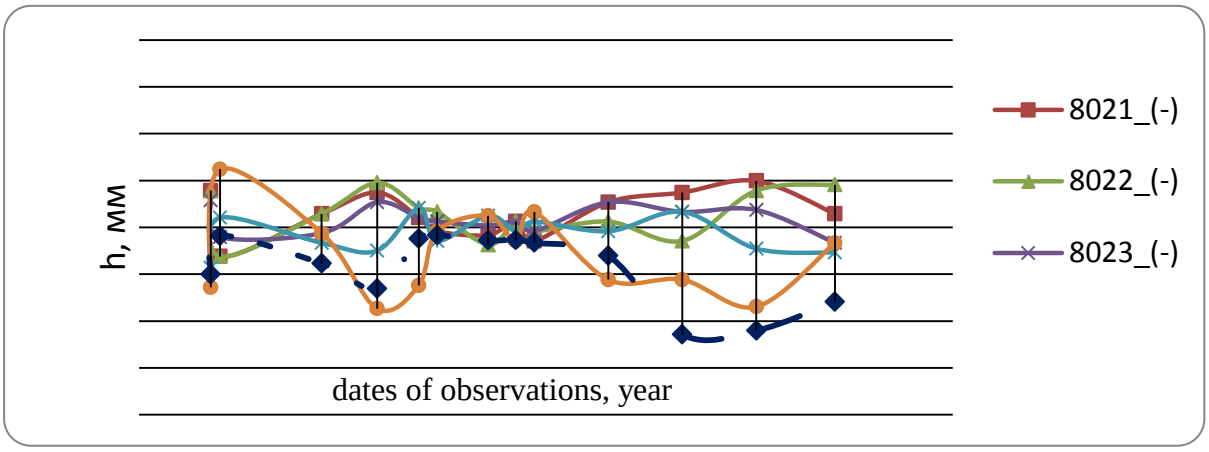

Figure 4: The centering of the negative component of the vertical movement process during blasting operations and landslide earth disposal

Centered values of the process negative component had mostly a positive trend of development, and the values of the positive component had a negative trend, that confirmed the above-noted compensational and inertial influence of the factors. In this case the centered values of both components of the process mainly reflect the natural character of its development with a slight technogenic impact. That's why they turned to be similar in value, and this factor allowed uniting the centered process into five realizations by averaging its values according to closely spaced adjacent sections and incorporating the values of individual remote sections. In total, we obtained five combined realizations of the centered process and two development graphs of negative and positive vertical displacements, characterizing the degree of influence of each of the considered technogenic impacts (Figure 5).

The next procedure consisted of modeling of five centered realizations in a kinematic form as a law of their distribution, represented by approximated standard in time and autocorrelation function with a zero expectation value, following the Gaus law of distribution in the profiles of mathematical models that were developed by Gulyaev. The designed forecast mathematical models PAVLOVSKAYA, KHOROSHILOV & NOSKOV (2013) in the form of approximate in time standards and autocorrelation function with zero expectation value have the following form:

$$m_x\left(t_j\right)=0;\ \frac{1}{\hat{\sigma}_x\left(t_j\right)}=0{,}8302\frac{1}{t_j}+0{,}3128;\ \eta_{\sigma t}=0{,}998. \qquad (1)$$

$$\hat{r}_x=0{,}84995^{\,-0{,}02802t_2};\ \eta_{rt}=0{,}475.$$

A received combined process (without a technogenic impact) is stationary, correctly distributed with the expectation value close to zero.

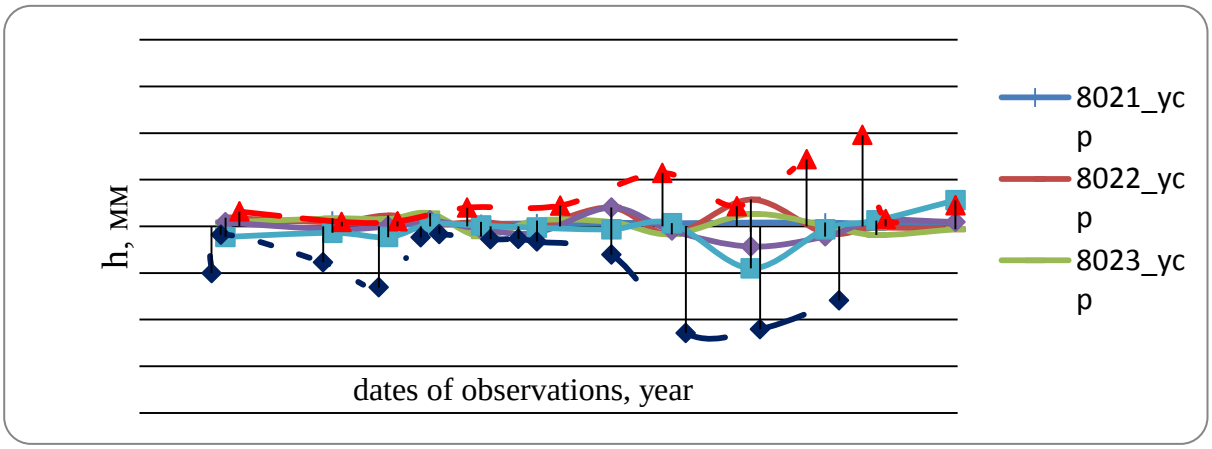

Figure 5: The united centered process of the negative and positive components in the form of five realizations

It should be noted that separate centering of the negative and positive process components allowed revealing a previously unknown nature of the impact in time and according to the intensity of two main technogenic impacts. This nature was expressed in the form of the changes of the observed mean benchmark displacement values. Meanwhile, the centered values of negative and positive components reflect mainly the evolution process, impervious to technogenic impacts. Therefore, these components can be regarded as a single process. The dotted borders of the averaged centered processes (Figure 5) restore the lost retrospective of blasting works and the landslide earth disposal works through geodetic data that is very important for further research. The available topographic1:5000 scale maps with explosion craters allow to calculate analytically a certain amount of the disposed rock material and to calculate the power of explosions for “ragging” the rock material.

All the mentioned solutions and the research done create the basis for parametric identification of the observed landslide process in a dynamic form presented by the negative and positive components as the two main influential factors. But the additional noise component model aimed at identification and analysis of unaccounted factors while forecasting the regularities of a sliding process can be made by means of the 1st- or 2nd - order autoregression DERUSSO, ROY & CLOSE (1970), KRAMARENKO, MAZUROV & PANKRUSHIN (2005).

For example, the dynamic model of the 2nd order and "input-output" type, describing a scalar process of displacements in a recurrent form under the influence of two main factors, has the following form:

$$\begin{aligned} x_k &= \phi_1 x_{k-1} + \phi_2 x_{k-2} + \beta_1 u'_k + \beta_2 u''_k + \gamma\omega_k; \\ \omega_k &= \lambda\omega_{k-1} + \mu\omega_{k-2} + \xi_k, \end{aligned} \qquad (2)$$

where x_k – output variable represented in the form of centered values of the positive and negative components as a single process, impervious to technogenic impacts on the *k*-th interval of a model discretization, step value is equal Δt;

u'_k, u''_k – two main impacts in the form of blasting works and earth disposal works;

ω_k – the joint action of unaccounted factors (noise component) in the form of the landslide slope reaction to blasting operations and earth disposal works;

ϕ_1, ϕ_2 – dynamic indices, reflecting the degree of influence of the displacement values x_{k-1} and x_{k-2} on x_k, i.e. inertial system properties;

β_1, β_2, γ – Indices, characterizing the degree of influence of two main impacts and the noise component on a displacement value;

λ, μ – model parameters of a noise component in the form of the 2nd order -autoregression;

ξ_k – So-called "white noise".

The parameters $\phi_1, \phi_2, \beta_1, \beta_2, \gamma$ are estimated according to the observation results (analytical calculations) for the temporal variation of the influencing factors and displacements; parameters λ, μ are assessed according to the residual errors of the sliding process approximation with the basic equation (2); ξ_k – an unestimated parameter**.**

The landslide process forecast model, designed according to Eq. (2) during the forecast period, has the following form (the last discretization interval is denoted by *N*):

$$\begin{aligned} \hat{x}_{N+1/N} &= \hat{\phi}_1 x_{N+i-1/N} + \hat{\phi}_2 x_{N+i-2/N} + \hat{\beta}_1 u'_{N+i} + \hat{\beta}_2 u''_{N+i} + \hat{\gamma}\omega_{N+i-1/N}; \\ \hat{\omega}_{N+i/N} &= \hat{\lambda}\hat{\omega}_{N+i-1/N} + \hat{\mu}\hat{\omega}_{N+i-2/N}, \end{aligned} \tag{3}$$

under $x_{N/N} = x_N, x_{N-1/N} = x_{N-1}, i = 1,2,3...,\ \hat{\omega}_{N/N} = \hat{\lambda}\frac{\varepsilon_N}{\hat{\gamma}} + \hat{\mu}\frac{\varepsilon_{N-1}}{\hat{\gamma}}$, where ε are residuals.

The calculated benchmarks displacements according to the designed forecast model of the landslide process by Eq. (3) can be subsequently compared with the benchmark displacement results according to the same model for a combined process in the form of temporal approximate standard and autocorrelation function with zero expectation with Eq. (1).

3 CONCLUSION

As a result of the research done, the methodology of a landslide process separation was developed in the form of two components, related to blasting works and earth disposal from the quarries was proved analytically. The technique of the transition to a centered normally distributed process of the landslide vertical displacements with zero expectation has been accomplished. It's important to note that this process was free from the influence of blasting and earth disposal operations. There also took place the procedure of a kinematic modeling of a combined sliding process. On the basis of the proposed parametric identification it's suggested to present the landslide process in the form of a dynamic second-order model that describes the scalar displacement process in a recurrent form, under the influence of two main factors. Then the results of the calculations according to different mathematical models were compared.

REFERENCES

Books:

KLYUSHIN, E., MIKHELEV, J., BARKOV, D.: *Practical course on Applied Geodesy. Geodetic support of constructing and engineering structures maintenance.* Moscow, Nedra, 1993.

Journal articles:

DERUSSO, P., ROY, R., CLOSE, CH.: *The state of space in control theory*. Moscow, Nature, 1970.

GULYAEV, A., PAVLOV, P.: *Geodetic studies of technological geodynamics at Boguchanskaya HPP*, Hydroengineering, № 9, p. 8-11, 1993.

KRAMARENKO, A., MAZUROV, B., PANKRUSHIN, V.: *Computer experiment on movements identification and constructions disorganized conditions and engineering geodynamics objects according to geodetic observations,* Geodesy and Aerial Photography, № 6, p. 3-14, 2005.

VASILIEV, E., GULYAEV, Y., PAVLOVSKAYA, O.: *Improving the geodetic studies efficiency of sliding slopes dynamics*, Geodesy and Cartography, № 9, p. 6-9, 2010.

PAVLOVSKAYA, O., KHOROSHILOV, V., NOSKOV, M.: *Technique of homogeneous landslide zones separation through the results of geodetic observations of aqueous benchmarks vertical displacements*, Geodesy and Aerial Photography, № 5, p. 31-34, 2012.

KHOROSHILOV, V., PAVLOVSKAYA, O., NOSKOV, M.: *Analysis and evaluation of a landslide dynamics on geodetic data under the conditions of blasting works and earth disposal*, Geodesy and Aerial Photography, № 4, p. 19-24, 2013.

Geodetic Monitoring of Contemporary Deformation Conditions of Near Surface Structures of South Siberia

Vyacheslav G. Kolmogorov
Siberian State Academy of Geodesy, Russian Federation

Abstract
The article focuses on the problems concerning geodetic monitoring of geodynamic processes in seismic active zones in South Siberia.

Keywords
Contemporary vertical movements of the earth's surface (CVMES), geodynamics, the CVMES velocity gradients, the earth's surface deformation.

1 INTRODUCTION

Nowadays the human society faces the problem – to define that possible degree of interfering into natural processes, that would make it possible, without interrupting technical progress, to avoid natural disasters, or, at least, to soften the danger. In order to solve this problem it's necessary to define diagnostic factors that will accurately and fully reveal the regularities of contemporary geologic processes evolution being influenced by technogenic effect. Such factors can be considered as contemporary deformations of earth's surface that are defined through the repeated precise geodetic measurements data.

In the 2-nd half of 20-th century there started the research of laws of spatio-temporal dynamics of the earth's surface parts deforming in West Siberia, and at the turn of 80-ties there took place the intensive geologic-geophysical exploration and obtained considerable amount of precise and high-precise relevelling data. One of the perspective scientific areas, aiming at solving ecological problems and improving exploration effectiveness is connected with geodynamic research.

On the first stage of geodynamic research special attention is paid to phenological (descriptive) geodynamics, aiming at geodetic, geological and geophysical data systematization, at complex geodynamic interpretation within the bounds of static (structural) and kinematic cartographic models. Scientific prerequisites for systematic research (monitoring) of contemporary earth's surface deformation to reveal mega-structural elements' peculiarities, are as follows:

1. the size and the direction of earth's surface deformation are expectedly determined not only by contemporary physic-chemical processes in deep earth's zones and upper mantle, but also by peculiarities of territorial geostructural elements distribution and their boundary zones, that were being formed during all the geological period and are naturally reflected in geophysical fields;
2. since the local structures distribution in sedimentation mass and regional pinchout zones and stratigraphic unconformity of sedimentary rock are controlled by regional blocks, boundary zones between them and innerblocking boundaries, reflected in contemporary earth's surface deformation, then the latter can be used to explore the hydrocarbons deposits location.

As a result of the above we can define the following aims of research for the nearest future:

1. to determine recent kinematic parameters of the region under investigation, that will allow to investigate local peculiarities of the deformation processes and to find out their interrelations with geological structure, to compile maps and charts that characterize a detailed dynamics of mega-structure under investigation;
2. to determine the territories of maximum earth's surface deformation by means of complex analysis of geodetic and geologic-geophysical data.

The principal research method is the correlation-regression analysis of precise relevelling data and geologic-geophysical data received from the territories of South Siberia, including southern parts of Western Siberian Plate (WSP) and Siberian Platform (SP), their joint zone (Yenisei Mountain Range), Altai-Sayans area (Asa) and Baikal Rift zone (BRz).

2 THEORETICAL BASIS AND EXPERIMENTAL BACKGROUND

The investigations in the West Siberia region were started in the 80-ties and first results were published in [1]. On the first stage there prevailed geotectonic aspect of studying contemporary tectonic activity in Siberia, which is the basis on “structural analysis” of repeated levelling data. The main idea of the analysis is: the complex spatio-temporal evolution process of lithosphere led to its significant differentiation from equally distributed geostructural elements of different kinds and categories from lithosphere plates, platforms of different ages, geosinclines, domes, troughs, fore and intermountain downwarpings to local structures. Because of various physical properties of rock and deep-zone substances, and also rock elements bedding, the mentioned non-homogeneities of geophysical environment, on the one hand, are naturally reflected in stationary geophysical fields, and on the other hand, predetermine the nature and peculiarities of spatial distribution of current crustal movements KOLMOGOROV & KOLMOGOROVA (1990).

The general idea about the nature and value of recent vertical movements of massive southern parts of Siberia is shown by graghs of day-time levels and datum points changing heights, obtained by means of first relevelling unadjusted data along the Kinel – Kuibyshev – Novosibirsk – Chita line during a 25-year period (Figure 1). The giant West Siberian trough is characterized as a vast territory of contemporary downwarping with a velocity of 6-12 mm per year. The sizes of anomalies of contemporary vertical earth's surface movements (CVMES) vary from 3 000 km (the first order structures) to 500 – 1000 km (the second order structures). Along the whole profile length the heights curve repeats in general the earth's surface. But nevertheless the recent and newest movements differ not only in velocities values and territorial boundaries of up- and downwarpings, but in amplitudes coincidence for all class structures, except faults.

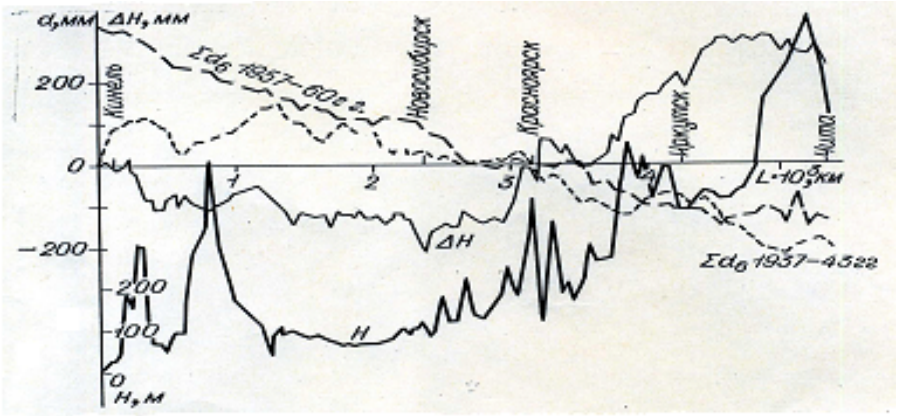

Figure 1: Line of repeated levelling Kinnel – Chita

H –high point of earth's surface, m; ΔH – heights changes, mm; d_6 – mean elevation difference, obtained with direct and reciprocal levelling, mm.

Thus, the analysis of unadjusted CVMES velocities along the profile definitely allows to divide recent movements into the regional (primary, directly connected with deep processes) and the local ones, which are elastic-tough resistance of rocks with different physical properties to complex strained conditions being caused by primary crustal movements, e.g. in fault zones. The tectonic-physical interpretation of abnormal movements change directly above the faults and the investigation of their formation and evaluation of their distribution prove the fact, that quick strained affect near the fault boundaries can be the consequence of crustal fault development. In accordance with the above, the principle of defining activated faults zones by CVMEC data is based upon the fact, that on these surfaces the concentration of abnormal values of movements velocities, their horizontal gradients, curvature changes of the surface etc. are fixed in narrow zones near the faults.

The CVMEC investigation on vast territories aiming at revealing long-period component of these movements and their regional features appearing in contemporary up-and-downwarpings and the transition zones is carried out by means of recent movement models mapping (Figure 2) KOLMOGOROV (1997).

The process of modeling CVESM includes:

1. Definition and evaluation of current movements through repeated levelling data;
2. CVESM velocity filtration by means of quadratic filter in order to eliminate measurement errors caused by random disturbances and high-mobility fault zones;
3. Detection and description of empirical correlation between the nature of CVESM velocities values and geologic-geophysical parameters.
4. Interpretation of CVESM velocities and their mapping.

Interpolating of CVESM velocities and their isobases mapping on territories, covered with random network of repeated levelling, is carried out on the method, based on using correlation relationships between CVESM velocities and geologic-geophysical earth's crust parameters KOLMOGOROV & KOLMOGOROVA (2000). The most effective method of CVESM velocities forecast is the so-called analogy method when standard area values reveal the correlation between the process under investigation and some value, measured on standard and prognostic areas, and the parameters values of the process under investigation are predicted according to the particular type of the relationship.

Assuming the CVESM velocities scalar field, drawn on map, for regular surface, and using differential geometry formulas through fundamental Gaussian values, they define its inclinations and curvatures, the axes vectors of maximal inclinations and curvatures, that are interpreted as the related components of earth's surface deformations.

The material concerning the current crust movement, accumulated so far, allowed to do the research into correlation links of different crust parameters in 2D space and, using methods of correlation cartography, it is possible to make a set of maps, showing the correlation between CVESM, earth's surface elevations, crust thickness and other geologic-geophysical parameters. For this purpose they use wide variety of ways of correlation-regression analysis that allows designing cartographic correlation models (KOLMOGOROV & KOLMOGOROVA (1990), KOLMOGOROV & KOLMOGOROVA (2000), KONTOROVICH & SURKOV (2000), KOLMOGOROV & KOLMOGOROVA (2002), KOLMOGOROV (2013)).

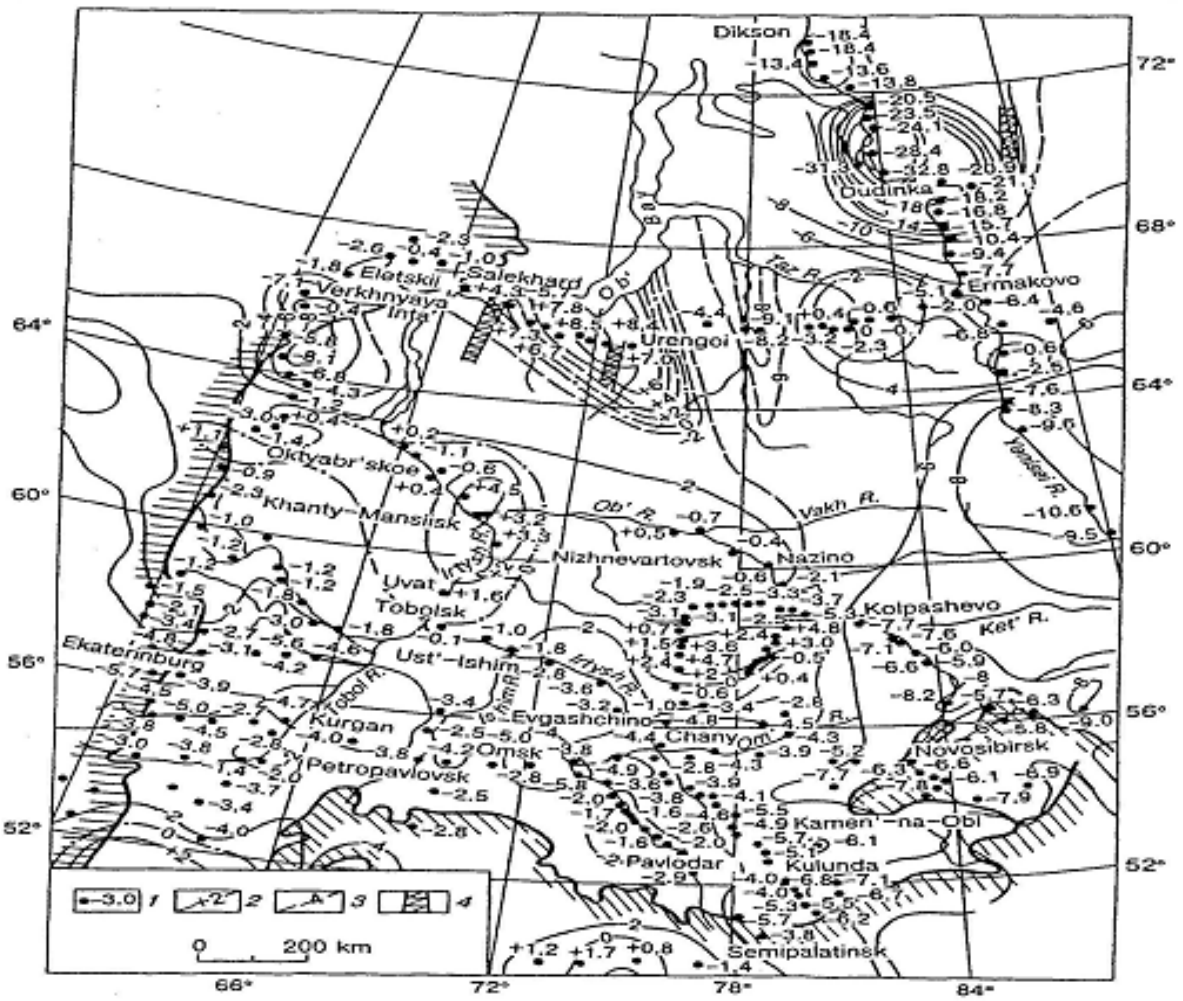

Figure 2: Map of current earth's surface vertical movements of West Siberia (according to geodetic data. **1− leveling datum and CVMES velocities**, **mm/year; 2 – isobases and values of velocities, mm/year**; **3 – hypothetic isobases, mm/year; 4 – zones of elevated horizontal gradients of PVMES velocities, year^{-1}**.

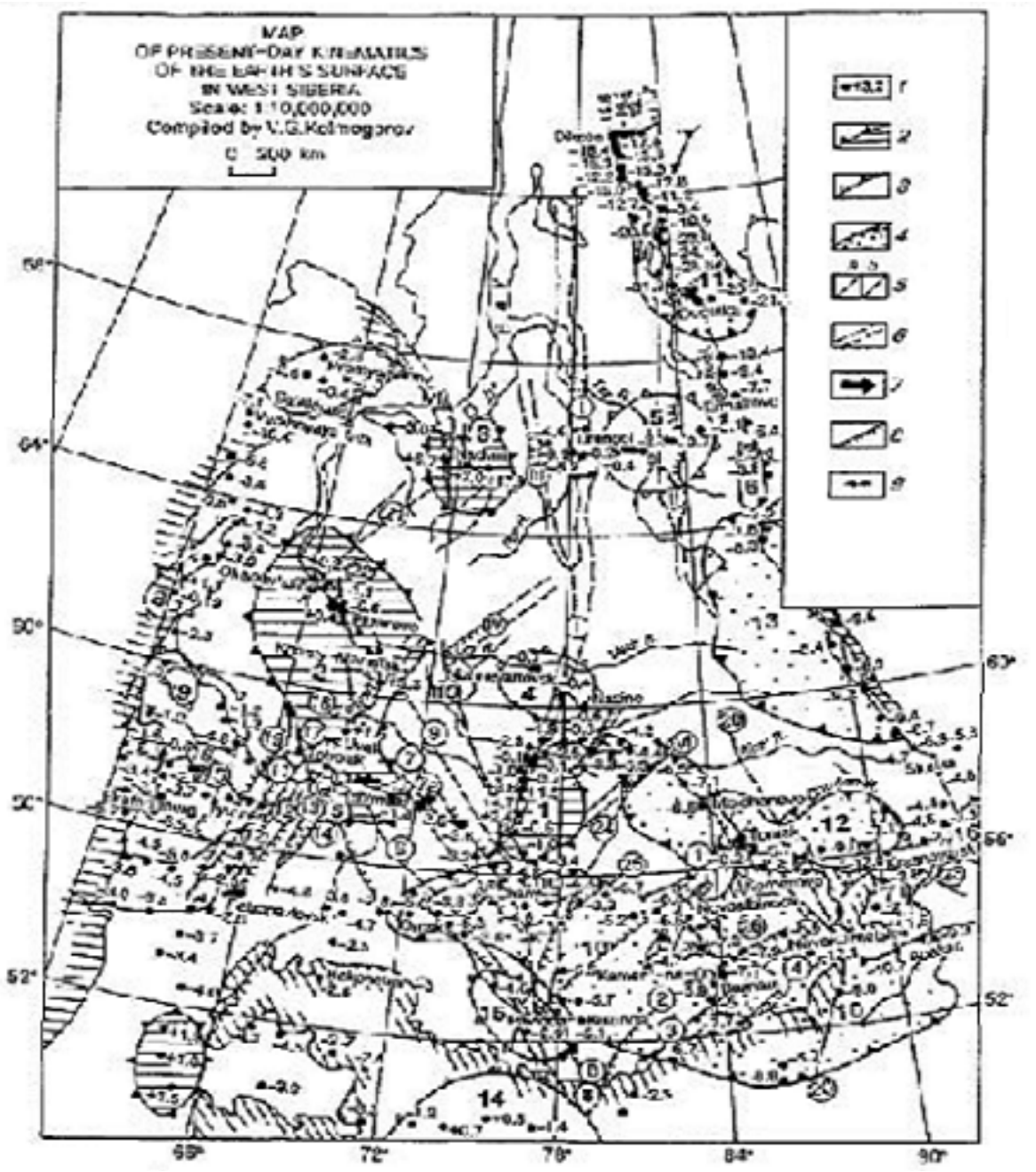

Figure 3: Map of recent kinematics of the earth`s surface in West Siberia. 1 – absolute velocities of recent up- and downwarpings, mm/year; 2 – ***absolute dome rises:*** **1 – Kaimus, 2 – Uvat-Khanty-Mansi/ 3 – Nadym, 16 – Angara-Kan;** ***3 – relative rises:*** **4 – Nizhnevartovsk, 5 – Taz, 6 – Turuckan, 7 – Bellyk, 8 – Kugigino, 9 – East-Uralian, 14 – Semipalatinsk monocline, 15 – Pavlodar;** ***4 –structures of intense downwarping:*** **10 – Kulunda-Kuznetsk, 11 – Ust`-Yenisei, 12 – Upper-Chulym, 13 – Kas-Yenisei; 5 –** ***faults recognized by geological-geophysical methods (a) and expressed in current deformations of the earth`s surface (b); 6 – graben-rifts*****: I – Koltogory-Urengoi, II – Khudosei, III – Khuduttei, IV – Agan, V – Ust`-Tym, VI – Chuzik.** ***Types of the earth`s surface deformations in zones of active faults: 7*** **– regional inclination (*ά*-deformation); 8 – predominant step-like S-deformation (normal and apthrust faults); 9 – predominant bending deformation with positive curvature. Encircled digits stand for fault numbers.**

3 AUTOMATED INFORMATION SYSTEM OF SEISMIC ACTIVITY MONITORING IN THE MOST DANGEROUS PARTS OF SIBERIA

The main aim of seismic activity monitoring is to recognize and investigate earthquake ***forerunners***. Such forerunners can be any abnormal geodynamic spatio-temporal phenomena, occurring before or during the earthquakes. The nature of such phenomena is complex and various, thus, for their registration and detailed investigation complex approach is required. The basic methods of this approach are the repeated geodetic and the geophysical monitoring methods. The latter can be referred to the observation with laser strain-metrical complex of the Institute of Laser Physics SB RAS (BAGAEV, ORLOV, RYBUSHKIN, SEMIBALAMUT & FOMIN, BAGAEV, ORLOV & PYATIGORETS (2006)).

The main advantage of the observation with this complex, as well as by the other geophysical (dipmetering, strain-metrical, hydrostatic, gravimetrical, by laser strain meter, etc.) methods is *continuity in time*. The main disadvantages of all these methods are:

a) *very small base*, which, compared with investigated regions, is just a point;
b) the necessity of providing *very strict observation conditions*, avoiding any impact (at first temperature variations and air humidity, atmosphere pressure) on measurement results, which requires significant expenses for special station equipment (in mines, basements of big buildings or construction of special laboratories).

Repeated geodetic measurements are a *discrete* method, and that is its disadvantage. However, the opportunity to carry out exact measurements in optimal repetition periods on vast territories possessing different morphostructural and tectonic conditions makes this method irreplaceable not only in investigating geodynamic conditions of region, but also in monitoring in epicenter zones for creating scientific prerequisites of earthquakes forecast.

At the end of the last century, in 80-ties about 50 geodynamic polygons of different kinds were set up in the Soviet Union. On prognostic polygons in seismic danger zones they built so-called “sites for deformation observations” (with measured lines of 2 – 5 km long) with geodetic constructions (quadrangles, chains of triangles and other shapes), on which they carried out highly-precise angular and linear measurements and levellings according to first-class high-precision program (average occasional error is less than 0,5 mm for 1 km of double way). The changes of measured geodetic elements were used to calculate for these shapes horizontal (dilatation and heave) and vertical (inclination changes and curvature) components of crustal deformation, that can appear as a scientific prerequisites to make earthquakes forecast, i.e., to define location, time and intensity of earthquake.

To control dynamic crustal processes it is proposed to create on regional polygon at least 2-3 “sites for deformation observations” with the area of 20-25 sq. km with the observatory in the center, where it is necessary to organize the following research activities:

- continuous temporal observations for varieties of geophysical fields (gravitation, magnetic, thermal, etc.), for time changes of plumb bob and inclinations of the earth's surface (tiltmeter), changes of short basis lengths (by laser strain meter), changes of elevation between fixed in certain order levelling bench marks (continuous measurements of the recent parameters can be carried out by means of hydrostatic levelling);
- discrete measurements of geodetic elements (horizontal and vertical angles, azimuths, line length and levelling elevations) on the points of “a site for deformation observations”, built on fault, by changes of which for the ground center it is possible to calculate the components of horizontal (dilatation and heave) and vertical (horizontal and vertical gradients of the earth's surface points vertical movements, earth's surface curvature changes) earth's surface

deformations, and also for the whole ground such characteristic as divergence (the information about inhomogeneous density of upper crustal layers) and rotor (the rotations of the ground or its separate parts);

- construction of “geodetic crossings” (geodetic vertical and horisontal network, levelling lines, alignment survey crossing disrupted structure) on the faults, located on “the ground”;
- synchronously with geodetic measurements on the points of the “site for deformation observations” should be carried out the discrete precise geophysical measurements of the abnormal gravitational and magnetic varieties.
- revealed on the “sites for deformation observations” temporal changes of certain geodynamic parameters (lengths, directions, geophysical fields anomalies, etc.) can be used as temporal corrections in the results of discrete regional geodetic (earth-based as well as satellite-based) and geophysical measurements.

The final research result of correlations, obtained with geodetic methods, of geokinematic paramerters with the geophysical ones should be the model of temporal change of crust strained-deformating condition on the site under investigation.

4 BASIC STAGES OF SOLVING GEODYNAMIC PROBLEMS

The investigations of subsurface structures deformation conditions in South Siberia are supposed to be carried out in 3 stages (KOLMOGOROV & KOLMOGOROVA (1990), KOLMOGOROV & KOLMOGOROVA (2000), KONTOROVICH & SURKOV (2000), KOLMOGOROV & KOLMOGOROVA (2002), KOLMOGOROV (2013)):

1. Data collection concerning CVESM in South Siberia during recent years (information about repeated precise and highly-precise levelling, conducted after a period of 1985-1986, their quality assessment);
2. Improvement of a comprehensive analysis of geodetic and geological-geophysical data, and their relations and correlations reveal, improvement of active faults zones revealing methods according to repeated levelling data, compilation of active faults charts of West Siberia, Yenisei Mountain Range, Altai-Sayan area;
3. Creating deformation models of the mentioned above mega-structures on their contemporary development stage and their tectonic-physical interpretation.

The main results are presented in the form of atlas that contains:

- the map set of kinematic parameters of earth's surface (CVESM velocities, curvature and inclinations changes) and active (on contemporary stage of their development) faults on West Siberia Plate, Yenisei Mountain Range, Altai-Sayan area;
- cartographic correlation models (2D) of the intensive geodynamic activity zones.

5 CONCLUSION

Practical application of the results, obtained during the investigation, is aimed at solving important problems, connected with formation of contemporary geomorphological image of investigated regions and localizations of geodynamic activity zones, which, as a rule, imply earthquake zones, iron and non-iron deposits, and also industrial objects, infrastructure etc. Short-periodic cycles of the earth's surface deformation development in fault zones can be used for creating scientific prerequisites for evaluation of strain-deformation conditions of upper crustal layers, the territories, covered with dense communication network, industrial and civil objects.

The monitoring results can be used for the following purposes:

- the impact of earth's surface kinematics on the geodetic stability by means of input necessary temporal corrections in coordinates;
- geodynamic zonation and compilation of correlation cartographic models;
- revealing of hydrocarbon deposits in geodynamically-active areas;
- forecasting of a deformation process in upper crustal layers according to geodynamic monitoring data, to take preventing measures to eliminate or to soften contemporary earth's surface deformations negative impact on industrial and civil objects;
- the research results can be used in educational process as an illustration in laboratory-practical classes, and also in writing projects works and master's thesis;
- the monitoring results can be edited as scientific publications and scientific-technical reports on related stages.

REFERENCES

Books:

KOLMOGOROV V.G. *Current geodynamic of Siberia according to the results of geodetic and geological-geophysical survey*. Novosibirsk: SSGA, 2013. – 236 p.

BAGAEV S.N., ORLOV V.A., RYBUSHKIN A. U., SEMIBALAMUT V. M., FOMIN U. N., *Two-frequency laser interferometric system for measuring linear movements*. Patent RU № 2082085.

Journal articles:

KOLMOGOROV V.G., KOLMOGOROVA P. P. *Modern kinematics of the earth's surface in South Siberia.* – Novosibirsk: science. – 1990. – 153 p.

KOLMOGOROV V.G., KOLMOGOROVA P. P. *The application of correlation cartography methods in geodynamic research of Western Siberia Plate*//Geodesy and cartography № 11, 2000. P. 30−38.

KONTOROVICH A.E., SURKOV V.S. *Western Siberia//Geology and natural resources of Russia. in six volumes.* T. 2./Senior Editor V.P. Orlov. 2 volume editor. SBR VSEGEI. – 2000. P. 447.

KOLMOGOROVA P. P., KOLMOGOROV V.G. *Current vertical movements of Altai-Sayan region and their connection with newest movements and seismicity*//Geology and geophysics, v. 43 № 6, 2002. P. 567−576.

BAGAEV S.N., ORLOV V.A., PYATIGORETS A.V. *Observation of earth`s osciallarions by a laser interferometric method*. Proceedings of SPIE 2006, vol. 6284, PP 628404-(12 pages).

KOLMOGOROV V.G. *Kinematics of the Earth`s surface in West Siberia from the results obtained by instrumental techniques*//Geology and Geophysics/ Vol. 38, 1997. – P. 1575−1585.

UAV-based photogrammetry: monitoring of a building zone

Jakob Unger, Martin Reich, Christian Heipke
Leibniz Universität Hannover, Germany

Keywords
UAS, monitoring, software comparison, orientation, 3D point cloud, DEM, orthoimage

1 EXTENDED ABSTRACT

Unmanned Aerial Vehicles (UAV) equipped with a camera offer the possibility to map distinct regions with a high flexibility and in short time compared to classical aerial photogrammetry. With a ground sampling distance at a level of a few centimetres they can be used for various tasks such as producing 3D point clouds, digital elevation models (DEM) and orthoimages (Remondino et. al., 2011; Haala et. al., 2013). The results can be used for inspection of industrial facilities, mapping of archaeological or agricultural sites, disaster site monitoring and mapping, etc. With the possibility to operate at small flying heights and with different viewing angles UAVs thus close the gap between terrestrial and classical aerial photogrammetry.
In this paper we present results of a project from the area of monitoring a building zone. Using UAV for that purpose offers the possibility to detect changes in geometry and surface material with a high frequency. In the project we used a Microdrones md4-200 micro-UAV vertical take-off and landing (VTOL) quadrocopter equipped with low-cost GPS and IMU. It has a maximum payload of 200g, hence we are highly limited in possible imaging devices. In our experiments we use two different setups: a Canon IXUS 100IS and a slightly heavier but more powerful PowerShot S110 that both were mounted looking downwards. An automatic capturing is achieved using the Canon Hack Development Kit (CHDK) in which a script mode enables capturing based on a predefined time interval. We acquired three different datasets of the building zone. For the processing of that data we compare three different software packages – commercial and non-commercial – that deliver the aforementioned products. To be able to compare the products of different epochs we use ground control points (GCP) measured by real time kinematic GPS.

The area of interest for the monitoring is the “zero:e-park” in Hanover, Germany, at present Europe’s largest zero-emission building zone. We acquired data in three epochs of an area of approximately 300x400m^2 over a period of four months with a flying height of 60m giving 3-5cm ground resolution with the different cameras. We then analysed the differences of the resulting DEMs for geometric changes from one epoch to the next and visualised the corresponding orthophotos to check the results. Each flight was based on the same predefined path of waypoints in automatic flight mode.
Because of the ongoing construction work we were not able to use manually marked targets for georeferencing. Instead we used the centre of man hole covers as GCPs. The accuracy of the processing chain was checked using independent check points. Comparable discrepancies in GCP and check points reveal realistic results. The different camera setups where compared too.
To analyse also the repeatability of our work we investigated the parameters describing stable planes, which we derived from the 3D point cloud (e. g. car parks and solar panels): we looked at the normal vectors, the distance between the planes and the flatness at different epochs.

The software packages we compared were the commercial products PhotoScan Professional by Agisoft and Pix4DMapper by Pix4D, and the open-source programme package MicMac by IGN Paris DESEILLIGNY & CLERY (2011). Input of each software package are the images of one epoch and precisely known GCP coordinates. The image coordinates of the GCPs and check points are measured manually in an assisted mode using PhotoScan. We use the same imagery and the same image

coordinates of the GCPs and check points in every software package to analyse the results based on comparable conditions. The GPS positions of the images are used only as initial values in bundle adjustment and to accelerate the matching and orientation process.
The comparison of the three software packages is done just for one of the epochs. In theory, we therefore expect to obtain identical results for the three packages. The orientation results are compared using remaining discrepancies in the GCP and check point coordinates. To examine the geometric quality of the 3D point clouds we investigate selected planes. The flatness highly depends on the matching algorithm, more precisely on the weighting between the data term and some smoothness constraint. Finally, orthoimages are compared visually and by investigating the positions of the GCPs.

Preliminary results show that detailed changes in height between epochs are obtained (Figure 1). Green depicts areas where the height increased whereas dark red means that it decreased. For example one can see where scaffoldings around buildings where dismantled (linear red lines around buildings), where parts of buildings where constructed and where ground was moved. This can be verified by consulting the corresponding orthoimages. Figure 2 shows an example of the details that can be seen in the images. In fact, these two examples show the ability for precise computations of volumetric changes that are of high value in many different fields.

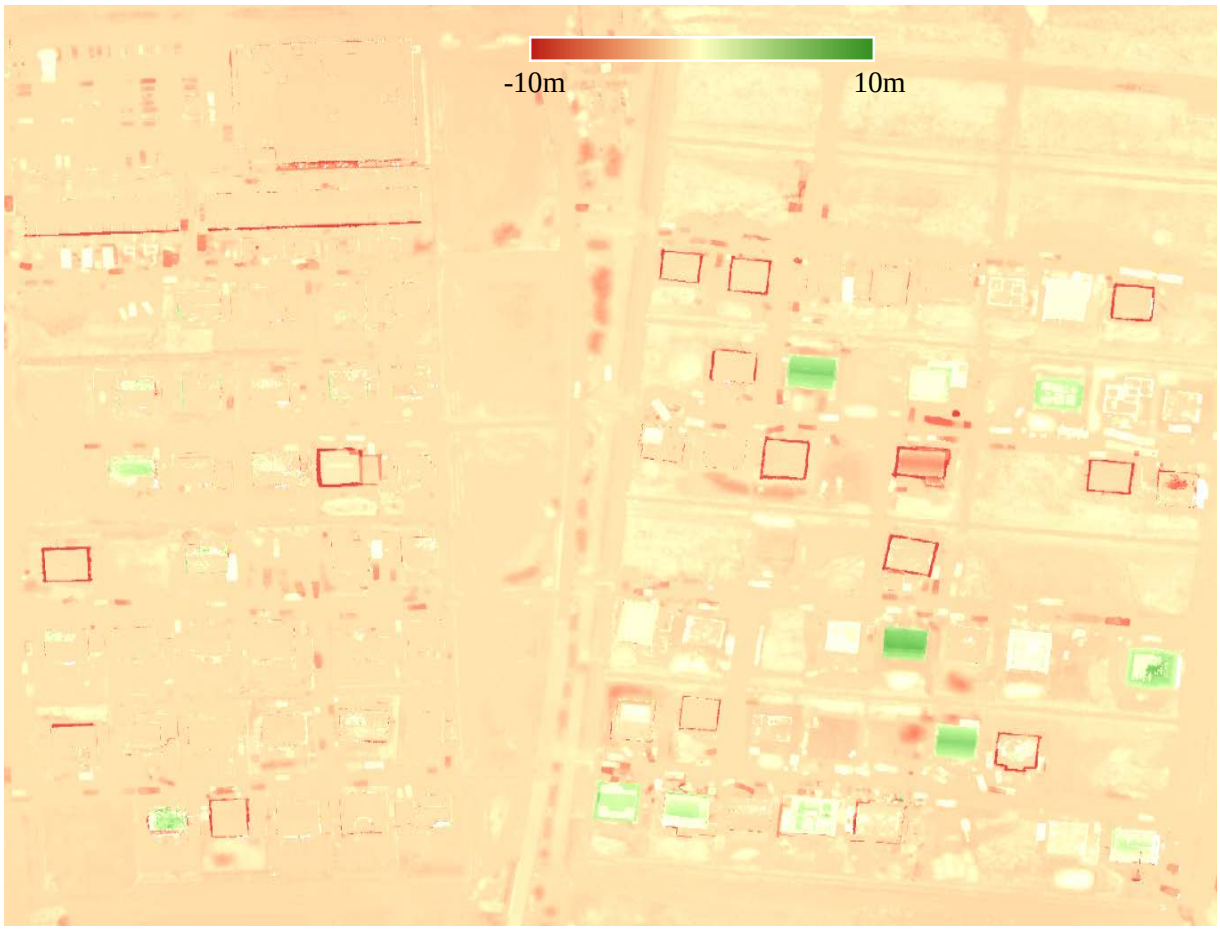

Figure 1: Difference of DEMs between two epochs

Figure 2: Detail of the difference of DEMs between two epochs and a corresponding orthoimage

REFERENCES

Books:

DESEILLIGNY, M. P., & CLERY, I. (2011). *Apero, an open source bundle adjustment software for automatic calibration and orientation of set of images*. In Proceedings of the ISPRS Symposium, 3DARCH11 (pp. 269-277).

HAALA, N., CRAMER, M., & ROTHERMEL, M. (2013). *Quality of 3D point clouds from highly overlapping UAV*. International Archives of the Photogrammetry, Remote Sensing and Spatial Information Sciences XL-1/W2, 183-188

REMONDINO, F., BARAZZETTI, L., NEX, F., SCAIONI, M., & SARAZZI, D. (2011). UAV *photogrammetry for mapping and 3D modelling – current status and future perspectives*. International Archives of the Photogrammetry, Remote Sensing and Spatial Information Sciences, 38, 1.

Technical Session 4: Construction Monitoring

TLS for Structure Monitoring

Ivo Milev[1], Desislava Staykova[2]
[1] technet-rail 2010 GmbH, Beuth University of Applied Science Berlin, Germany,
[2] technet-rail 2010 GmbH

Abstract
The evolution of the laser scanning technology during the last decade offers a new possibility for surveying of large areas. In particular during the last two years the scanning technology becomes a part of the infrastructure monitoring. The benefit of using such technology is the closeness to the continuous methods used in the structural engineering as example the Method of Finite elements. The classical geodetic method using TPS leveling and GNSS are giving just a limit description how the deformation processes are going on. The monitored points are sparse and do not give full description of the movement processes in the closest network. It means the classical deformation networks analysis are just a generalization of the impact caused by the deformation.

Keywords
Infrastructure monitoring, Laser scanning technology

1 LASER SCANNING TECHNOLOGY

Within the last few years an interest of exploiting the laser scanning data for deformation measurements and monitoring purposes rises up. In this paper are presented two different approaches for monitoring and investigation of structural engineering objects. The data analysis is result of special created mathematical model based on the Finite elements theory and the strain stress analysis.

1.1 Terrestrial laser scanning (TLS) for the purposes of deformation monitoring

Monitoring of the behavior of infrastructure objects has always been of high priority for the structural engineering. The needs or precise modeling and detailed geometrical characterization of the object could not be covered of the traditional surveying methods which require the usage a huge number of points for describing the objects surface. The density of such benchmarks is low and does not fulfill the need of representation the deformations for the entire area of interest. The development of the laser scanning technology introduces a new way for deformations monitoring. The high scanning speed, dense measurement of huge amount of points and high accuracy gives advantage of the TLS in comparison with other technologies used for structural monitoring. Compared with the technologies using single point monitoring approaches where the deformations detection is limed to specific benchmarks, the TLS provides high data redundancy. Combined with proper software products this technique offers the possibility for high accurate surface modeling and displacement detection in the millimeter area. As the TLS is a remote sensing measurement technology the impact over observed points and network is minimized.

A new approach for deformation measurement and a-posteriori analysis is developed. The measurement technique comprises in itself all advantages of the TLS, GNSS, geotechnical and meteo-sensors. Using the combination of scanning technology with prisms gives the possibility for wide area coverage, detailed surface monitoring and accuracy control. The solution is based on the combination between high density point cloud and accurate mathematical model for surface modeling and displacements detection.

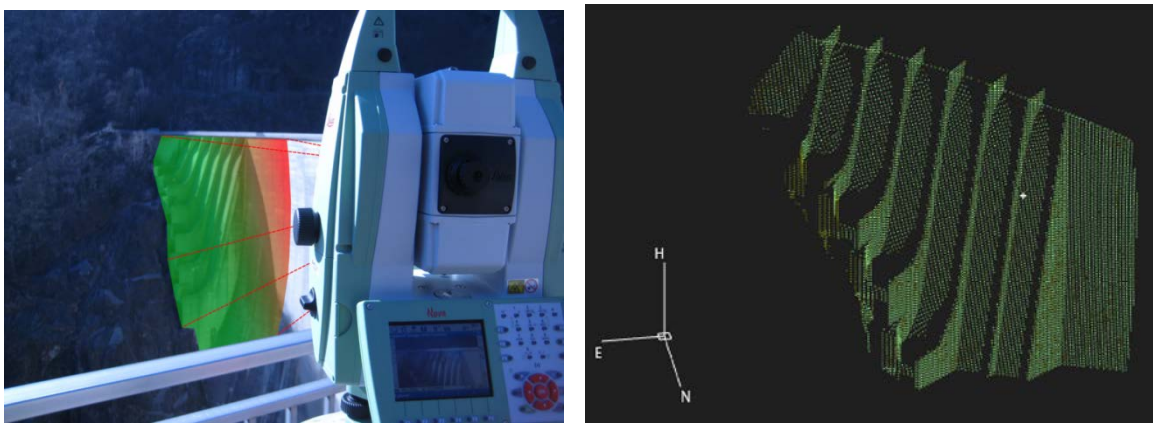

Figure 1.1: Scanned area of interest (© Leica)

The developed *n.Vec Technology* brings all processes from point cloud processing to deformation detection and documentation into one synchronized system. The single scans from the reference epoch are filtered for non-surface scans features (ghosts) and are merged together to create a common null scan with the highest possible accuracy. Each single point coordinate in the merged cloud is corrected to the optimal adjusted position. The advantage of this process is a mathematic description of the scanned surface. Based on the mathematical model the point cloud of the scanned area can be separated into different parts which best fit and describe the body form.

The *n.Vec Technology* uses normal vectors to determine movements in man-made and natural structure objects. For each point is calculated the normal vector and the shortest distance to the closest part of the null scan. Through comparison of the normal vectors from the current epoch to the reference are determined the deformations and their direction, and the volume changes of the observed object. The so calculated movements are documented and as color-coded deformation maps.

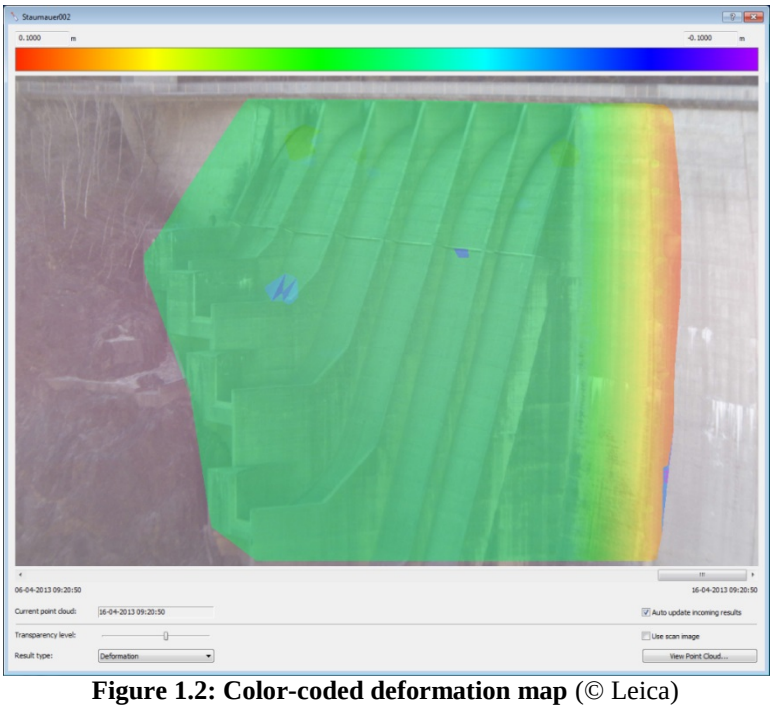

Figure 1.2: Color-coded deformation map (© Leica)

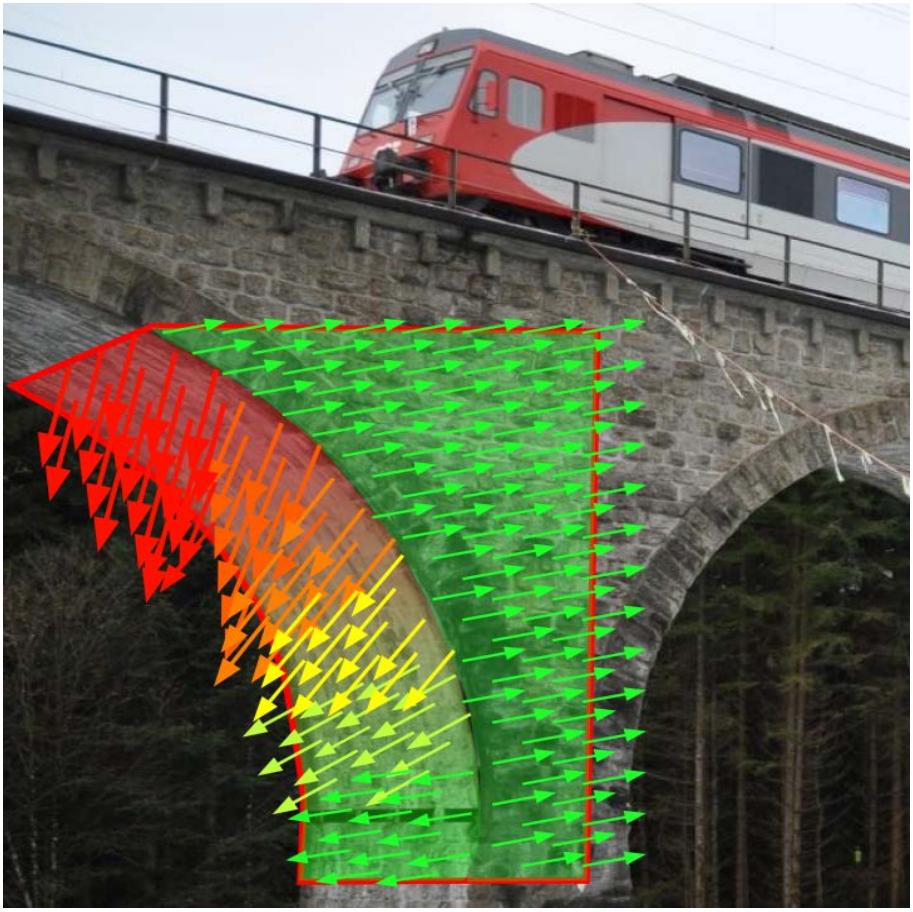

Figure 1.3: Calculated normal vectors in deformation direction (© Leica)

1.3 Mobile Laser Scanning (MLS)

The development of Mobile Laser Scanning with terrestrial and water-based vehicles in various engineering fields such as measurements of highways, streets, railways, cities areas, coastal areas and ports has a rapid progress in the last years.

As a response of the growing interest to the MLS technology and its application for engineering purposes a new approach of mobile scanning system with a-posteriori data adjustment is developed. The goal of the performed set of scanning projects was to be proved the usage and the accuracy of the MLS systems for the needs of the engineer surveying in the area of deformation analysis and the land administrations for monitoring and documenting the as-built street network.

1.3.1 The system

The system consists of fully integrated laser scanner in combination with GNSS, IMU sensors and DMI (Distance Measuring Indicator) aiming to determine precisely the position of the vehicle. Using the combination of the laser range, scan angle, position of the scanner, orientation of the platform from GNSS and IMU data, and recorded from the DMI data, for each scanned point are calculated the georeferenced coordinates even in the places with low or no GNSS signal. Considering the accuracy requirements and point cloud density diverse system configurations of laser scanner and INS, driving speed and rate of data acquisition are used. The so modified system gives possibility for the user for collecting big amount of high accurate data for short period of time.The data acquisition and processing are done in continuous way which minimizes the error factors.

1.2.2 Accomplished Projects

Dependent on the scanned area and conditions were performed measurements with different system configuration. Processing of the raw data, calculation of the georefernecd coordinates for each scanned point and ghost removing procedures were performed. The end result is a high density point cloud which can be used for detection of displacements in the structure of the object and of surface

deformations. The created workflow ensures high accurate transition from the raw measurement data to 3D point clouds into desired coordinate system. The usage of special developed functions based on the finite element method and strain-stress analysis enables quick and accurate data adjustment and a-posteriori deformation analysis. The applied for the scanned area mathematical algorithms give the possibility for detection of deformations in the street surface less than 3 mm relative to the datum surfaces.

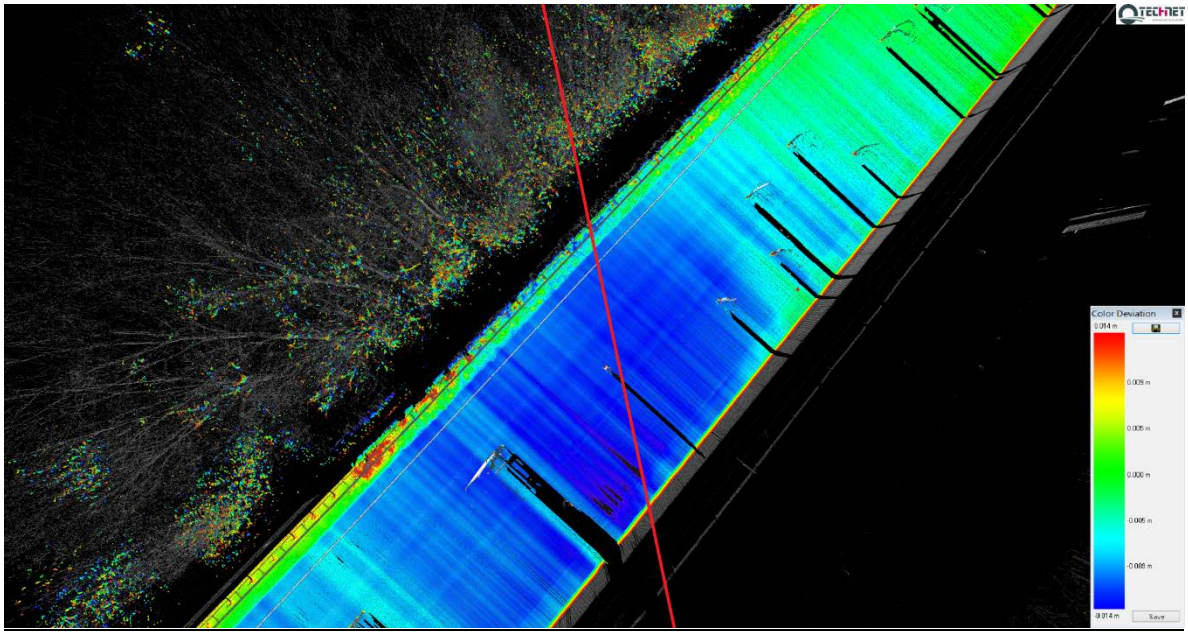

Figure 2.1: Color-coded deformation point cloud as result from the comparison between the current and the null epoch of measurement (© technet-rail 2010)

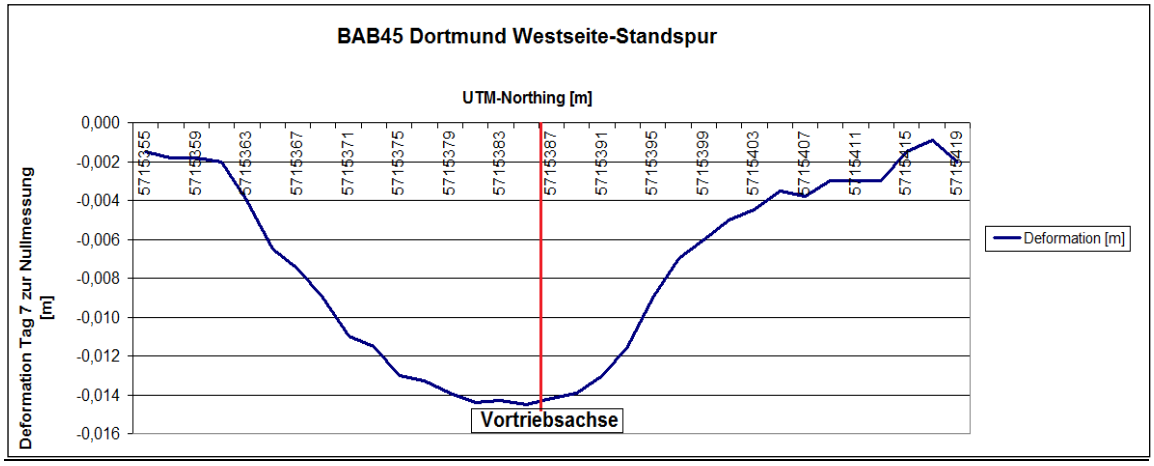

Figure:2.2: Diagram representing the deformation of the surface w.r.t the null epoch (© technet-rail 2010)

2 THE FINITE ELEMENTS METHOD

The finite elements method is a powerful and versatile analysis tool. It is used for solving problems with loadings, complicated surfaces, to obtain solution for the boundary values problem.

The used finite element method is the Ritz-Galerkin method which is using special subspaces of trial functions. The main feature of these subspaces is that the basis functions vanish over all but a fixed number of elements into which the given domain is divided. The triangular elements are the elements most often used by engineers when solving boundary value problems in two variables. The reason is obviously that it is easy to approximate an arbitrary boundary by a polygon and to triangulate the polygonal domain. If a piecewise linear functions are used as trial functions, the approximation of the

boundary by a polygon is a natural one. If are used functions which are piecewise polynomials of a higher degree, it cannot be expected to retain the same accuracy along the curved part of the original boundary as inside the domain or along the polygonal part of the boundary. Numerical evidence is given in '*The finite element method in domains with curved boundaries, Internat. J. Numer. Met. Engrg.'* And at the same time the curved elements are proposed as more suitable for use along the curved part of the boundary (ZLAMAL M (1973)).

2.1 Application of the Finite elements method and the stain stress analysis

The laser scanning technique acquires dense 3D data point over an area of interest. The scanned object in his structure consists of big amount of points which allows the implementing of mathematical methods (Finite elements method) for surface modeling and studying the objects behavior. For investigation the deformations of large areas is used the Lagrange polynomial description which uses a mesh of elements representing some fixed reference state for strain MCMEEKING & RICE (1975).The modeled domain it is divided into a system of smaller bodies (elements) connected with two or more common points (nodes) or boundary lines into an intern network. Connecting the elements together, the filed becomes a polynomial interpolated into the entire structure. There are four stiffness terms: small strain stiffness, initial load stiffness, initial strain stiffness, and initial stress stiffness. In the analysis, all of these must be calculated for each increment of deformation. The increment of deformation must be small in any case to ensure that the constitutive rate moduli do not change significantly from one increment to the next MCMEEKING & RICE (1975).

3 CONCLUSIONS

The TLS and MLS techniques methods provide fast, high accurate and complete scanning of infrastructure objects (dam walls, bridges, railways, highways, street network). The data acquisition and processing are done in a continuous way which negligees the impact of operator errors. The software data processing ensures high quality, reliability and accuracy of the adjusted measurements. The end products are base for performing of real time deformation analysis and monitoring of structure objects. The results of the performed projects proved the fully integration of TLS and MLS technology with the a-posteriori software data processing and adjustment as a unprecedented method for monitoring of infrastructure objects.

REFERENCES

Books:

MILEV I., *Integrierte Modelle zur physikalischen Interpretation Geodätischer Deformations-untersuchungenn*, genehmigte Dissertation, Bauingenieurwesen und angewandte Geowissenschaften der Technischen Universität Berlin zur Erlangung des akademischen Grades, 2001

Journal articles:

MCMEEKING M.R., RICE J.R., *Finite-element formulations for problems of large elastic-plastic deformation.*,Int. J. Solids Structures, Pergamon Press ,1975, Vol.11, pp.601-616.

ZLAMAL M., *Curved Elements in the Finite Element Method. I,* Siam Journal on Numerical Analysis, Vol. 10, No. 1 (Mar., 1973), pp. 229-240.

Links:

technet-rail 2010 GmbH: http://www.technet-rail.de

Automated Recognition of Roadbed Deformations (defects) Using Laser Scanning Data

Maxim A. Altyntsev
Siberian State Academy of Geodesy, Novosibirsk, Russian Federation

Abstract
Highlights of laser scanning data applications for roadbed crack identification are considered. The analysis of image classification results taken from a mobile laser scanning system is carried out. The technique of automated crack identification from laser scanning data and the use of TerraSolid and IDIMA software are presented.

Keywords
Mobile laser scanning, image classification, roadbed defects

1 INTRODUCTION

One of the most important tasks in road facilities is automatic identification of defects in the roadbed. Roadbed defects are appeared eventually under the influence of various factors. The most common defects are cracks. If cracks are not repaired, it leads to the road havoc. Therefore, all places where the cracks appear should be revealed in time and repaired.

Today the roadbed crack identification is solved by field reconnaissance of roads. This method is highly labour-consuming, takes a lot of time and does not enough accurate. Mobile laser scanning allows reducing the volume of field works, increasing the speed and the accuracy of crack identification DEGOVCOV (2012).

Mobile laser scanning is one of advanced method of surveying. It is widely used in town planning, architecture, electric power industry, road facilities, oil and gas industry. Mobile laser scanning data can be used for creation of topographic maps, 3D models, cross and longitudinal, and road certification ZAMPA & CONFORTI (2009), SEREDOVICH & ALTYNTEV (2013).

2 THE TECHIQUE

All roadbed defects are well identified by mobile laser scanning data. This is achieved by simultaneous analysis of laser points in display mode by the reflected signal intensity and images taken by digital cameras equipped with a mobile laser scanning system. Medium and large cracks are well identified by the laser point intensity, whereas the smallest ones by images. To increase the rate of crack identification by images it is recommended to apply existing algorithms and develop new automated image classification ones. Having the data of interior and exterior orientation of images, crack coordinates of classified pixels can be determined in world coordinate system. Point clouds are obtained in the same coordinate system. The elements of interior and exterior orientation of images are calculated during calibration of mobile laser scanning system.

The results of Novosibirsk area surveying carried out in August 2012 were used for the development of automated crack identification technique. The surveying was carried out by Lynx Mobile Mapper M1 system. IDIMA and TerraSolid software was used for investigations (http://jena.ru/catalog/laser_scaning_systems/lynx (2014)).

IDIMA software contains a toolbox for automated image classification. The nonadaptive image classification algorithm is implemented in this software. Classification is carried out on the basis of object self-organization of any image into robust homogeneities which are correleted with each other in a consistent structure (CS-strucrure) OSTROVSKY, RUMYANTSEV & FADEEV (2012).

To extract certain groups of objects in IDIMA software using images taken from digital cameras equipped with the mobile laser scanning system, it is necessary to create a training sample using area masking. For creating a training sample several pixels of any determined object should be selected. In our case these pixels relate to cracks. Masks delete from processing certain image areas. What is concerned crack identification, all areas not relating to a roadbed should be masked. Otherwise, the result of classification will be unsatisfactory. For example, pixels relating to cars, trees and other objects can be selected. The CS-structure created by the masked image differs from that created by the image without masked areas. It is connected with simultaneous analysis of the whole image while creating CS-structure. The less variety set of objects for analyzing image area the more detailed CS-structure will be created for an image with similar brightness characteristics for the set of object.

IDIMA software for initial image creates several various structures, allows applying them for classification and to choose certain set of structures. One of initial images used for crack identification and an image with a superimposed mask is shown in Figure 1. An example of several structures constructed by this image is shown in Figure 2.

Figure 1: The initial image

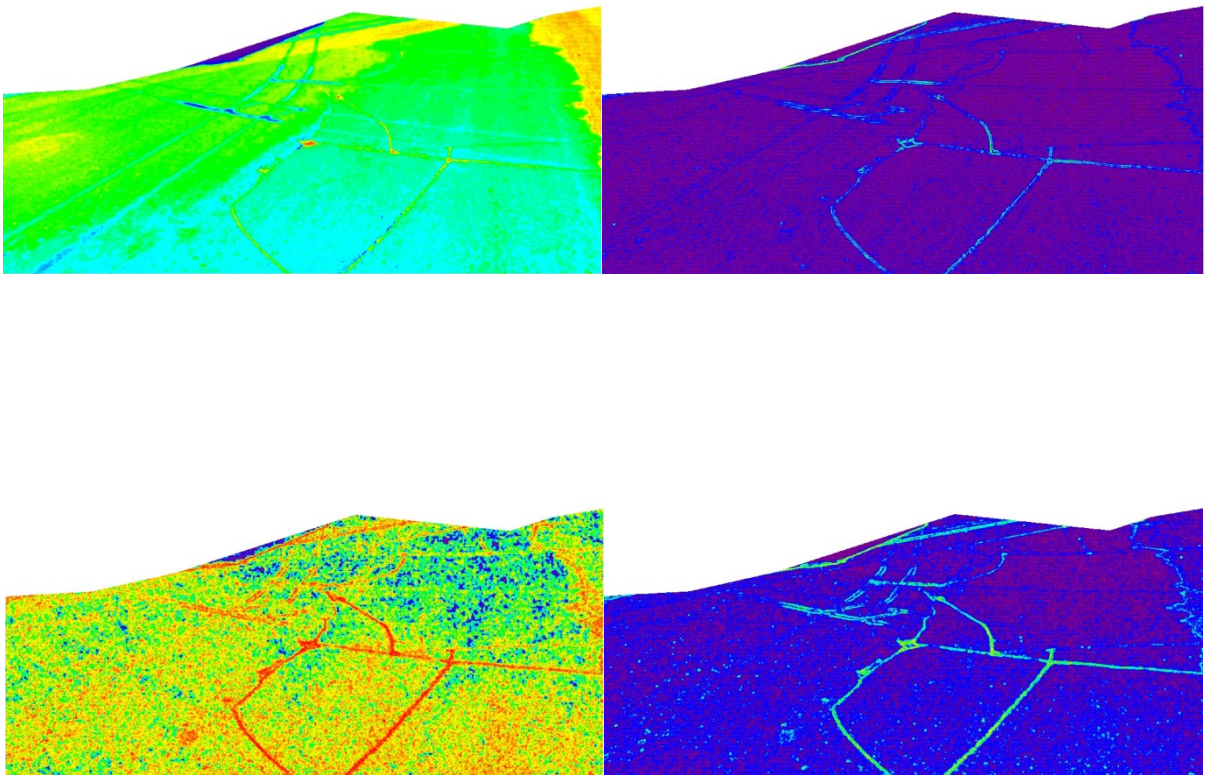

Figure 2: Structures created by the initial image

Figure 2 shows that varying structures extract image detailes by differently ways. Using these structures a training sample was created and classification process had been implemented. The result of crack identification in software IDIMA is shown in Figure 3a.

The reliability of image classification depends on a quality of created training sample, masking results, characteristics of extracted objects, quantity of shadows. Cracks can be not recognized if they are in a shadow area. The less area a crack occupies the more complicated to recognize it automatically, the more incorrectly classified pixels are on the resulting image, and the more a noise.

Practically all crack areas have been completely recognized on the classified image but there are still some other pixel groups recognized as cracks.

The crack coordinates in the world coordinate system can be determined by TerraSolid software tool used for painting laser points according to colors taken from images. The matter of this technique is that initial images in TerraSolid project work directory are replaced by images with recognized cracks. The laser points matching by cracks were painted in red color as in images (Figure 3b). Painted laser points can be separately saved.

a) b)

Figure 3: Crack identification result: a) in images, b) painted laser points

3 CONCLUSION

Thus, the technique of automated roadbed defect recognition can be schematically presented as shown in Figure 4.

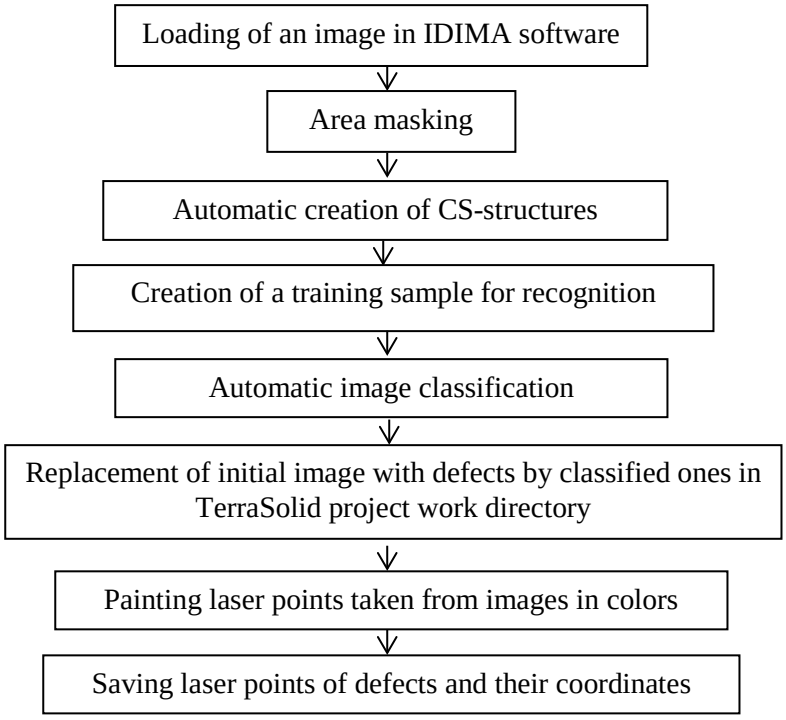

Figure 4: The technique for automated recognition of roadbed defects using laser scanning data

Main disadvantages of the technique are as follows: the necessity to process each image individually, online mask and a training sample creation. For the development of fully automatic technique for roadbed defect recognition additional investigations are necessary for CS-structures namely to determine the impact of various external factors on pixel brightness in CS-structures obtained from images with cracks. If there is a need to determine any dependence between defect brightness in CS-structure, time and image acquisition conditions, and size of defects, it is necessary to develop a new software or to improve the existing one for defect recognition providing the opportunity of applying the pixel brightness average value relating to the certain object class, that is relating to the fixed training sample. Also batch mode of image processing should be included in that software.

REFERENCES

Books:

OSTROVKSY, E.A., RUMYANTSEV, S.V., FADEEV, V.A.: *The IDIMA Software Is a Nonadaptive Classification of Objects Based On Remote Sensing Data*, issue 1, p. 12-17, 2012.

Journal articles:

DEGOVCOV, A.A.*: Mobile Laser Scanning Technology For a Design and Survey Works*. Interexpro Geo-Siberia-2012, Novosibirsk, proceedings, vol. 3, p. 140-144, 2012.

SEREDOVICH, V.A., ALTYNTEV, M.A.: *Application of Mobile Laser Scanning Data For Creation of Topographic Plans*. Interexpro Geo-Siberia-2013, Novosibirsk, proceedings, vol. 3, p. 96-100, 2013.

ZAMPA, F., CONFORTI, D.: *Mapping with Mobile Lidar*. GIM International, issue 4, vol. 23, p. 35-37, 2009.

Links:

http://jena.ru/catalog/laser_scaning_systems/lynx on February 25, 2014.

Technical Session 5: Deformation Analysis and Time Series Analysis

Time Series Analysis for Construction Monitoring

Martin Metzner
Institute of Engineering Geodesy, University of Stuttgart, Germany

Abstract
The main points and first options for the analysis of measurements in terms of time are pointed out in the article. First, the measurements must be pre-processed, so that any trend contained is removed and the values of the measurement series are present in equidistant intervals. Then the actual time series analysis begins. In particular, the autocovariance and the autocorrelation function are used, which enable to identify the underlying processes of a time series. For this some typical processes and examples to interpret autocovariance and autocorrelation functions are shown. Furthermore, the cross-covariance and cross-correlation functions are presented that help to compare two time series with each other and the relationship (especially the temporal shift) between them. In order to eliminate any influence of the periodic effects from the time series, the general scope of filters are introduced based on a low-pass filter, which is calculated based on a moving average.
At the end a view on frequency analysis is presented, particularly in terms of ensuring the analysis in the time domain.

Keywords
Time Series, autocovariance function, autocorrelation function, cross-covariance function, cross-correlation function, filter

1 INTRODUCTION

In many areas of everyday life one comes into contact with time series - often data and their sequence are presented in graphics in the news. To pick up a few examples of such series of observations, the monthly unemployment figures or the almost continuously documented stock indexes can be mentioned. In geodesy, especially in the field of deformation measurements, automated measurement systems leads to time series HEUNECKE et. al. (2013). Because of the development of technology and measurement sensors (odometer, total stations, GNSS-sensors, etc.) and its automation usually the measured values are digital, with sampling rates up to several readings per second, which can be evaluated computer-aided. In the context of construction monitoring time series and time series analysing become one important method KUHLMANN et. al. (2013). Different objects, like dams, buildings and bridges i.e. ROBERTS et al. (1999); ROBERTS et. al., (2004); HUDNUT et. al. (1998) were monitored and analysed. Also online monitoring systems are developed, based on the measurement of time series KÄLBER & JÄGER (2001).
In general a series of observations respectively a time series *x(t)* can be characterized as a realization of a stochastic process *X(t)*. A stochastic process is a random process which is represented as a sequence of random variables in dependence of time – the parameter *t*. $x(t_i)$ describes an observed value at the time t_i. According to the mentioned measuring systems the observed value can be a length, a coordinate, etc. In opposite to a deterministic process, which can be predicted completely, a stochastic process isn't exactly predictable and is non-reproducible at any point. In context of this article discrete realisations of time series as well as continuous realisations of stochastic processes should be named time series *x(t)* (DIN 18709-5, 2010).

In practice a time series is not considered as repeated observation of an invariant random variable, but the time series represents a time variant random variable. Consequently, there is a time-ordered sequence of observed values for each time point $t_i \in T$ as realization of a stochastic process. In practice, a discrete realization of a continuous stochastic process will be present, meaning *T* describes

the set of integers ($\mathbb{Z}$) (DIN 18709-5, 2010). Furthermore, the total number of measured values will be finite and can be specified by the parameter n (with $n \in \mathbb{N}$).
This is also the context for the measurement period $T = n \cdot \Delta t$, with the sampling rate Δt as the time difference of two (measuring) points of time t_i (with $i = 1 \ldots n$).
In this paper, the discrete case is considered essentially and therefore, the corresponding empirical functions are given in the following.

2 PREPARING THE DATA

To evaluate a time series, at least the deterministic trend and the usually stochastic time series are to be separated. Since the time series must be equidistant to apply the algorithms of time series analysis, the time series must be examined for gaps in the data and these are then filled with interpolated values.

2.1 Trend

The mentioned deterministic parts that can be contained in a time series are usually called trend. This is modelled in a time series analysis and, if present, is removed by the time series (Figure 1). The trend can be modelled using smooth mathematical functions, in the simplest case a straight line, or at periodic trends with the help of suitable sine functions CHATFIELD (2004). If the trend from a time series is completely eliminated, then this is the stationarity of expected value, i.e. the expectation values of all observed values are identical CHATFIELD (2004).

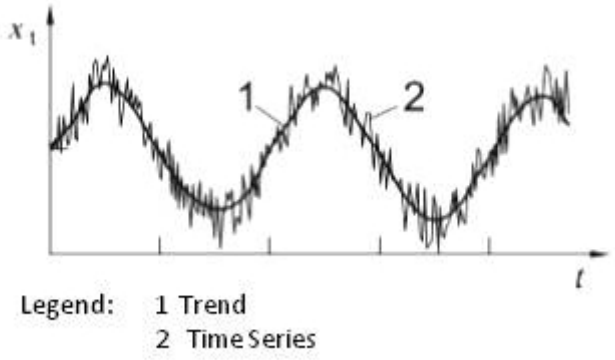

Figure 1: Time series and trend DIN 18709-5 (2010)

2.2 Stationarity and Ergodicity

In connection with the mentioned stationarity of the expected value, the stationarity criteria and ergodicity are explained. Both properties are generally required in practice, if time series are investigated.

The definition of stationarity includes that the prohability function, and thus the expected value of the time series and the autocovariance function are independent of the time NEUNER & FOPPE (2009). By the ergodicity property is described that the properties of the overall process are included in one realization, and therefore can be derived from this HEUNECKE et. al. (2013)

2.3 Data Gaps

For generating the series of measurements usually a constant sampling rate is needed (equidistance), wherein the sampling rate is the distance between two discrete measurements of the time series. In this context, the so-called Nyquist frequency is important, which is derived from the given sampling rate.
The Nyquist frequency is the name given to the highest frequency that can be reconstructed on the basis of the discrete series of measurements. As mentioned previously, the algorithms of time series

analysis assume equidistant data series. However, data series in reality often contain data gaps. Reasons for data gaps are malfunction or failure in the automatic data capture or eliminated outliers. In order to eliminate data gaps, corresponding, similar or the existing measured values matching data must be inserted NEUNER & FOPPE (2009). Before filling the gaps, first, a statistical evaluation of the measurement series, usually depicted in a histogram, should be performed.
In Figure 2 as an example data gaps can be seen in a real series of measurements (measurement of coordinates by a tachymeter: 1700 readings), which should be recorded at a sampling rate of one hour. It is easily seen that in this case small gaps occur more frequent than large gaps - a typical characteristic of automated measuring systems.

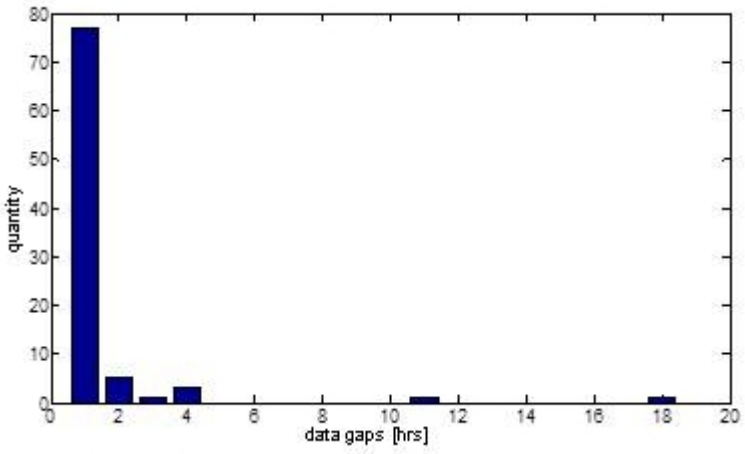

Figure 2: Numbers and size of data gaps ZHOU (2012)

For filling, especially of small data gaps, there are different methods in use, of which some are presented below RUNKLER (2010).

$z(t_i)$ is the calculated value replacing a value to fill a gap in the original series of measurements. i (with $i = 1,2, \dots, n$) is the index that marks the gap or the outliers in the original series of measurements. The series of measurements including gaps and without outliers is denoted with $y(t)$, which is converted using the values $z(t_i)$ in the series of measurements $x(t)$ for time series analysis. In other words $x(t)$ is the final time series without gaps and outliers – ready for the time series analysis.

- *Substitution of outliers by the maximum or minimum value:*

  Qutliers can be replaced by the still permitted minimum or maximum value of the valid data.

  Where:

$$z(t_i) = \begin{cases} \max\{y(t)\} & \text{for } z(t_i) \text{ larger,} \\ \min\{y(t)\} & \text{for } z(t_i) \text{ smaller,} \end{cases} \quad (1)$$

  with $max\{y(t)\}$ or $min\{y(t)\}$ is called the maximum value or minimum value of the valid data $y(t)$, which takes the place of the missing or replaced value $z(t_i)$

- *Substitution of outliers or fill of gaps with the global mean:*

  Another possibility is to replace an outlier or to fill a gap by using the global mean value of the measurements RUNKLER (2010):

$$z(t_i) = \frac{\sum_{j=1}^{n} y(t)}{n}. \quad (2)$$

For large gaps in the data more complex algorithms, given in the following, are called (Runkler, 2010):

- *Linear interpolation:*

$$z(t_i) = \frac{y(t_{i-1})+y(t_{i+1})}{2}. \quad (3)$$

Values can be calculated for replacement by simple linear interpolation. Herein, $y(t_{i-1})$ is the last value before a gap in the original series of measurements and $y(t_{i+1})$ the next available value in a series of measurements. A gap of more than one value is present in the original series, the above formula for linear interpolation must be adjusted accordingly, to produce a complete series of measurements of $x(t)$ with equidistant measurements.

- *Non-linear interpolation, for example by polynomial 3rd Order (cubic):*

Non-linear interpolation methods can be used alternatively, for example, higher order polynomials or splines. In the simplest case, the quadratic interpolation can be used. If this doesn't lead to success, the cubic interpolation as described in equation (4) is used to calculate the missing values:

$$z(t_i) = a_0 + a_1 t_i + a_2 t_i^2 + a_3 t_i^3. \quad (4)$$

To calculate the coefficients of the cubic interpolation five observed values before and five observed values after the gap are used to estimate the coefficients a_0, a_1, a_2, a_3 by the method of least squares. If within these five observed values a data gap occur again, then this value will be skipped and another value will be used for the calculation of the coefficients. About the number of used observed values there is the condition that the number is sufficient to estimate the coefficients successfully. For the determination of the four coefficients of the cubic interpolation four observed values will be satisfying the needs. To calculate an over determined solution and reconstruct as closely as possible the characteristic curve of the measurement series, more values should be added, as previously stated.

With the well prepared data (stationary and without trend, no gaps) the actual time-series analysis can start.

3 COVARIANCE AND CORRELATION

With the help of variance and covariance or the correlation coefficient dependencies between two variables can be identified. The variance in this case indicates a measure of accuracy for a measurement variable and the covariance is a measure of the linear dependence between two random variables. Since the numerical value of the covariance allows no clear statement regarding the stochastic dependence, a normalized quantity is calculated using the correlation coefficient, which is independent of the numerical values of the covariance and variance measure. In time series analysis dependencies have to be investigated. For this, the algorithms for variance, covariance and correlation valid for individual random variables will be generalized accordingly to time series. The equations for calculating the autocovariance are given here and in the following. The stationarity of the series of measurements is assumed, in other words, the trend is already eliminated. As for a single value, the variance can be calculated as follows for a discrete time series:

$$s^2 = \frac{1}{n-1}\sum_{j=1}^{n}\left(x_j - \bar{x}\right)^2 \text{ , with } \bar{x} = \text{mean value of the time series} \quad (5)$$

and $n =$ total number of individual values of the time series. The discrete autocovariance function is given by:

$$\hat{C}_{xx}(k) = \frac{1}{n-k-1}\sum_{j=1}^{n-k}(x_j - \bar{x})(x_{j+k} - \bar{x}); \quad k = 0,1,\dots,m \leq {}^{n}/_{10}. \tag{6}$$

The autocovariance function is calculated only up to $k = m \leq {}^{n}/_{10}$, since a sufficiently accurate estimation for $\hat{C}_{xx}(k)$ is possible only up to this value (Heunecke et . al., 2013). m indicates the number of values used to calculate the autocovariance. If one calculates the autocovariance function for $k = 0$, i.e. calculating $\hat{C}(0)$, this leads again to the empirical variance s^2. The autocovariance function allows to describe and analyse the relationship between the measured values of one series of measurements. k stands for the degree of shift in the time series. For $k = 1$ the temporal shift of the sampling rate corresponds exactly to Δt. The autocovariance function expresses with $k = 1$ the connection between the neighbored values, with $k > 1$ the relationship between the values which are further away. If the autocovariance function for $k > 0$ converges to zero slowly, a high trend of conservation of the measurement series can be assumed, i.e. consecutive random variables change very little NEUNER & FOPPE (2009).

In addition by calculating the correlation coefficient as a normalization of variances and associated covariances, the so-called autocorrelation function is obtained as a normalization of the autocovariance function:

$$\hat{R}_{xx}(k) = \frac{\hat{C}_{xx}(k)}{\hat{C}_{xx}(0)}. \tag{7}$$

By the normalization, the function values of $\hat{R}_{xx}(k)$ lie in the interval $[-1,1]$. The graphical representation of the autocorrelation function, also referred as “correlogram”, shows the correlation coefficients for different time differences k (so called “lag”). The graphic representation can already lead to first interpretations of the properties and the leveling of the time series, for example, these can be tested for stationarity. Assuming that the measurements are random, the autocorrelation function for all time difference is close to zero. In real data this is however not always clearly detectable (see Figure 3). In this example, yet different influences can be read, in particular, periodic influences on the time series can be still assumed.

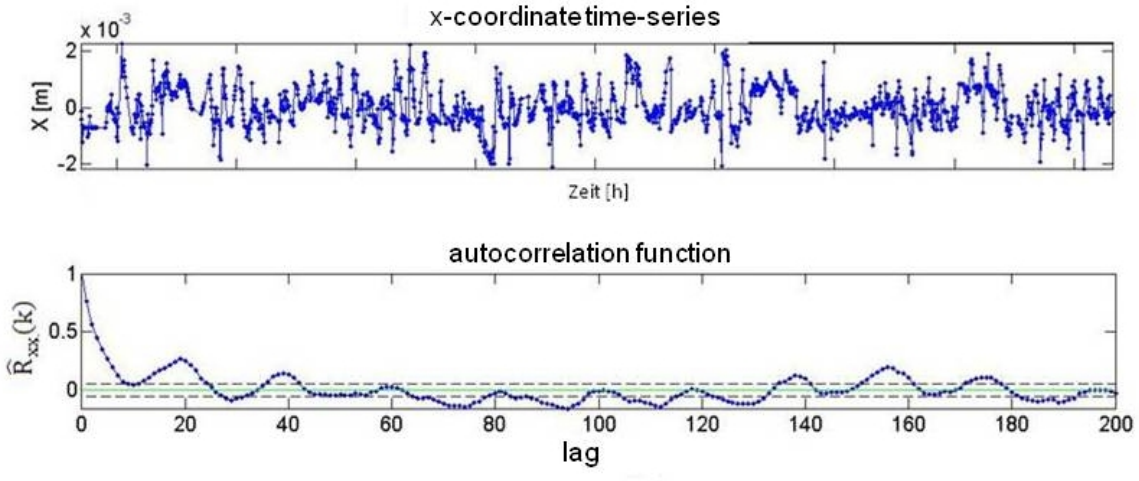

Figure 3: Time series and related empirical autocorrelation function WANG (2012)

With the previously introduced functions, the relations between the measured values of a time series can be investigated. With the cross-covariance and the cross-correlation function of two time series, the dependencies between them can be analysed. An example of this is the determination of the cross-covariance for a time series of observations of a total station (x, y, z coordinates), and a time series of temperature observations.

As a result of such an analysis, for example, the information whether and when the change in the temperature also causes a change in the observed coordinates. Generally, the closeness of two time series as a function of their mutual (temporal) shift is determined with the cross-covariance function or the cross-correlation function. The degree of match is defined by the correlation coefficient. The empirical cross-covariance function is given by:

$$\hat{C}_{xy}(k) = \frac{1}{n-k-1}\sum_{j=1}^{n-k}(x_j - \bar{x})(y_{j+k} - \bar{y}). \quad (8)$$

Here x_j describes a single value of the time series $x(t)$ and y_j describes a single value of the time series $y(t)$.

The requirement for the calculation of $\hat{C}_{xy}$ is that both time series with n equidistant measurements in equal sample length Δt of the same sample rate T are available. The cross-correlation function is again a normalization of the cross-covariance function:

$$\hat{R}_{xy}(k) = \frac{\hat{C}_{xy}(k)}{\sqrt{\hat{C}_{xx}(0)\cdot\hat{C}_{yy}(0)}}. \quad (9)$$

4 TYPICAL PROCESSES

After the demonstration of the algorithms for the analysis of time series, some typical processes and their behaviour will now be shown in the time domain using the following graphics. Typical processes are using the terms “white noise process”, “red noise process” (or Gauss-Markov-Process) and “coloured noise process”. A white noise process is a process in which there is no correlation between temporally adjacent values. All the covariances are zero, and thus the autocorrelation function for all of the values is zero, except for $k = 0$. Here the function assumes the variance as function value (Figure 4a)) HEUNECKE et. al. (2013). Formally, white noise processes are referred to as a stochastic process, which at each point of time having an identical distribution and being stochastically independent for the random variables for all the other points of time. In reality, usually red noise processes occure (Gauss-Markov-Process) (Figure 4b)). Formally, it is defined as a stochastic process for which the stochastic dependence decreases with increasing time interval between the values. This is expressed in the appearance of autocorrelation function decreasing with increasing displacement and striving towards zero.

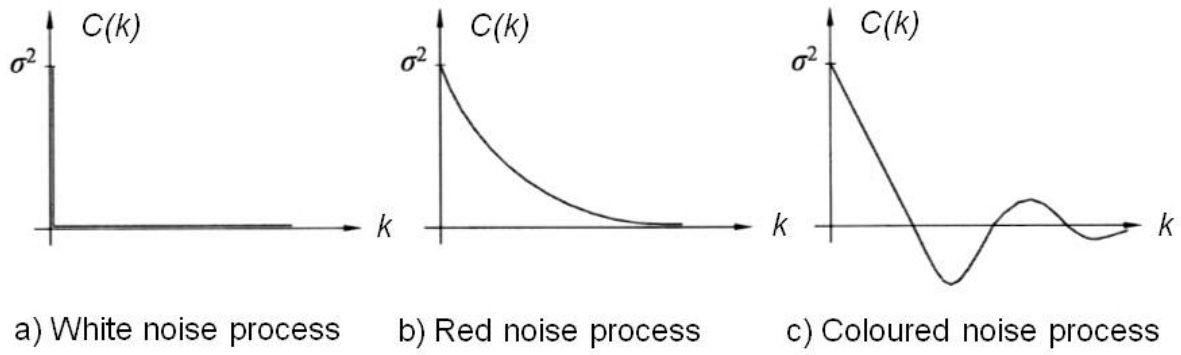

Figure 4: White, red and coloured noise processes HEUNECKE et. al. (2013)

A coloured noise process (Figure 4c)) is a Gauss-Markov-Process which is overlaid by periodic influences. Formally, it is a stochastic process, in which the red noise process is superimposed by periodical functions.

In the following some additional examples of empirical time series and their corresponding autocorrelation functions are shown. The examples are taken from CHATFIELD (2004). First, a time series can be seen with short-term correlation (Figure 5). This is characterized by two or three large correlation values unequal to zero and the tendency of the other coefficients to zero.

For the measurements related to the average, this means that one or two more measurements follow a value with a positive sign, also exhibit a positive sign. The same concept is true for measured values

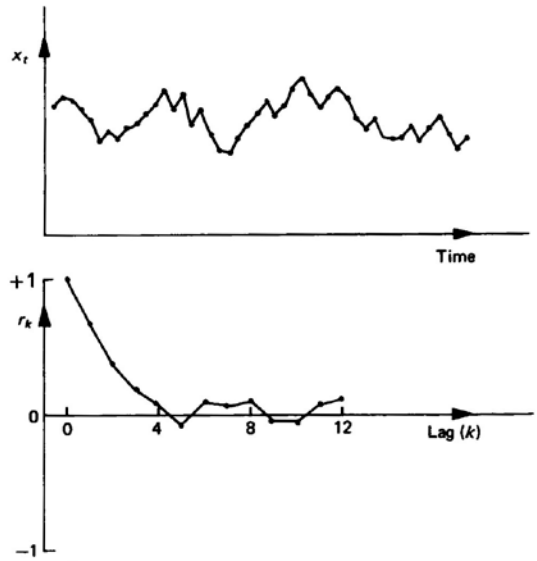

Figure 5: Time series with short term correlation CHATFIELD (2004)

with a negative sign. Periodic effects are visible in the appearance of autocorrelation function by a periodic function. If such periodic influences are identified as a trend that should be eliminated from the time series, the successful elimination can also be tested graphically. In Figure 6 an autocorrelation with periodic influences can be seen in the top view.

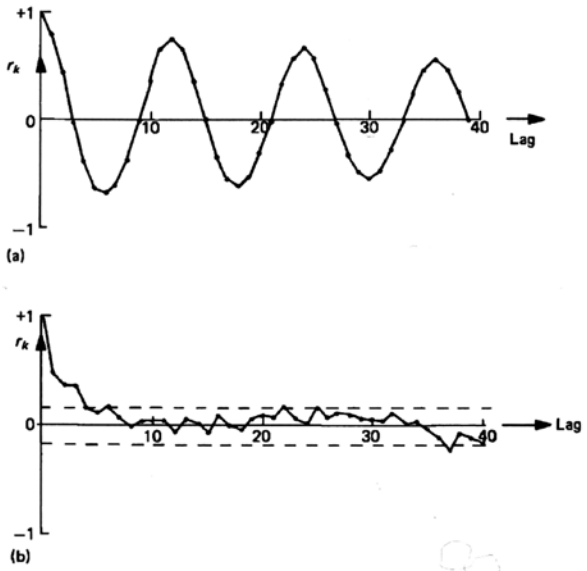

Figure 6: Elimination of periodic influences CHATFIELD (2004)

After the elimination of these influences the result is shown in the lower of figure 6. The autocorrelation function now fluctuates within a certain range around zero, where the range limit here is $\pm 2/\sqrt{n}$. Values which are outside this range are significantly different from zero in accordance with CHATFIELD (2004). The stationarity of a time series can be checked in the graphical representation. Figure 7 shows an example for a non-stationary time series. The time series contains a trend. This is also illustrated by the fact that even at high displacement rates ($k \cdot \Delta t$) does not reach an autocorrelation value of zero.

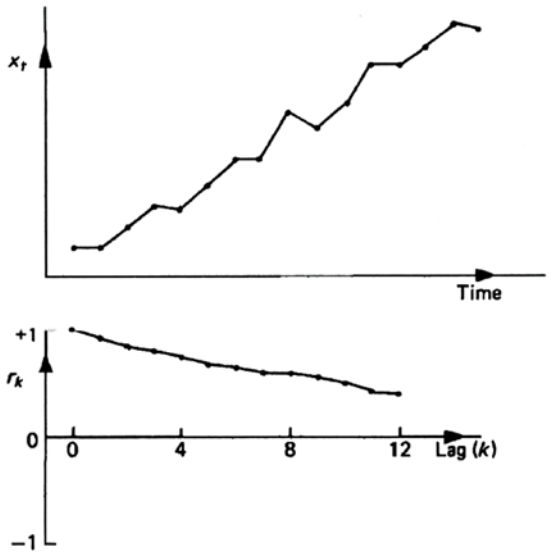

Figure 7: Non-stationary time series CHATFIELD (2004)

5 BASIC FILTERING

One difficulty in the analysis of time series is the detection of a continuous process by discrete values. Due to a limited sample rate high frequencies cannot be detected. Conversely, the elimination of certain frequencies detected in time series may be a task of the time series analysis. This aim can be achieved if, for example, a lowpass filter is applied on the time series. With this high frequencies are eliminated. Conversely, highpass filters are used to remove low frequencies in the measurement series and to focus on the study of high frequencies.

In general terms, the filter is always a function that transfers a time-dependent process $x(t)$ into another time-dependent process $y(t)$, thereby changing the spectrum of the process. An example of a lowpass filter is the calculation of a moving average (DIN 18709-5, 2010). In the discrete case applies here:

$$\mathrm{y(t)} = \frac{1}{2\mathrm{B}+1}\sum_{-\mathrm{B}}^{+\mathrm{B}} \mathrm{x(t-k)}. \tag{10}$$

The variable $2B$ resp. the term $2B + 1$ is referred as the filter length, and $y(t)$ represents the filtered time series $x(t)$. A highpass filter may also be generated using a lowpass filter. Substracting, the filtered time series $y(t)$ from the original time series $x(t)$, as rest, a time series z(t) with removed low frequencies is calculated (DIN 18709-5, 2010). Besides the two mentioned filters, lowpass and highpass filters, there are also combinations of these filters possible. These combinations then give a bandpass filter (there are only certain frequencies passed through) or a band-stop filter (there are only certain frequencies filtered out). These filters were generated in analogy to the construction of a highpass filter. Effects of such filtering process are also visible in the representations of the autocorrelation function.

In Figure 8, a periodic process is shown. After filtering out the low frequencies of this process, the image of the autocorrelation (Figure 9) is significantly changed. In addition to the reduced amplitude, the frequency of the periodic process moves down to slightly higher frequencies. Using the autocorrelation function, the influence and the result of filtering is therefore assessed and clearly visible.

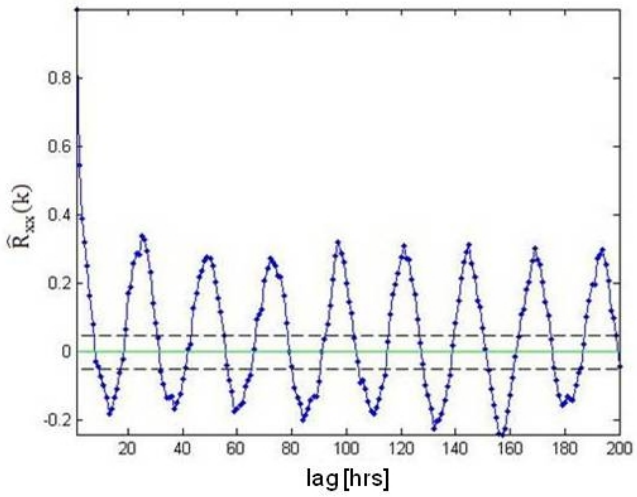

Figure 8: Autocorrelation function including low frequencies WANG, (2012)

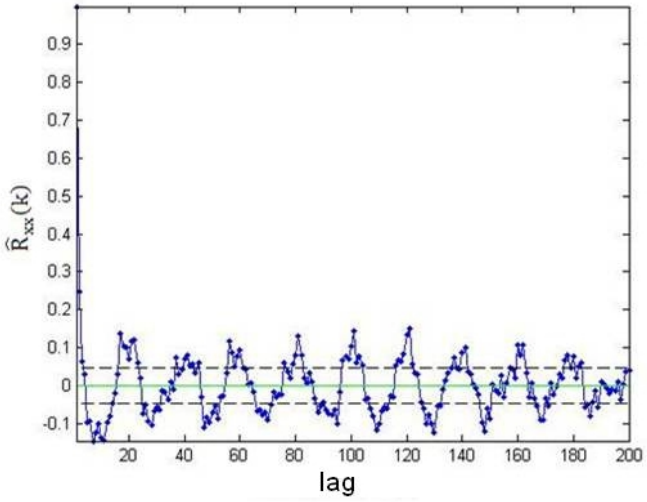

Figure 9: Filtered autocorrelation function WANG (2012)

6 POSSIBILITIES OF ANALYSIS IN THE FREQUENCY RANGE

The autocovariance function and the autocorrelation function are the natural tools to analysis stochastic processes, i.e. a series of measurements in the time domain. At this point the possibilities of analysis in the frequency domain are shortly explained. Usually one tries to eliminate periodic effects from the data in a pre-processing step in time series analysis. This can in particular be supported in determining the periods by analysis in the frequency domain. In a periodogram, these frequencies can be detected and analysed.

A periodogram is formed for example by the transfer of the time series in the frequency domain by a Fast Fourier Transformation (FFT). In the following, the examples for such an analysis are shown. In Figure 10 a time series for a coordinate that was determined using a total station is given.

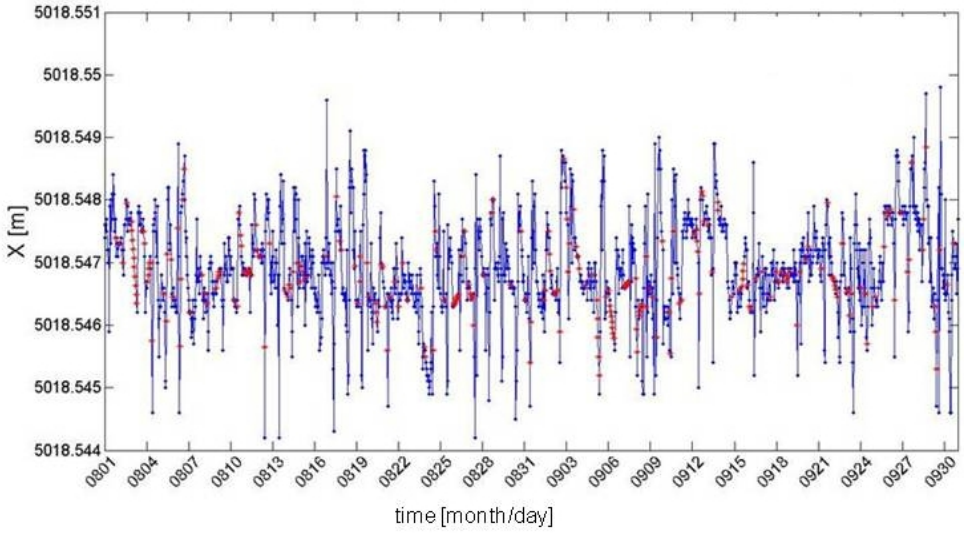

Figure 10: x-coordinates time series WENJUAN (2010)

Linear trends, gaps and outliers were removed in pre-processing. Visualizing the autocorrelation function of the coordinate (Figure 11), periodic effects are obviously included.

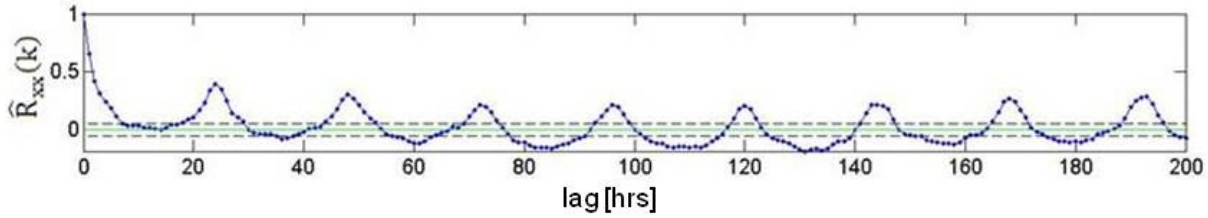

Figure 11: Autocorrelation of x-coordinates WENJUAN (2010)

To investigate these effects in more detail, now a FFT was calculated and the result is shown in a periodogram (see Figure 12). Frequencies can be detected which are dominant in the time series.

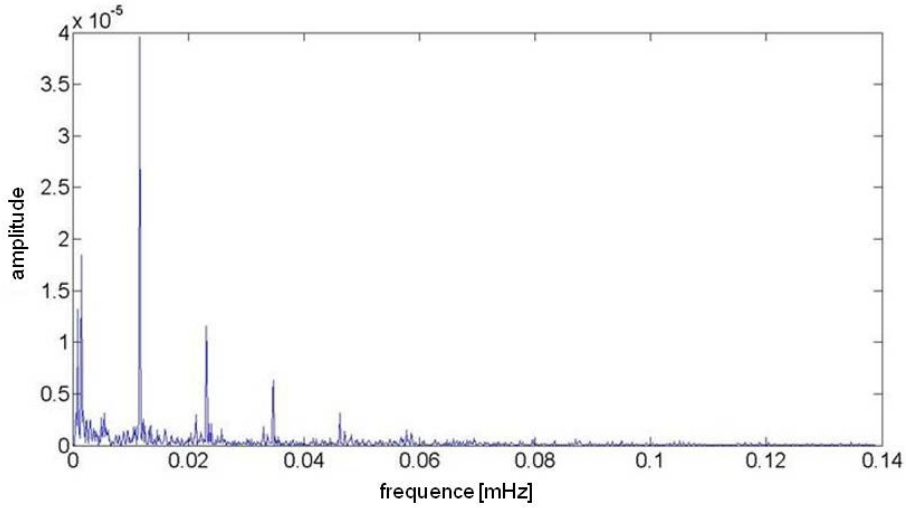

Figure 12: Periodogram of the x-coordinates

If one removes these frequencies (in this case, an 8-day period) and shows the modified time series shown in the autocorrelation domain, these periodic effects have been almost removed (Figure 13).

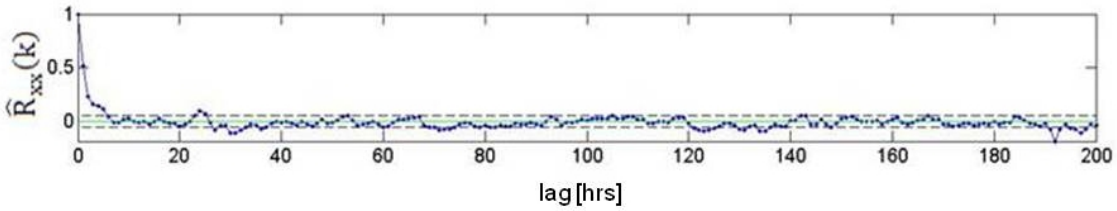

Figure 13: Autocorrelation function of the x-coordinate after removing periodical effects WENJUAN (2010)

Transforming the modified time series again in the frequency domain, significant changes, can be visualized particularly in the magnitude of the amplitude (Figure 14).

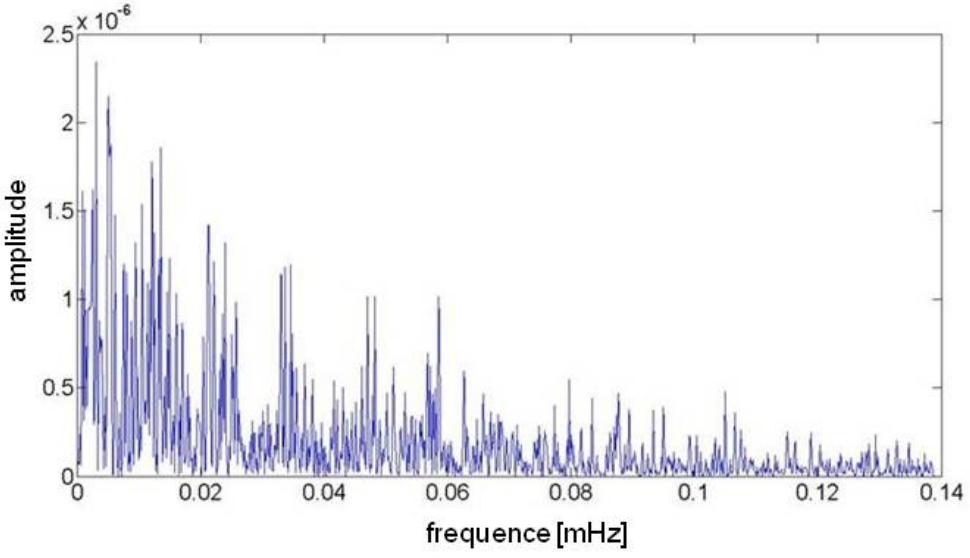

Figure 14: Periodogram of the x-coordinates after removing periodical effects WENJUAN (2010)

7 CONCLUSIONS

With the presented techniques the first steps towards a time series analysis can be done. Important to mention is that before the analyses starts, the time series must be in proper state. This means the time series must be available without gaps, outliers and trend. The algorithms shown require the stationarity and the ergodicity of the time series. These algorithms of time series analysing in the time domain are the autocovariance function and the autocorrelation function. For interpretation of the results of these functions the theoretical and typical processes were mentioned. To improve the time series analysing also filter can be used to pre-process the time series and to delete unwanted influences inside the time series or to point out certain aspects which should be investigated. First steps towards the analysing of a time series in the frequency domain were also presented.
With this algorithms and options of analysing the first steps towards the analysing of time series in context of construction monitoring were given.

ACKNOWLEDGEMENTS

The authors would like to thanks Prof. Schwieger for the support and Ms. Wenjuan Hu, Ms. Ye Zhou, and Ms. Xu Wang for preparing, realising and partly analysing the measurements within her master thesis at IIGS, University Stuttgart.

REFERENCES

Books:

CHATFIELD, C.: *The Analysis of Time Series: An Introduction.* Chapman & Hall London, 2004.

DIN 18709-5, Normenausschuss Bauwesen (NABau) im DIN: *Begriffe, Kurzzeichen und Formelzeichen, in der Geodäsie – Teil 5: Auswertung kontinuierlicher Messreihen*, Beuth Verlag, 2010.

HEUNECKE, O.; KUHLMANN, H.; WELSCH, W.; EICHHORN, A.; NEUNER, H.: *Auswertung geodätischer Überwachungsmessungen.* In der Reihe: Möser, M.; Müller, G.; Schlemmer, H. (Hrsg.): *Handbuch Ingenieurgeodäsie*, Wichmann Verlag, Berlin, 2013.

NEUNER, H.; FOPPE, K.: *Grundlagen der Zeitreihenanalyse im Zeitbereich*. In: Foppe, K. (Hrsg.): 85. DVW Seminar: *Zeitabhängige Messgrößen – Verborgene Schätze in unseren Daten*, Wissner-Verlag, Augsburg, 2009.

RUNKLER, T.: *Data Mining: Methoden und Algorithmen intelligenter Datenanalyse*, Vieweg+Teubner, Wiesbaden, 2010.

WENCHUAN, H.: *Time Series Analysis for Construction Monitoring*, Masterarbeit, Institut für Ingenieurgeodäsie, Studiengang Geoengine an der Universität Stuttgart (unveröffentlicht), 2010.

WANG, X.: *Time Series Analysis for Construction Monitoring – Detailed analysis of high frequencies*, Masterarbeit, Institut für Ingenieurgeodäsie, Studiengang Geoengine an der Universität Stuttgart (unveröffentlicht), 2012.

ZHOU, Y.: *Zeitreihenanalyse*, Studienarbeit, Institut für Ingenieurgeodäsie, Studiengang Geodäsie und Geoinformatik an der Universität Stuttgart (unveröffentlicht), 2012.

Journal articles:

KUHLMANN, H., SCHWIEGER, V., WIESER, A., NIEMEIER, W.: *Ingenieurgeodäsie – Definition, Kernkompetenzen und Alleinstellungsmerkmale*. Zeitschrift für Vermessungswesen, Heft 6, Wißner Verlag, p. 391-399, 2013.

HUDNUT K. W. and BEHR J. A.: *Continuous GPS monitoring of structural deformation at pacoima dam*, Seismological Research Letter, 69(4), p. 299-308, 1998.

KÄLBER, S., JÄGER R.: *GPS-based Online control and Alarm System (GOCA)*, 10th FIG International Symposium on Deformation Measu rements, Orange, California USA, March 19– 22, 2001.

ROBERTS G.W., DODSON A. H. and ASHKENAZI V.: *Twist and deflection: monitoring motion of humber bridge*, GPS World, 10(10), p. 24-34, 1999.

ROBERTS G., MENG X. and BROWN C.: *From St Paul's to the Tate Modern; Overcoming problems in monitoring bridge deflections using GPS*, 1st FIG International Symposium on Engineering Surveys for Construction Works and Structural Engineering, Nottingham, United Kingdom, June 28– July 1, 2004.

Time-Spatial Analysis for Low-Cost GPS Time Series

Li Zhang
Institute of Engineering Geodesy, University of Stuttgart, Germany

Abstract
The Institute of Engineering Geodesy (IIGS) is currently developing an automatic low-cost GPS monitoring system, which includes u-blox single frequency GPS receivers. In the first tests, the Trimble Bullet III GPS antennas (costs less than 100 €) with the self-constructed L1-optimized choke rings already obtained an accuracy, that almost met the requirements of geodetic applications. However, the accuracy of the system, particularly in shadowing environment, still needed to be improved. For this purpose, time series analysis of the three-dimensional GPS coordinates is carried out. This will prepare the construction of low-cost GPS antenna/receiver arrays for monitoring.

Measurements with closely-spaced antennas are carried through to find spatial correlations additional to the well-known temporal correlations. The multipath effects should be visible in the coordinates as periodic and trigonometric functions. They should be estimated and taken into account for the processing strategy to deliver improved coordinate accuracy. Furthermore the spatial correlation between the antennas should also be investigated and used for improving the coordinate accuracy.

The aim is the development of a stabile method using time and spatial correlation of multiple antennas to improve the results of low-cost GPS receivers to enable structural health monitoring.

Keywords
Low-cost GPS, monitoring, multipath effects, time-spatial analysis, time series, correlation

1 INTRODUCTION

Monitoring of structures and natural objects, such as landslides, rock glaciers, dams and bridges is one of the main tasks of engineering geodesy. Automation and continuity of measurements are the trends of the monitoring. The data collection and processing of the GNSS receivers can be realized automatically and continuously. They are able to measure the three-dimensional positions and achieve accuracies in mm range in relative mode by using carrier phase measurements. Besides, compared to traditional measurement instruments (for example tachymeters and leveling) and modern areal measurement instruments (for example terrestrial laser scanners and terrestrial radar scanners), the direct line-of-sight is not necessary and their measurement accuracies are not sensible to weather conditions. However, the geodetic GNSS receivers are expensive (some cost more than 20 000€), so that they are not suitable for the area-wise measurement.

Besides the geodetic GNSS receivers, there are also many low-cost single-frequency GPS receivers, which are developed for the mass market and whose price is below 100 €. Many preliminary researches at the Institute of Engineering Geodesy, University of Stuttgart (IIGS) showed that those low-cost GPS receivers, by using the carrier phase data, reach an accuracy which almost meets the requirements of geodetic applications SCHWIEGER (2007), SCHWIEGER (2008), SCHWIEGER (2009). Based on these preliminary successful experiences, IIGS is currently developing an automatic low-cost GPS monitoring system using u-blox GPS L1-receivers ZHANG et al. (2012), ZHANG & SCHWIEGER (2013). Since they are cost-effective, many receivers can be applied at the same time. That means, a high spatial discretization of the object can be provided by using low cost GPS receivers.

The general weakness of the GNSS receivers is that, their signals are disturbed from the multipath effects, so that their accuracies particularly in shadowing environment needs to be improved. Usually, there are only short baselines up to several kilometers for monitoring of objects in engineering

geodesy. The most GNSS errors, such as ionosphere and troposphere errors can be ignored for short baselines, but the multipath effects cannot be eliminated in differential mode. For this reason, the multipath effects are the dominating errors for short baselines.

The authors try to reduce the multipath effect on the one hand by applying self-constructed L1-optimized choke ring (chapter 2), in another words, by improving the hardware; on the other hand by considering the time and spatial correlation between the closely-spaced antennas (chapter 3), it means by data processing. The first investigations are carried out and the results will be presented in this paper.

2 MITIGATION OF MULTIPATHEFFECT USING L1-OPTIMIZED CHOKE RING

It is well-known that the accuracies of GNSS receivers are affected by multipath effects, even in shadowing free environment. Since the reflected signals come not only from the vertical reflectors, but also from the ground.

Part of the multi-path effect can be reduced by special construction or design of GNSS antennas such as choke ring and full spectrum GNSS antennas TOPCON (2014). However, the prices of geodetic antennas are very high, so that they are not cost-effective solutions. Furthermore, the commercial chock ring is not optimized for single frequency GPS receivers, so that it is not the optimal solution here. The reason will be given later in this chapter.

In TAKASU & YASUDA (2008), several low-cost GPS L1-frequency antennas and receivers were tested in combination. The tests show that good antennas have a higher positive impact on the result than good receivers. For this reason, three types of low-cost antennas (u-blox ANN-MS, Vimcom 96/1 and Trimble Bullet III; each of them costs less than 100 €) were tested in combination with the u-blox LEA-6T receiver at IIGS ZHANG & SCHWIEGER (2013).

To reduce undesirable multipath effects, the u-blox ANN-MS antenna is shielded with a self-constructed ground plate. Vimcom 96/1 and the Trimble Bullet III antennas are shielded with self-constructed L1-optimized choke rings.

As described in FILIPPOV et al. (1998), multipath effects can be reduced by a certain depth of the choke ring antenna. The depths of the choke rings should be about 1/4 of the wavelength of the signal, for the frequencies of L1 and L2 they are approximately 4.7 cm and 6 cm. The commercial choke rings have depth of about 5.6 cm, which is a compromise between L1 and L2 and so the multipath effects are not reduced absolute optimally for single frequencies. The self-constructed choke ring has a depth of 4.5 cm and is thus optimized for L1-frequency ZHANG & SCHWIEGER (2013).

First of all, the antennas with different shieldings are compared in ZHANG & SCHWIEGER (2013). The result shows the Trimble Bullet III antennas have the best performance. Further measurements were than carried out to verify, if the self-constructed L1-optimized choke ring performs better than the ground plate by using the same antenna. The results show that the accuracies with choke rings are about 40% better than with ground plates. The details will not be shown here, since it is not the focus of this paper.

Antenna phase center offset (PCO) and phase center variations (PCV) are also main errors, which cannot be eliminated in differential mode. They can be mixed with the multipath effects and they change with the shieldings, such as ground plate and choke ring ZEIMETZ & KUHLMANN (2008). For this reasons, before the comparison of choke ring and ground plate, the antennas were individually calibrated with choke ring and ground plate by University of Bonn, Institute of Geodesy and Geoinformation. It is an absolute anechoic chamber calibration.

The PCO of the Trimble Bullet III antenna are both in sub-mm with choke ring and ground plate in east and north-component. The PCV are shown in Figure 1. So it can be found out, that the PCV of the Trimble antenna with choke ring is much smaller and more homogeneous and more rotationally symmetric than it is with the ground plate.

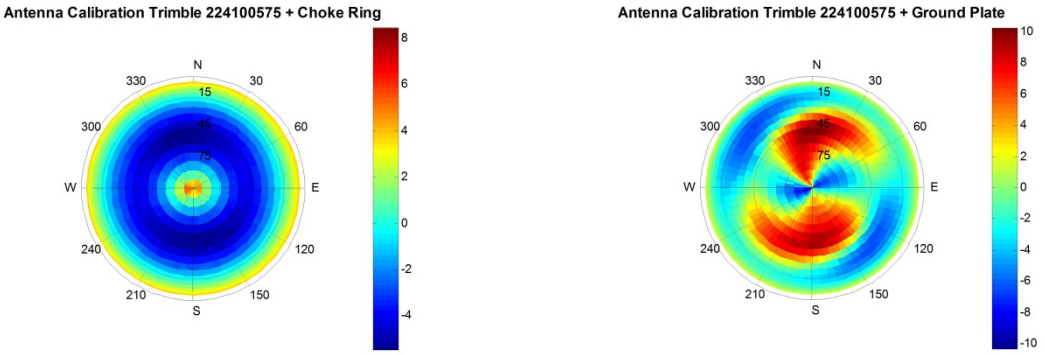

with choke ring with ground plate

Figure 1: PCV of one Trimble Bullet III antenna with choke ring

The accuracies were improved sub-mm range by using the antenna calibration data. The antennas were calibrated individually; individual calibration means that each antenna has its own calibration data. The individual antenna calibration is expensive and costs much more than the antenna itself. The question arises, whether type calibration for those low-cost antennas is enough or whether single calibration is necessary. The results in Zhang and Schwieger (2013) showed that the results with type calibration are the same as with individual calibration. That means, on the base of the research carried through up to now, the type calibration for this antenna with choke ring is enough.

3 TIME-SPATIAL ANALYSIS OF MULTIPLE LOW-COST GPS ANTENNAS

3.1 Background and Basic Idea

The accuracy of the low-cost GPS receivers and antennas were improved by the self-constructed L1-optimzed choke ring. However, there is still potential to improve the accuracy. The reference stations are usually equipped with the best high-end geodetic receivers and antennas. However, it is well-known that even some SAPOS (Satellitenpositionierungsdienstder deutschen Landesvermessung) reference stations are suffering from multipath effects WANNINGER (2000). Since only a part of reflected signals, such as the signal from ground and part of signals above the horizon, can be eliminated or minimized by the choke ring. There are still parts of reflected signals, probably with high elevation angle that cannot be eliminated, so that the accuracies are affected.

Many researchers have worked on the multipath effects and tried to find their characteristics and to eliminate them. Multipath effect has usually typical period of sidereal day, since it depends on the geometry constellation between satellites, antennas and the location of reflectors in the vicinity; normally the position of reflectors and antennas do not change and the satellite position repeat after a sidereal day. The multipath effect can be defined mathematically by considering the geometric relationships and the reflection coefficient of reflectors GEORGIADOU & KLEUSBERG (1988). However, the positions and the reflection coefficient of reflectors in reality are so complicated, that the multipath effects cannot be modelled exactly. Therefore, they cannot be distinguished from the other errors and the real movements of the antennas very well.

The multipath effects of reference stations were already investigated by many researchers WANNINGER (2000), BILICH et al. (2004), ZEIMETZ et al. (2009). It was assumed that the reflected signals only come from ground, for a typical antenna height of about 1.5 meter, the typical dominating multipath period varies from 5 to 45 minutes. However, for the antennas mounted on non-uniform surfaces such as landslides and dams, the situation will be more complicated, especially if the environment is not free from shadowing.

In WANNINGER (2000), the multipath effects can be detected and reduced, if the L1 and the L2 carrier phase were observed in a combined way. But for the L1-freuquence receiver, there is no data from the L2-frequency. In BILICH et al. (2004) and ROST (2011), the time series using signal-to-noise ratios (SNR) were investigated and the multipath effects can be reduced.
Most researches up to now are based on observation data, mainly ranges based on the phase data. Since the information at disposal for the research is the coordinates from the GNSS measurements, an idea arises to develop a coordinate-based method, to reduce the errors of multipath effects and the other errors. In KUHLMAN (2003), ZEIMETZ et al. (2009) and LI (2013), the time series of GPS coordinates were analyzed. Different filters such as Kalman filer model with shaping filer and FIR-filter have been applied on the coordinates to separate the noise such as multipath effects and the real deformations. The correlation in time series was analyzed and taken into account.
As mentioned before, since the low-cost receivers and antennas are cost effective, more receivers and antennas can be mounted on the monitored object. The multipath effects cannot change rapidly in a small area, since the environment or reflectors do not change rashly. So if several antennas are set closely, the multipath effect or any other errors should change slowly, so that the coordinates of these antennas are highly spatial correlated. An approach that considers the spatial correlation and improves the accuracies of GPS coordinates will be introduced in this paper.
In this chapter, the time series of low-cost GPS antennas will be analyzed at first. Then, the spatial correlation of the multiple closely-spaced low-cost GPS antennas will be investigated. The aim is to improve the accuracies by considering the time and spatial correlations between the antennas.

3.2 Test Scenario

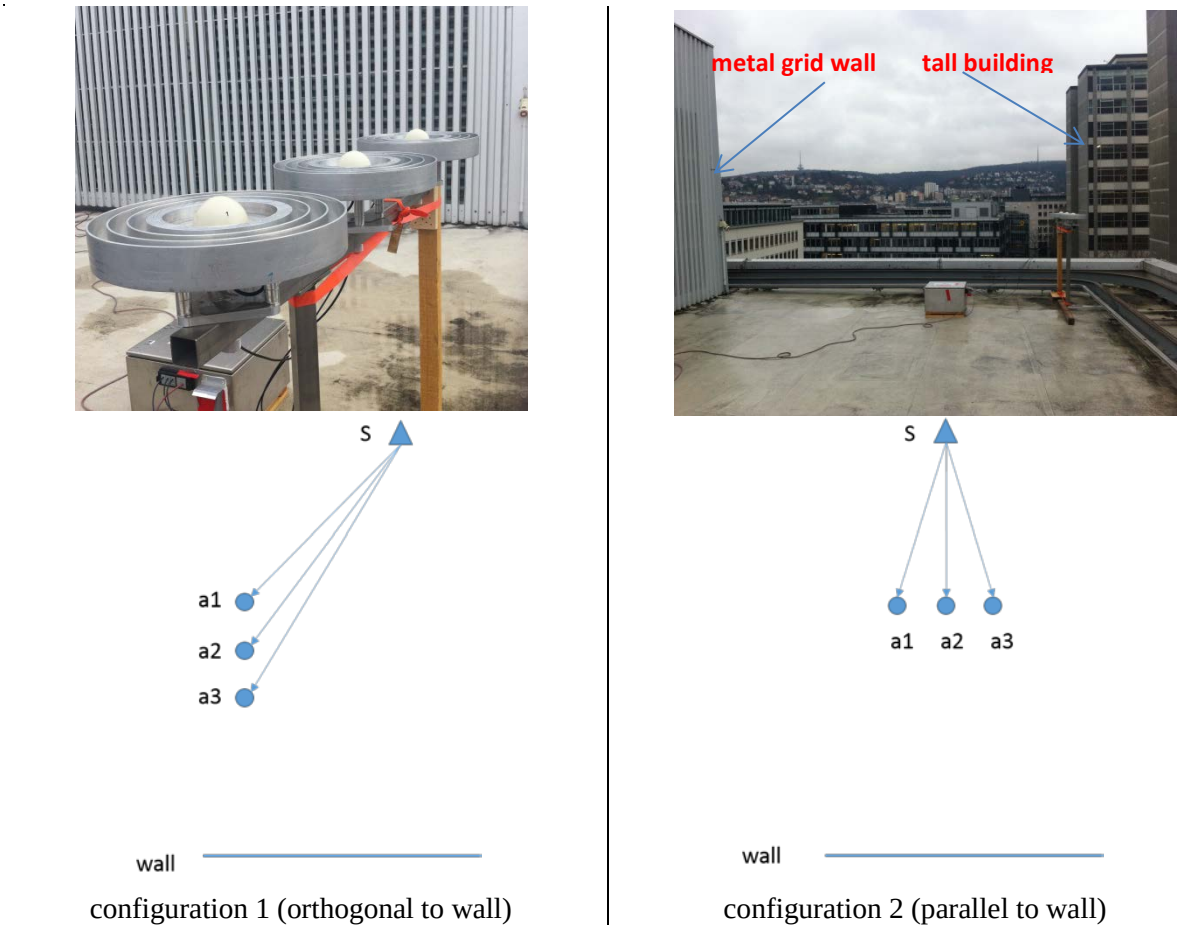

configuration 1 (orthogonal to wall) configuration 2 (parallel to wall)

Figure 2: Two test configurations (not scaled)

Three antennas with the choke ring were tested on the roof of the IIGS building (compare Figure 2). A metal grid wall is near the antennas (about 5 meters away) and a tall building is about 50 meters away (compare Figure 2 right). It is supposed that most multipath effect originate from the metal grid wall and the ground; the satellites configuration is not so ideal due to the tall buildings. As one can see from figure 2 left, the surface of the metal grid wall is not flat but constructed, so that it is not the simple specular reflection, if the signals are reflected on it.
The three antennas were arranged in two configurations: orthogonal (configuration 1) and parallel (configuration 2) to the wall. It is expected that the multipath effect change much more in configuration 1 than in configuration 2 for the antennas.
There is a SAPOS reference station in about 500 meters away from the IIGS building. This reference station was taken as reference station and the three low-cost antennas were taken as rover stations for the calculation of baselines. The distance between two adjoining antennas is 50 centimeters. The distances between the antennas cannot change, since they are mounted on the same holder (see Figure 2). Three antennas are numbered as a1, a2 and a3. The distance between the a2 (the middle one) and the wall is about 4.2 meters in configuration 1 and about 5.1 meters in configuration 2 and the antenna heights are all about 1.2 meters. The GPS raw data (UBX-format) were stored directly from EVK-6T UBLOX (2014) with 1 Hz sampling rate. The antennas were measured in configuration 1 for about 9 days and in configuration 2 for about 20 days.

3.3 Time Series Analysis of Low-Cost GPS Antennas

3.3.1 Data Pre-processing

The raw data was processed with the free software TEQC (TEQC 2014) and wa1 (WA1 2014). The results are UTM-coordinates for three baselines (coordinates difference in east, north and height direction) for every second. Since the amount of data is huge, only results of one day for each configuration were analyzed in detail till now. One day solution was divided into 24 hourly solutions, so that some short periodic effect can be found.

The given coordinates of the antennas are unknown; the mean value of the coordinates can be calculated as an approximation for the given coordinates. The standard deviations which describe the repeatability of the measurements are defined as parameter for the accuracy of the measurements. For monitoring, repeatability or accuracy of the measurements is the most important and decisive parameter. For this reason, the standard deviations will be mainly discussed in this paper.

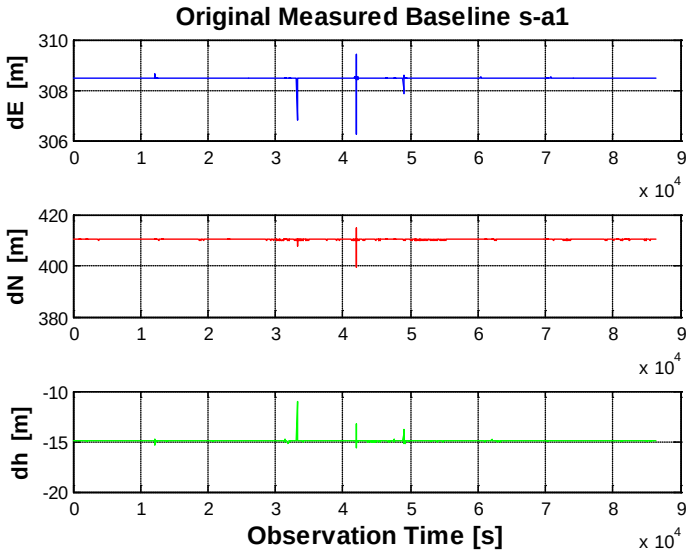

Figure 3: Example for an original measured baseline

Figures 3 shows an example for one original measured baseline, as visible, it makes no sense to calculate the mean values and standard deviations, if there are so many obvious outliers. So at first, the outlier were detected and defined, if difference to the mean value were lager than 4.7 (the multipath effects may reach 1/4 of the wavelength of the signal, meaning 4.7 cm for L1-frequency) centimeters in one of the coordinates' component. The mean value and the standard deviations were calculated again. Then, the three sigma rule NIEMEIER (2008) was used to detect the other "smaller" outlier. The mean value and standard deviation were estimated again by excluding all the detected outliers. The outliers and some gaps (actually there are almost no gaps) were linear interpolated. Figure 4 is an example for a baseline after detection and interpolation of outliers. On average, about 5% outliers are detected and interpolated.

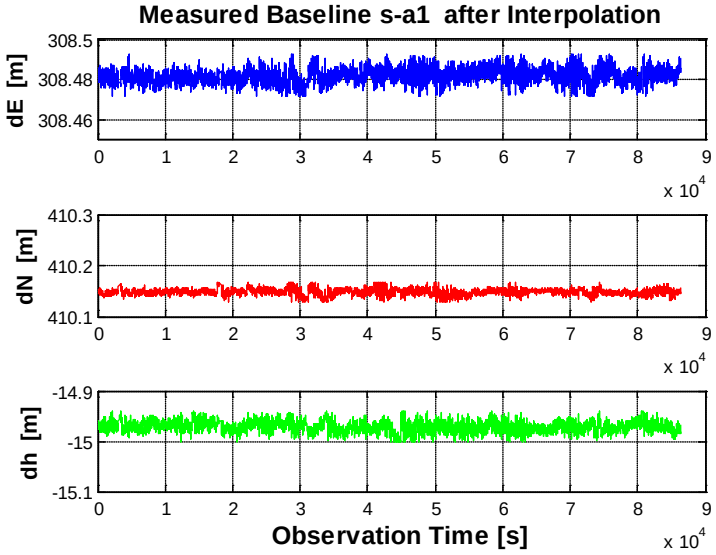

Figure 4: Example for a baseline after detection and interpolation of outliers

$$x(t) = a_0 + b_0 t \tag{1}$$

$$x(t) = \sum_k a_k \cos(2\pi f_k t) + b_k \cos(2\pi f_k t) \tag{2}$$

The linear and periodic trend should be eliminated, so that the time series is stationary. Stationary is an important precondition for the analysis of time series CHATFIELD (2004); METZNER & SCHWIEGER (2014). The parameters a_0 and b_0 (compare equation (1)) of the linear trend and the parameters a_k and b_k of periodic trend (compare equation (2)) can be calculated by adjustment. $x(t)$ is the time series of coordinate components. f_k is the dominating frequency, that can be found in frequency domain (compare section 3.3.3). The significance of the parameters should be tested by t-test like $t_{a_0} = \hat{a}_0 / s_{a_0}$, the $\hat{a}_0$ and s_{a_0} are the estimated parameter and its standard deviation from the adjustment results FOPPE & NEITZEL (2014). In the time series of coordinates that were chosen for analysis, there are no significant linear and periodic trends.

3.3.2 Data Analysis in Time Domain

The autocovariance function describes the correlation in the time series and the discrete autocovariance function can be defined as equation (3). The normalized autocovariance function is the

auto-correlation function (see equation (4)), it can vary from 1 to -1. It can only be calculated up to m=n/10, so that the calculation is statistic significant HEUNECKE et al. (2013).

$$\hat{C}_{xx}(k) = \frac{1}{n-k-1}\sum_{j=1}^{n-k}(x_j - \bar{x})(x_{j+k} - \bar{x});\ k = 0,1....m = n/10; \tag{3}$$

$$\hat{K}_{xx}(k) = \frac{\hat{C}_{xx}(k)}{\hat{C}_{xx}(0)} \tag{4}$$

Figure 5 shows one example of an autocorrelation function of one baseline in all coordinates' components. Since it is a one day solution, there are 86400 seconds and 1/10 of it is shown up to 8640 seconds. The autocorrelation function is symmetric at zero and its maximum is always at the zero and equal to 1. Besides, it can be seen that, after about 1000 seconds (about 16 minutes) there is almost no correlation visible. This autocorrelation function visualizes that the process consists of typical white noise, Gauss-Markov-process and colored noise.

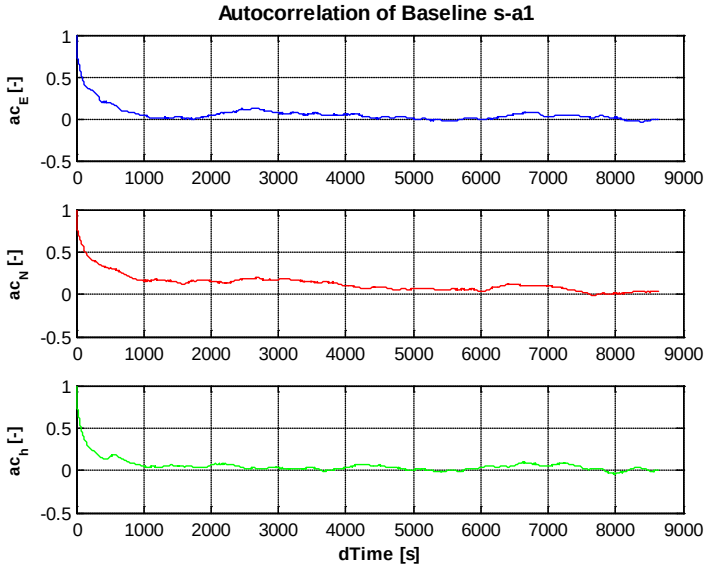

Figure 5: Example for Autocorrelation Function of one Baseline

The autocorrelation function reflects the time correlation within one time series. If the time correlation between the two time series is considered, it is called cross-covariance function, the definition can be found in equation (5). The normalized cross-covariance function is cross-correlation function (see equation (6)), it can also vary from 1 to -1.

$$\hat{C}_{xz}(k) = \frac{1}{n-k-1}\sum_{i=1}^{n-k}(x_i - \bar{x})(z_{i+k} - \bar{z});\ k = 0,1....m = n/10; \tag{5}$$

$$\hat{K}_{xz}(k) = \frac{\hat{C}_{xz}(k)}{\sqrt{\hat{C}_{xx}(0)\hat{C}_{zz}(0)}} \tag{6}$$

Figure 6 shows an example for the cross-correlation between two baselines in each coordinates' components. The cross-correlation is asymmetric at zero, to give an impression, the cross-correlation for the negative time difference is also shown in Figure 6.

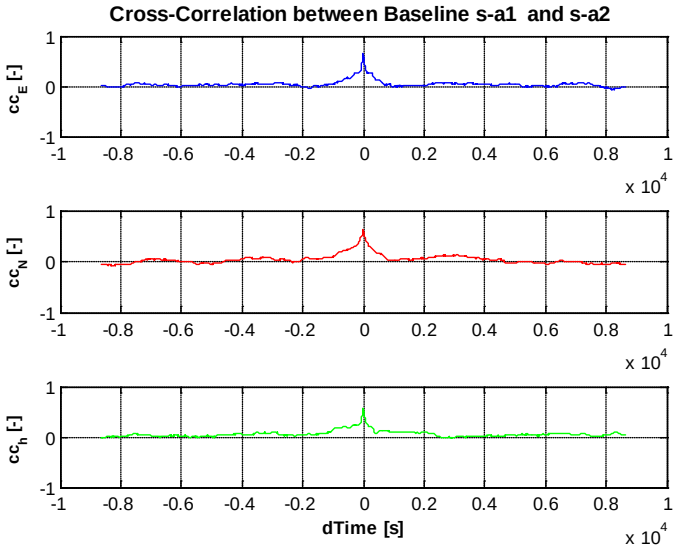

Figure 6: Example for Cross-Correlation Function between two Baselines

Here in Figure 6, the cross-correlation functions between the two baselines vary from about 0 up to 0.64 in east, 0.63 in north and 0.57 in height component. The maximum of a cross-correlation function does not have to occur at a time shift of zero. However, the results show that the maximum is always at zero, which means the error has an influence on every antenna at the same time and there is no time delay for different antennas. Furthermore, as expected, the autocorrelation shows higher maximum values (the maximum of autocorrelation function is always 1) than the cross-correlation between two baselines. The cross-correlation functions between the baselines will be discussed in section 3.4 more in detail, since they deal with the information about the spatial correlation.

3.3.3 Data Analysis in Frequency Domain

Some properties of the time series such as periodic effect cannot be found easily in time domain, but in frequency domain. Fourier transformations of the autocovariance and cross-covariance function are called spectrum and cross-spectrum in frequency domain. The procedure and the formulas for the transformation can be found in HEUNECKE et al. (2013) and CHATFIELD (2004). They will not be presented in this paper.

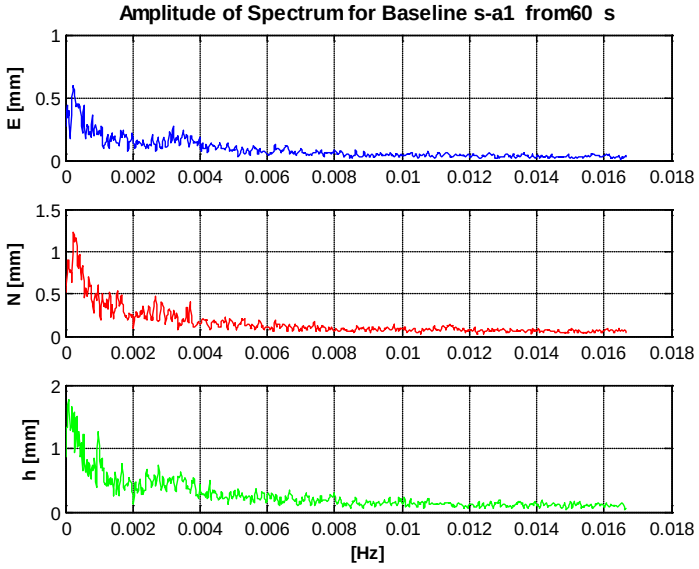

Figure 7: Example for Amplitude Spectrum of one Baseline (one day solution)

Figure 7 shows the amplitude spectrum of one baseline. The amplitudes for the high frequencies (> 1/60s) are very small, so that they can be ignored. Therefore, only a part of frequencies are presented. It seems to be that some trends remain in data. For example, the dominant period in Figure 7 is about 18 hours for each component. This period was taken for the adjustment in section 3.3.1. As mentioned before, the parameters were not significant, it means, there are no trends in data.

If only one hour solution is analyzed (compare Figure 8), the dominating period is about half an hour. It seems to be that long periods are visible in the data that cannot be calculated significantly with the chosen observation intervals. This effect should be analyzed in detail in the future, maybe different observation intervals (for example several days, several hours) should be taken and the periodic effect should be analyzed. However, the typical short periods resulting from the ground reflected multipath are vanished, since the choke ring is used.

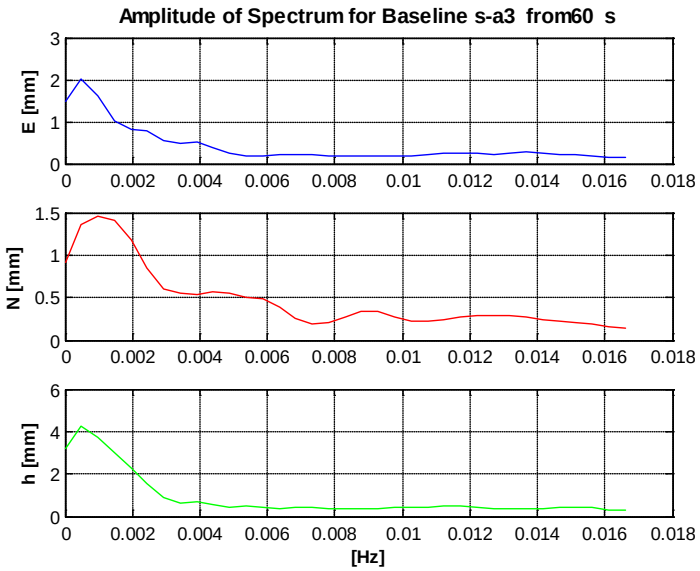

Figure 8: Example for Amplitude Spectrum of one Baseline (one hour solution)

3.4 Spatial Correlation Analysis of Closely-Spaced Low-Cost GPS Antennas

Since the antennas are closely-spaced, it is expected that their errors are highly correlated. As noticed in section 3.3.2 the cross-covariance functions were calculated, its normalized form is the cross-correlation function. For three baselines, three sets of cross-correlation functions, they are cross-correlation functions $\hat{K}_{s-a1,s-a2}$, $\hat{K}_{s-a1,s-a3}$, $\hat{K}_{s-a2,s-a3}$ can be obtained (in all the three coordinates' components, so there are 9 cross-correlation functions altogether).

As mentioned before, the maximum of the cross-correlation functions in the results are at time shift of zero. It means the influence of the error happen at the same time for every antenna. If only the maximum of each cross-correlation functions, called K_{12}, K_{13}, K_{23}, were taken and compared, as expected, for both configurations, it is always $K_{12} < K_{13}$ and $K_{23} < K_{13}$, since the distance between the antenna 1 and 3 is the biggest. Furthermore, the general the cross-correlations K_{12}, K_{13} and K_{23} of the configuration 2 is bigger than of configuration 1, since the change of environment of configuration 1 is more than that of configuration 2 for the three antennas.

The similar effect can be also found in the accuracies of the coordinates. In configuration 1, the standard deviations of the coordinates are antenna 1 > antenna 2 > antenna 3, they are about 5 to 6 mm in north, 3 to 4 mm in east and 9 to 11 mm in height (one day solution). Since the distances between the antennas and the metal grid wall are antenna 1 < antenna 2 < antenna 3. In configuration 2, since

the distance between the wall and the antennas are the same, their standard deviations are almost the same. They are about 3 mm in east, 5 to 6 mm in north and 9 to 10 mm in height (one day solution). The cross-correlations and accuracies seem to be very reasonable and realistic.

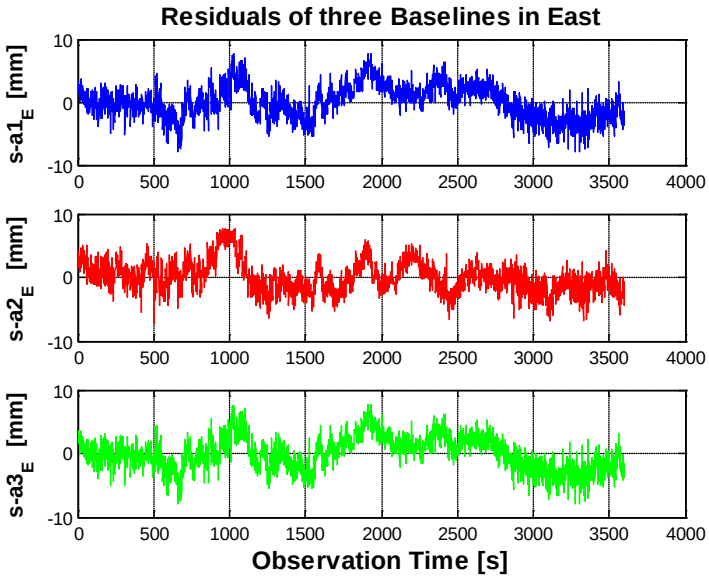

Figure 9: Example for Residuals of the three Baselines in East (one hour solution)

Figure 9 shows an example for the residuals of three baselines in the east component (one hour solution in configuration 2). The errors have a similar effect on the closely-spaced antennas. Since the distance between the adjoined antennas is the same, if the error influences change exactly spatially linear, the error of antenna 2 should be average of the errors of antenna 1 and antenna 3. However, the change of errors is not exactly spatially linear, but the cross-correlation contains information about this similarity, it can be used here. One simple approach was applied to improve the accuracy by using the spatial cross-correlation between the baselines. For example, the coordinates of antenna 2 can be corrected by the coordinates of antenna 1 and 3 by considering the cross-correlation. $x_{2\_cor}(t)$ can be calculated by equation (7). $x_1(t)$ to $x_3(t)$ on the right side are the original coordinates' residuals in east, north and height component. It means the coordinates of antenna 2 are corrected by the weighted mean of the antenna 1 and 3, the weightings depend on the cross-correlation between the antennas. As mentioned before, if the errors change exactly spatially linear, the error of antenna 2 will be completely eliminated, it means the $x_{2\_cor}(t)$ will be zero. Since it is not the case, the error of antenna 2 cannot be completely eliminated but reduced (compare table 1 and 2).

$$x_{2\_cor}(t) = x_2(t) - \left(\frac{K_{12}}{K_{12}+K_{23}} \cdot x_1(t) + \frac{K_{23}}{K_{12}+K_{23}} \cdot x_3(t) \right) \tag{7}$$

K_{12} and K_{23} depend on the chosen observation intervals processed and the configurations of the observations. The K_{12} and K_{23} vary from about 0.3 to 0.5 for a one day solution and from about 0.2 to 0.8 for a one hour solution in configuration 1; they vary from about 0.55 to 0.65 for one day solution and from about 0.35 to 0.8 for a one hour solution in configuration 2.

For testing this approach, a one daily solution and four hourly solutions were taken from the each configuration. The tables 1 and 2 show the original and improved standard deviation of baseline s-a2 by applying the approach. Generally, almost all the standard deviations were improved (only one exception gray marked in table 2). The percentage of improvement is varies obviously (maximum is 46%), on average about 21% for configuration 1 and 25% for configuration 2.

Table 1: Original and Improved Standard Deviations of Baseline s-a2 (Configuration 1)

Configuration 1	Original standard deviation [mm]			Improved standard deviation [mm]		
s-a2	E	N	h	E	N	h
Day solution	3.3	6.2	9.4	3.0	5.4	8.2
1. hour	1.9	4.1	5.4	1.7	2.5	5.1
2. hour	3.7	16.6	10.0	2.8	13.2	7.5
3. hour	2.7	5.3	16.6	1.5	3.5	10.6
4. hour	4.0	5.5	8.4	3.6	4.1	7.3

Table 2: Original and Improved Standard Deviations of Baseline s-a2 (Configuration 2)

Configuration 2	Original standard deviation [mm]			Improved standard deviation [mm]		
s-a2	E	N	h	E	N	h
Day solution	3.3	5.7	9.5	2.3	4.1	7.0
1. hour	2.0	3.2	5.8	1.4	1.9	5.9
2. hour	2.5	3.1	5.8	2.2	2.0	5.6
3. hour	2.1	3.0	5.9	1.5	1.7	4.3
4. hour	2.4	3.3	10.7	2.0	2.1	7.3

From these first test results, it can be seen that the approach that takes the spatial correlations into account can improve the accuracies of the results. The linear combination of the corrections is the simplest assumption. In the future, the spatial correction should be analyzed more in detail and more reliable and sophisticated approaches have to be developed.
This type of the approach may have some problems to distinguish the errors from real deformations, because the deformations have a similar effect, so that the real deformations cannot be detected. The errors, particularly the multipath effects, and the deformation should be separated correctly. This step should be investigated in the future.

4 CONCLUSIONS AND OUTLOOK

In this paper, methods were introduced to improve the accuracies of the low-cost GPS receivers and antennas. One of them was realized by using the L1-optimized choke ring. Compared to a normal ground plate, the choke ring can improve the accuracies about 40%.
Another improvement was realized by analysing the time and spatial correlation of some closely-spaced antennas. But it is obviously, that there are still some problems of finding the short period trends, it will be the focus of future work. And it is expected that the potential to improve the accuracy within this method will be impressive.
After considering the spatial correlation between the closely-spaced antennas, the accuracies of the results were already improved about 20 to 25% for the chosen data. Up to now, the baselines between the antennas, that means the baselines a1-a2, a1-a3 and a2-a3 were not analysed. Since their distance is known, these geometry conditions can be considered as additional information for detect and modelling the multipath effects in the future.
Furthermore, a lot of new experimental works are in progress. For example, more antennas, such as an antenna-array with 9 antennas (compare figure 10) are arranged to have higher spatial discretization, so that the changes of the spatial correlation can be calculated in different directions. And their spatial correlations should be analyzed and modelled.
The goal is to detect the effect of multipath errors or other errors in real time or in near real time by applying more closely-spaced low cost GPS antennas and considering the time and spatial correlations in the future.

Figure 10: Nine Antennas and Receivers Array

ACKNOWLEDGEMENTS

The help of Wa1 software provider, Prof. Dr. Wanninger from Geodetic Institute of Technical University of Dresden is highly appreciated. The authors thank also the Institute of Geodesy and Geoinformation, University of Bonn for the antenna calibrations.

Finally, the authors thank Mr. Martin Knihs of the IIGS for his help with the practical measurement and particularly for the construction of the choke rings.

REFERENCES

Books:

CHATFIELD, C.: *The Analysis of Time Series: An Introduction*. Chapman & Hall London, 2004.

HEUNECKE, O.; KUHLMANN, H.; WELSCH, W.; EICHHORN, A.; NEUNER, H.: *Auswertung geodätischer Überwachungsmessungen.* In der Reihe: Möser, M.; Müller, G.; Schlemmer, H. (Hrsg.): Handbuch Ingenieurgeodäsie, Wichmann Verlag, Berlin, 2013.

LI, L.: *Separablity of deformations and measurement noises of GPS time series with modified Kalman filter for landslide monitoring in real-time*. München 2013, ISBN 978-3-7696-5110-2, II+10 S, 2013.

NIEMEIER, W.: *Augleichungsrechnung*. Walter de Gruyter, Berlin, New York, 2008.

ROST, C.: *Phasenmehrwegereduzierung basierend auf Signalqualitätsmessungen geodätischer GNSS-Empfänger*. München 2011, ISBN 978-3-7696-5077-8, 167 S,2011.

Journal articles:

BILICH, A., LARSON, K. M., AXELRAD P.: *Observations of signal-to-noise ratios (SNR) at geodetic GPS site CASA: Implications for phase multipath.* Proceedings of the Centre for European. Geodynamics and Seismology, 23, 77-83, 2004.

FILIPPOV, V., TATARNICOV, D., ASHJAEE, J., ASTAKHOV, A., SUTIAGIN, I.: *The First Dual-Depth Dual-Frequency Choke Ring*. Proceedings of the 11th International Technical Meeting of the Satellite Division of The Institute of Navigation (ION GPS 1998), Nashville, TN September 15 - 18, 1998.

FOPPE, K.; NEITZEL, F.: *Von der Zufallsgröße zur Trendschätzung im vermittelnden Ausgleichungsmodell – Grundlagen zur Zeitreihenanalyse für Praktiker*. Zeitabhängige Messgrößen – Ihre Daten haben (Mehr-)Wert. 129. DVW-Seminar on 26. - 27. 02. 2014 in Hannover, Wißner Verlag, Augsburg, 2014.

GEORGIADOU, Y., KLEUSBERG, A.: *On Carrier Signal Multipath Effects in Relative GPS Positioning*. Manuscripta Geodaetica, 13:172-179, 1988.

KULMANN H.: *Kalman-filtering with coloured measurement Noise for deformation analysis. Proceedings*, 11th FIG Symposium on Deformation Measurements, Santorini, Greece, 2003.

METZNER, M; SCHWIEGER, V.: *Analyse von Messreihen im Zeitbereich.* Zeitabhängige Messgrößen – Ihre Daten haben (Mehr-)Wert. 129. DVW-Seminar on 26. - 27. 02. 2014 in Hannover, Wißner Verlag, Augsburg, 2014.

SCHWIEGER, V.: *High-Sensitivity GNSS – the Low-Cost Future of GPS?*. Proceedings on FIG Working Week 2007, Hongkong SAR, 13.-17.05. 2007

SCHWIEGER, V.: *High-Sensitivity GPS - an availability, reliability and accuracy test.* Proceedings on FIG Working Week, Stockholm, Sweden, 14.-19. 06. 2008.

SCHWIEGER, V.: *Accurate High-Sensitivity GPS for Short Baselines.* FIG Working Week, Eilat, Israel, 03.-08.05.2009.

TAKASU, T., YASUDA, A.: *Evaluation of RTK-GPS Performance with Low-cost Single-frequency GPS Receivers.* Funai Laboratory of Satellite Navigation, Tokyo University of Marine Science and Technology. Tokio, Japan, 2008.

WANNINGER, L.: *Carrier Phase Multipath Calibration of GPS Reference Stations.* Proceedings of ION GPS 2000, Salt Lake City, UT, 2000.

ZEIMETZ, P.; KUHLMANN, H.: *On the accuracy of absolute GNSS antenna calibration and the conception of a new Anechoic Chamber*, FIG Working Week 2008, 14.-19.06, Stockholm, Sweden, 2008.

ZEIMETZ, P.; ELING, C.; KUHLMANN, H.: *Analyse von GPS-Referenzstationsbeobachtungen mit Methoden der Zeitreihenanalyse.* Zeitabhängige Messgrößen – Verborgene Schätze in unseren Daten. 85. DVW-Seminar on 07. - 08. 09. 2009 in Kassel, Wißner Verlag, Augsburg, 2009.

ZHANG, L., STANGE, M., SCHWIEGER, V.*: Automatic Low-Cost GPS Monitoring System Using WLAN Communication.* FIG Working Week 2012, 6.-10.05.2012, Rom, Italy, 2012.

ZHANG, L., SCHWIEGER, V.: *Investigation regarding different antennas Combined with low-Cost receiver*. FIG Working Week 2013, 06.-10.05.2013, Abuja, Nigeria, 2013.

Links:

TEQC: http://facility.unavco.org/software/teqc/teqc.html, last accessed on February 2014.

TOPCON:http://www.topconpositioning.com/sites/default/files/PN_A5_DataSheet_7010_2088_RevB_lg.pdf, last accessed on March 2014.

UBLOX: http://www.u-blox.com/, last accessed on March 2014.

WA1: http://www.wasoft.de/wa1/index.html, last accessed on February 2014.

Technical Session 6: Monitoring by Laser Scanning

Combining Laser Tracker and Laser Scanner Data

Annette Schmitt
Institute of Engineering Geodesy, University of Stuttgart, Germany

Abstract
Laser scanner as well as laser tracker may be used for quality control in industry and construction. Both measuring systems have their pros and cons with respect to accuracy and with respect to pointwise and areawise measuring. This contribution focuses on the integration of both techniques in one data set. Therefore the registration is realized using wooden balls as common targets.

The registration could be done with a RMS of 1 mm. Afterwards the flatness of a timber element is analysed using laser scanner data and laser tracker data. The exemplary result reveals a non-significant flatness of the analysed timber element.

The investigation is carried through within the project “Robotic Fabrication in Timber Constructions” that aims to show the feasibility of the combination of robotic fabrication, computational design, simulation processes and 3D-surveying.

Keywords
Laser Tracker, Laser Scanner, Registration, Timber Construction

1 INTRODUCTION

In an industrial environment laser trackers are often used for quality control SCHWARZ (2009). Laser scanners are also used for quality control, for example on building sites STENGELE (2010). Laser trackers can be used for measuring object points and lines, e.g. edges. Also surfaces can be calculated by means of this data with an accuracy of around 10 µm. Laser scanners are suited to estimate surfaces from the data. A combination of these two instruments is used for a project dealing with robotic timber construction. Timber is a living material. The production accuracy from known personal progress reports for wooden elements is between 0.5 mm and 1 mm.

2 MEASUREMENT SYSTEMS

2.1 Laser Scanner

Laser scanners are established in 3D-data acquisition since many years. They are used for example in forensic, architecture, and planning tasks in factory buildings KERN (2007). However, they are not that often used for quality control of work pieces. For this task normally triangulation laser scanners will be used SCHWARZ (2007).
In this contribution a laser scanner is used in combination with a laser tracker. The used laser scanner is the Leica HDS7000, which is structurally identical with the Z+F Imager 5010 from Zoller+Fröhlich. This instrument is a phase shiftbased laser scanner. A range noise of 0.3 mm RMS at ten meters within a reflection of 80 % is given by the manufacturer. The laser scanner also shows an angle accuracy of 0.007° RMS in horizontal and vertical direction Z+F (2012). In Figure 1 the used laser scanner is shown.

Figure 1: Leica HDS7000

2.2 Laser Tracker

The laser tracker was developed in the 1980s by Dr. Kam Lau, the founders of Automated Precision Inc. (short API) API (2010). Laser trackers are polar measuring systems with two kinds of distance measuring systems. One distance measuring system is the absolute distance measuring system, short (ADM). The other one is an inferometric distance measuring system (IFM), which is based on the Michelson-Interferometer from 1881 MICHELSON (1881). Laser trackers may include both or one of the two techniques. As the name implies, the laser tracker can automatically follow the reflector. There are three different methods for this beam guidance. So, the beam can be guided through the optical rotation centre of the tracker, with cardanic stored mirrors at the optical centre or with the reflection from a precise ball in the optical centre. All systems use a beam splitter and a positionsensitive diode inside the way of beam JATZKOWSKI (2011). In Figure 2 **Figure** the principle of laser tracker is shown in a simplified way.

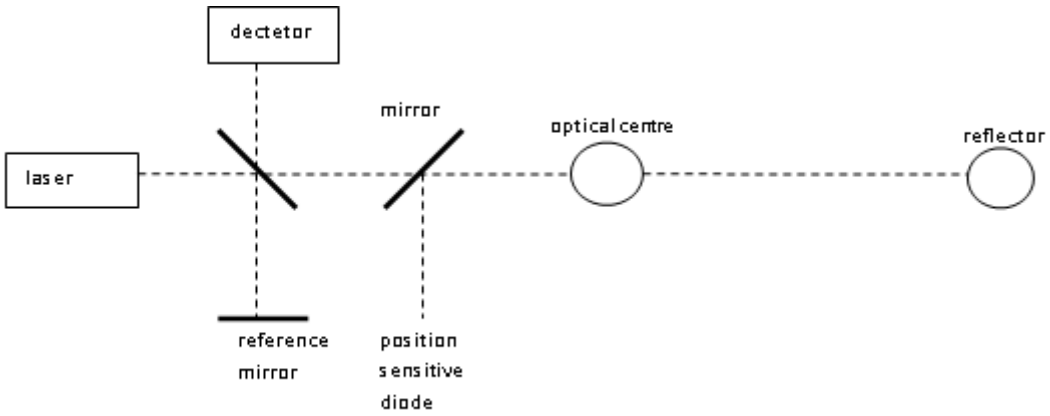

Figure 2: Principle of laser tracker JATZKOWSKI (2011)

For these investigations the API Radian is used, see Figure 3. By static measuring with spherically mounted retroreflectors, short SMR, and in interferometric mode, it delivers an accuracy of ±10µm. The software to control the laser tracker offers different measuring methods, like discrete points measuring und scanning. So it is possible to measure lines and, with an adapter, edges. For measuring hidden parts of an element, the IntelliProbe360™ can be used in combination with the API Radian. This instrument is wirelessly connected to the data processor of the laser tracker.

Figure 3: API Radian

Figure 4: IntelliProbe360™

2.3 Integration and Comparison of Laser Tracker and Laser Scanner

Both systems are polar systems, so they are measuring angles and distances. As shown before, the laser tracker has got two methods of distance measuring whereas the laser scanner has only one method. The laser tracker always needs a reflector which can be a SMR or an IntelliProbe360™. On the other hand a laser scanner does not need any marked target.

Mostly laser scanners are mainly used to measure 3D-surfaces, but not to measure discrete points. In principle, lines can be measured with both systems. However, the lines which are measured by the laser scanner are arbitrary profiles and not defined lines. The lines measured by the laser tracker can be anywhere inside the measuring range. The laser tracker can measure discrete points and surfaces. By using adapters it is also possible to measure edges with the laser tracker. This is impossible with a laser scanner. Edge detection with a laser scanner is only possible in post processing. The edges have to be calculated, for example with segmentation of planes and following intersect of these planes. KERN (2003).

The data acquisition resulting from these systems is realized in different ways. The laser scanner has only to be set to a defined place and started by the operator. The laser tracker measures a target, e.g. a SMR which has to be moved by the operator. The operator selects the parts of objects which should be measured and starts the selected measuring mode. If there is more than one position of the laser tracker, the registration between the positions can be done in real-time during the control process.

Depending on the measuring task and on the used control software, the postprocessing with laser tracker can be realized between two measurements. For example, during a quality control the position and the diameter of holes in e.g. a working piece can be calculated in some milliseconds. It is also possible to directly create a report of the data and the calculations.

The postprocessing for the laser scanner data costs more time than the one for laser tracker data, because the data has to be imported into software like Leica Cyclone. If an area is scanned by more than one position, the registration has also to be done in postprocessing. For the registration, laser scan targets should be used, because an automatic registration without targets is CPU-intensive and does not guarantee that the registration will be successful. Normally, automatic registration only works for objects with a rough and striking structure. Afterwards it is also possible to calculate for example the position and the diameter of a hole in a working piece.

As shown before, the accuracy level of the two measurement systems is different. The laser tracker is more accurate than the laser scanner. This is caused on the way of distance measuring. The laser scanner achieves an accuracy of submillimetres for short distances. The laser tracker achieves an accuracy of some 10 µm in interferometric mode API (2014 b).

Table 1: Comparison of Laser Tracker and Laser Scanner

	Laser Tracker	Laser Scanner
Polar system	Yes	Yes
Distance measuring	IFM, ADM	ADM
Reflector	Yes	No
Discrete point measurement	Yes	No
Line measurement	Yes	Only profiles
Surface measurement	Postprocessing	Postprocessing
Edge detection	With adapter	Only post processing
Handling	By User	Semi-automatically
Accuracy	Static measurement: ± 10 µm	Distance noise for 10m: ± 0.3 mm rms

3 REGISTRATION OF LASER TRACKER AND LASER SCANNER DATA

For the registration of laser tracker data and laser scanner data there is a need of known points in both instrumental coordinate systems. Thus targets are needed, which can be measured by laser tracker and laser scanner. It is costly to measure 3D-targets with the laser tracker. Due to the reflection property of smooth steel, it is not possible to measure the SMR with the laser scanner. So, another target has to be selected. Following the 3D-targets of a laser scanner, wooden balls are chosen, because they have approximately the same size like the SMR and are available at the institute.

Figure 5: Wooden Ball

3.1 Control of Wooden Ball

To verify the diameter, four balls are measured by laser tracker and IntelliProbe360™ in the scanning mode. The scanning mode is chosen, because it is a fast way to collect data of a surface. The spheres of the balls are calculated in Spatial Analyzer® using hundred points. The results are shown in Table 2: Results of sphere calculation from Laser Tracker data.

Table 2: Results of sphere calculation from Laser Tracker data

Ball	Diameter [mm]	RMS [mm]
1	38.810	0.11
2	38.879	0.15
3	38.871	0.15
4	38.888	0.16

The next step, after measuring the size of the balls with the laser tracker, is to check them with the laser scanner. For that reason, the four balls are scanned. Here, also spheres are calculated, the results are shown in Table 3: Results of sphere calculation from Laser Scanner data.

Table 3: Results of sphere calculation from Laser Scanner data

Ball	Diameter [mm]	RMS [mm]
1	37.76	0.21
2	37.16	0.21
3	37.19	0.21
4	36.75	0.21

The results of the calculation from laser scanner data shows the calculated diameter is around 1 mm smaller than the calculated diameter from the laser tracker data. The differences between the size of the SMR, which is 1.5'' or 38.1 mm, and the measured size of the wooden balls are tested for significance.

Table 4: Difference between diameter of wooden balls from laser scanner data and of SMR

Ball	Difference [mm]
1	0.34
2	0.94
3	0.91
4	1.35

The 3D measurement accuracy of the laser scanner is given with 0.3 mm for a distance of 10 m. The quantil from Gaussian distribution is ±1.96, so a duplex test with a significant level of $\alpha = 0.5$. The results are shown in Table 5: Results of test.

Table 5: Results of test

Ball	Test statistic	Significant?
1	1.13	No
2	3.13	Yes
3	3.03	Yes
4	4.50	Yes

The test shows that, besides the first ball, all diameters calculated from laser scanner data are significantly different from the diameter of the SMR. For that reason the calculated centre points of the sphere, which are used for registration with laser tracker data, have to be corrected by an offset. The offset has to be added only to z-coordinate, because the wooden balls and the SMR are set on a fixed adapter with a hollow.

3.2 Registration with wooden balls

The registration with the wooden balls is done in Spatial Analyzer®. The first step is the calculation of the centres of the wooden balls from laser scanner data, because these are the identical points for the registration with the laser tracker data.

Table 6: Results of sphere calculation from laser scanner data

Ball	Diameter [mm]	RMS [mm]	Distance [m]
1	38.62	0.17	2.1502
2	39.88	0.18	1.7240
3	40.23	0.17	3.1124
4	39.55	0.18	3.3372

Table 6 shows the results of the sphere calculation for the registration. Compared with the results from 0, the diameters of the spheres are different. It seems to be possible that the diameter differences are dependent from the distance. More important is the influence if eliminating noisy points and cleaning the data. Investigations have shown that the diameter changes in the level of some millimetres if the data cleaning is realized in different ways. In Figure 6 the arrangement of targets and the position of the laser scanner are shown.

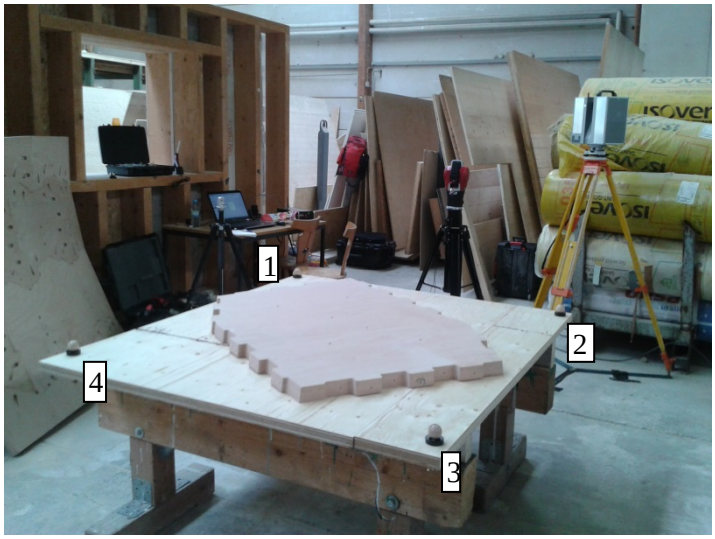

Figure 6: Measurement arrangement

Due to the diameters, which depend on the distances from laser scanner data, the offsets have to be calculated individual. The results are shown in Table 7.

Table7: Offsets in z-axis

Ball	Offset[mm]
1	-0.3
2	-0.9
3	-1.1
4	-0.7

With the corrected z-coordinates a Helmert transformation, in Spatial Analyzer® called best-fit transformation, between the laser tracker data and the laser scanner data is calculated in Spatial Analyzer®. Within the laser tracker measurements, the positions of the fixed adapter around the wooden elements are measured with the SMRs. The result of the best-fit transformation with all four points shows that point 1 is an outlier. After deleting this point, the results turn out as shown in Table 8.

Table 8: Result of Registration

	X [mm]	Y [mm]	Z [mm]	3D [mm]
Max Error	0.201	0.173	0.002	0.265
RMS Error	0.143	0.130	0.001	0.193

With this result the analysis of the data can be done. So as an example, the flatness of the surface of an element can be checked.

4 ROBOTIC FABRICATION IN TIMBER CONSTRUCTION

4.1 Project description

For the project *Robotic Fabrication in Timber Constructions*, three institutes at the University Stuttgart, the Institute for Computational Design, the Institute of Building Structures and Structural Design and the Institute of Engineering Geodesy, are cooperating with industrial partners and partners from the state Baden-Württemberg. They develop a timber construction system which combines robotic fabrication with computational design, simulation processes and 3D-surveying ICD (2014).
The fabrication with industrial robotics offers more manufacturing possibilities and the development of innovative, material-oriented and adaptive construction systems. The result of this project will be a demonstrator pavilion for the state horticultural show *Landesgartenschau 2014* in Schwäbisch Gmünd. The demonstrator pavilion is presented in Figure 7 ICD (2014).

Figure 7: Model of the demonstrator pavilion for Landesgartenschau 2014 ICD (2014)

The pavilion will be made of 243 wooden elements which will be produced by industrial robots. The elements, which consist of plywood with a thickness of 50 millimeters, are preformatted by a CNC-machine and afterwards processed by the robots. In Figure 8, the production process and an exemplary wooden element are shown.

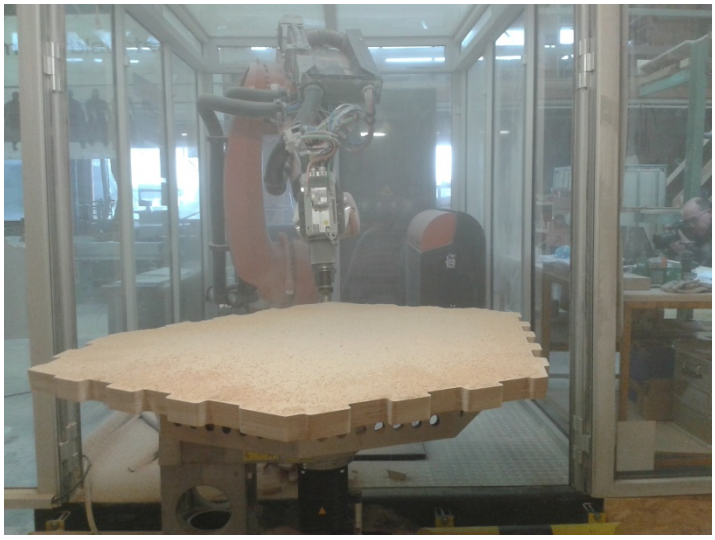

Figure 8: Robotics produces a wooden element

The surveyor's part in this project is the quality control of the elements and, when the pavilion is built up, the deformation analysis using laser scanning data. The quality control is done by the laser tracker. The results of the laser tracker measurements are compared to the given design model. Some of the elements are scanned.

4.2 Application example

The registration as shown in 0 is calculated for a different wooden element. The position of the laser scanner, laser tracker and the identical points are not changed when scanning the other element. The calculations for the first element are shown in 0. For the second element the results are shown in this chapter. Figure presents the given design model taken from CAD system.

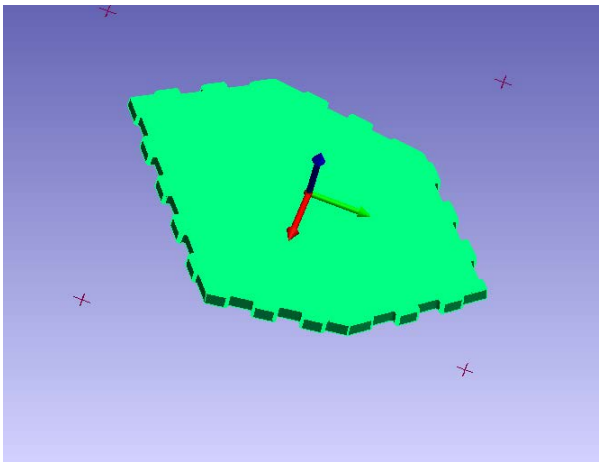

Figure 9: CAD Model of Element 2 (screenshot from Spatial Analyzer®)

At first the offset of the wooden balls have to be calculated from laser scanner data. In Table 9 the results of the sphere calculation, the offset and the distance between laser scanner and points are shown.

Table 9: Offset for Element 2

Ball	Diameter [mm]	Offset [mm]	Distance [m]
1	40.8	-1.4	2.1518
2	39.7	-0.8	1.7238
3	41.7	-1.8	3.1133
4	41.7	-1.8	3.3387

The next step is the best-fit transformation. In this transformation, point 1 is an outlier, too. The results of the transformation with point 1 are shown in Table 10.

Table 10: Results of best-fit-transformation

	X	Y	Z	3D
Max Error	0.557	0.452	0.006	0.626
RMS Error	0.424	0.323	0.004	0.937

The results are comparable for the two examples. The laser tracker registers with respect to the CAD model of the element. So, the comparison between the CAD Model and the laser scanner data is possible, since the laser scanner data and the laser tracker data are registered with each other. It is also possible to test the flatness of the element. To investigate the flatness, the CAD model is compared to the laser scanner data. To do this comparison in Spatial Analyzer®, the laser scanner data has to be thinned out. This is due to the fact that Spatial Analyzer ® cannot work with more than 2.000.000 points. The comparison is done by means of the function *Relationships* in Spatial Analyzer, which calculates the deviation between the points and the surface of the CAD model NEWRIVERKINEMATICS (2012). The results of this comparison are shown in Figure 10:

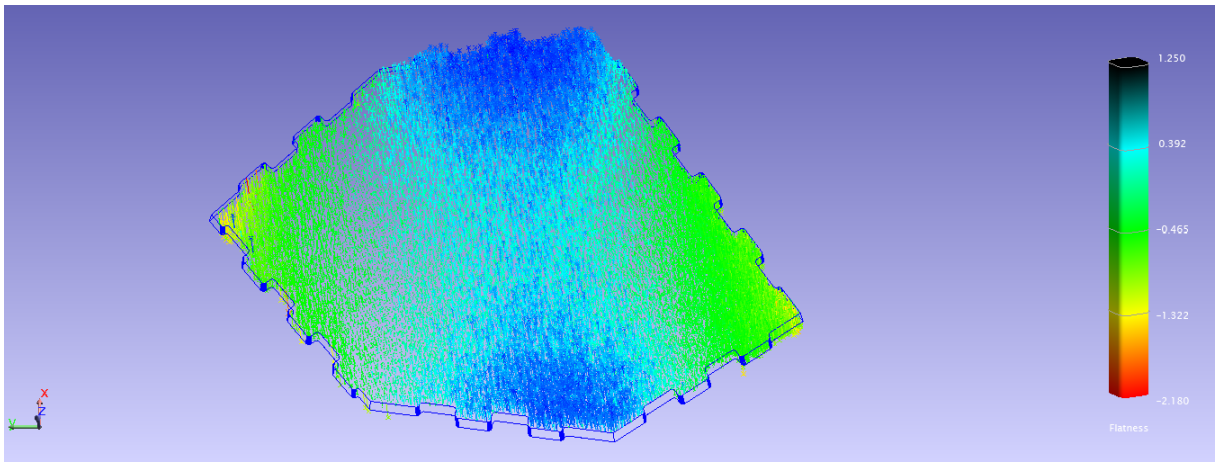

Figure 10: Flatness calculated from laser scanner data

As shown in Figure 10 the element is deformed, but not as assumed. The element looks like a valley with two hills. In the blue areas the element differs between -0.8 to 2.5 mm from the CAD model. But this is due to the noise from the laser scanner data. The RMS in z-direction for the top area of the element is 1.5 mm. A statistical test assuming Gaussian distribution shows that the element deviates significantly from flatness.

With the data additional from the laser tracker the flatness and the expansion in x- and y-direction of the element could also be controlled. The measured areas of the element are the edges. They are measured with the IntelliProbe360™ and a specially designed adapter. The flatness test is also done with the function *Relationships* from Spatial Analyzer®. For the laser tracker, the minimum difference between element and CAD model is -1.537 mm and the maximum difference is 0.895 mm. The RMS is 0.682 mm. If this result is tested assuming Gaussian distribution, the results of laser scanner are proven. The result is shown in Figure 11.

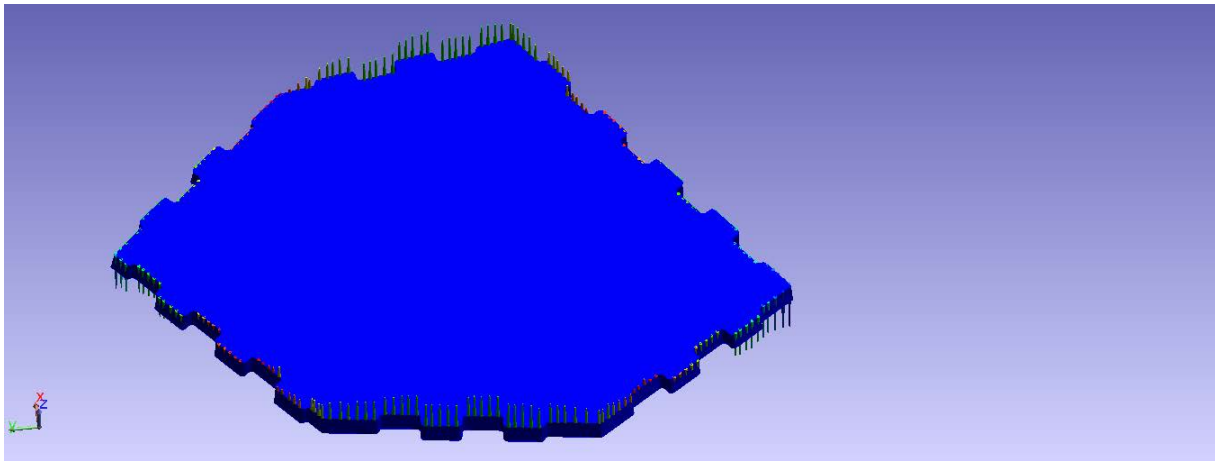

Figure 11: Flatness calculated from laser tracker data

The expansion in x- and y-direction with respect to the CAD model is shown in Figure 12. In x-direction the expansion differs from -0.599 mm to1.160 mm. In y-directions the difference between CAD model and the element is between - 1.186 mm to 0.293 mm with respect to the CAD model. The RMS in x-direction is 0.568 mm, in y-direction 0.547 mm. Statistical tests show that the maximum values are significantly different from the ones the CAD model. The given manufacturing tolerance in the robotic fabrication is expected to be ±0.25 mm. The expansion in x- and y-direction is partly out of tolerance. For the builders of the pavilion means, they have to compensate these differences.

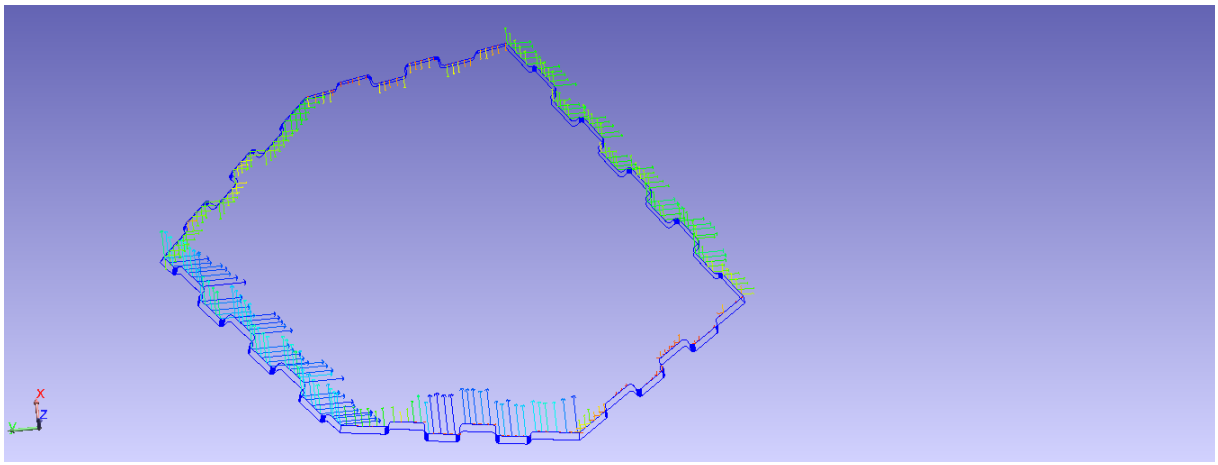

Figure 12: Expansion of element

5 CONCLUSIONS

These investigations show a possibility to use laser tracker and laser scanner for one data set. The registration of both measuring systems can be realized with wooden balls as targets. The preparations for the registration are calculating spheres and their centres from laser scanner data and to correct them by an offset. The offset is the difference between the diameter of the calculated sphere and the diameter of the SMR. After the registration, the data sets can be analysed. One analysis realized was the test with respect to flatness.

The analysis of laser scanner data and laser tracker data can be realized in Spatial Analyzer®. The disadvantage of Spatial Analyzer® is that it needs a long time to process the data and cannot really work with more than 2.000.000 points from scanner data. For this reason the registration from laser scanner and laser tracker data will be done in Leica Cyclone in a current master thesis.

ACKNOWLEDGEMENTS

The authors would like to thank Mathias Stange for the support and the help. Furthermore these investigations are partly funded by EFRE European Union, Cluster Forst und Holz, Land Baden-Württemberg, KUKA Roboter GmbH, Landesgartenschau Schwäbisch Gmünd 2014 GmbH, Müller Blaustein Holzbau GmbH and Landesbetrieb Forst Baden-Württemberg.

REFERENCES

Books:

JATZKOWSKI,P.: *Ressourceneffiziente Kalibrierung von 5-Achs-Werkzeugmaschinen mit Tracking-Interferometern*. Dissertation. Apprimus Verlag, Aachen, 2011.

NEWRIVERKINEMATICS: *Spatial Analyzer® User Manual*. New River Kinematics Inc. Williamsburg, Virginia, USA, 2012.

MICHELSON, A.: *The relative motion of the earth and the luminiferous ether*. American Journal of Science and Arts, 08/1881, p. 120-128, 1881.

SCHWARZ, W.: *Trends in der geodätischen Messtechnik und in ihren Anwendungsfeldern*. Allgemeine Vermessungs-Nachrichten, 03/2009, p. 115 – 127, 2009.

STENGELE, R. et. al.*: Vermessung im Gotthard-Basistunnel: Vortriebsvermessung, Laserscanning und Langzeit-Monitoring*. Ingenieurvermessung 2010, Wunderlich, T. (Hrsg.), Herbert Wichmann Verlag, Heidelberg, 2010.

KERN, F.: *Terrestrisches Laserscanning kurz & bündig*. http://www.architekturvermessung.de/05-Literatur/doc/laserscanning_fkern.pdf, last accessed on March 4, 2014.

ZHUANG, H, ROTH, Z. S.: *Modeling gimbal axis misalignments and mirror center offset in a single-beam laser tracking measurement system*. International Journal of Robotics Research, Number 3, 1993.

Links

API: http://www.apisensor.com/index.php/about-de/history-de, last accessed on February 17, 2014.

API: http://www.apisensor.com/images/API_pictures/product_module_picture /p_ip360_01_2009_md.png, last accessed on March 4, 2014, a.

API: http://www.apisensor.com/images/ProductLiterature/

SpecSheets/Radian%20Spec%20Sheet%20EN0812_web.pdf, last accessed on March 4, 2014, b.

API: http://www.apisensor.com/images/ProductLiterature/SpecSheets /intelliprobe360%20wireless%20spec_EN0812_web.pdf, c.

ICD: http://icd.uni-stuttgart.de/?p=10046, last accessed on February 24, 2014.

Z+F: http://www.zf-laser.com/fileadmin/ editor/Datenblaetter/ Datenblatt_Z_F_IMAGER_5010_D_kompr.pdf, last accessed on March 4, 2014.

Terrestrial Laser Scanning for Monitoring of Tunnel Deformations

Ekaterina I.Gorokhova
Siberian State Academy of Geodesy, Russian Federation

Abstract
A great attention in tunnel maintenance is given to monitoring tunnel lining. Meanwhile, along with external visual examination to reveal breaks and deformations, laser scanning is carried out for determining tunnel geometrical parameters (ring ellipticity, tunnel axis declination and cross sectional deformations). The techniques offered for determination of tunnel deformation parameters using TLS data are considered.

Keywords
terrestrial laser scanning, tunnel, deformations, accuracy, 3D model, cross-section

1 INTRODUCTION

Tunnels are an important and necessary link in transport infrastructure, not only for cities, but the whole country as well. Therefore, geodetic and surveying works are the responsible process at all stages of any tunnel construction and maintenance. The higher a quality of surveying and mine-surveying works in tunnels, the better their quality, terms and further operational phase. In the course of tunnel maintenance under the influence of various loads the tunnel lining deformations take place. For determination of their values and declinations from permitted values there is necessity for continuous in-situ measurements.

Investigations in this field make contribute to achieving higher accuracy both during measurements and processing.New developments allows automating tunnel works and reducing the measurement time.

As a result of practical investigations, a technique was developed for determination of deformations by TLS data processing in Cyclone, RapidForm, RealWorks Survey, MatLab.

Analysis based on TLS data obtained from terrestrial laser scanning in the Novosibirsk subway tunnels, transport tunnels of West Siberian Railway in Kemerovo and Sverdlovsk Region (Figures 1, 2) was carried out.

Figure 1: A portal of railway tunnel in Kemerovo Region

Figure 2: A view of the Novosibirsk subway tunnel.

2 A TECHNIQUE FOR DEFORMATION MONITORING

Tunnel surveying was done by the terrestrial laser scanner Leica ScanStation C10. For the relative orientation of neighbouring scans spherical targets were applied (a diameter of 70 mm). Three of them were set up in places of mutual neighbouring scans overlapping. Cylindrical targets used for the exterior orientation of scans were set up on the reference points B13, B14, B15, B17, B20, B22, B23 by means of a pole and a bipod.

Terrestrial laser scanning was carried out at each station with coverage 360° x 100° and angular increment 0.04°. Before surveying a scanner was levelled by means of a built-in electronic level. Scanning stations were chosen based on existing camera lockout condition, niches and portals. The average distance between scanning stations is 25 m. Then laser scanning data was processed.

A data processing algorithm is presented in Figure 3.

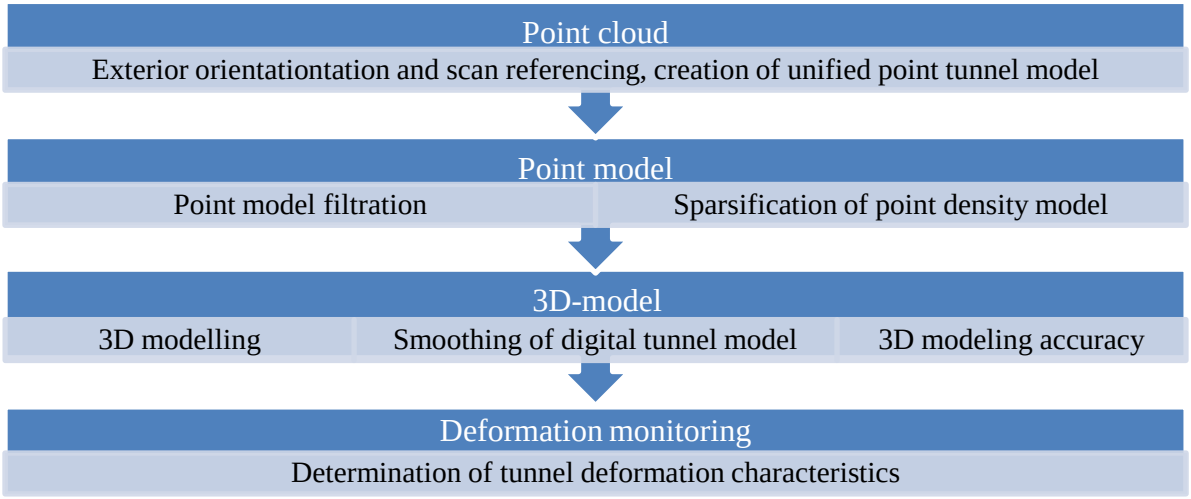

Figure 3: Scan data processing algorithm

At the first stage of office works for tunnel scan data processing the exterior orientation of scans was performed as a result of which a unified point model was obtained in world coordinates. Then the model was exported in Leica Cyclone software.

At the second stage the point model filtration was done in Cyclone software to remove noises and redundant information not belonging to the tunnel lining surface and distorting the image of internal tunnel contour.

Point model environment with unnecessary points was selected by the “Polygonal Fence Mode” special function and deleted by “Fence – Delete Inside” function.

Leica HDS Cyclone hasn’t the option for sparsification of density point model, after filtration that is why the model was exported to RealWorks Survey software. The sparsification of density point model was done with the Sampling function up to the value 1 point per 1.9 cm^2. This operation allowed simplifying the point model for the post processing and saving the necessary sampling of tunnel model.

For creating triangulation 3D model (Mesh) a point model was processed in Trimble RealWorks Survey and RapidForm using specialized filters and Mesh scanline algorithms. For example, in RealWorks Survey software 3D cylindrical surface was created with the Mesh Editing Tools and Mesh Creation functions. In RapidForm software for this purpose there was a Mesh Buildup Wizard function by means of which the following problems were solved:

- To delete the rough results of 3D modeling. Using the scroll-box the number of polygons in a Mesh-surface was decreased or increased to delete rough results of a triangulation and create the correct triangles;
- To smooth a three-dimensional Mesh-surface of a tunnel (polygon approximation, smoothing of tunnel 3D model and partial processing of "holes" appeared as a result of triangulation errors. Using the Find Defect function existing defects of creation (crossing polygons, small clusters, etc.) were found on a surface of 3D model and eliminated by the Healing Wizard function. Hereafter, the Fill Holes function was used hole patching up on a digital tunnel surface left after re-triangulation.

As showed the experience in objects modelling based on TLS data, in some software products the 3D surface is created incorrectly due to the incorrect process of triangulation caused by a complicated object). Therefore, it such surface should be smoothed that is to delete rough results of triangulation. This operation is realized differently in various software products. If a vector object model is created as a Mesh-surface, this operation is necessary. If a 3D model is created in form of NURBS-surface (by spline - functions), then smoothing isn't required.

As a result, 3D tunnel model becomes more reliable and ready to be used for accuracy assessment of 3D model creation, tunnel monitoring, etc.

After TLS data processing the accuracy assessment and quality control were performed for the results of total station surveying of the tunnel using coordinates of 132 control points. The maximum discrepancies of these points were 0.031 m, and RMS error was10 mm (Figure 4).

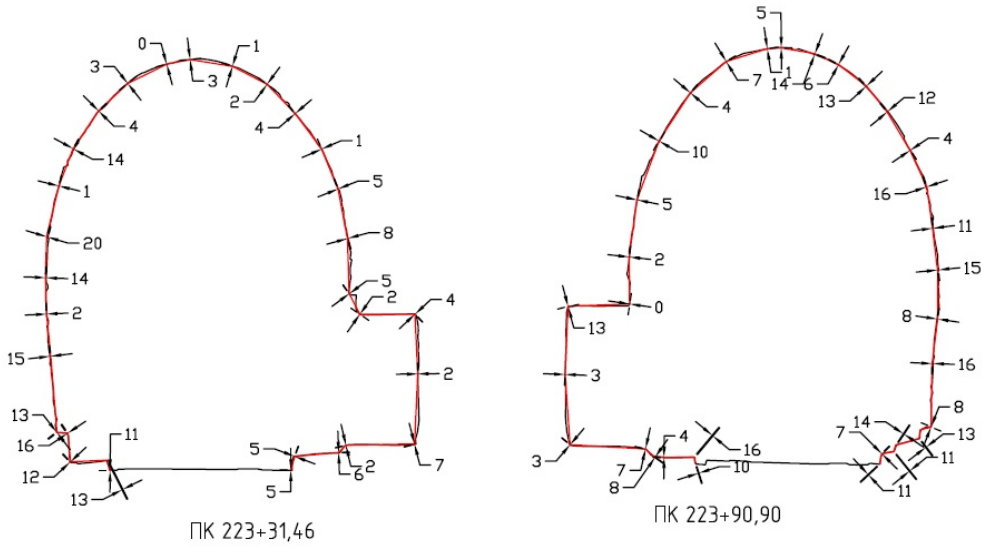

Figure 4: Example of control measurements by a total station and their compare with obtained sections.

Then data were exported in the Cyclone and RealWorks Survey software and the accuracy assessment for 3D modelling was executed along with the assessment of tunnel condition. In this case discrepancies of consequent spatial point position on 3D model of tunnel surface and its point model were measured. About 121 measurements were performed. The maximum discrepancy for model point position was 0,011 m and RSM error was 0.008 m.

The office processing of TLS data is finished by the assessment of railway tunnel conditions and determination of geometrical parameters giving evidence of tunnel deformations. To analyse the a tunnel's health the following procedures were used:

1. Comparison of design and actual *K*-sections (obtained by terrestrial laser scanning data) located every 10 m on a smoothed tunnel section. Such technique allows revealing a declination of a tunnel under construction from the designed value, deformation monitoring during construction, when maintenance begins, and during tunnel maintenance
2. Comparison of tunnel cross-sections obtained for different dates of tunnel scanning. In this case the assessment of tunnel condition will be compared with the characteristics of its similar cross-sections obtained for different observation epochs. This technique is aimed at the regular monitoring of railway tunnels. Its advantage is that it allows comparing not only separate cross-sections taken from 3D model, but 3D models of tunnel created for different dates themselves.

Comparison of cross-sections was made in the Cyclone software in interactive mode. Designed (or a model of particular epoch) and real 3D models of tunnel`s surface were loaded in Cyclone software. Cross-sections of both kinds of models were created at a given distance. Tangent lines are drawn in distinguished points being under maximal loads. The perpendicular to this tangent line is restored from the points to the crossing with real cross-section. The measured values characterizing a condition of internal tunnel lining are plotted in the table. Then the same is made for the next cross-section. For the whole tunnel 341 measurements were taken. The maximum discrepancy in geometry differences of internal tunnel lining were 22 mm, and a mean difference was 11 mm (Figure 5).

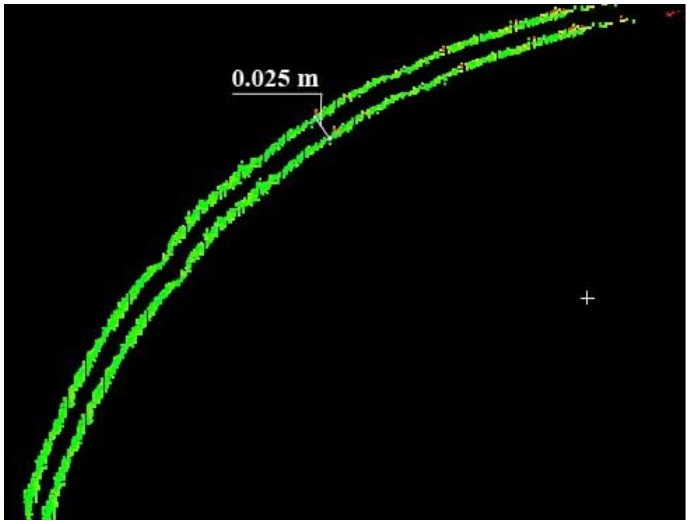

Figure 5: Measurement of deviations

3 THE EXPERIENCE WITH USING MATLAB SOFTWARE FOR DETERMINATION OF TUNNELS DEFORMATIONS

The determination of geometry declination values in Cyclone cannot be done automatically. It is inconvenient and makes longer the time for data processing. We made an attempt to process measured data in MatLab for the purposes of automating measurement processes.

Plotting tunnel cross-sections and calculations were made in the built-in Simulink software package. This package gives a wide range of opportunities for the user in updating library blocks, creating own libraries, and drawing up new libraries of blocks.

In modeling a user may choose own method for solution of differential equations, change modelling time (with fixed or variable period) and follow the processes taken place in the system. The results of modeling can be presented in the form of schedules or tables.

Another advantage of Simulink software package is that it allows filling up libraries of blocks by means of auxiliary programs written both in MATLAB language and C + +.

Data loading in MatLab software is performed from *.pts format. After loading the cross-sections are plotted on spline basis – approximation and least squares method.

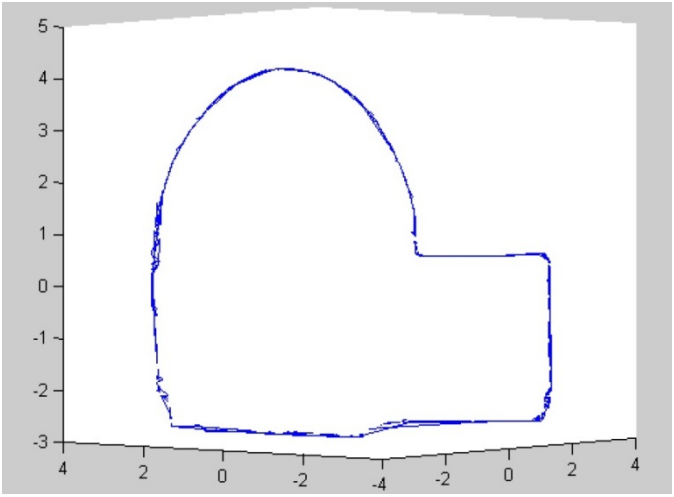

Figure 6: An example of a cross-section in MatLab.

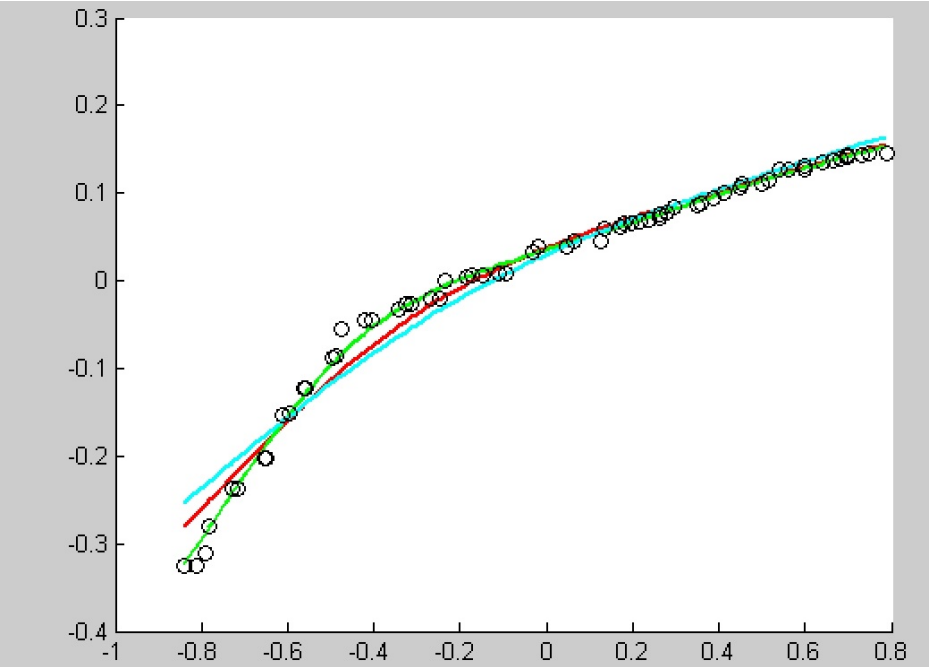

Figure 7: Example of plotted section comparison:
Green profile – on the basis of NLS data
The blue – on a basis of total station data
The red – designed value.

4 CONCLUSION

As a result of investigations, the technique for tunnel deformation monitoring was developed and tested. The deviation values of internal tunnel line geometry allow carrying out the necessary calculations and making a report on a magnitude of tunnel's wear, the necessity of its reconstruction or closing. Hereinafter the author is planning to extend deformation analysis in MatLab software which opens wide opportunities for solving such kind of problems.

REFERENCES

Books:

SEREDOVICH, V.A.: *Terrestrial laser scanning*. Siberian State Academy of Geodesy, Novosibirsk, 2009.

PIEGL, L., TILLER, W.: *The Nurbs Book*. Springer, Berlin, 1997.

Journal articles:

GOROKHOVA, E.I., IVANOV, A.V.: *Experience of application for terrestrial laser scanning technology in railway tunnels*, Proceedings of International scientific congress "Interexpo GEO-Siberia-2009", p. 257 - 260, 2009.

KOMISSAROV, AV., GOROKHOVA, E.I.: *Substantiation of parameters for tunnels surveying with terrestrial laser scanning*, Geodesy and Aerophotography, 3/2011, p. 81 – 85, 2011.

NEUNER, H., SCHMITT, C., NEUMANN, I.: *Modelling of terrestrial laser-scanning profile measurements with*, Proceedings of the 2nd Joint international Symposium on Deformation Monitoring, Nottingham, England, 2013.

HEIKER, A., KUTTERER, H.: *Integration of observations and models in a consistent least squares adjustment model*, Proceedings of the 1st International Workshop on the Quality of Geodetic Observation and Monitoring Systems, QuGOMs. München, 14.-15.04.2011.

KUTTERER, H., NEUMANN, I.: *Recursive least-squares estimation in the case of interval observation data*, International Journal of Reliability and Safety, Jg. 5, 3/4/2011, S. 229–249, 2011.

PAFFENHOLZ, J.-A., ALKHATIB,H., KUTTERER,H.: *Direct geo-referencing of a static terrestrial laser scanner*, Journal of Applied Geodesy, Jg. 4, 3/2010, S. 115–126, 2010.

TLS for Calibrating Finite Element Models

Bimin Zheng
Institute of Engineering Geodesy, University of Stuttgart, Germany

Abstract
In Baden-Württemberg the façade of many old buildings are made of sandstone. Sandstone erosion is caused by physical and chemical influences. Extreme thermo-hygro conditions can cause significant damage like cracking. In this paper terrestrial laser scanning (TLS) was used for detection of thermo-hygro deformations of sandstone. The sandstone facade is scanned in several epochs using Leica phase based scanner. The first measurement serves as reference measurement. The measurements are repeated roughly every four weeks to evaluate the deformation of the facade. Using the measurement data, the facade surface can be described by a number of local area normal vectors and volume elements with respect to a predefined idealized reference surface. By comparing the facade surface reconstruction over several epochs, the deformation of the facade can be evaluated. Statistical hypothesis tests are used for the deformation analysis. A three dimensional finite element model (3D FEM) was used for the modelling of the temperature influences. In the best case this model can be calibrated by geodetic measurements.

Keywords
TLS, hygro-thermo deformation, 3D FEM, Statistical hypothesis test

1 INTRODUCTION

The main building of University of Applied Sciences Stuttgart (HFT) was built from 1867 to 1873. During World War II the building was destroyed in 1944 in the interior by bombs. The perimeter was damaged by fire. From 1948 to 1953, the building was rebuilt MEYER (2012). The façade consists of sandstone, which is in Baden-Württemberg the most popular construction material for the historical city architecture (Figure).

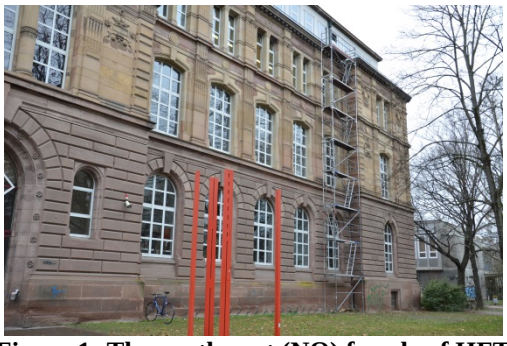

Figure 1: The north-east (NO) façade of HFT

The deformations on the façade can be divided in elastic, plastic, chemical and crack-caused changes. They are mainly a result of hydric swelling, temperature deformations, change of the materials and are normally superimposed ZHENG et al. (2013). Some decay forms like scaling, blistering, sandy decay etc. are very difficult to be recognized by human eyes. There are hardly any methods to monitor non-destructively rapid decay processes. Twenty years ago an approach to determine the surface changes and losses as well as the depth of surface loss and the velocity of the damage processes was presented GRASSEGGER et al. (1990). This is one attempt to combine cultural heritage research with engineering geodesy for monitoring purposes.

In our research terrestrial laser scanning takes the great challenge to monitor the precise deformation of the size of the damage and the velocity of the processes. The point clouds of the façade in each scan epoch will be used for FEM analysis and also to determine local normal vectors and local volumes. In order to detect the surface deformations, the change of local normal vectors and change of volume will be calculated between scan epochs. At the end the results from geodetic measurements will be compared with FEM thermal analysis.

2 DATA ACQUISITION

According to the definition of the types of damage GRASSEGGER (1997) many types of damages on the NO façade are observed. For our research two areas of the façade were chosen in which there are at least 4 different types of damage like alveolarization, crack, detachment, graffiti and algae. Each area is around 2x2 m^2 (Figure 2).

Figure 2: Two areas on the façade (left: area 1, right: area 2)

In this paper the analysis of stone 1 in area 1 will be presented as an example (Figure 3).

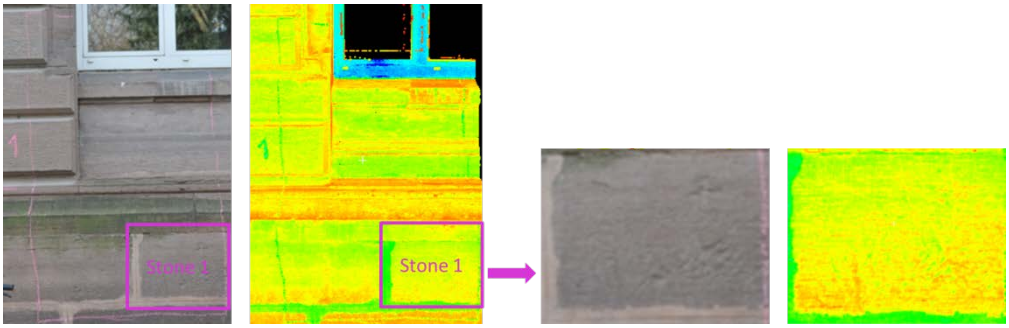

Figure 3: Stone 1 in area 1

Leica HDS 7000 was used for the data acquisition. This phase scanner has a measurement range of more than 100 m. According to the measurement configuration the horizontal distance between the façade and the laser scanner standpoint is around 15m. In order to keep the resolution on the façade under 2 mm the following combination for the scan modus (Table 1) was chosen for all the scans.

Table 1: Scan modus for all 5 epoch scans ZHENG et al. (2013)

Area [m^2]	Angle increments (Hz/V)	Quality (Frequency)	Scanning duration [min]	Resolution
4	Ultra High (0.009°/0.009°)	Premium (254 kHz)	5 min	2mm

In this scan modus the angle increments are 0.009° for horizontal (Hz) and vertical angle (V). The scan frequency is 254 kHz. The higher the scan frequency is, the better the quality LEICA (2012).

Both areas were scanned in 6 different epochs. In the first scan there were not enough control points for a robust geo-referencing ZHENG et al. (2013). For the fourth scan the weather data were not

available. Therefore 4 measurements were used in this research. The first measurement took place on 13th March 2013. The average of temperature and humidity for each scan epoch is shown in Table 2.

Table 2: Temperature and humidity during the scanning ABUSHARKH (2014)

Epoch	Date	Time	Average Temperature [°C]	Average Humidity [%]
1	13/03/2013	13:00-15:00	-2.0	76.96
2	08/04/2013	10:00-12:00	5.5	58.48
3	07/06/2013	10:00-12:00	21.5	54.92
4	21/06/2013	10:00-12:00	19.5	61.95

In order to guarantee all the scans from different epochs are realized in the same coordinate system, a local coordinate system was defined (Figure 4). Four points were chosen as control points for geo-referencing. The laser scanner was set up at almost the same place in each epoch. This guarantees that the angle of incidence between laser beam and façade changes only a few amounts between the different epochs. The average registration error is 3 mm WEI (2013).

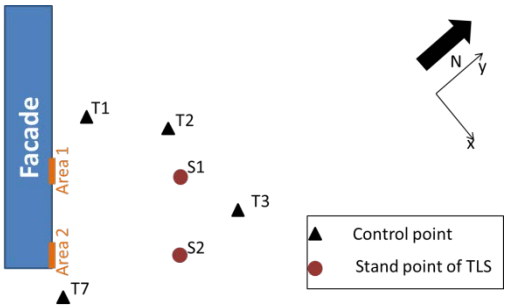

Figure 4: Measurement configuration ZHENG et al. (2013)

3 MODELLING AND DATA ANALYSIS

After geo-referencing all the point clouds are available in the same local coordinate system. The point clouds were processed in several steps (Figure 5). Point cloud of stone 1 in epoch 1 was chosen for the FEM simulation. In the deformation analysis all the other point clouds were compared with the point cloud of epoch 1. In order to calculate and describe the deformation between two different epochs, the local normal vectors and the local volume change were chosen for comparison. Other methods to describe the point cloud based deformation analysis can be read in ELING (2009), GENECHTEN et al. (2009), GORDON (2007) and OLSEN (2010). The classifications of both comparisons were visualized. Then the statistical tests were carried out for the deformation analysis. At the end the geodetic measurements were compared with the FEM simulation results.

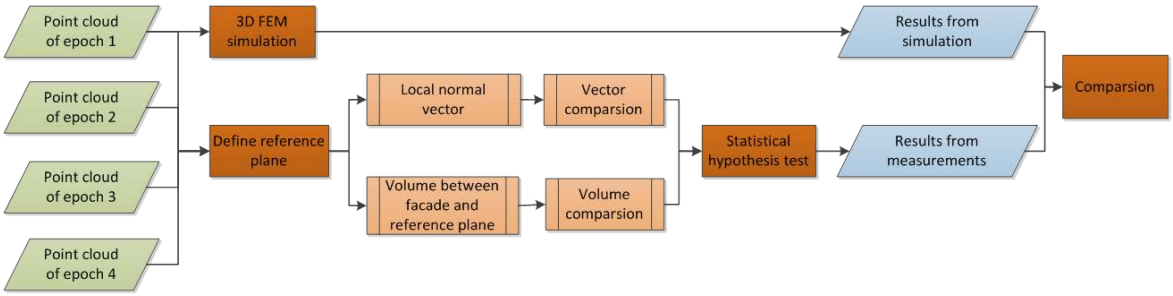

Figure 5: Overview of the processing

3.1 Modelling by FEM simulation

In our research finite element program Macroscopic Space Analysis (MASA) was used for the simulation process. MASA is mainly intended to be used for the nonlinear analysis of concrete and reinforced concrete structures OZBOLT (2010). In the MASA program a 3D model based on the thermo-hygro-mechanical coupling between thermal, hygral and mechanical properties of concrete is implemented (OZBOLT et al., 2008b). Commercial pre- and post-processing package FEMAP is used for preparation of input data and visualization of FEM analysis results (OZBOLT, 2010). FEMAP provides affordable and very powerful finite element analysis (FEA) software to the designer. It is a specially developed Windows solution including pre-and post-processor for advanced engineering finite element analysis but not for non-linear FEM analysis. For the investigation of this contribution non-linear FEM is required.

3.1.1 Data processing of FEM simulation

The data processing consists of mainly two steps Figure 6. In the first step a mesh was created from the point cloud using Geomagic. A local coordinate system which is applied for the solid elements in FEM simulation was defined for the mesh in AutoCAD. Then FEMAP was started to create solid elements, define material properties and constrains for FEM ABUSHARKH (2014). After running FEMAP all the files for MASA were generated.

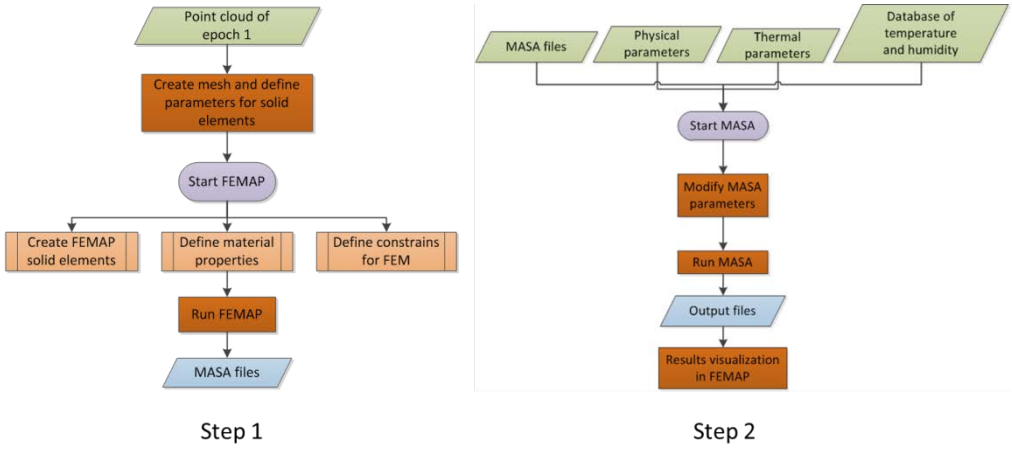

Figure 6: Data processing of FEM simulation

In step 2 physical parameters of the stone, thermal parameters and hourly temperature data were imported into MASA (OZBOLT et al., 2008a). MASA modified those parameters and chose the thermal model for the FEM simulation. After these steps MASA was run to get the simulation results. In the end the displacements of the façade surface were shown in response to the change of temperature in FEMAP.

3.1.2 First results of FEM simulation

The thickness of the stone is 20 cm. At a first approach the thermal extension is modelled. The influence of relative humidity is neglected in this contribution. The origin of the local coordinate system was defined in the lower left corner behind the façade surface (Figure 7). The z-axis points to the façade surface. The y-axis shows up. The distance between two nodes is about 2 cm. In this research it is assumed that the stone is constrained at xz-plane. There are 23880 solid elements. The humidity was not considered.

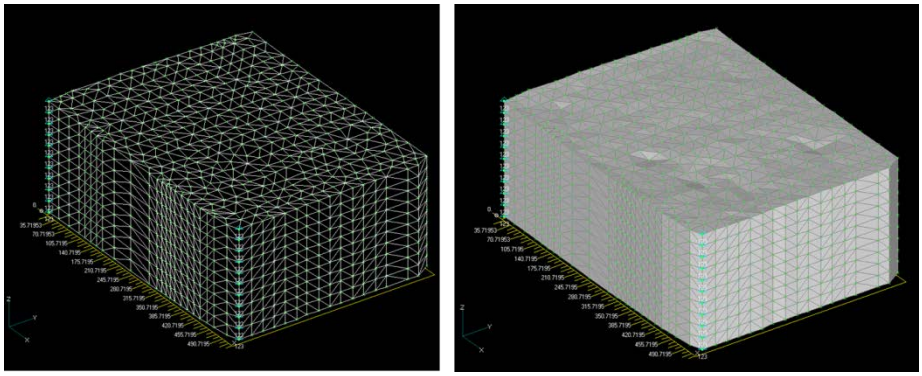

Figure 7: Solid elements in FEMAP (left: mesh, right: solid elements)

The point cloud of epoch 1 was set as start situation. In this research the focus lays on the façade surface. The displacements of the façade surface are shown along the z-axis. From 13th March 2013 to 8th April 2013 the temperature change is 7.5°C. The maximal displacement is colorized in red and below 0.008 mm. The area near the upper edge has almost no displacement (Figure 8, left). The biggest temperature change is 23.5°C between epoch 3 and epoch 1. The maximal displacements focus on the lower area of the stone and are around 0.024 mm. In the orange part the displacements have the average of 0.017 mm. The minimal displacements are in the top part of the stone (Figure 8, middle). In the third FEM simulation the area of maximal displacement (0.027 mm) is reduced. 85% part of the façade surface has an average displacement of 0.021 mm (Figure 8, right).

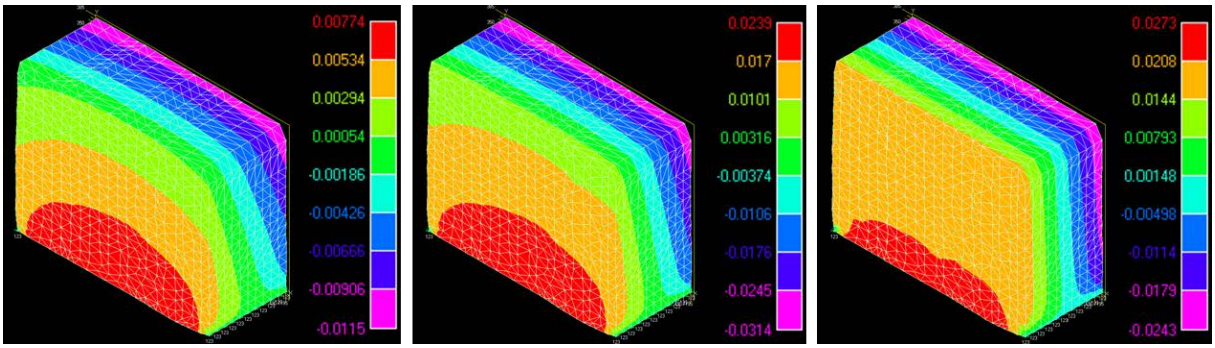

Figure 8: FEM simulations for epoch 2, 3, 4 (the colour scalars are different in those three simulations)

The result of thermal analysis shows that the temperature change does not have a big influence on the surface deformation. The maximal displacement in those three simulations is 0.027 mm along z-axis.

3.2 Data analysis using normal vectors and volume elements

In the local coordinate system of the point clouds, the façade is perpendicular to the xy-plane. The z-axis orients to the zenith direction (Figure 9Figure , left). In order to realize the volume calculation a reference plane has been found by coordinate transformation. After the transformation the façade lays parallel to the xy-plane (Figure 9, right) ZHENG et al. (2013). The x-y plane is now defined as the reference plane for the deformation analysis.

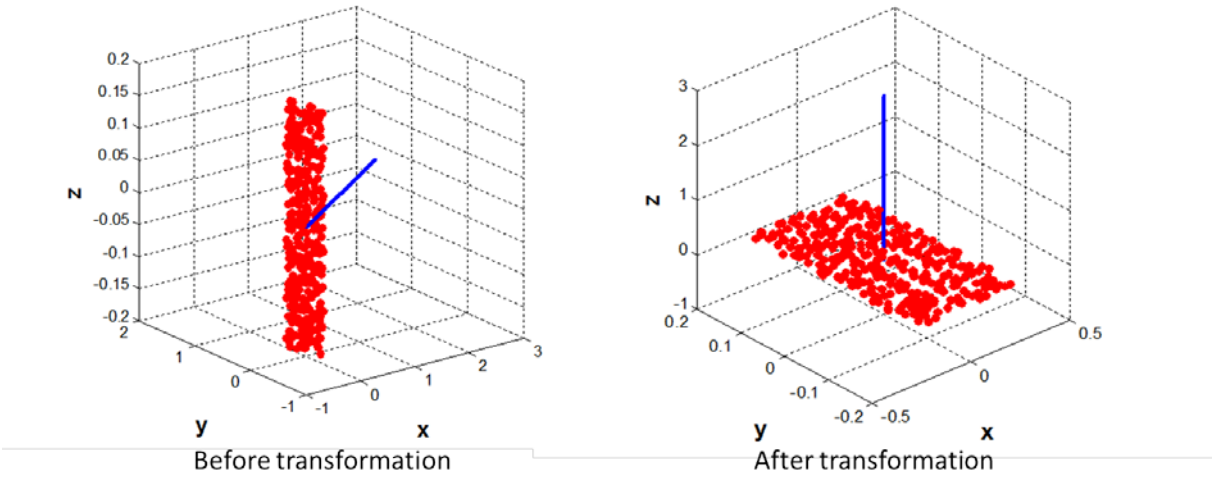

Figure 9: Define the reference plane

3.2.1 Comparison of the local normal vectors

Based on the research ZHENG et al. (2013) the point cloud of the stone was divided into many regular grids which have side length of 2 cm using Matlab. In order to get a normal vector which is not depending on the surface estimation needed for deformation analysis of volumes, in every grid a best fitted plane was estimated. The plane is a two-dimensional vector space in R^3 defined with 3 points P_1, P_2, P_3 that are not lying on a straight line. If vector product is built KÜHNEL (2013), LAU (2011)

$$n = (P_2 - P_1) \times (P_3 - P_1), \tag{1}$$

where n is a vector which is perpendicular to the plane. The shortest distance from the plane to the origin d is obtained by projection of any point P_i on the normalized vector n_0:

$$d = \frac{n \cdot P_i}{|n|} = n_0 \cdot P_i. \tag{2}$$

The plane is uniquely described by the normal vector and the distance of the plane to the origin d:

$$\frac{1}{\sqrt{n_x^2 + n_y^2 + n_z^2}} \begin{bmatrix} n_x \\ n_y \\ n_z \end{bmatrix} \cdot \begin{bmatrix} x_i \\ y_i \\ z_i \end{bmatrix} + d = 0 \tag{3}$$

,

with the condition:

$$r(x) = \sqrt{n_x^2 + n_y^2 + n_z^2} - 1 = 0 \tag{4}$$

In each area in every epoch around 475 grids are computed, and therefore the same number of normal vectors have to be calculated (Figure 10). Because of many small rough structures on the stone surface the normal vectors of each grid are not always parallel to z-axis. The angles between normal vectors and z-axis are colorized in each grid. (Red: 0.7-0.8, orange: 0.6-0.7, yellow: 0.5- 0.6, green: 0.4-0.5, white: 0.3-0.4, gray: 0.2-0.3, dark gray: 0.1- 0.2, black 0-0.1 in rad.)

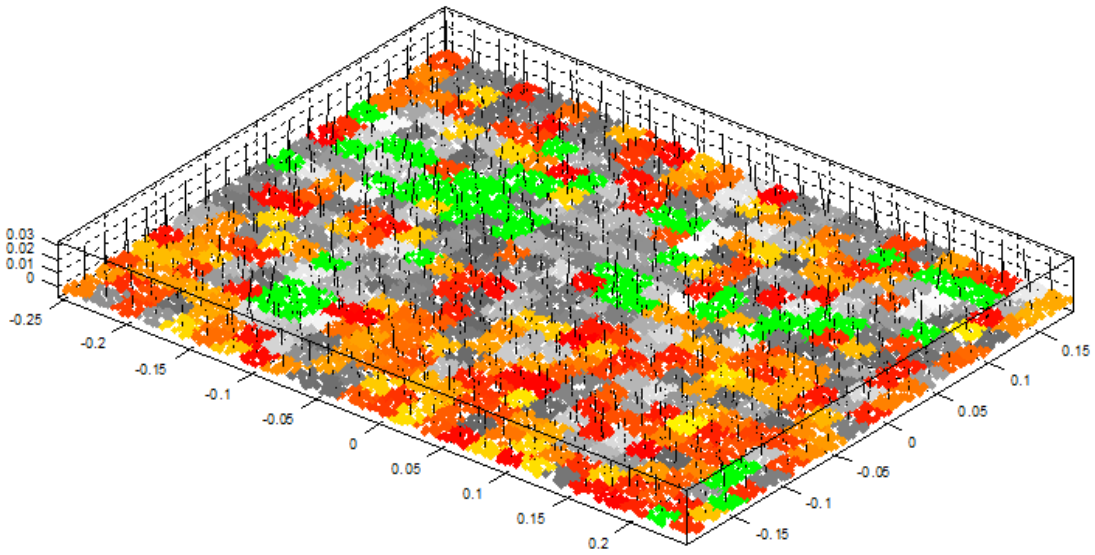

Figure 10: Local normal vectors of stone 1 in epoch 1

The difference between two normal vectors in different epochs and their absolute values were calculated. With respect to the angle in radiant between normal vector n_{i_epoch1} of grid I in epoch 1 and the normal vector n_{i_epochj} of grid I in epoch j the grids were colourised (Figure 11**,** left). The angle differences of normal vectors have to be tested for their significance KÜHNEL (2013). For this case normal distributed values and the significance level of α=0.05 was assumed NIEMEIER (2008). For the normal vectors first of all the accuracy σ_{ni}^{j} of the normal vector I in epoch j was derived taking into account all the computation steps beginning with the standard deviations of the laser scanner observations. The authors have to note that correlations between the observations have not been considered for the error propagation in this contribution. The standard deviation of the angle between two normal vectors can be calculated as following:

$$\sigma_{\Delta\alpha_i^{j-1}} = \sqrt{(\sigma_{ni}^{j})^2 + (\sigma_{ni}^{1})^2} \ . \tag{5}$$

The respective test value may be computed by

$$y = \frac{\left|\Delta a_i^{j-1}\right|}{\sigma_{\Delta\alpha_i^{j-1}}} \tag{6}$$

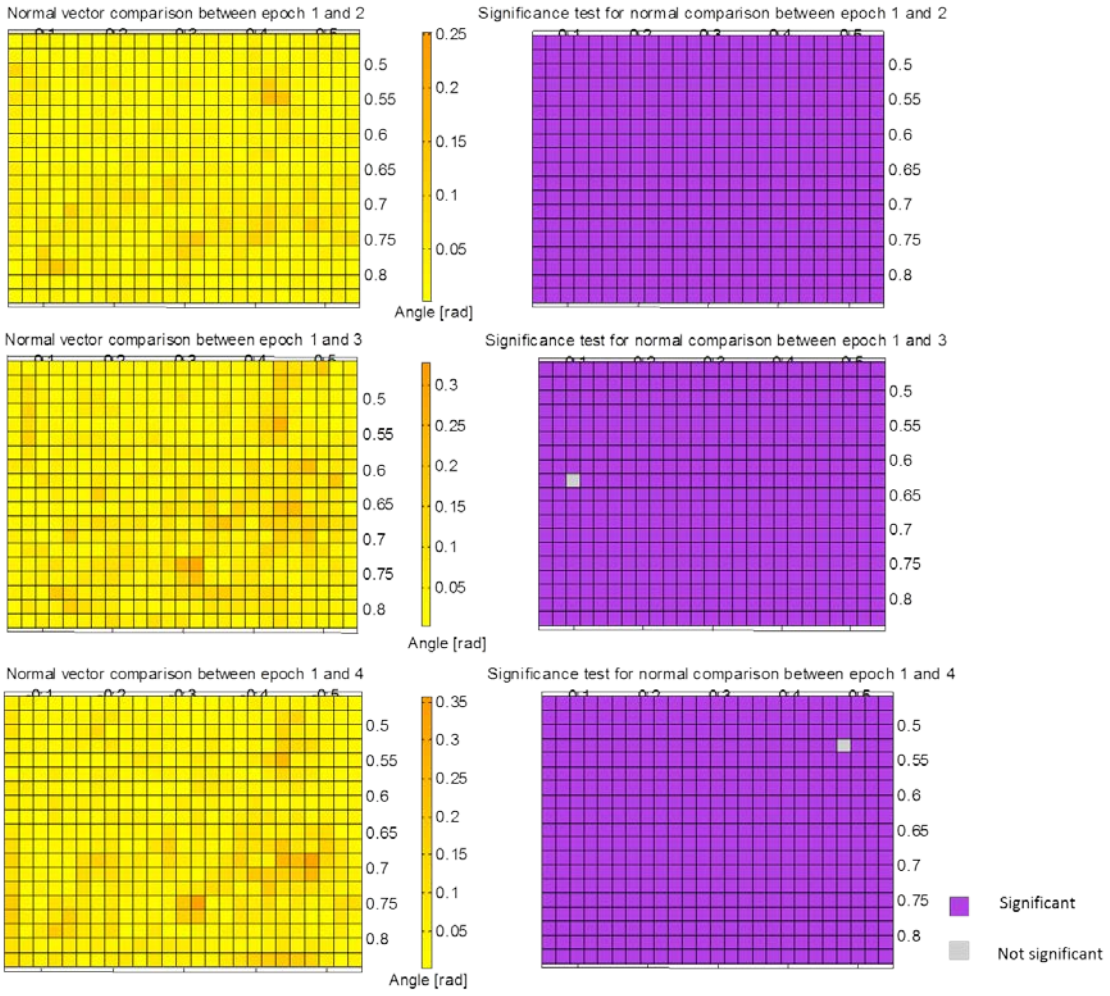

Figure 11: Angle differences between two epochs (left) and significance test (right)

Table 3: Comparison of normal vector angles

Epoch 1 – 2		Epoch 1 -3		Epoch 1 – 4	
$\Delta\alpha_{min}$ [rad]	$\Delta\alpha_{max}$ [rad]	$\Delta\alpha_{min}$ [rad]	$\Delta\alpha_{max}$ [rad]	$\Delta\alpha_{min}$ [rad]	$\Delta\alpha_{max}$ [rad]
0	0.25	0	0.34	0	0.36

Table 3 gives an overview about the interval of the differences. Most all of the angles are in interval between 0 rad and 0.2 rad. The maximal angle difference of 0.36 rad between two normal vectors is calculated for the comparison of epochs 1 and 4. Particularly with regard to the change of temperature it can be seen that the normal vectors with big differences concentrate in the area where the surface is not flat. A supposition is that in this area deformations are more active than the other areas. Almost all the angle differences are significant (Figure 11, right).

3.2.2 Comparison of the local volume

It is necessary to use the reference plane (xy-plane, Figure 9, right) to calculate the volume between the point clouds and the reference plane (Figure 12). In each regular grid a surface was reconstructed from the points by polynomial of 2nd degree KÜHNEL (2013):

$$z = f(x, y) = P_{00} + P_{10}\, x + P_{01}\, y + P_{20}\, x^2 + P_{11}\, xy + P_{02}\, y^2 . \quad (7)$$

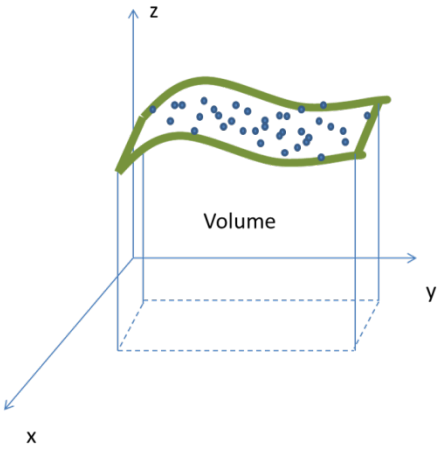

Figure 12: Volume between the reference plane and point cloud

The parameters P_{00}, P_{10}, P_{01}, P_{20}, P_{02} and P_{11} are the coefficients of the polynomial and were estimated in an adjustment using Gauss-Helmert Model. X, y and z are the coordinates of the points FRITSCH (2009). The volume between this surface and the xy-plane was calculated for every grid KÜHNEL (2013):

$$V_i = \iint \int_{0}^{Z=f(x,y)} dzdydx \,. \tag{8}$$

The volume behind each grid from epochs 2, 3 and 4 was compared with the volume of epoch 1. The differences of the volumes were calculated. With respect to the change of the volume the grids were colourised (Figure 13, left). The volume differences between epoch 1 and 2 are below 0.04 cm³. The volume differences of epoch 1-3 and epoch 1-4 are bigger (about 0.05 cm³ to 0.09 cm³). The maximal volume difference 0.089 cm³ can be found between epoch 1 and 4 (Table 4).

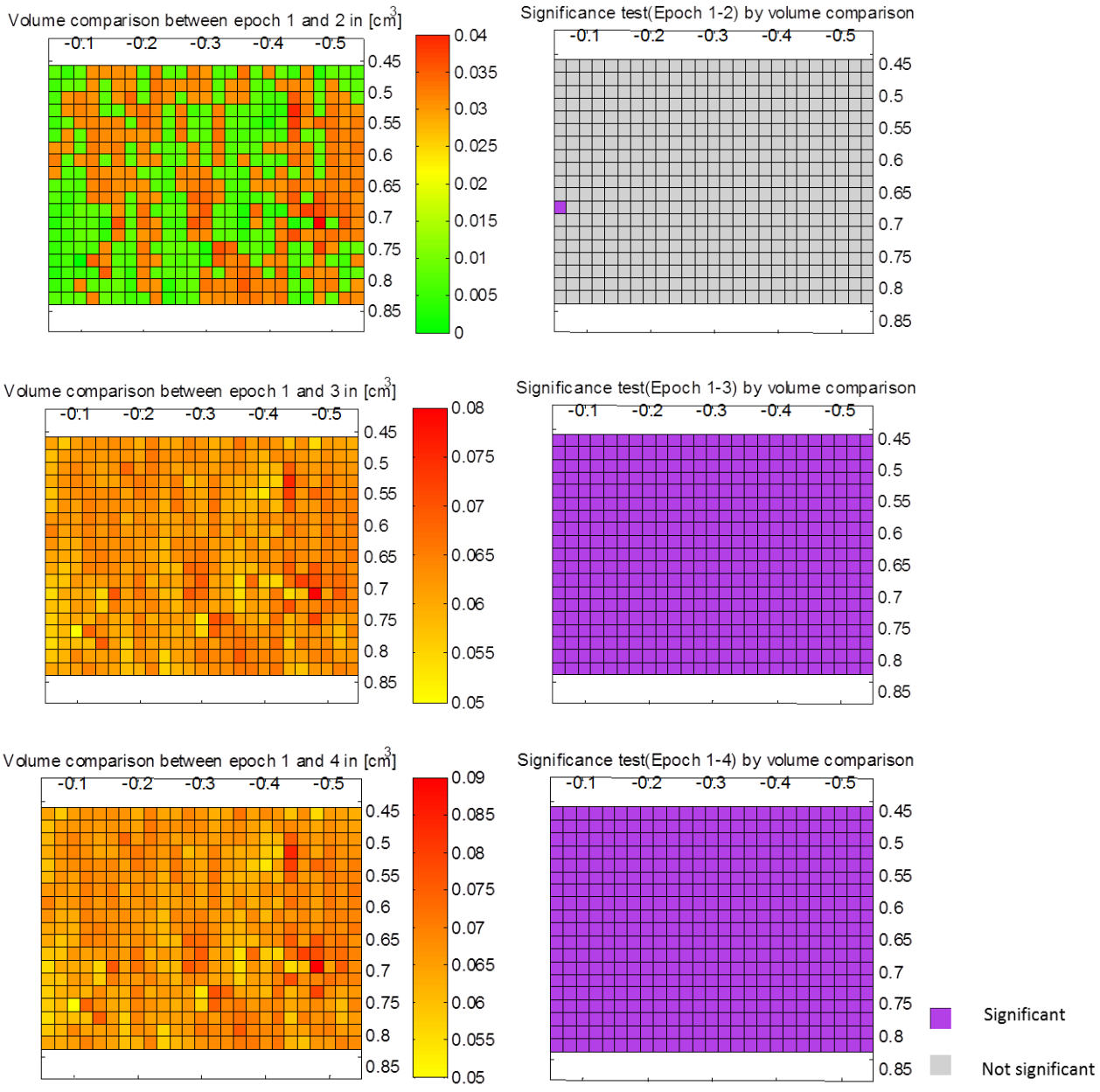

Figure 13: Volume differences between two epochs (left) and significance test (right)

Table 4: Comparison of volume differences

Epoch 1 – 2		Epoch 1 -3		Epoch 1 – 4	
ΔV_{min} [cm^3]	ΔV_{max} [cm^3]	ΔV_{min} [cm^3]	ΔV_{max} [cm^3]	ΔV_{min} [cm^3]	ΔV_{max} [cm^3]
0.002	0.039	0.050	0.078	0.052	0.089

For the standard deviation of the volumes again the observations of the laser scanners have to be considered. The approximation error of the surface reconstruction is of great importance for the covariance propagation following e.g. equation (7) and (8) delivering finally the standard deviation of the volume differences $\sigma_{V_{i\_epochj}}$. The significance of the volume differences have to be tested. The respective standard deviation is

$$\sigma_{\Delta V_i^{j-1}} = \sqrt{(\sigma_i^j)^2 + (\sigma_i^1)^2} \tag{9}$$

The test value is calculated by

$$y = \frac{\left|\Delta V_i^{j-1}\right|}{\sigma_{\Delta V_i^{j-1}}} \tag{10}$$

The statistical tests were realized for the volume comparison of all epochs (Figure 13, right). From the results of the significance test it can be seen that the volume changes from epoch 1 to epoch 3 and 4 are significant. The volume differences between epoch 1 and 2 which are smaller than 0.04 cm^3 and almost not significant. The standard deviation of the volume differences $\sigma_{V_{i\_epochj}}$ is always in the interval [0.013cm^3 – 0.025cm^3] for this research.

3.3 Comparison between FEM and geodetic measurements

From the geodetic measurements significant deformations in epoch 3 and 4 have been found. But the displacements in FEM simulation in those two epochs are not visible. A reason for that is the temperature variation alone causes no relevant deformation. This also corresponds to the statement in previously published research OZBOLT et al. (2008a). The magnitude of thermal expansion ΔZ_T and hygral expansion ΔZ_H can be separated calculated by rule of thumb. Therefore other material properties like water saturation and water absorption are ignored. The expansions Δz are perpendicular to the material layers. The expansion based on humidity change is between 5 and 1.5 times bigger than thermal expansion (Table 5).

Table 5: Thermal and hygral expension

	Epoch 1-2 [mm]	**Epoch 1-3 [mm]**	**Epoch 1-4 [mm]**
Δz_T	0.011	0.035	0.032
Δz_H	0.056	0.067	0.045

From volume differences ΔV_i^{j-1} the displacements along the z-axis can be calculated by

$$\Delta z_i^{j-1} = \frac{\Delta V_i^{j-1}}{4cm^2} \tag{11}$$

The maximal and minimal displacements are shown in Table 6.

Table 6: Calculated displacements from geodetic measurements

Epoch 1 – 2 [mm]		**Epoch 1 -3 [mm]**		**Epoch 1 – 4 [mm]**	
Δz_{min}	Δz_{max}	Δz_{min}	Δz_{max}	Δz_{min}	Δz_{max}
0.050	0.098	0.125	0.195	0.130	0.223

The biggest displacement of 0.223 mm is between epoch 1 and 4. The displacements from the comparison between epoch 1 and 2 are below 0.1 mm. The magnitude of the displacements from geodetic measurements is around 8 times bigger than the displacements from FEM simulation. Though, the detected deformations in geodetic measurements as well as in FEM simulation have the similar growth trend.

From the comparisons above it is obviously to see the influence of humidity can not be ignored in the FEM simulation. In the next research it is necessary to use a combined hygro-thermal model for FEM simulation. All the material properties like relative humidity, water saturation, water absorption and water permeability must be considered in this coupled analysis model.

4 CONCLUSIONS

It is possible to detect the deformation of the façade surfaces by using laserscanning measurements. However, the scanning modus and scanning configuration should be carefully chosen regarding the point's 3D position accuracy and the point resolution on the object. The scanning duration in each epoch was about 10 minutes per stone.

By the calculation of normal vectors and volumes and their changes respectively it is possible to describe the change of the façade surface completely. The volume changes are below 0.09 cm^3. The extreme volume differences like 0.089 cm^3 lay in the area with many small rough structures. The volume differences are significant for all grids in epochs 3 and 4. The quality of surface reconstruction may have a great influence on the detection of deformations ZHENG et al. (2013). In the next step the correlation between the surface parameters and the volume accuracy must be analysed. This may increase the significance of the parameters normal vector and volume difference. Besides, for the surface structures like edges, a better reconstruction method is needed since an edge needs another representation than a 2^{nd} order surface fitting.

Obviously the temperature influence describes the deformations not completely. It is expected that the humidity will have a high influence on the deformation simulation OZBOLT et al. (2008a). In the next step the humidity parameters will be combined with temperature data in FEM simulation. Also the exact information about the cross-section of the façade is needed to define the constrain-condition in FEM. In the best case the calibration of this model using geodetic measurements can be the target.

ACKNOWLEDGEMENTS

First I would like to take this opportunity to thank all colleagues who have supported this study through their professional and personal support. Particularly I would like to thank Mr. Professor Josko Ozbolt. He provided us with MASA software in time and gave me an important overview about FEM analysis. At the same time I would like also to thank his colleagues Mr. Periskic and Ms. Bosnjak for their strong support to solve the problems when we use the software.

I would like to thank Ms. Professor Grassegger and her colleagues for providing the research object and literatures. Finally, I would like to thank my doctorate supervisor Mr. Professor Schwieger for his useful advice and detailed corrections during his busy business trip.

REFERENCES

Books:

ABUSHARKH, M.: *Analysis of damage dynamics on the North-East façade of the HFT Stuttgart using Finite Element Method (FEM),* Master-Thesis (in processing), Institute of Engineering Geodesy, University of Stuttgart, March 2014

ELING, D.: *Terrestrisches Laserscaning für die Bauwerksüberwachung.* Wissenschaftliche Arbeiten der Fachrichtung Geodäsie und Geoinformatik der Leibniz Universität Hannover, Nr. 282, 2009

FRITSCH, D.: *Ausgleichungsrechnung II,* lecture script, Institute of Photogrammetry, University of Stuttgart, 2009

KÜHNEL, W.: *Differentialgeometrie: Kurven-Flächen-Mannigfaltigkeiten.* Springer Spektrum, ISBN: 9783658006143, Wiesbaden, 2013

LAU, D.: *Grundbegriffe der Mathematik, algebraische Strukturen 1, lineare Algebra und analytische Geometrie, numerische Algebra und Kombinatorik*, Springer, ISBN: 9783642194429, Berlin, 2011

LEICA: *Leica HDS 7000 User Manual,* 2012

MEYER, C.: *Schadenserfassung durch Kartierung an der HFT-Stuttgart, Bau I, NO-Natursteinfassade und Bewertung der Ursachen*, Bachelor-Thesis (unpublished), Department of Civil Engineering, University of Applied Sciences Stuttgart, 2012

NIEMEIER, W.: *Ausgleichungsrechnung.* 2. Auflage. Walter de Gruyter, Berlin, 2008

OZBOLT, J.: *Finite element code MASA (MAcroscopic Space Analysis).* General introduction for MASA, Institute for Construction Materials, University of Stuttgart, 2010

WEI, X.: *Analysis of damage dynamics on the North-East façade of the HFT Stuttgart using Leica Laser-Scanner HDS7000*, Master-Thesis (unpublished), Institute of Engineering Geodesy, University of Stuttgart, July 2013

Journal articles:

GENECHTEN, B., DEMEYERE, T., HERINCHX, S., GOOS, J., SCHUEREMANS, L., ROOSE, D., SANTANA, M.: *Terrestrial Laser Scanning in Architectural Heritage – Deformation Analysis and the Automatic Generation of 2D Cross-Sections.* Proceedings of the CIPA XXII International Symposium, Kyoto, Japan, 11-15 October 2009

GORDON, S., LICHTI, D.: *Modelling Terrestrial Laser Scanner Data for Precise Structural Deformation Measurement.* Journal of Surveying Engineering, Vol. 133, No.2, 2007

GRASSEGGER, G., ECKSTEIN G.: *Schadensvermessung an Natursteinen. Photogrammetrische und naturwissenschaftliche Untersuchungen, Präzisionsvermessung zum zeitlichen Verlauf der Steinschäden.* Denkmalpflege in Baden-Württemberg, 19. Jahrgang, Stuttgart, 1/1990

GRASSEGGER, G.: *Die Verwitterung von Natursteinen an Bauten und Baudenkmälern.* Ebner Verlag, Ulm, S. 434-440, 1997

OLSEN, M., KUESTER, F., CHANG, B., HUTCHINSON, T.: *Terrestrial Laser Scanning-Based Structural Damage Assessment.* J. Comput. Civ. Eng., 24(3), 264-272, 2010

OZBOLT, J., GRASSEGGER, G., VAN DER VEKEN, P., PERISKIC, G., REINHARDT, H. W.: *Experimental and numerical study of hygro-thermo-mechanical properties of „Schilfsandstein" from Baden-Württemberg.* Environmental Geology, Springer-Verlag, vol. 56, Page 535-546, 2008a

OZBOLT, J., PERISKIC, G., REINHARDT, H. W., ELIGEHAUSEN, R.: *Numerical analysis of spalling of concrete cover at high temperature. Computers and Concrete*, International Journal, 5, 279-293, 2008b

ZHENG B., SCHWIEGER, V., GRASSEGGER, G.: *Detection of hydrothermal deformations of sandstone using laser scanning.* Proceedings of "2nd Jonit International Symposium on Deformation Monitoring (JISDM)", Session 12, Nottingham, 10th Sep. 2013

Links:

http://weatherspark.com/, last accessed on 03rd March, 2013

http://www.plm.automation.siemens.com/de_de/products/velocity/femap/, last accessed on 04th March, 2013

Detecting and Modelling Fine Structures from TLS data

Annette Scheider
Institute of Engineering Geodesy, University of Stuttgart, Germany

Abstract
In this investigation the abilities of area-wise measurements to detect fine structures are investigated. Terrestrial laser scanners using phase shift method surveyed objects with a width of less than 1 cm over a short distance. In a first step, fine structures must be detected in the point cloud. Therefore adequate filters must be chosen and applied. The amount of mixed pixels in the point cloud is reduced. For this purpose the spatial orientation of each triangulated face is compared to a threshold; points which are part of faces with an angle larger than this defined view angle are eliminated. The filtered point cloud can be used to model structures with a diameter and width respectively of a few millimetres either by geometric primitives, by faces or by representing element axes.

Keywords
Point Cloud, Laser scanner, Fine Structures

1 INTRODUCTION

A new branch of architecture is dealing with granular substances by emulating natural constructions like snow. DIERICHS & MENGES (2012) describe these structures (*aggregates*) as unbound systems on the one hand being stable but on the other hand being reconfigurable within a short time. In favour of this the term “aggregate architecture” was introduced DIERICHS & MENGES (2012). The Institute of Computer-Based Design (ICD) of University of Stuttgart researches on this topic. For that purpose, they have developed special granules (Figure 2) which are able to build large cantilever structures DIERICHS (2014). One example of a cantilever dome is shown in Figure 1. The elements have four to ten legs and are made of synthetic material. Every element leg converges, but the geometry of different legs is not completely symmetric; their width decreases from ca. 5 mm (close to the centre) to ca. 2 mm at the end points.

Because the behaviour of these elements during the construction process should be described, it is simulated e.g. with discrete element method simulation DIERICHS (2014). The next step is to build up an aggregate structure by filling a specified amount of granules on a removable fundament either manually or by a robot. To validate the simulated model, it has to be compared to the real structure. So measurements are required.

Consequently the idea was born to monitor aggregate structures composed of fine granular elements with geodetic methods. Multiple surveying techniques and methods have been considered (see next chapter) before area-wise acquisition methods were chosen. So a point cloud represents the measured object.

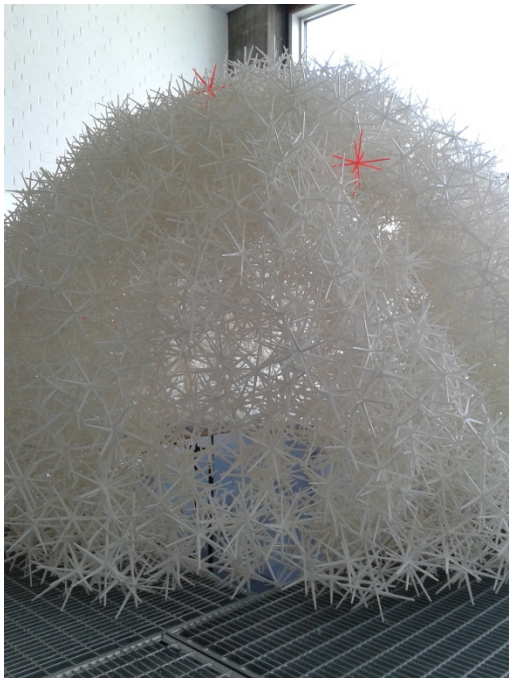

Figure 1: Aggregate Structure – Cantilever dome of granulates

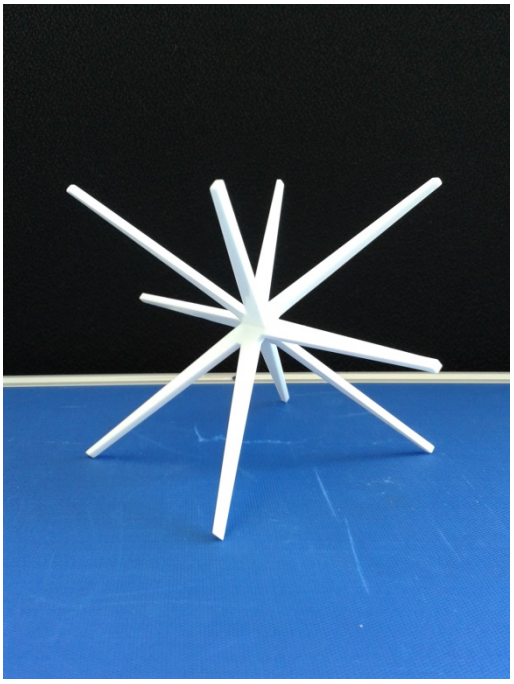

Figure 2: Single granular element

2 CHALLENGE TO MEASUREMENT TECHNIQUES

2.1 Different adequate measurement techniques

Measurement of fine structures without any kind of surface structure is always a challenge. Several measurement techniques have been considered to decide which of them is suitable to survey aggregate structures. Particularly the orientation of the element axes can be reconstructed by measuring the endpoints and the central point of an element. So first of all a point-wise monitoring was considered. A disadvantage of this monitoring method is that it is necessary to touch the points of interest with any kind of reflector or sign. This may deform the fragile elements or even the complete aggregate structure. Measuring single points is also quite work-intensive for large structures consisting of thousands of single elements. Point-wise monitoring would only be adequate for the survey of single granular elements (Figure 2). So reference values can be determined for some selected elements.

In this case, only laser trackers or theodolite measurement systems fulfil the requirements of detecting fine structures: They can reach a much higher accuracy than total stations and only a minimum of contact respectively no contact during the measurement procedure is necessary. Often laser trackers are combined with hand-held probing instruments. These instruments determine their spatial orientation, so the offset between measured point (reflector) and stylus tip will be applied to the coordinates by the measurement software.

Alternatively, area-wise measurement methods can capture contactless numerous points in a short time. But the resulting point clouds are distributed automatically by the optical characteristics of the instrument, so it is not possible to measure directly specified points. Also shadowing may affect the availability of the measured points. Despite these disadvantages, area-wise measurement method was chosen because it is the only possibility to survey a complex aggregate structure within a specified time window. It can be assumed that the structure is stable within this time interval.

Point clouds can be produced by several measurement methods, e.g. cameras, structured-light scanners, laser scanners and hand-held scanners.

Hand-held scanners which are combined with laser trackers or measuring arms measure fine structures with a high accuracy. PAULUS et. al. (2014) scan young barley plants to protocol the steam volume of the growing plants. Within a volume of few metres, small structures can be scanned all around.

Unfortunately, measurements of large structures would take a plenty of time and many individual placements of the measuring instrument would be needed.
Photogrammetric methods offer a variety of options to create point clouds of small elements with a high accuracy: Photos taken by a single camera or by multiple cameras can be evaluated with special algorithms to create point clouds e.g. dense image matching method for close range applications WENZEL et. al. (2013). For that purpose the images must overlap. Inside an area overlapped by many images, a completeness of 60% - 100% can be achieved WENZEL et. al. (2011). To get a detailed three dimensional point cloud, a large number of photos is necessary. Besides it is easier to create a point cloud if there is any kind of structure on the surface of the object. It is possible to tag an artificial structure. Consequently, objects can also be surveyed by structured-light scanners with a high accuracy GÜHRING (2002). Light stripes are projected to the element while a camera records it. But the projector and the camera have only a defined view field, so measurements of a large structure are work intensive and require lots of stations.
Point clouds being produced by methods of close range photogrammetry represent fine structures with few noisy points. Hence close range photogrammetry is a good option to survey fine structures.

2.2 Terrestrial laser scanner

Generally, terrestrial laser scanners cannot achieve an accuracy level comparable to laser trackers or close range photogrammetry, but their advantage is the large view field: Panoramic laser scanners STAIGER (2003) can measure the environment within 360° in horizontal direction and more than 300° vertically. Different resolutions and quality levels can be chosen, which define the scan duration.

Laser scanners produce a three dimensional point cloud by measuring distances, horizontal and vertical angles. For distance measurements a laser beam is emitted, reflected by an object and sent back to the receiving part of the distance measurement unit. Because the laser beam is divergent, not only a point but approximately a circle is projected to the object surface. This diameter is the limiting size to detect fine structures. The size of this area depends to the range to the laser scanner. For Leica HDS 7000 the diameter is already 3.5 mm in a distance of 0.1 m from the scanner LEICA GEOSYSTEMS (2011).
HEBERT & KROTKOV (1991) explain that “the range is measured by integrating over the entire projected spot”. The measured distance is represented by one point in the point cloud. Similar to total stations, laser scanners measure the distance either by pulsed time of flight (PTOF) method or by phase shift method SCHULZ (2007). Thus, the same problems affect distance measurements. Here, a scanner with phase shift technique was used; therefore so-called mixed pixels appear.
The term mixed pixels was defined by HEBERT & KROTKOV (1991). These points arise if the laser beam is reflected partly by the object itself and partly by another object behind (see Figure 3). So the effect of mixed pixels always occurs at edges of objects. Filters can reduce them but often they cannot be completely eliminated, particularly for small objects. In this case only a small number of circles and points respectively are located entirely on the surface of the fine object. If the object width is smaller than the beam diameter, it is only represented in the point cloud by mixed pixels.

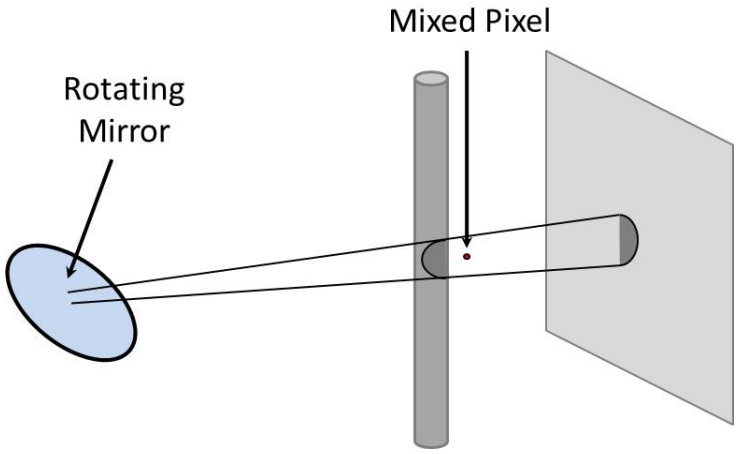

Figure 3: Origin of Mixed Pixels

To detect a fine structure, mixed points must be detected with an adequate filter which must often be adapted to the particular situation. Another approach would be to reconstruct the structure and edges respectively by analysing the mixed pixels themselves.

3 DETECTION OF FINE STRUCTURES

It should be investigated whether point clouds being measured by terrestrial laser scanners can be filtered in a way so that fine structures can be detected and modelled respectively. For that purpose points on the object must be separated from measurement noise and mixed pixels as well as other disturbing influences.

3.1 Detection of single structures

Before the point clouds of the granular elements or complete aggregate structures are captured, suitable resolution and quality levels must be determined. For this purpose simpler objects like sticks were investigated and analysed in SCHAAL (2013). The HDS 7000 from Leica Geosystems was used to scan sticks with a thickness of 2 cm down to 2 mm within a distance of less than 5 m. SCHAAL (2013) shows that structures with a diameter of less than 4 mm can hardly be detected. Even for sticks with a diameter of 5 mm, the point cloud includes noisy points with a curved shape (see Figure 4a). For smaller structures the point cloud contains an insufficient number of points located on the object itself. Either they are identified as isolated points or the mentioned noisy points cover them, so the object shape seems to be curved.
According to the analysis in SCHAAL (2013) the resolution levels *Superhigh* respectively *Ultrahigh* (20,000 resp. 40,000 points/rotation) shall be used with high or premium quality, so that the rotational velocity of the mirror is compressed by a factor 4 resp. a factor 8 compared to the highest possible rotational velocity.
Detecting structures in a point cloud is a pre-processing step of modelling these structures. Mixed pixels must be selected and eliminated. For that purpose a triangulated mesh of the point cloud is created. It consists of triangulated faces and measured points as vertices. Mixed pixels can be detected by considering the view angles of the faces. Lots of commercial software (e.g. GEOMAGIC, 2014) or freeware (e.g. MESHLAB, 2014) offers tools to select these faces according to a threshold angle. Here, point cloud processing was performed by *MeshLab*. For the sticks, the threshold view angle is defined with 82° and for the granular elements with 85°.
Remaining triangular faces caused by mixed points can often be detected by searching for isolated faces. Again a threshold must be inserted to define the minimal number of surrounding faces. Detected faces and their vertices are eliminated. The resulting point cloud still contains noise points but their number is obviously reduced and the object itself can be detected like it is shown in Figure 4b and Figure 5.

Filtering of scanned granular elements causes more challenges. End points of the granules are hardly detectable. In most cases, they are represented by mixed pixels. This is the reason why the element edges seem to be curved versus end points (Figure 5). Also legs pointing towards the laser scanner are often eliminated because an insufficient number of points is located on these parts.

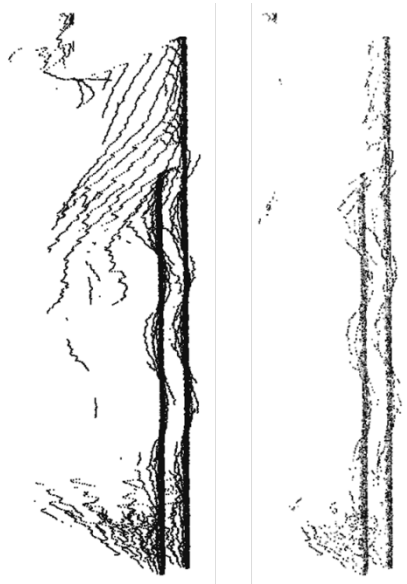

Figure 4: (a) Point cloud of scanned sticks (b) filtered point cloud (Meshlab)

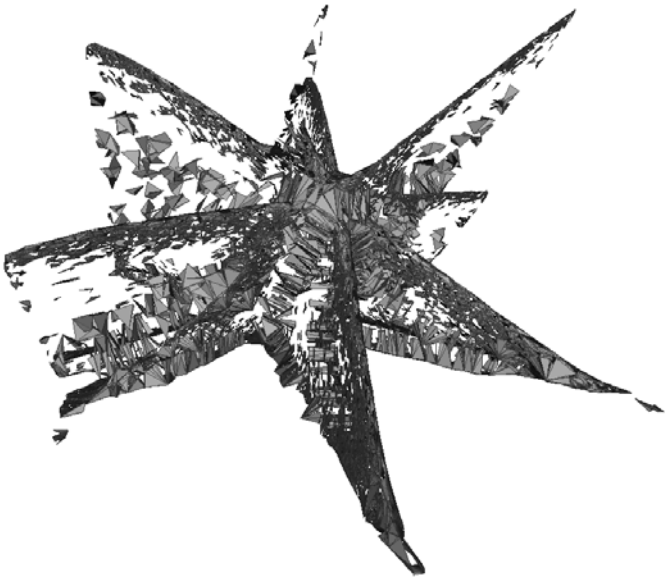

Figure 5: Granular element – number of faces is reduced by criterion "view angle" (MeshLab)

3.2 Detection of composed structures

Aggregate structures are composed of many granular elements. Because of the dense connection, they shadow parts of elements being behind them. So it is hardly possible to find an uninterrupted granular element in the point cloud. The described process may reduce small isolated parts of granular elements. In a further step, the filter must be adapted to distinguish between the object itself and mixed points. However the filtered point cloud improves the detection of the aggregate structure (Figure 6 and Figure7).

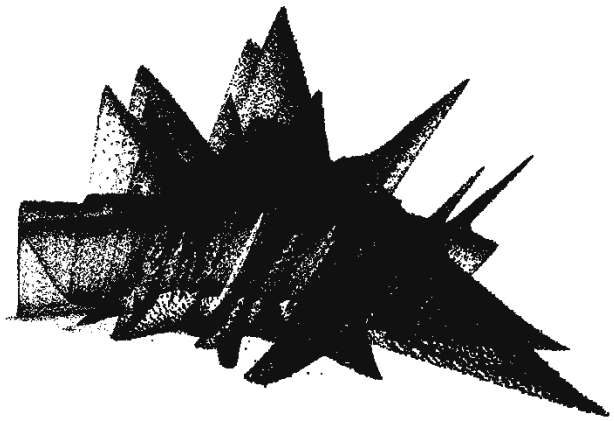

Figure 6: Measured Point Cloud of a composed aggregate structure

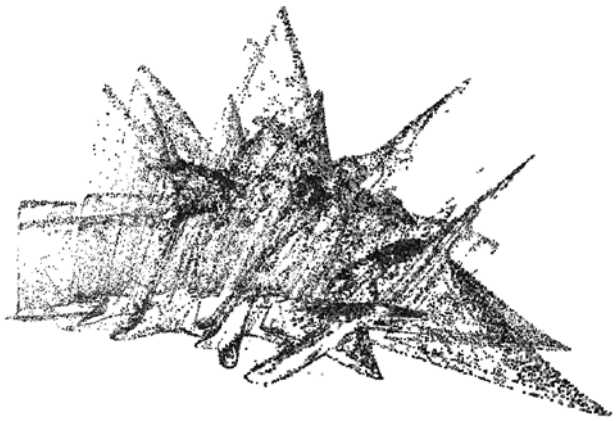

Figure 7: Filtered Point Cloud of a composed aggregate structure

Large composed structures are normally surveyed from multiple stations. It is often meaningful to reduce the number of mixed pixels before the point clouds are registered. In a registered point cloud, disturbing points and triangulated faces respectively cannot be detected by a predefined view angle. Consequently they cannot be separated from the object itself.

4 MODELLING OF STRUCTURES

After noise reduction the objects can be modelled in different ways. The complete structure can be considered by modelling the surface or the volume by faces and solids respectively. Another approach is to model the single elements. For detailed models, they can also be described by faces or solids. If only the position and the spatial orientation should be analysed, elements can be described by straight lines or curves.

Here, two different objects are considered: Cylinders and granular elements.
SCHAAL (2013) uses the software Geomagic to estimate cylinders out of the scanned sticks. After filtering the point cloud (see 3.1) cylinders are estimated for the chosen points. According to the remaining points on the object in single scans, cylinders can be estimated for sticks with a diameter larger or equal to 4 mm. Registered point clouds contain more points on the object so even cylinders with a diameter of 3 mm can be estimated in many cases. If there are too many noise points around the object, an estimation of cylinders is not possible.

In the modelling process for granular elements, their legs are represented by axes and lines respectively. Because the legs of the elements are convergent to their ends, the line is assumed to run from one end point to the opposite one. The accuracy of these virtual lines depends to the position accuracy of the detected end points and represents only an approximated orientation.
To calculate the axis of the granular elements, the position of the element centre is required. Currently the approximated position is determined manually. In future, the element centres shall be determined automatically. Because the size of the element is known, a sphere with a radius corresponding to the length of element legs is defined. Points outside this sphere are assumed to be mixed pixels or belong to other objects and are eliminated. A convex hull is created around the points within the sphere to detect end points of the element legs. Because mixed pixels have not been deleted completely, some of them might also be part of the convex hull. Therefore all points which form the convex hull are separated and analysed. First the distances between the particular points are calculated. Because all points are part of the sphere, maximum distances should be close to the sphere diameter for points on opposed legs of the element. Multiple point combinations fulfil this requirement. For all candidates the spatial orientation is computed which is used to segment the amount of detected lines for the particular axes. The next step is to reconstruct the particular axes. For each end point of a line, the amount of possible candidates is centred by calculating the mean coordinates. The candidate with minimum distance to the mean end point is chosen as approximated end point. The representing virtual lines are added Figure 8.

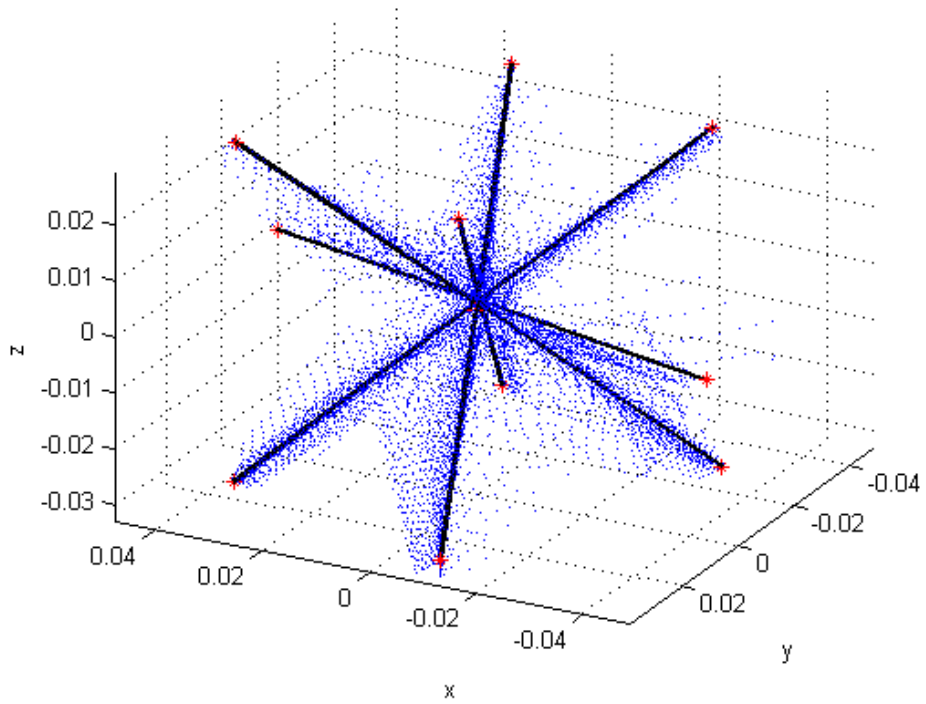

Figure 8: Granular element with approximated element axes

5 CONCLUSION

Detecting and modelling fine structures from point clouds by area-wise monitoring are a challenge. It requires special acquisition methods and special processing algorithms. Elements with a diameter or width down to 4-5 mm can be surveyed by terrestrial laser scanners using phase shift method for distance measurements. But the detectable width depends to the offered resolution of the scanner and the measuring distance. Point clouds have to be filtered to detect the structures and elements. For that purpose, a filter level must be defined which deletes enough mixed pixels or other noise points to recognize the structure itself but which does also not eliminate too many points on the object itself. Smaller structures can be captured either with hand-held scanners in combination with measuring arms and laser trackers respectively or with photogrammetric methods.

It might be possible to combine all these methods to acquire structures with lots of fine details in an efficient way. Thereby mixed pixels within the point cloud indicate edges or fine structures. For example parts which cannot be reconstructed by a laser scanner point cloud are added by a point cloud which is created using images. In this case, adequate registration methods are necessary.

Currently, precognition concerning the shape and size of fine structures is necessary to model them, e.g. diameter of cylinders or length of element legs. A more detailed analysis may automatize the estimation of diameters or radius. Also the detection of element centers or the elimination of background segments may be improved by automation.

In future investigations, detected and modelled structures can be compared to the results received by photogrammetric methods.

6 OUTLOOK

Aggregate structures can be deformed quite easily because of their flexible behaviour: They adapt perfectly to the acting forces, because the single element itself can be deformed to a certain level. Additionally they may be arranged in a new way like in a fluid DIERICHS & MENGES (2012). So deformation tests will be conducted. Deformations can be detected by modelling the single elements (position and orientation) and compare them for different epochs. But this modelling process is very laborious. For quick results it is more convenient to model to complete aggregate structure as a volume or surface. After filtering the measured point cloud, the structure can be composed of solids e.g. tetrahedrons which are not allowed to overlap. So the volumes can be compared for different epochs. Changing volumes indicate deformations. The location of the deformed region is determined with further analysis.

The surface of a structure can be composed by a newly connected mesh representing a non-convex hull. According to the principle of Delaunay triangulation, no other points shall be located within each triangle. Here, this principle must be adapted to the 3D space. A second surface of another epoch can be intersected with the first one and deformations can be recognized. It is also possible to compare a point cloud measured at another epoch to the surface and take the deviations as indicators for deformation.

ACKNOWLEDGEMENTS

The author would like to thank Ms Karola Dierichs (Institute of Computer-Based Design, University of Stuttgart) and Ms Carolin Schaal for their support. Ms Dierichs offered us the opportunity to scan aggregate structures within her project. Ms Schaal investigated the resolution capability of laser scanners for measurements of fine structures (cylinders) in her bachelor thesis.

REFERENCES

Journal articles:

DIERICHS, K., MENGES, A.: *Aggregate Structures – Material and Machine Computation of Designed Granular Substances.* Architectural Design, Vol. 82/2, p. 74-81, 2012.

GÜHRING, J.: *3D-Erfassung und Objektrekonstruktion mittels Streifenprojektion.* PhD Thesis, University of Stuttgart, Deutsche Geodätische Kommission, Reihe C, Nr. 560, München, 2002.

HEBERT, M., KROTKOV, E.: *3-D Measurements From Imaging Laser Radars: How good are they?* IEEE/RJS International Workshop on Intelligent Robots and Systems IROS'91 in Osaka, Japan, 1991.

PAULUS, S., RIEDEL, S., KUHLMANN, H.: *Automatic Extraction of Stem Parameters out of 3D Laser Scanned Barley Plant Point Clouds*. Beiträge zum 17. Internationalen Ingenieurvermessungeskurs Zürich 2014, p. 403-415, 2014.

SCHAAL, C.: *Untersuchung des Auflösungsvermögens eines Laserscanners bei der Aufnahme feiner Strukturen*. Bachelor Thesis, University of Stuttgart, not published, 2013.

SCHULZ, T.: *Calibration of a Terrestrial Laser Scanner for Engineering Geodesy*. Phd thesis, ETH Zürich, Institut für Geodäsie und Photogrammetrie an der Eidgenössischen Technischen Hochschule Zürich, 2007.

STAIGER, R.: *Terrestrial Laser Laserscanning – Technology, Systems and Applications*. 2nd FIG Regional Conference, Marrakech, Morocco, December 2-5, 2003.

WENZEL, K., ABDEL-WAHAB, M, CEFALU, A., FRITSCH, D.: *A Multi-Camera System for Efficient Point Cloud Recording in Close Range Applications*. LC3D workshop in Berlin, 2011.

WENZEL, K., ROTHERMEL, M., FRITSCH, D., HAALA, N.: *Image Acquisition and Model Selection for Multi-View Stereo*. Int. Arch. Photogramm. Remote Sens. Spatial Inf. Sci., 2011., Vol. XL-5/W1, pp. 251-258, 2013.

Links:

DIERICHS, K.: http://www.karoladierichs.net/category/projects, last accessed on February 24, 2014.

GEOMAGIC: http://www.geomagic.com/de/, last accessed on February 26, 2014

LEICA GEOSYSTEMS: *Leica HDS 7000 – Product Specifications*. 2011. http://hds.leica-geosystems.com/downloads123/hds/hds/HDS7000/brochures-datasheet/HDS7000_DAT_en.pdf, last accessed on March 5, 2014

MESHLAB: http://meshlab.sourceforge.net/, last accessed on February 26, 2014.

Technical Session 7: Geodetic Monitoring for Mining

Future Challenges of the Small Atomic Oscillators Used in GNSS Monitoring Systems for Structures and Natural Objects

Konstantin M. Antonovich, Nikolay S. Kosarev
Siberian State Academy of Geodesy, Novosibirsk, Russia

Abstract
The installation of small atomic oscillators in GNNS receivers and satellites open new possibilities for using them in monitoring structures and natural phenomena and objects. The advantages are considered.

Keywords
GNSS, receiver, small-size atomic clock, measurement accuracy.

1 INTRODUCTION

All applications of satellite navigation systems are based on the signal propagation time measurements from the satellite to the receiver. Therefore the accurate timing information has the decisive significance. The time is necessary for the observer's position fixing in the inertial space, and for satellite precise positioning. In this case it is important to measure the distance between a satellite and a receiver. To provide a distance error no less 1 mm the time should be known as less as $0.3 \cdot 10^{-11}$ seconds.

To have such accuracy of distance measurements to a satellite making by the one-way method the atomic clock is required to be in a receiver too.

It is important not only the clock oscillator stability but also their size and the mass. The present-day to the product miniaturization has touched GNSS technologies as well SHKEL (2011). Some laboratories are are engaged in the development of the small-size atomic clock. The National Institute of Standards and Technologies of USA and some powerful companies (Honeywell, Symmetricom, Kernko) have started to develop the small-size atomic clock production technologies. The small-size atomic clock MACH was developed in Russia at the Frequency Standard Laboratory of the Physical Institute of the Russian Academy of Science. Some characteristics of modern oscillator types are given in Table 1.

Table 1. The characteristics of modern oscillators

Oscillator Characteristics	On the base of atomic ray tube	Traditional rubidium frequency standard	Precision quartz crystal oscillator	Small-size atomic clock
Long-duration relative frequency instability, for 1 hour	10^{-13}	10^{-12}	10^{-10}	$5 \cdot 10^{-12}$
Cost, thousands of rubles	3000	100	18	less than 30
Volume, cm^3	10000	200-500	60	less than 50
Input power, W	100	~12	~3	0,3

In compare with precision quartz crystal oscillators the application of the small-size atomic clock together with a GNSS receiver has the following advantages:

- The signal lock time becomes shorter; observations are more stable in close conditions and urban areas;
- There is no necessity to introduce the receiver clock error for each epoch. This reduces the number of unknowns in equations for calculation of coordinates and its increments, increases the system equations conditioning resulting to the accuracy increase of and the reliability of results.
- The decrease of noise of direct observations and derived measurements (single, double and triple differences and their combinations).

Small atomic oscillators are also used for the development of new GNSS measurement processing methods. Checking technique of code and carrier phase measurements by geometric range differences is considered. This technique is based on approximate base station coordinates and data taken from navigation message ANTONOVICH (2011), ANTONOVICH (2012a), ANTONOVICH (2012b), ANTONOVICH (2012c), KOSAREV (2012a), KOSAREV (2012b).

However, there are other sources of errors because of reducing errors from the same source leads to the accuracy increase only in case of reducing the impact of other error sources among which the most serious are the multipath, some kinds of interference, and ionospheric scintillations. The use of filters can improve the problem solution ANTONOVICH (2011), ANTONOVICH (2012a), ANTONOVICH (2012b), ANTONOVICH (2012c), KOSAREV (2012a), KOSAREV (2012b).

Owing to the application of small atomic oscillators together with GNSS receivers for measurements the accuracy is higher than that provided by standard quartz generator-based receivers. We consider that the measurement errors in plane for distances less than 10 km between stations will be approximately 1 mm + 0.1 ppm·D (D is a distance between reference stations) at the duration of observation about several minutes.

The application of small-size atomic oscillators in geodetic monitoring structures and natural objects can provide quantitative, quick and accurate solving integer-valued phase ambiguities because of the receiver clock correction is constant and the carrier phase pseudorange equation contains only three unknown variables (three coordinates). From other side, using small atomic oscillators allows error reducing in determination of geodetic height MISRA (2001). This is the most important in structural monitoring using GNSS technologies LUCCIO (2002).

2 CONCLUSIONS

The small atomic oscillators open a new era for GNSS techniques for technology used for geodetic monitoring of structures and natural objects.

REFERENCES

Journal articles:

ANTONOVICH, K. *On the way of the continuous carrier phase control during GNSS observations* [Text] / K. Antonovich, N. Kosarev // Material collection of the International Exhibition and Scientific Congress «GEO-SIBERIA-2011», 19-29 April 2011, Novosibirsk, V. 1, part 2. – Novosibirsk: SSGA, 2011. – P. 164-168.

ANTONOVICH, K. *The use of geometrical range for control of GNSS measurements* [Текст] / K. Antonovich, N. Kosarev // Material collection of the International Exhibition and Scientific Congress «INTEREXPO GEO – SIBERIA – 2012», 10 – 20 April 2012, Novosibirsk, V. 1, part 2.– Novosibirsk, SSGA, 2012 a, – P. 245 – 250.

ANTONOVICH, K. *The control method of code and phase pseudoranges in coordinate domain* [Text] / K. Antonovich, N. Kosarev // Geodesy and aerial photography. – 2012 b, – №2/1. – P. 11 – 15.

ANTONOVICH, K. *The estimation of multipath means of code data* [Text] / K. Antonovich, N. Kosarev // Navigation Satellite Systems, their role and value in modern life: thesis report of the Second International Scientific and Technical Conference, dedicated to the 30th anniversary of the launch into orbit the first Navigation Satellite of "GLONASS" (10–14 October 2012, Zheleznogorsk) / edited by N. Testoedov; «Information satellite Systems»; Siberian State Aerospace University. – Krasnoyarsk 2012 c, – P. 213 – 215.

KOSAREV, N. *Consideration of the effect of the atmosphere of control carrier phase in the GPS – observations* [Text] / N. Kosarev// The Earth Sciences in modern stage: Material collection of the Forth Scientific and Practical International Conference (25.04.2012). Moscow: Publishing house of «Sputnik+», 2012 a, – P. 114 – 118.

KOSAREV,N. *The reconstruction of carrier phase: problems and solutions* [Text] / N. Kosarev // Bulletin of SSGA. – 2012 b, – Vol. 1 (17): Novosibirsk, SSGA, 2012. – P. 53 – 60.

LUCCIO M. The Concrete and the Clay: Monitoring Large-Structure Deformation [Text] / M. Luccio // GPS World. – 2002. – No. 8. – P. 16-20. – English.

MISRA, P.N. Global Positioning System. Signals, Measurements and Performance [Text] / P.N. Misra, P. Enge – USA: Ganga-Jamuna Press. – 2001. – 390 p. – English.

SHKEL A. M. Microtechnology Comes of Age [Text] / A.M. Shkel // GPS World. – 2011. – No. 9. – P. 11 – 15. – English.

Links:

http://www.aetechnologies.ru/dev/mach/

The Assessment of Geomechanical Situation in the Neighborhood of Designed Open Pit-Side Contour Convergence with Shafts in Mine Development

Tulegen T. Ipalakov[1], Erik K. Nurzhumin[2]
[1]D. Serikbayev East-Kazakhstan State Technical University, Republic of Kazakhstan,
[2]S. Seyfullin Kazakh Agrotechnical University, Republic of Kazakhstan

Abstract
The paper suggests tentative assessment of geomechanical condition in the neighborhood of designed open pit-side contours convergence with shafts during multiple-purpose mining of the deposit using probabilistic approach.

Keywords
Mine, resistance, risk assessment, uncertainty, probabilistic analysis, safety factor

1 GENERAL INFORMATION ABOUT AN OBJECT

The given paper studies the option of the opencast development using spiral ramp (Figure 1). The distance from the mine bench crest to the shaft “Ventilyatsionnaya” (ventilate) was 62 m with the design factors of the pit wall with safety bench width of 10m and the bench batter of 75 degrees. The distance to the shaft “Kapitalnaya” is 44 m.

Deposit mine “Yubileynoye” (Jubilee) can be conditionally referred to the mines in “high-strength” massifs; their walls are a fortiori stable because their bench crest is conditioned mainly with the wall structure and transport communication system parameters. That is why the calculation of stability in the area of convergence with permanent mines has been done taking into account the mine geometric parameters on the first place.

The influence of the mine space on perimeter massif is expressed in the occurrence of stress concentration zone and relieving zones, stress vector direction alteration, shear load increase near the wall.

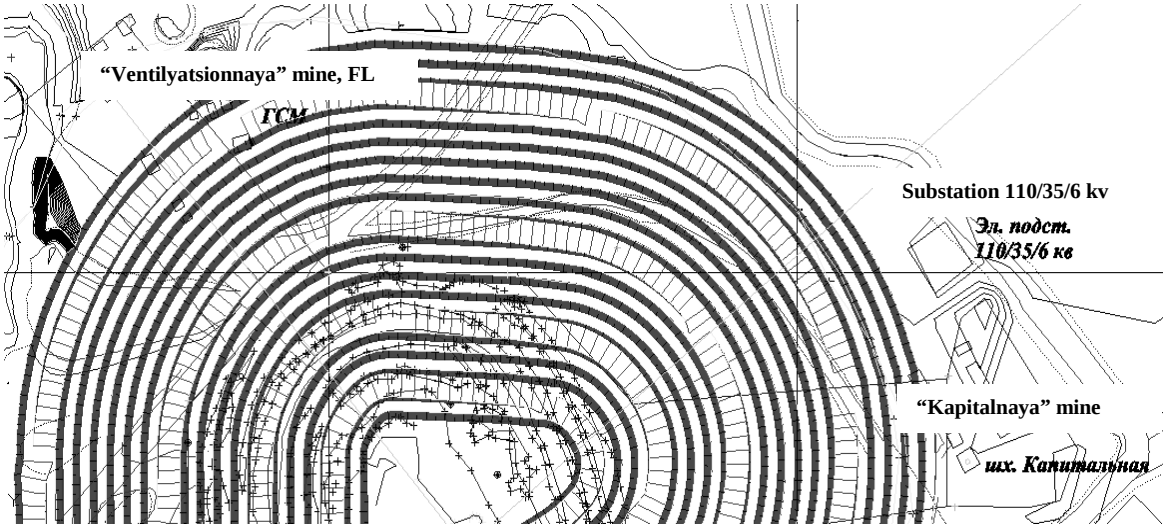

Figure 1: The diagram of underground mine objects location
"Ventilyatsionnaya" (ventilate) mine, FL; Substation; "Kapitalnaya" main

2 THEORY

Modern concept of operating complex anthropogenic structures including mines suggests the transition from the ideology of "complete safety" to the ideology of "acceptable risk". To do this it is necessary to analyze and develop the system of risk management that is, decreasing the latter to the acceptable level.

Risk occurrence is caused by uncertainties which occur on different stages of resistance calculating.

Systematic analysis of uncertainties and assessment of geotechnical object risk can be solved on the basis of probabilistic approach. The advantage of this approach is in the deformation occurrence probability as an important indicator of the pit wall resistance state. Probability calculation input parameters (initial data) and the results are considered as probability distribution and not as discrete assessments of slopes done by determined methods.

Probability approach uses all values of physical-mechanical properties of lithological differences making the mine wall slope deformation and possible combinations of different factors influence are considered. In the result of calculation we get the probability density function of safety factor values.
Detailed probability calculation allows improving significantly the analysis quality and accuracy, to assess the mine walls deformation danger.

Long-term experience of using probabilistic methods for calculating the resistance of mine benches and walls at foreign enterprises has allowed to develop specific criteria to assess deformation occurrence probability ($P_{обр}$). Reference SULLIVAN (2007) presented acceptable bounds of deformation occurrence probability under different geomechanical conditions. Below the Table shows major geomechanical risks that may occur under different designs of the mine wall in the area of convergence with "Ventilyatsionnaya" shaft.

Table 1: Major geomechanical risks

Potential geomechanical risks	The distance of mine wall convergence with the shaft, m				
	97	116	134	141	152
	Slope batter, degrees.				
	78	80	82	83	84
Sliding surfaces corresponding to global minimum of the wall resistance cross the borders of shaft guard pillar, which may cause the deformation of shaft massifs.	+	+	-	-	-
Inadmissible level of deformation occurrence probability	-	-	-	-	+
The guard pillar and shaft are in the zone of stress concentration comparable with the massif rock strength	-	-	+	-	+

3 PRACTICAL APPLICATIONS

Nevertheless, we must note that the shown above calculations have been done for the conditions that mainly take into consideration the wall geometrics. If negative engineering-geological factors are revealed in the process of detailed geomechanical exploration of the deposit, it will be necessary to do more complete analysis with more accurate distance of the mine wall convergence with the shafts on the further design stages. Besides, one must pay attention to the fact that the upper part of the shaft and guard pillar are in the tensile stress zone (Figure 2), where the direction of stress resultants indicates the presence of potential sites where the process of the massif additional crack formation and rock fragmentation are possible. It is necessary to note that under such capacities of benches and walls in the shaft area there is a serious danger of deformation occurrence in case of disconfirmation physical-mechanical properties of deads under their changing to down. The method of decreasing stress-strain properties (SSR) has determined that if there is 20% decreasing of rock bond and 15 % angle of internal friction decreasing, glides may occur; their mechanism is shown in Figure 3 (on the example of “Kapitalnaya” mine area). The mentioned above stress-strain properties alteration, especially near “Ventilyatsionnaya” mine, there is an oxide zone there, may be conditioned by several revealed factors such as negative structural, engineering-geological, hydrogeological and other features of massif rocks forming outline zones, and also under the influence of anthropogenic factors (mass explosions on the ground and underground) in the pointed areas.

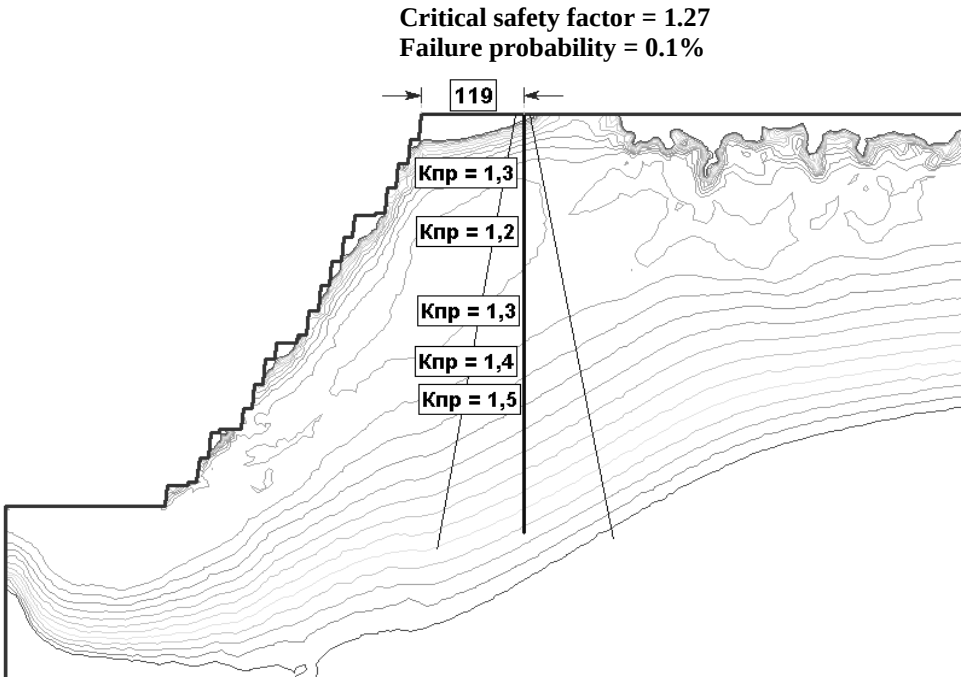

Figure 2: Results of calculation the resistance of the system "the mine wall – the shaft of "Kapitalnaya" mine using finite element method (slope angle is 84 degrees, the mine wall slope is 58 degrees, safety bench width is 10 m)

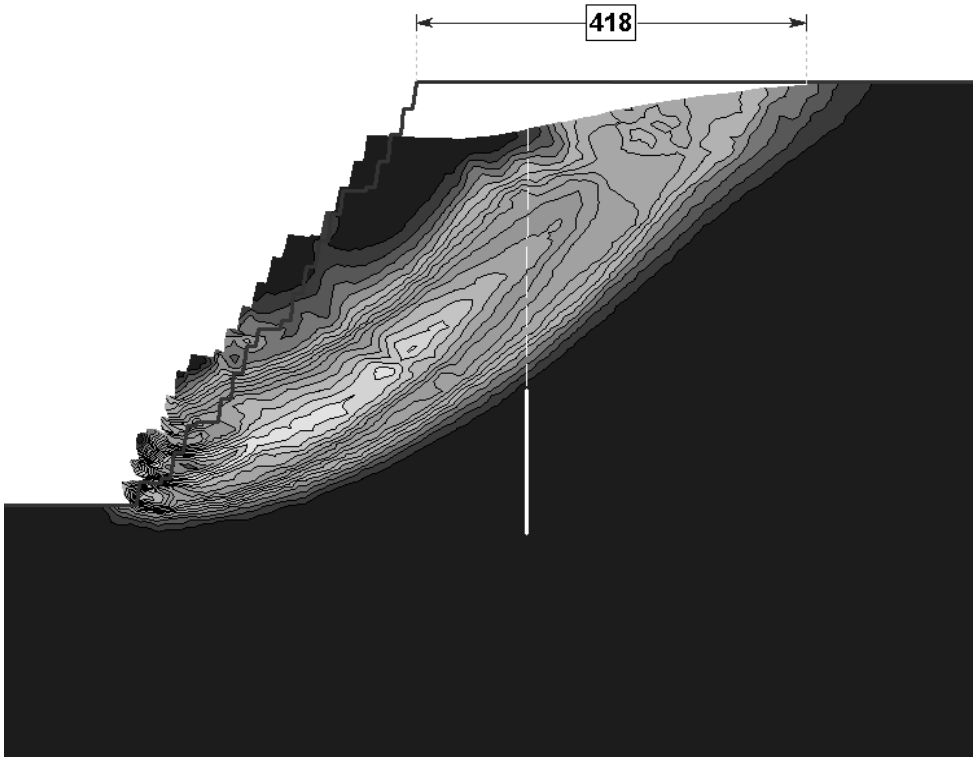

Figure 3: Mechanism of possible deformations in the mine "Kapitalnaya" shaft area at decreasing stress-strain properties of outline massifs below critical safety factor

4 CONCLUSIONS

1. The results of resistance calculations done in the area of mine walls and mine shafts convergence using the original geological data being at the moment revealed the area of possible alteration of walls and benches design factors, with the objective to increase the distance between the pointed objects. The permissible estimated slope batter is 83 degrees for the mine “Ventilyatsionnaya”. The distance to the mine shaft will be increased up to 141 m if the safety bench width is 10 m. The permissible estimated slope batter is 84 degrees for the mine “Kapitalnaya”. The distance to the mine shaft is 119m correspondingly. Such wall structures will allow to decrease the negative influence of the mine on guard shaft pillows and mine industrial sites.

2. The pointed walls factors are close to critical which is supported by the calculations using the method of decreasing stress-strain properties (SSR). Thus, if there are changes (decreasing), 20% of estimated rock adherence and 15% of internal friction angle, there may occur deformation with rather serious effect. That is why, in spite of the conditions dictated by the deposit opening structure it is necessary to use the given parameters on quite limited wall sites for the construction of final outlines.

3. Having the objective of decreasing geomechanical risk on the given mine sites, it is necessary:

– First of all to make geomechanical drilling and to make a range of laboratory examining of structural, strengthening properties of rock massifs, to specify the degree of their alteration due to anthropogenic effect, to study hydrogeological conditions;

– To develop practical recommendations for the wall structure on final outlines, in geomechanical zones 1 and 4 of the existing mine, to open experimental-industrial sites, and to foresee conducting the necessary cycle of experimental-industrial and experimental works for the prognoses and analysis of geomechanical condition of the layout massif in their designs.

REFERENCES

Books:

IPALAKOV, T.T., Parshakov A.T. Resource saving technology of control the mine walls resistance on the basis of probability analysis. Monograph. Edit.EKSTU, Ust-Kamenogorsk, March 2013, 145 p.

Journal articles:

DUNCAN, J.M. State of the art: limit equilibrium and finite element analysis of slopes, / J. M. Duncan // Journal of Geotechnical Engineering. 1996. - pp 577-596.

DUNCAN, J.M. The accuracy of equilibrium methods of slope stability analysis / J. M. Duncan, G. Wright // Engineering Geology. - vol. 16. 1980. - pp 5-17.

SULLIVAN, T.D. (2007). Hydromechanical coupling and pit slope movements. In Y. Potvin (ed.), Slope Stability 2007 – Proceedings of the 2007 International Symposium on Rock Slope Stability in Open Pit Mining and Civil Engineering, Perth, 12-14 September 2007, pp. 3-43.

IPALAKOV, T.T., Apshikyt B. Slope resistance under influence of earthquake. Proceeding of International Forum “Innovative technologies in mine survey”, February 15, Karaganda, 2013, p. 106-108

IPALAKOV, T.T., Parshakov A.T. Resource saving technology of control the mine walls resistance. Materials of International scientific conference “Innovative technologies of collecting and processing geo-space data for natural resources management”, September 18 – 19, 2012. Almaty, 2012 p. 5 – 10

List of authors

Maxim A. Altyntsev
Department of Engineering Geodesy and Mine Surveying
Siberian State Academy of Geodesy
10, Plakhotnogo St.
630108, Novosibirsk
Russian Federation
Tel.: +79529152980
Email: mnbcv@mail.ru

Konstantin M. Antonovich
Department of Physical Geodesy and Remote Sensing
Siberian State Academy of Geodesy
10, Plakhotnogo St.
630108, Novosibirsk
Russian Federation
Tel.: +73833610159
Email: kaf.sastronomy@ssga.ru

Eugene I. Avrunev
Department of Cadastre and Territorial Planning
Siberian State Academy of Geodesy
10 Plakhotnogo St.
630108, Novosibirsk
Russian Federation
Tel: +3833443173
E-mail: kadastr204@yandex.ru

Joel van Cranenbroeck
CGeoS – Creative GeoSensing sprl-s
Rue du Tienne de Mont, 11
BE-5530 MONT, Yvoir
Belgium
Tel.: +32(0)81413657
Fax: +32(0)81412602
Email: joel@creative-geosensing.com

Alexey V. Dubrovsky
Director of “Digitaizer” Laboratory
Siberian State Academy of Geodesy
10, Plakhotnogo St.
630108, Novosibirsk
Russian Federation
Tel.: +73833610109
Fax: +73833443060
Email: avd5@mail.ru

Alexander I. Fyodorov
Institute of Cadastre and Environmental Management
Department of Geomatics and Property & Infrastructure
Siberian State Academy of Geodesy
10, Plakhotnogo St.
630108, Novosibirsk
Russian Federation
Tel.: +73833610709
Email: fai2012@ngs.ru

Natalia V. Fyodorova
Institute of Cadastre and Environmental Management
Department of Geomatics and Property & Infrastructure
Siberian State Academy of Geodesy
10, Plakhotnogo St.
630108, Novosibirsk
Russian Federation
Tel.: +73833610709
Email: fai2012@ngs.ru

Ilgiz A. Giniyatov
Department of Cadastre and Territorial Planning
Siberian State Academy of Geodesy
10 Plakhotnogo St.
630108, Novosibirsk
Russian Federation
Tel.: +3833443173
E-mail: kadastr204@yandex.ru

Ekaterina I. Gorokhova,
Siberian State Academy of Geodesy
10, Plakhotnogo St.
630108, Novosibirsk
Russian Federation
Tel.: +73833432955
Email: e.gorohova@ssga.ru

Tulegen T. Ipalakov
Department of Geodesy, Land Management, and Cadastre
D. Serikbayev East-Kazakhstan State Technical University
19, Serikbayev Str.
070010, Ust-Kamenogorsk
Republic of Kazakhstan
Tel.: +77779858113
Fax: +87232540776
Email: TIpalakov@ektu.kz

Reiner Jäger
Institute of Geomatics at IAF/HSKA
University of Applied Sciences Karlsruhe
Moltkestr. 30
76133 Karlsruhe
Germany
Tel.: +49(0)7219252620, -2598
Fax: +49(0)721-9252597
E-mail: reiner.jaeger@hs-karlsruhe.de
Website: www.goca.info

Alexander P. Karpik
Siberian State Academy of Geodesy
10, Plakhotnogo St.
630108, Novosibirsk
Russian Federation
Tel.: +73833433937
Fax: +73833443060
Email: rector@ssga.ru
Website: http://www.ssga.ru

Kaisar Khasenov
Department of Geodesy, Land Management, and Cadastre
D. Serikbayev East-Kazakhstan State Technical University
19, Serikbayev Str.
070010, Ust-Kamenogorsk
Republic of Kazakhstan
Tel.: +77779858113
Fax: +87232540776
Email: Hasenovkb@gmail.com

Valery S. Khoroshilov
Department of Physical Geodesy and Remote Sensing
Siberian State Academy of Geodesy
10, Plakhotnogo St.
630108, Novosibirsk
Russian Federation
Tel.: +73833432911
Email: khoroshilovvs@mail.ru

Vyacheslav G. Kolmogorov
Department of Geomatics and Property& Infrastructure
Siberian State Academy of Geodesy
10, Plakhotnogo St.
630108, Novosibirsk
Russian Federation
Tel. +73833443660
Fax +73833443060
Email: vyacheslavgeorgievich@mail.ru

Nikolay S. Kosarev
Department of Physical Geodesy and Remote Sensing
Siberian State Academy of Geodesy
10, Plakhotnogo St.
630108, Novosibirsk
Russian Federation
Tel.: +73833610159
Email: kosarevnsk@yandex.ru

Martin Metzner,
Institute of Engineering Geodesy
University of Stuttgart
Geschwister-Scholl-Str. 24 D
70174 Stuttgart
Germany
Tel.: +49(0)71168584043
Fax: +49(0)71168584044
Email: martin.metzner@ingeo.uni-stuttgart.de

Ivo Milev
technet-rail 2010 GmbH
Beuth University of Applied Science Berlin, Germany
Goethe Strasse 42
10625 Berlin
Germany
Tel.: +49(0)3054840785
Fax: +49(0)3054826798
Email: ivo.milev@technet-rail.de

Hans Ni
Beijing iSpatial Co Ltd PR China
Room 1207, Building 1, Huihuang International Plaza
Shangdi Street 10, Haidian District, Beijing
PC 100085
RP China
Tel.: +861059713414
Fax: +861059713424
http://www.ispatial.com.cn

Erik K. Nurzhumin
Department of Geodesy
S. Seyfullin Kazakh Agrotechnical University
62, Prospect Pobedy
473028, Astana
Republic of Kazakhstan
Tel.: +77172397947

Olga G. Pavlovskaya
Department of Higher Mathematics
Siberian State Academy of Geodesy
10, Plakhotnogo St.
630108, Novosibirsk
Russian Federation
Tel.: +73833443300
Email: pavlovskaya@ssga.ru

Marzhan Rakhymberdina
Department of Geodesy, Land Management, and Cadastre
D. Serikbayev East-Kazakhstan State Technical University
19, Serikbayev Str.
070010, Ust-Kamenogorsk
Republic of Kazakhstan
Tel.: +77779858113
Fax: +87232540776
Email: MarzhanRakh@mail.ru

Annette Scheider,
Intitute of Engineering Geodesy
University of Stuttgart
Geschwister-Scholl Str. 24D
70174 Stuttgart
Germany
Tel.: +49(0)71168584057
Fax: +49(0)71168584044
Email: annette.scheider@ingeo.uni-stuttgart.de

Annette Schmitt
Institute of Engineering Geodesy
University of Stuttgart
Geschwister-Scholl Str. 24D,
70174 Stuttgart,
Germany
Tel.: +49(0)71168584065
Fax: +49(0)71168584044
Email: annette.schmitt@ingeo.uni-stuttgart.de

Desislava Staykova
technet-rail 2010 GmbH
Goethe Strasse 42
10625 Berlin
Germany
Email: desi.staikova@technet-rail.de

Volker Schwieger
Institute of Engineering Geodesy
University of Stuttgart
Geschwister-Scholl Str. 24D
70174 Stuttgart
Germany
Tel.: +49(0)71168584040
Fax: +49(0)71168584044
Email: volker.schwieger@ingeo.uni-stuttgart.de

Uwe Stilla
Photogrammetry and Remote Sensing,
Technische Universitaet Muenchen
Arcisstr. 21
80333 Muenchen
Germany
Tel.: +49(0)8928922671
Fax: +49(0)8928923202
Email: stilla@tum.de

Jakob Unger,
Intitute of Photogrammetry and GeoInformation
Leibniz Universität Hannover
Nienburger Straße 1,
30167 Hannover
Germany
Tel.: +49(0)5117622323
Email: unger@ipi.uni-hannover.de

Igor G. Vovk
Department of Applied Informatics and Information Systems
Siberian State Academy of Geodesy
10, Plakhotnogo St.
630108, Novosibirsk
Russian Federation
Tel.: +7383343 853
Email: vovkig383@rambler.ru

Karl You Xiangjun
Beijing iSpatial Co Ltd PR China
Room 1207, Building 1, Huihuang International Plaza
Shangdi Street 10, Haidian District, Beijing
PC 100085
RP China
Tel.: +861059713414
Fax: +861059713424
http://www.ispatial.com.cn

Li Zhang
Institute of Engineering Geodesy
University of Stuttgart
Geschwister-Scholl Str. 24D
70174 Stuttgart
Germany
Tel.: +49(0)71168584049
Fax: +49(0)71168584044
Email: li.zhang@ingeo.uni-stuttgart.de

Bimin Zheng,
Institute of Engineering Geodesy
University of Stuttgart
Geschwister-Scholl Str. 24D
70174 Stuttgart
Germany
Tel.: +49(0)71168584061
Fax: +49(0)71168584044
Email: bimin.zheng@ingeo.uni-stuttgart.de